Summer 2007

Novel model of cerebrospinal fluid dynamics based on hemodynamically driven cyclic brain compliance variation

Bruno A. Mantilla
New Jersey Institute of Technology

ABSTRACT

NOVEL MODEL OF CEREBROSPINAL FLUID DYNAMICS BASED ON HEMODYNAMICALLY DRIVEN CYCLIC BRAIN COMPLIANCE VARIATION

by
Bruno A. Mantilla

This study provides a novel explanation for the Cerebro-Spinal Fluid (CSF) flow pattern observed in phase contrast cine-MRI studies. CSF dynamics has been traditionally explained as a bulk flow from the site of production to the site of absorption. Studies done with phase contrast cine-MRI show a more complex CSF movement, that is not explainable by the bulk flow paradigm. This study describes a mechanism explaining how the energy delivered by the heart in each cycle is responsible not only for the blood flow, but also for the CSF circulation. This mechanism is based on a cyclic variation of brain compliance, dependent on the blood volume inside the brain vessels. As the cardiac cycle changes the blood volume inside the vessels, it also conditions a compliance cycle of the brain tissue.

For better comprehension of the mechanism, a conceptual model, mathematical model and computer model are described. To capture the essence of CSF dynamics a three compartmental model is created representing: the ventricular system, the intracranial subarachnoideal space, and the spinal subarachnoideal space. The implemented driving function represents the blood volume variation with time produced by the cardiac cycle. In turn it determines cyclic changes in brain parenchyma compliance. Brain parenchyma compliance changes as a function of the blood volume inside the brain vessels; therefore, during systole the compliance diminishes, during

diastole compliance increases. As brain tissue compliance changes the CSF volume inside each compartment is redistributed. Cyclic compliance variation of brain tissue creates a pulsatile CSF flow. The CSF dynamics model is also used for the analysis of altered CSF dynamics; Normal Pressure Hydrocephalus and Idiopathic Intracranial Hypertension are explained as a consequence of altered compliance of the brain tissue.

NOVEL MODEL OF CEREBROSPINAL FLUID DYNAMICS BASED ON HEMODYNAMICALLY DRIVEN CYCLIC BRAIN COMPLIANCE VARIATION

by
Bruno A. Mantilla

A Dissertation
Submitted to the Faculty of
New Jersey Institute of Technology
in Partial Fulfillment of the Requirements for the Degree of
Doctor of Philosophy in Biomedical Engineering

Department of Biomedical Engineering

August 2007

APPROVAL PAGE

NOVEL MODEL OF CEREBROSPINAL FLUID DYNAMICS BASED ON HEMODYNAMICALLY DRIVEN CYCLIC BRAIN COMPLIANCE VARIATION

Bruno A. Mantilla

Dr. William Hunter, Dissertation Co-Advisor — Date
Chair, Department of Biomedical Engineering, NJIT
Professor, Department of Biomedical Engineering, NJIT

Dr. Richard Foulds, Dissertation Co-Advisor — Date
Associate Professor, Department of Biomedical Engineering, NJIT

Dr. Stanley Reisman, Committee Member — Date
Professor, Department of Biomedical Engineering, NJIT
Professor, Department of Electrical and Computer Engineering, NJIT

Dr. John Tavantzis, Committee Member — Date
Professor, Department of Mathematics, NJIT

Dr. Sergei Adamovich, Committee Member — Date
Assistant Professor, Department of Biomedical Engineering, NJIT

Dr. Max Roman, Committee Member — Date
Assistant Research Professor, Department of Biomedical Engineering, NJIT

BIOGRAPHICAL SKETCH

Author: Bruno Antonio Mantilla

Degree: Doctor of Philosophy

Undergraduate and Graduate Education:

- Doctor of Philosophy in Biomedical Engineering, New Jersey Institute of Technology, Newark, NJ, 2007
- Master of Science in Biomedical Engineering, New Jersey Institute of Technology, Newark, NJ, 2002
- Neurosurgeon, Universidad Militar Nueva Granada, Hospital Militar Central Bogota, Colombia, 1985
- Doctor in Medicine, School of Medicine, Universidad del Rosario, Hospital San José-Bogotá, Colombia, 1980

Presentations and Publications:

Mantilla, B., et al., Cerebrospinal Fluid Normal Dynamics, Proceedings of the BMES 2005 Annual Fall Meeting, October 2005, Baltimore, Maryland.

Mantilla, B., et al., Relation between Brain Parenchyma Compliance and Normal and Abnormal Cerebrospinal Fluid Dynamics, Proceedings of the Third Annual Symposium of Neural Hydrodynamics, May 2005, Columbus, Ohio.

Mantilla, B., et al., Cyclical Variation of Brain Parenchyma Compliance as the Pump for Cerebrospinal Fluid, Proceedings of the BMES 2004 Annual Fall Meeting, October 2004, Philadelphia, Pennsylvania.

Mantilla, B., Foulds, R.A., Integrated Biomedical Education Using Studio-Based Learning, Proceedings of the Partnership for Educational Bioengineering Laboratories (PEBEL) , June 2004, Lansdowne, Virginia.

Mantilla, B., Foulds, R., Bergen, M., Studio Classes Modeled on Complex System Theory in Order to Increase Creativity and Critical Thinking, Proceedings of the 30th IEEE Northeast Bioengineering Conference, Springfield ,Massachusetts, April 2004.

Mantilla, B., Foulds, R., A Computational Model of the Spastic Behavior of the Lower Limb, Proceedings of the 29th IEEE Northeast Bioengineering Conference, Newark, New Jersey, March 2003

Foulds, R., Bergen, M., Mantilla, B., Integrated biomedical engineering education using studio-based learning, Engineering in Medicine and Biology Magazine, IEEE Volume 22, Issue 4, July-Aug. 2003 Page(s):92 - 103

'cause only dreams make the world spin as it should

Empezamos Como Un Sueño

I

En el seno de la madre,
Se conjura…
Primoroso Sueño,
Con azúcar y cristal
nos convierte en realidad.

Empezamos como un sueño…
Y empezamos a soñar

En la aurora,
nuevo Sueño;
escondido tras la bruma,
Con olor a incertidumbre,
Se levanta,
Majestuoso
Entonando su cantar…
nos llama,
nos cita,
Y nos hace suspirar

Empezamos como un sueño…
Y empezamos a soñar

I I

El…Se extiende,
Se desplaza,
Y con mil otros se entrelaza
Haciendo al mundo girar…

Empezamos como un sueño…
Y empezamos a soñar

Nos evade,
Se esconde…
Reaparece y nos sonríe;
De nuevo su llamar…
Gigante Sueño que nos guía,
Que nos lleva
Jugueteando día a día,
Lentamente al mas allá.

Empezamos como un sueño…
Y empezamos a soñar

III

Que la fuerza de tus sueños te sonría,
Cada día,
Renovando tu cantar.
Y te lleve
Floreciendo en la vida.
Y te aguarde,
A las puertas del olvido
Con alegría, amor y paz

Empezamos como un sueño…
Y nos vamos a soñar…

ACKNOWLEDGMENT

Special thanks go for my mentor and friend, Dr. Richard Foulds, also my co-advisor, who was able to transcend the scientific arena to establish human, sincere and open communication. I hope we can keep it for a long time. Thanks to Dr. Hunter, my co-advisor and chair of BME, who kept me working while I studied. Also special thanks for Dr. Reisman, Dr. Tavantzis , Dr. Adamovich, and Dr. Roman, each one of you gave me an exceptional friendship, and generously provided me with your unique wisdom and knowledge. Dr. Kristol, you provided useful advice since my first day in BME. Dr Collins talking with you is always inspirational and rewarding. Dr. Arinzeh, it is simply "so good" swapping ideas with you.

Very special words for my family: Silvia, Juan Jose, and Juliana, I know it was tough leaving everything behind, but we knew we could do it; thanks for helping me "in the battle", we ought to keep it up! The future is here, and it is yours.

Father you will always be an inspiration and an unmatchable example. To my mother, sisters, and brothers: even though it is not easy to reach your standards, I still feel your strong support coming from a far distance.

I would like to thank Mr. German Correa for always being there without needing to be asked.

Thanks to my fellow graduate students, in special to the "Lab Gang", Darnell, Amanda, Quin Yin, Kate, Diego, Chemu, and Kai; also to the "Non-Linear Dynamics Gang", Anne Marie, Diane, and Jason; for that special magic spelled between us, we need to keep it that way.

Thank you Ms. Naporano and Ms. Price for your invaluable help in everyday activities.

TABLE OF CONTENTS

TABLE OF CONTENTS
(Continued)

LIST OF TABLES

LIST OF FIGURES

LIST OF FIGURES
(Continued)

LIST OF FIGURES
(Continued)

LIST OF FIGURES
(Continued)

LIST OF FIGURES
(Continued)

LIST OF FIGURES
(Continued)

Figure **Page**

LIST OF FIGURES
(Continued)

Figure **Page**

CHAPTER 1

INTRODUCTION

Numerous studies had been published trying to model and to understand pathological conditions of Cerebrospinal Fluid (CSF) dynamics, mainly hydrocephalus, and to a lesser extent, Idiopathic Intracranial Hypertension. Even though it will seem logical to understand the normal situation before attempting to understand the abnormal situation, this has not happened. Comparatively little effort has been devoted to understand the normal CSF circulation. It has been assumed for a long time the existence of a permanent bulk flow from the site where CSF is formed to the place where CSF is absorbed. This assumption has been one of the pillars where the analysis of multiple models of CSF dynamics lies. Amazingly, without checking the existence of a presumed and needed pressure gradient between the site of formation, choroid plexus, and the assumed absorption site at the brain convexity, the arachnoid villi, bulk flow is still found in most physiology texts as the accepted mechanism of the CSF dynamics. Notwithstanding, work done by Greitz et al., and by Naidich et al. with Magnetic Resonance Imaging (MRI) in the early 90's, documents a complex oscillatory CSF flow pattern that contradicts absolutely the previously accepted paradigm.

This work is focused on understanding the relation and functioning of the CSF/ ventricular system from a physics and hydrodynamics point of view. A novel concept is introduced in which cyclical changes of the ventricular and subarachnoideal wall's compliances are necessary conditions for the normal movement of CSF. Moreover, these cyclical changes of the brain compliances are dependent on the amount of blood present

inside the brain vessels. As a consequence, the compliance's cyclical variations are intimately bound to the cardiac cycle.

The importance of the physical structure and behavior of the brain tissue are emphasized, not only from a biological, but also, most important, from a material science point of view. Although, this is not intended to be an exhaustive review of anatomy and physiology of the CNS, essential features are introduced in order to better comprehend the relation between structure and derived physical functioning of the system. The bulk properties of the brain tissue as well as basic concepts of hydrodynamics are taken into consideration. Also, the origin of viscoelastic properties of the brain and its relation to the structure are reviewed.

Finally, to explain the normal CSF flow inside the brain and spinal canal, a conceptual model, followed by a mathematical analysis and a computer model are developed. By merging knowledge from basic anatomy, histology, physiology, physics, mechanical engineering, material science, hydrodynamics and control systems, novel concepts and new mechanisms emerge. Mechanisms and concepts here presented provide a better explanation of the CSF system dynamics.

CHAPTER 2

STRUCTURE AND PHYSIOLOGY OF THE NERVOUS SYSTEM

2.1 Brain Structure

The brain could be described in a very simple way as a hollow sphere with thick walls, made of soft material, divided into two hemispheres. The brain is enclosed in a rigid vault, the cranium. It is suspended in an aqueous medium, the cerebrospinal fluid, and surrounded by three covering membranes for its protection: the dura mater, the arachnoid and pial membranes. The brain is continued as the spinal cord through a large aperture, the Foramen Magnum, located at the base of the skull.

During embryological evolution of the brain, three distinctive regions are formed: the forebrain or anterior brain, the midbrain or middle brain, and the hindbrain or posterior brain. The forebrain includes the cerebral cortex, the diencephalic structures, basal ganglia and the connections between them. The cerebral cortex, which is divided into right and left hemispheres, constitutes about two-thirds of the brain mass and lies over and around most of the remaining structures of the brain. It is the most highly developed part of the human brain and is responsible for high mental superior functions as thinking, perceiving, creating strategies, comparing, handling abstract concepts and producing and understanding language. The lateral ventricles lay beneath the cortex, one in each hemisphere. The third ventricle is located deep in the midline surrounded by diencephalic structures.

The midbrain constitutes the smallest of the three divisions, and it is formed exclusively by the mesencephalon. Through the mesencephalon a medial fine and

cylindrical canal, the Sylvius' Aqueduct, connects the third and fourth ventricles. The midbrain forms the superior portion of the brainstem.

The hindbrain includes the pons, medulla oblongata and cerebellum. The pons and medulla oblongata connect the anterior and midbrain to the spinal cord. The pons and medulla oblongata form the inferior portion of the brainstem, and they are involved in the control of many basic functions, such as heart rate, breathing, eating, and sleeping. The inferior portion of the brainstem accomplishes these tasks by directing the spinal cord, other parts of the brain, and the body to perform the appropriate actions. It is also the highway where all the nerve impulses coming from, and into, the superior centers of the CNS travel into the spine. The cerebellum, which represents only one-eighth of the total weight of the brain, is a prominent structure located dorsally to the brainstem. It works with the frontal cortex, and several structures in the pons, in developing new movement strategies by using vestibular, visual and propioceptive information. The fourth ventricle is a cavity filled with CSF, located beneath the cerebellum and dorsally to the pons and medulla. The fourth ventricle connects on the top to the Sylviu's Aqueduct; and at the bottom to the subarachnoideal space, via the two lateral foramen's of Luschka, and a medial foramen of Magendie.

2.2 CSF and the Ventricular System

The Cerebrospinal fluid, (CSF), is a clear bodily fluid composed mainly of water. It is formed by active and passive mechanisms in the ventricular system at a constant rate of 0.35 ml/min. The CSF specific gravity (1.004 - 1.007 g/cm ^{3}) is barely greater than water. CSF viscosity at 37 Celsius is similar to water (6.9 X 10-4 Pa-s). CSF composition is

slightly different from serum; it is composed of a lower amount of proteins, glucose, and potassium, and has a lower Ph. (Table 2.1). Sodium, chloride, and magnesium values are slightly higher in CSF than in plasma. Few white blood cells are typically present in the CSF; a range between 0-5 cells/mm ^{3} in adults is considered normal (0-8 cells/ mm ^{3} in infants). No red blood cells should be present. Thus, CSF behaves as a Newtonian fluid, with density and viscosity similar to water.

CSF production has been frequently attributed to the choroid plexus in the interior of the ventricular system, but probably it is also formed by the ependymal lining of the brain's ventricles. CSF travels from the interior of the ventricles into the subarachnoideal space and is absorbed intracranially in at least in two places:

- Arachnoid Granulations (arachnoid villi, Pacchioni's granulations) located at the convexity over the brain cortex.
- Lymphatic system of the face, mainly in the perinasal area.
- Absorption has been also reported to occur also at the dural cuffs surrounding the vertebral nerves emerging from the spinal cord.

In summary, the Cerebrospinal fluid, (CSF), is formed inside of the ventricles, travels through the ventricles, and exits through the foramens of Luschka and Magendie entering the Cisterna Magna into the subarachnoideal space. The subarachnoideal space is filled with CSF, and surrounds the spinal cord, brainstem, cerebellum and cerebral cortex.

Table 2.1 CSF Composition

Component	CSF	Serum
Water content (%)	99	93
Protein(mg/dl)	35	7000
Glucose(mg /dl)	60	90
Osmolarity(mOsm/lt)	295	295
Na (meq/lt)	138	138
K (meq/lt)	2.8	4.5
Ca (meq/lt)	2.1	4.8
Mg (meq/lt)	0.3	1.7
Cl (meq/lt)	119	102
pH	7.33	7.41
Specific Gravity	1.004 - 1.007 g/cm^3	NA (variable)

The ventricular system is located inside the brain, and is formed by a series of cavities interconnected by narrow passages, and filled with CSF. Beneath the cortex of each cerebral hemisphere, a large lateral ventricle extends from the frontal(frontal horns) into the temporal (temporal horns) and occipital (occipital horns) lobes.

The third ventricle is a single midline cavity located between the two lateral ventricles and is surrounded by diencephalic structures. The interventricular foraminae of Monroe connects on each side of the third ventricle with the lateral ventricles. The cerebral aqueduct of Sylvius is a thin canal, located inside the dorsal midbrain, connecting the third ventricle to the fourth ventricle. The fourth ventricle is another single

cavity, located on the dorsal region of the pons and medulla oblongata, and beneath the cerebellum. At the fourth ventricle, the lateral foramens of Luschka, and the mid foramen of Magendie connect the fourth ventricle to the subarachnoideal space. These apertures open into enlargements of the subarachnoideal space known as the cisterna pontis and the cisterna magna, respectively.

CSF circulation has been traditionally addressed as a bulk flow moving unidirectionally from inside the lateral ventricles, through the ventricular system into the subarachnoideal space. As we will discuss later this traditional approach has been challenged due to direct measured data. (Johnston 2000, Penn 2005) Also, Penn documented in dogs and humans that the variation of the intra-ventricular pressure, the intra-parenchymal pressure, and the subarachnoideal pressure in the brain convexity, occurred in tandem. Penn also published that the difference in pressure between the intraventricular and cranial-subarachnoideal space was less than 1 mm Hg.; which was the sensitivity limit of the transducer used during the procedure. As a consequence, the concept of the pressure gradient between the intraventricular and subarachnoideal pressures is inexistent or has a magnitude of less than one mm Hg.

Even though the mechanism by which the CSF travels through the ventricular system and subarachnoideal space is not well understood, it has been attributed to forces formed by:

- Pressure gradients created by the production and absorption of CSF. (Dandy 1919, Johnston 2000, Sherwood 2004)
- Pressure waves generated by pulsatile arterial blood flow, choroid plexus pulsations and brain expansion. (Linninger, 2005, Egnor 2000)
- Currents induced by ependymal cilia. (Johnston 2000, Sherwood 2004)

None of these mechanisms provide a suitable explanation of the complex movement pattern of CSF. Thus, there exists a need to provide a suitable mechanism that explains CSF flow between compartments. In particular, the current theories do not account for the fact that the pressure in the three compartments equilibrates nearly instantaneously due to Pascal's Law, and the absence of valves between the compartments.

No definite CSF compartmental volume distribution has been universally established, but it is accepted that most of the CSF resides in the intracranial subarachnoideal space (≈90 cc) followed by the spinal subarachnoideal space (≈35 cc) and the ventricles (≈25 cc). The calculated total amount of cerebrospinal fluid is about 150 ml, and a daily average production of 500 ml is accepted, indicating a turnover between 3 -4 times a day.

The structure of the Central Nervous System, due to the essence of its function, is uniquely characterized by the absence of solid supporting structures (no bone), and contractile elements (no muscle).

The brain can be divided into three distinct components enclosed in a rigid structure with fixed volume:

- Vascular component: composed of arteries, capillaries and venous structures.
- Cellular component: composed of neurons and glial cells.
- Cerebrospinal fluid component: composed of cerebrospinal fluid.

These three components are viewed as non compressible. Since the three components are enclosed in a rigid structure, the total volume is fixed; so, in order for anyone of them to increase, there is a need for a decrease in either or both of the other two components. If this condition is not satisfied, the consequence will be an exponential

increment of intracranial pressure. (Chong 2002, Greitz 1992, Chestnut 1991, Chestnut 1994)

This study reviewed the structural relationship, and modeled and analyzed the dynamic relationship between these three components, in an effort to disclose the mechanism by which the CSF is accommodated and driven inside the brain and spinal regions.

Of the three previously discussed components of the brain, the arteries are the most firm elements of the system. Also, the arteries are the only ones capable to introduce any type of mechanical energy into the system, and they behave in a pseudo-elastic manner. Moreover, the arteries are the only identifiable source that can sustain a cycling variation of the contained-volume from an identified source. During systole, arteries increase their content and during diastole they decrease their content. As a consequence, the arterial-wall circumferential stress is also cyclic, and dependent upon the cardiac cycle. Structurally, arteries form a successive pattern of continuous and iterative divisions creating a fractal profile.

In the cellular compartment, the cells extend numerous appendices interlocking each other and creating a network, or lattice, where they suspend themselves in close relation and attach to the cerebral vessels. The close relation between vessels, neuroglia and neurons is not only structural but also functional. This is evidenced by the close attachment of the neuroglia to the vessels with their podocytes on one side, and with the close physical relation with the neurons on the other, functioning as an intermediary, helper and controller between the vessel's diameter and the neuronal needs. The fact that neurons are dependent upon continuous delivery of oxygen and glucose from the vessels creates an obvious structural dependence of the cells around the vessels. Thus, the whole

brain is constructed in a fractal-like, complex and hierarchically structured way. This has formed the brain architecture in what is known in material science as a Hierarchically Structured Material.

In each heart cycle an approximate 15% of the stroke volume, at rest, is sent into the brain. As blood comes in, an increment of the brain volume is produced; also the increment in volume inside the vessels distends the vessels' walls, increasing their circumferential and axial stress. Due to the architecture of the intracranial brain arteries, the brain parenchyma does not receive the incoming blood simultaneously. It has been communicated by neuroradiologists that frontal lobes first receive the incoming blood, followed by the parietal and occipital lobes. Also the venous drainage starts earlier at the superficial venous territory, from the cortex, than the venous drainage from the deep structures around the ventricles.(Taveras 1978 , Scott 2003)

As illustrated in Figure 2.1, it has been documented that during systole CSF exits the cranium into the spinal canal matching the amount of blood coming into the brain. This fact confirms the Monroe-Kellie theory in which a volume exchange is needed in order to avoid an increment in the intracranial pressure. (Greitz 1992, Kotani 1992, Naidich1993)

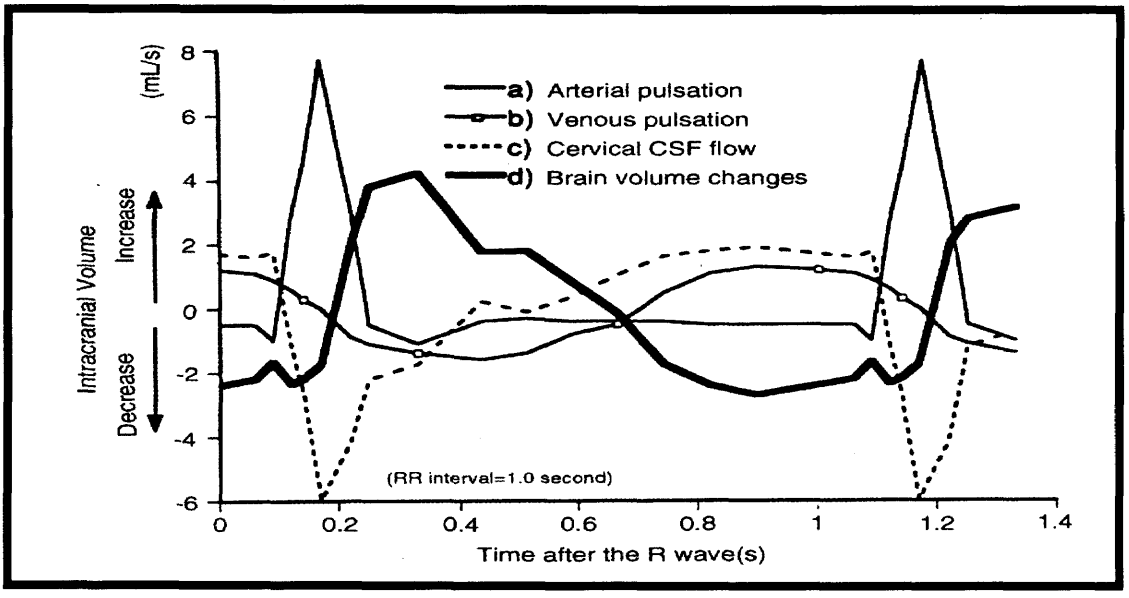

Figure 2.1 Cerebrospinal fluid (CSF) and human cerebral blood flow (CBF) changes during a cardiac cycle. Note the mirror image of the CSF flow and the Cerebral Blood flow; and how they correlate with a change in the brain volume.
From: Greitz D, Wirestam R, et al., Pulsatile movement and associate hydrodynamics studied by magnetic resonance phase imaging. The Monroe- Kellie Doctrine revisited. Neuroradiology 34: 370-380,(1992)

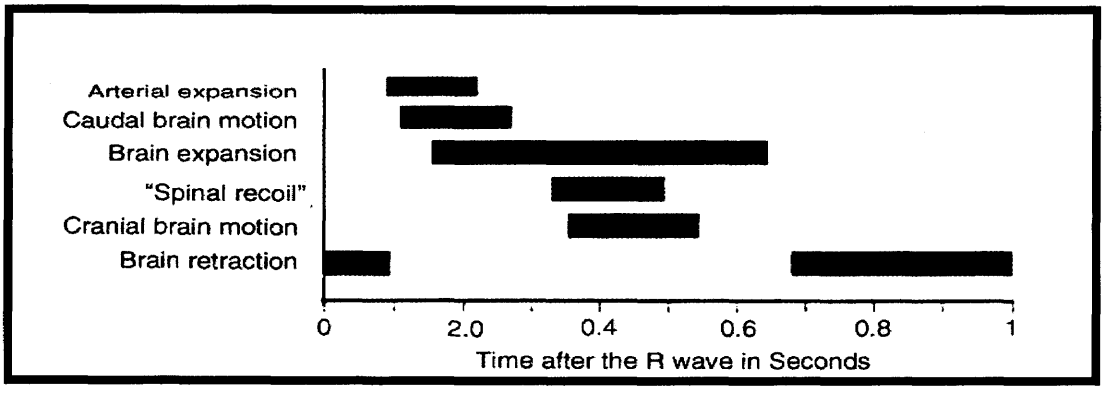

Figure 2.2 Human cerebral blood flow and brain changes during cardiac cycle.
From: Greitz D, Wirestam R, et al., Pulsatile movement and associate hydrodynamics studied by magnetic resonance phase imaging. The Monroe- Kellie Doctrine revisited. Neuroradiology 34: 370-380,(1992)

Greitz also documented a close relation between the cardiac cycle and a sequence of mechanical events occurring inside the cranium. Soon after the R wave is seen in the electrocardiogram, the arteries in the neck present diameter expansion, followed by a downward displacement of the brain structures, then the brain starts moving upwards, and finally the brain starts to retract until it reaches its initial size (Figure 2.2).

As the anatomical structure of the CSF compartment is quite complex, these CSF compartment is treated, from here onward, as a CSF-Compartmental System composed of three compartments: the ventricular, subarachnoideal and spinal compartments. Before MRI was available, the study of CSF implied invasiveness and, as a consequence, a possible perturbation of the system. Since the arrival of Phase Contrast Cine MRI has enabled the non-invasive study of CSF flow dynamics to become a reality. Greitz et al. in 1992 made measurements of brain displacement, blood flow and CSF flow. Naidich et al. in 1993 made a time correlated study of the displacement of "normal CSF pulsation". These publications documented a complex pattern of CSF oscillations happening in the ventricular, subarachnoideal and spinal compartments, and related them in time with the R wave of the electrocardiogram; and by extension, they are also related to the cardiac cycle, and cerebral blood flow. These studies are the backbone to the assumptions made in the present model. They showed that the CSF movement is oscillatory, complex and multidirectional.

The ventricular system is formed by a set of four ventricular cavities (two Lateral, the Third, and the Fourth Ventricles), the intracranial subarachnoideal space (subdivided into a convexity region , and a set of basal cisterns), the spinal subarachnoideal space(divided by the dentate ligaments into dorsal and ventral areas), six orifices connecting the compartments (two Foramens of Monroe, two Foramens Lushcka, the Foramen Magendie, and the Foramen Magnum), and one duct (Sylvius Aqueduct). In his original description, Naidich uses six different cavities or compartments (III ventricle, aqueduct, IV ventricle, cisterna magna, dorsal spinal, and ventral spinal), three foramens (Monroe, Magendie and Magnum) and one duct (Sylvius Aqueduct) to describe the CSF flow during one cardiac cycle.

In an effort to extract the information from an anatomically-detailed study, and to convert it into a system dynamics focused explanation, and in order to make a fair transition with out doing an over-simplification, a two step adaptation process was presented in this research, where the changes could be better appreciated.

The first step was to extract the information shown at an anatomically based description of the CSF flow, starting in diastole and evolving into eight (8) successive equally spaced time frames during a complete cycle. To extract the information, it is fundamental to understand the changes of the flow magnitude and direction, based on the anatomy, during each stage of the cycle. Equally important is to interpret these changes in view of the hypothesis presented here. (Figures 2.4, 2.5 and 2.6)

Figure 2.3 modified from Naidich et al., is a close-up image centered at the junction of the diencephalon with the brain stem; where several structures are used as a reference for the phase contrast Cine MRI images. As this picture shows a structural T1-weighted image, the CSF appears in a dark gray tone. The third ventricle is labeled with the number three (3) in white, at the top of the picture. The pons is labeled with a letter P. The fourth ventricle is labeled with the number four (4) in white, behind the pons. The Cisterna Magna, located beneath the fourth ventricle is labeled by the letter C. The aqueduct is seen between the third and fourth ventricles, and is detailed by the small black arrow heads. The dorsal (d) and ventral (v) portions of the cervical spine are shown at the bottom. The foramen of Monroe is shown at the top of the Third Ventricle where the points of two arrows (one black and one white) coincide. This image shows a mid-sagittal section of the brain, where it could be seen a representative of each of the compartments hosting CSF in its interior. Thus, this image is very appropriate for a follow-up and examination of the CSF movement during the cardiac cycle. During a

phase contrast cine MRI the still elements of the structure become blurry; while the moving elements of the structure are highlighted and could be tagged for directionality. In the study done by Naidich , shown here, the CSF moving in a cephalic direction is seen in a dark gray color, meanwhile the CSF moving in the caudal direction is seen in bright white color.

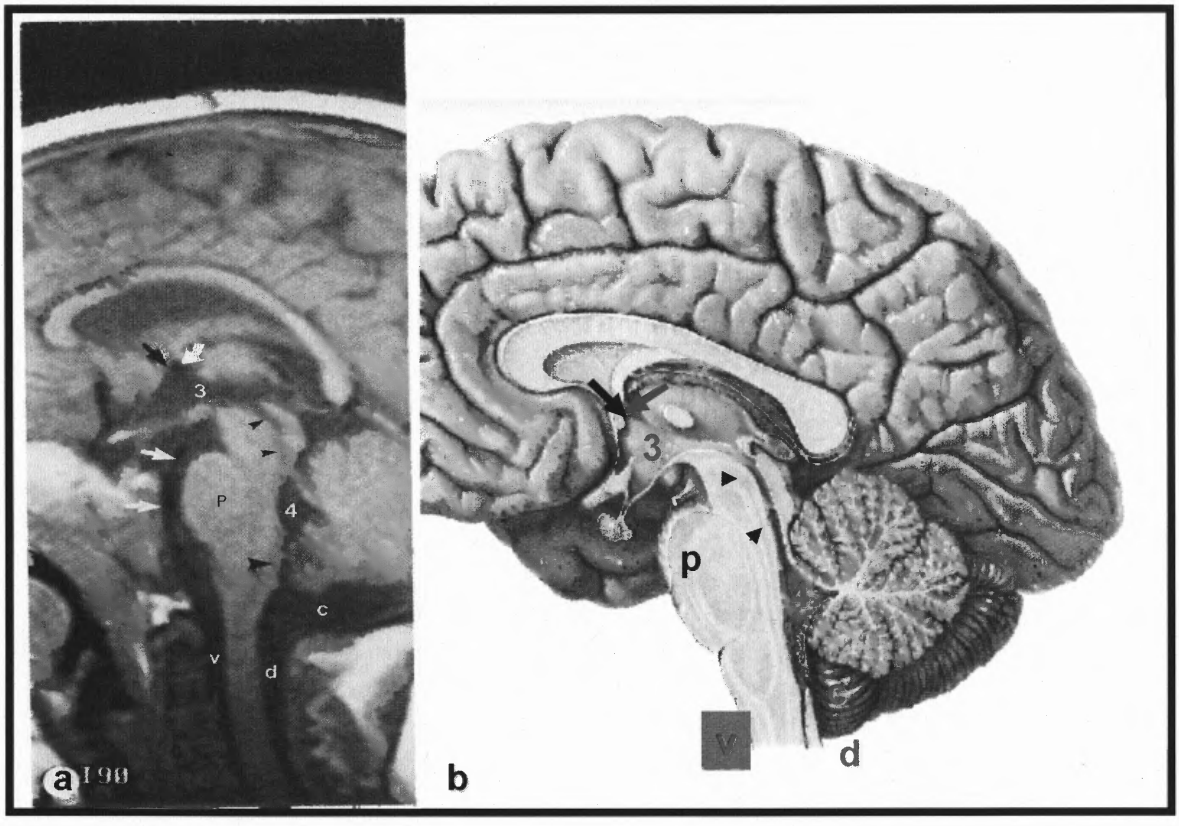

Figure 2.3 a) T1 structural MRI showing a close-up of a mid- sagittal view of the brain. CSF is shown as dark gray; brain structures in light color. Note, Third Ventricle (3), Fourth Ventricle (4), Pons (P), Cisterna Magna (C), dorsal(d) and ventral(v) regions of the cervical spine. Small black arrow heads pointing at the Sylvius Aqueduct at the midbrain. Large black arrow head showing the Foramen of Magendie, connecting the inferior portion of the Fourth Ventricle to the subarachnoideal space at the Cisterna Magna. Note the Foramen of Monroe at tip confluence of two arrows, one black and one white, at the top of the Third Ventricle. Two white arrows show the Prepontine Cisterna, in front of the Pons.
b) Brain anatomic specimen showing the same structures as in a.
Adapted from: Naidich et al. ,Neurosurg Cli N Am 4(4): 677-706(1993)

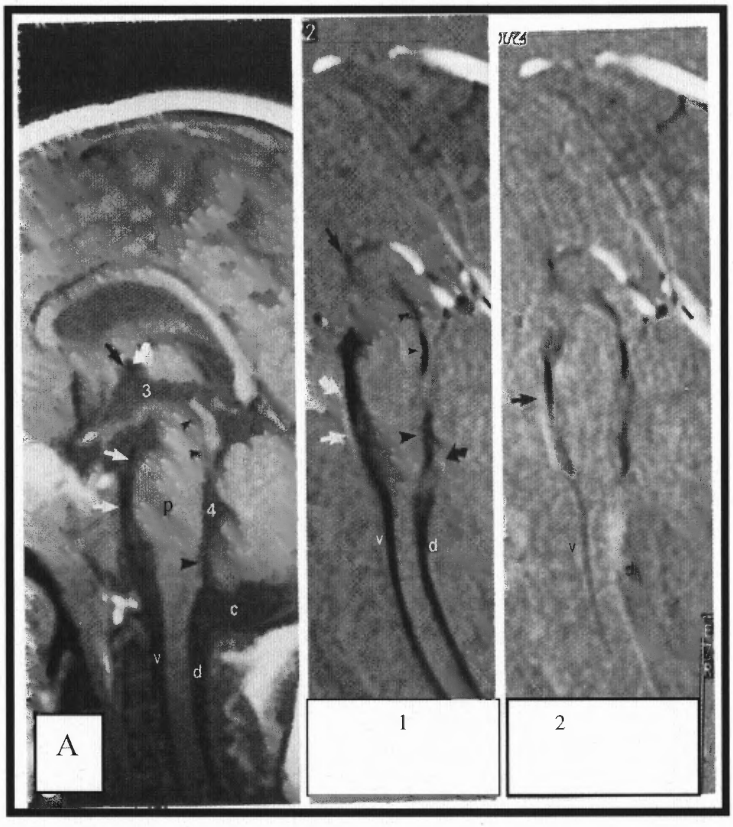

Figure 2.4 Phase-Contrast Cine MRI of CSF normal oscillations. Image A shows a close-up of the normal T1 structural MRI image of the brain, which is used as a reference for the phase-contrast cine MRI. Here, stages 1 and 2 show the initial sequence of phase-contrast cine MRI. Stages1 through 8 show the complete and characteristic flow pattern of CSF during one cycle. Continues on Figures 2.5 and 2.6.
Adapted from: Naidich et al. ,Neurosurg Cli N Am 4(4): 677-706(1993)

- Stage 1: The starting point of the sequence is at the end of heart diastole where all the CSF compartments show a cephalic direction of CSF flow. During these stage the brain vessels have the least amount of blood in their interior, thus compliance of the system is at its highest value.

- Stage 2: An initial caudal movement of CSF is noted to start in the dorsal area of the cervical spine. Compared with Figure 1, on Figure 2 could be seen a change in color of the CSF at the dorsal region of the cervical spine. A more bright and white color is seen, showing a caudal direction of the CSF flow in the dorsal region of the cervical spine. As the heart systole starts pumping blood into the brain, the compliance of the structures inside the cranium start diminishing, and the CSF starts to be expelled into the spinal compartment.

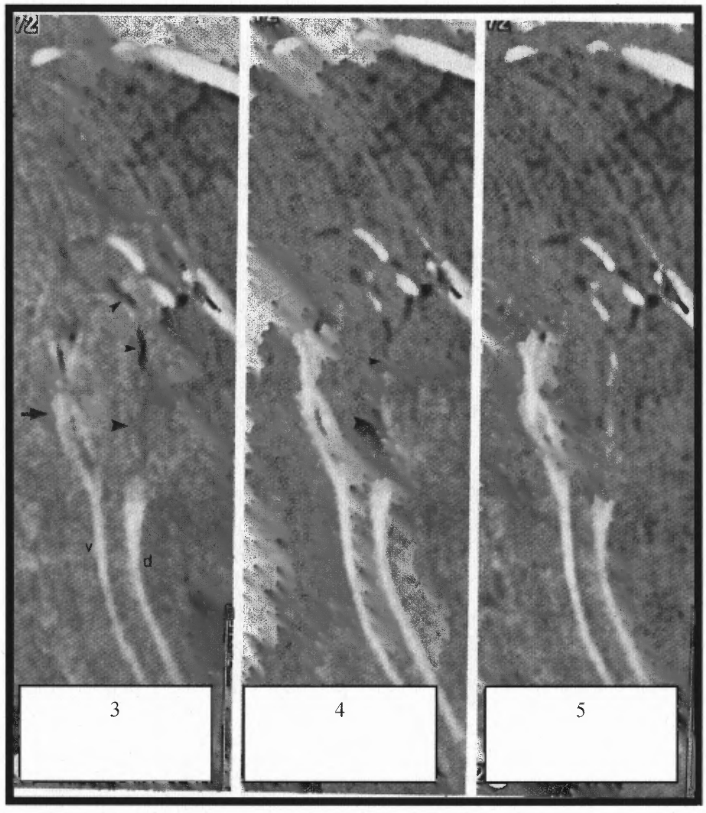

Figure 2.5 Phase-Contrast Cine MRI of CSF normal oscillations.
Stages 3 to 5 show the sequence of phase contrast cine MRI, showing the characteristic flow pattern of CSF during one cycle.(continue).
Adapted from: Naidich et al. ,Neurosurg Cli N Am 4(4): 677-706(1993)

- Stage 3: Cisterna magna, dorsal and ventral spinal regions are showing a caudal direction of the flow. At the inferior portion of the ventricular system, the flow is shifting towards a caudal direction (large arrow head), while at the superior portion (small arrow heads) the flow is still going in cephalic direction. The increased amount of blood inside the brain vasculature continues to diminish the compliance of the brain parenchyma; as a consequence more CSF is diverted into the spinal compartment. As the CSF is diverted from the Cisterna Magna, which forms part of the intracranial-subarachnoideal space, the fluid inside the lower portion of the ventricles starts to flow into the subarachnoideal space.

- Stage 4: Bright CSF intensity at Cisterna magna, dorsal and ventral spinal regions is showing a caudal direction of the flow. The less bright intensity of the CSF at the inferior portion of the ventricular system is showing the flow starting to go caudally (large arrow head). The flow at the superior portion of the ventricular system is shifting direction (small arrow head), being reflected in a diminished intensity of the CSF signal at this level. The amount of liquid that had already left the subarachnoideal space, starts creating a gradient between the interior of the ventricles and the subarachnoid space, at the Cisterna Magna. As the CSF reaches the Cisterna Magna it rapidly flows into the spinal compartment.

- Stage 5: Flow at the Cisterna Magna, the inferior portion and superior portion of the ventricular system is going caudally. Dorsal and ventral spinal regions are still showing a caudal direction of the flow, but their intensity and width are starting to wax, showing a diminished flow in respect to the previous stage. This stage is named as Peak Systolic. At peak systole, the amount of blood inside of the cerebral vasculature is at its highest value. At this stage the vessels are engorged, and the circumferential stress of the vessels is at its highest value; therefore the stiffness of the vessels has increased at its maximum, and the compliance of the brain tissue has decreased to its minimum.

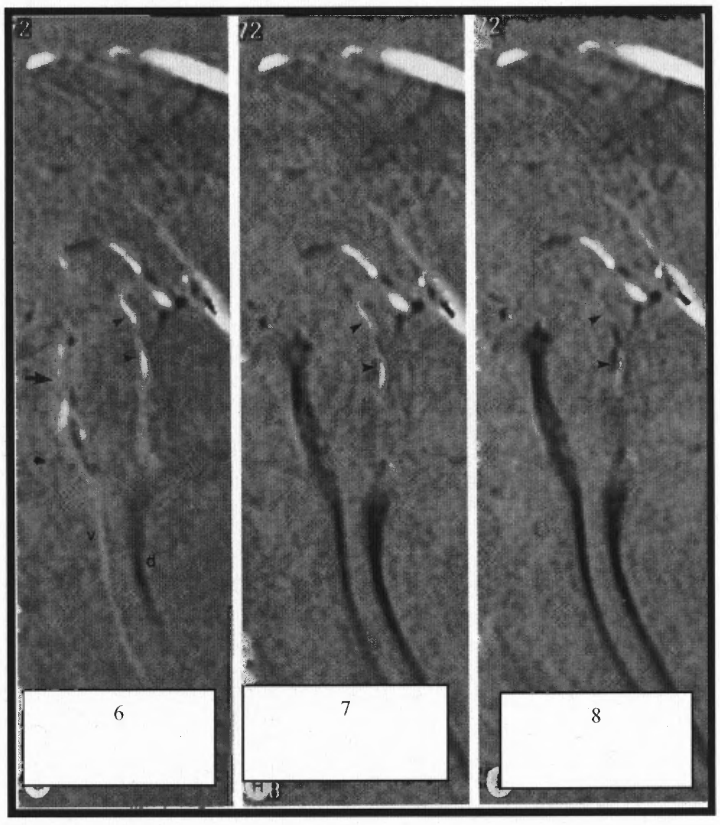

Figure 2.6 Phase-Contrast Cine MRI of CSF normal oscillations.
Stages 6 to 8 show the sequence of phase contrast cine MRI, showing the characteristic flow pattern of CSF during one cycle.
Adapted from: Naidich et al. ,Neurosurg Cli N Am 4(4): 677-706(1993)

- Stage 6: The flow at the inferior portion and superior portion of the ventricular system continue going caudal. While the Cisterna Magna is still going caudal, its intensity is fading, reflecting a decrement in the amount of flow in that direction. The dorsal and cervical spinal regions are starting to change the direction of the flow. When the heart systole finishes, and the venous drainage starts depleting the vessels, the compliance of the brain starts a slow return to its original value, which is reflected in the direction of the CSF flow.

- Stage 7: The flow at the superior portion of the ventricular system is still going caudal, while in the inferior portion, the CSF flow is starting to change into cephalic direction. Subarachnoideal and spinal compartments are already flowing in cephalic direction. The compliance has definitely increased inside of the cranium, and the CSF is coming back into the skull.

- Stage 8: Mixed signals come from the upper region of the ventricular compartment, showing the flow changing into cephalic direction; while in the rest of the compartments a defined cephalic flow direction is already established. The system is nearly at stage 1, and soon will be ready to start a new cycle. The vessels are slowly reaching the expected state towards the end of the diastole; where it is expected to have the least amount of blood inside of the brain vessels, and the compliance of the brain to be at its highest value.

The second step is to perform an equivalent description of CSF flow, in a simplified three compartmental system, emphasizing the changes in direction and magnitude as a function of time (Figure 2.8). Before this analysis is done, it is important to remember that the most posterior and inferior portion of the subarachnoideal space, the cisterna magna, is situated behind the cerebellum. As it name suggests, it has called the attention of many anatomists because of its big size, location and connections. Situated beneath the cerebellum, at the very end of the cranial cavity, just on top of the Foramen Magnum, the Cisterna Magna is the place where the three compartments meet. Not withstanding it is part of the subarachnoideal space, in a sense the Cisterna Magna acts as a hall way, or a three duct manifold connecting the three compartments.

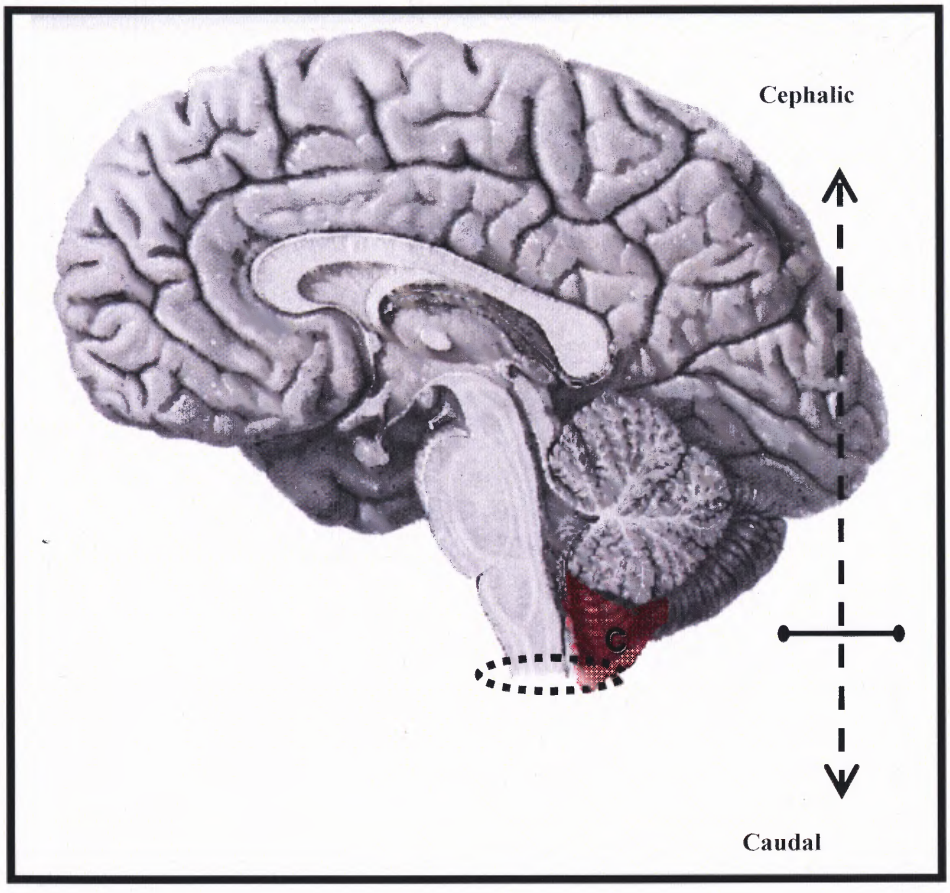

Figure 2.7 CSF Normal Flow Reference Points. Cisterna Magna, in red, is situated beneath the cerebellum, on top of the Foramen Magnum. Foramen Magnum represented by doted circle. Cisterna Magna, which constitutes part of the subarachnoideal space, is the anatomical place where the three compartments meet.

The phase contrast cine MRI study done by Naidich could be easily understood if a hypothetical sensor is located in the Cisterna Magna, looking to the direction of the flow into each compartment. The results of this hypothetical study will originate the following CSF flow stages:

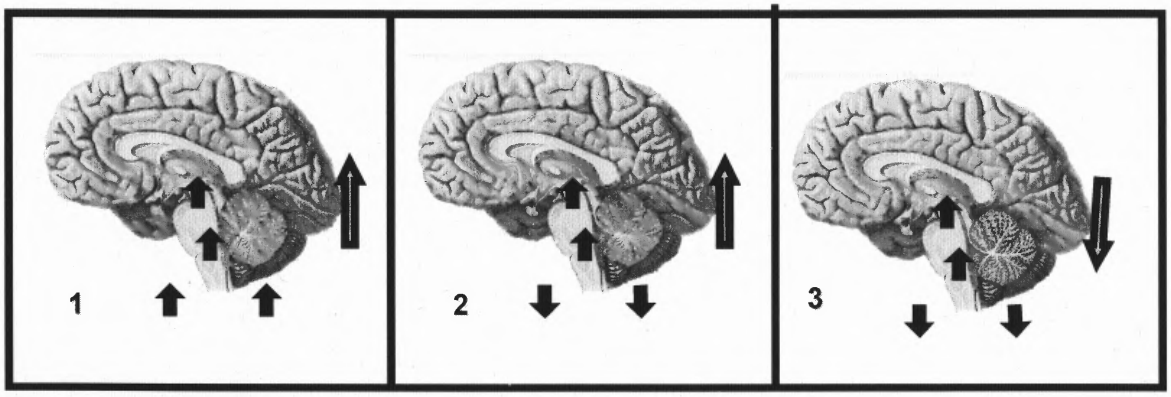

Figure 2.8 CSF Normal Flow, stages 1, 2, 3.

- Stage 1: The starting point in time is at the end of heart diastole, where the CSF flow is directed in a cephalic direction in all the compartments.

- Stage 2: An initial movement of CSF is noted to start going caudal in the spinal compartment.

- Stage 3: Subarachnoideal and spinal compartments are showing a caudal direction of the CSF flow. CSF flow in the Ventricular compartment is still going in a cephalic direction.

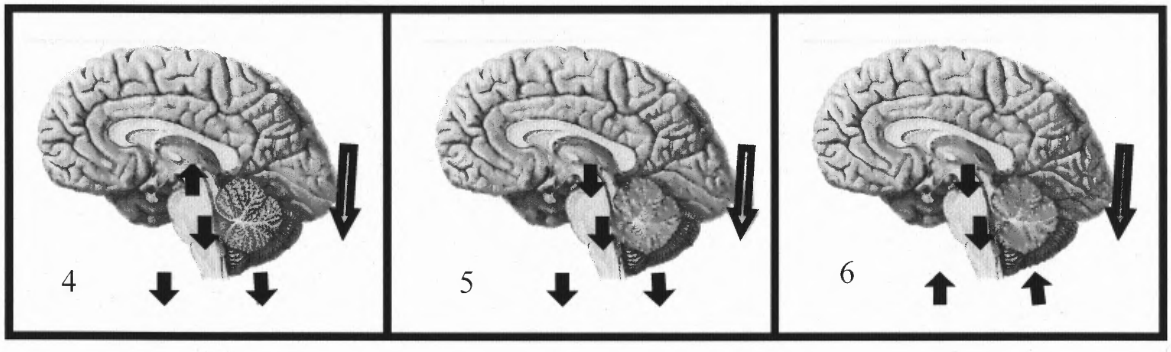

Figure 2.9 CSF Normal Flow, stages 4, 5, 6.

- Stage 4: Subarachnoideal and spinal compartments are showing a caudal direction of the CSF flow. CSF Flow in the Ventricular compartment is shifting direction.

- Stage 5: CSF Flow in all compartments is going in caudal direction. CSF flow in the Spinal compartment is starting to slow down. This stage is named as Peak Systolic.

- Stage 6: CSF flow in the Ventricular compartment is going caudal. Flow in the Subarachnoideal compartment is still going caudal, but begins to slow down. The spinal compartment is changing the direction of the flow.

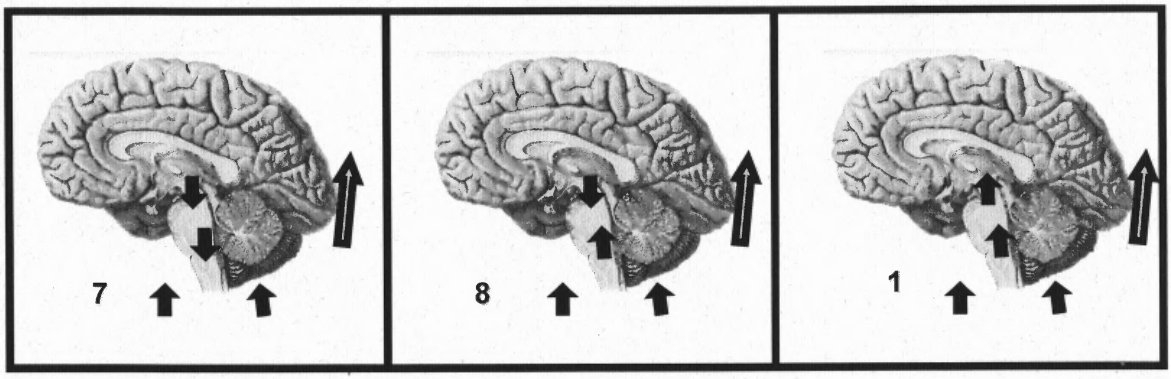

Figure 2.10 CSF Normal Flow, stages 7, 8, 1.

- Stage 7: Flow in the Ventricular compartment is still going caudal, but starting to slow down. Subarachnoideal and spinal compartments are flowing in cephalic directions.

- Stage 8: The ventricular compartment starts changing flow into cephalic direction; while in the rest of the compartments a defined cephalic direction is already established. The system is preparing to start a new cycle at stage 1 (Table 2.2).

Table 2.2 Normal CSF Oscillations During Cardiac Cycle, in the Simplified Three Compartmental System

Stage	Compartment	Cephalic	Caudal	Slow Down	Changing Direction
1	Ventricular	↑↑			
	Subarachnoideal	↑↑			
	Spinal	↑↑			
2	Ventricular	↑↑			
	Subarachnoideal	↑↑			
	Spinal		↓↓		
3	Ventricular	↑↑			
	Subarachnoideal		↓↓		
	Spinal		↓↓		
4	Ventricular				↓↑
	Subarachnoideal		↓↓		
	Spinal		↓↓		
5	Ventricular		↓↓		
	Subarachnoideal		↓↓		
	Spinal			↓	
6	Ventricular		↓↓		
	Subarachnoideal			↓	
	Spinal				↓↑
7	Ventricular			↓	
	Subarachnoideal	↑↑			
	Spinal	↑↑			
8	Ventricular				↓↑
	Subarachnoideal	↑↑			
	Spinal	↑↑			

It is a real challenge to find an explanation of this series of changes in the direction of the CSF flow. However, these changes in direction could be well explained if a dynamic-wall container approach is done. By a dynamic-wall container, it is meant a container in which its walls physical properties (compliance/ stiffness) are able to change in time. By varying independently the walls' compliance, the amount of maximum possible storage of each compartment is changed, and the volumes are shifted between compartments, even if they are all under the same pressure. The present study takes into consideration strategies used by anesthesiologists and critical care physicians to reduce the stiffness of the brain. (Piper 1993, Chestnut 1991, Chestnut 1994) The common factor in all these strategies is trying to reduce the diameter, and axial and circumferential stresses of the arteries in the brain. So, if changes in the vessel's circumferential and axial stresses effectively change the brain compliance, an underlying mechanism for changing brain compliance normally exists (Bhadelia 1998, Czosnyka 1999, Chong 2002). As is explained in this chapter, Equations 2.3 and 2.12, the increased volume inside the vessels produces an increased stiffness, which is the same as a decreased compliance off the brain. This is the link between cardiac cycle and cerebral blood flow on one end, and change in brain compliance and CSF flow on the other.

Marmarou characterized brain compliance in a study considered a classic. He measured intraventricular pressure directly by placing a needle inside the ventricle of twenty infants. Then he measured the pressure variation at regular intervals after first extracting, and then adding fixed volumes of CSF. In that way, Marmarou produced the ventricular compliance curve by plotting delta volume vs. delta pressure at regular intervals. He defined the compliance curve as an exponential. Linear approximations to

the compliance exponential curve, in the physiological interval between seven and eleven mm Hg, were used in the present model. (Shulman and Marmarou)

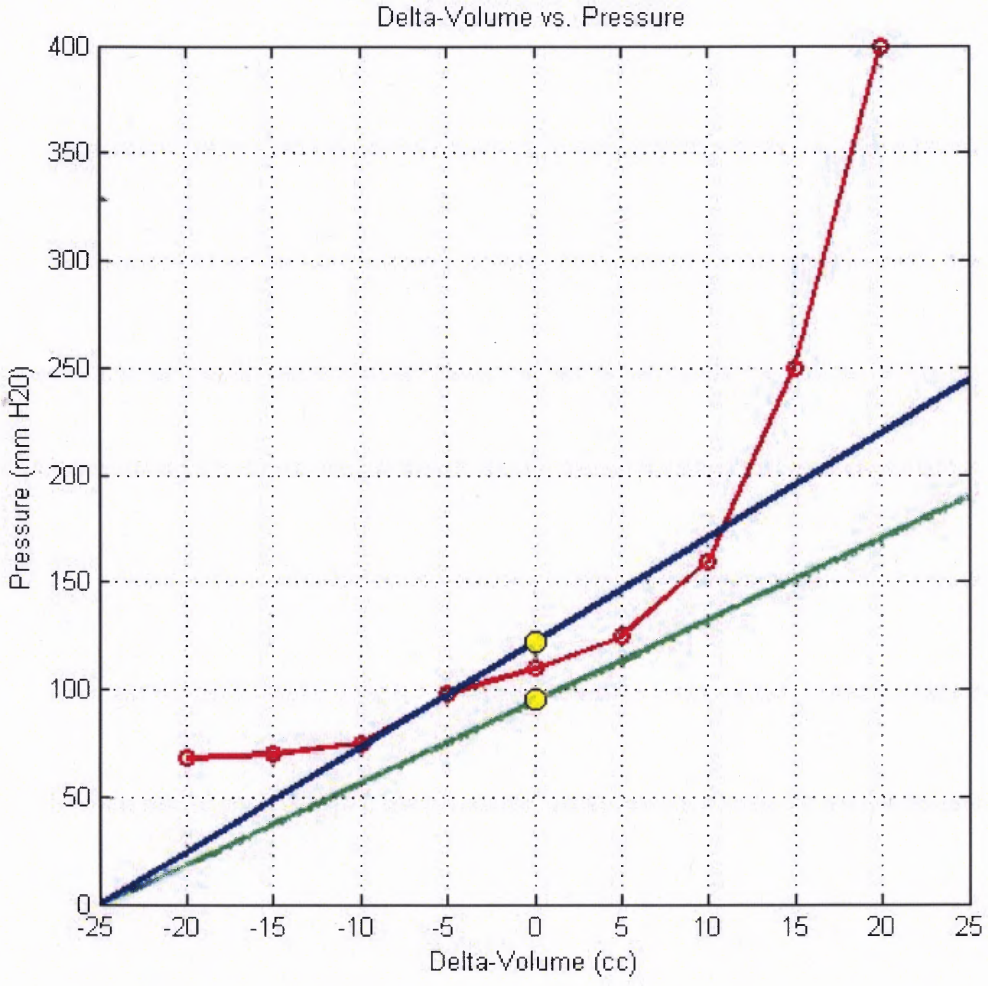

Figure 2.11 Transfontanelar measurement of ventricular compliance curve in red, with linear approximations used in the present model in green and blue. Yellow dots show the range of the intraventricular compliance during the computer model simulations.
Modified from Shulman and Marmarou, Pressure- Volume considerations in Infantile Hydrocephalus, in Developmental Medicine and Child Neurology 1971

2.3 Histology of the CNS

The brain and spinal cord are formed by two types of cells closely packed together: neurons and glial cells. They are intimately associated in a structural and functional relation. The tridimensional (3D) deposition of the fibers and cells, form an intricate and interlocked structure; similar to a scaffold. This scaffold, in turn, is also closely related to the vessels in order to control the amount of blood, oxygen and nutrients needed for an adequate function and survival of the neurons. As will be reviewed later, these type of histological relations represents a hierarchically structured material; which accounts for several of the physical properties of the brain tissue.

Neurons represent 10% of the whole population of cells in the nervous system. The neuron structure is formed by a cell body and by two types of cytoplasmatic extensions: the dendrites and the axons. The size of the neurons' cell body varies from 5 μm in the cerebellum to 150 μm in the motor cortex, and its cytoplasmatic extensions could vary from a few microns in the short communicating interneurons, up to more than a meter for those transmitting and receiving signals from the peripheral nervous system, and spinal cord. Neurons produce local, regional, intrahemispheric, interhemispheric and extended connections to the brainstem and spinal cord. These interconnections between neurons create a lattice or scaffold through the whole brain parenchyma. The microtubules of the neuron cytoskeleton are protein structures that not only define and maintain the shape of the axons, and presumably of the dendrites, but also have important functions as highways for the movement of substances produced in the cell body. This structural design is reinforced by the interaction with glial cells, mainly astrocytes and oligodendrocytes, which gives local support between the neural fibers, the cell bodies and vessels inside the CNS.

Representing 90% of the whole cellular population, glial cells derive their name from the Greek word for glue; thus reflecting the first hypothetical role assigned to them. Although the glial cells include astrocytes, oligodendrocytes, ependimal cells and mycroglia, due to their structural importance only the first two will be reviewed.

Initially considered just as mere supporters, astrocytes have gained recognition for their important role in the control of the vessel's diameter, and in the regulation of permeability for certain substances. From the structural point of view, their podocytes play an important role by engulfing and attaching the vessels on one end, and on the other end, they are in close proximity with regional neurons. Astrocytes play an important role controlling regional vascular responses, and setting environmental needs for the correct neuronal/vascular interaction (Figure 2.12). Structurally they segmentally reinforce the neural fibers lattice, and create a structural linkage between vessels, neuronal fibers and neurons.

In the CNS the oligodendrocyte wrap their cell membrane around the axons or dendrites forming the myelin sheath. The oligodendrocyte extends its cell membrane covering several different nearby neurons. In this manner the oligodendrocyte also serves as a local reinforcement of the lattice already formed by the neural fibers, astrocytes and vessels.

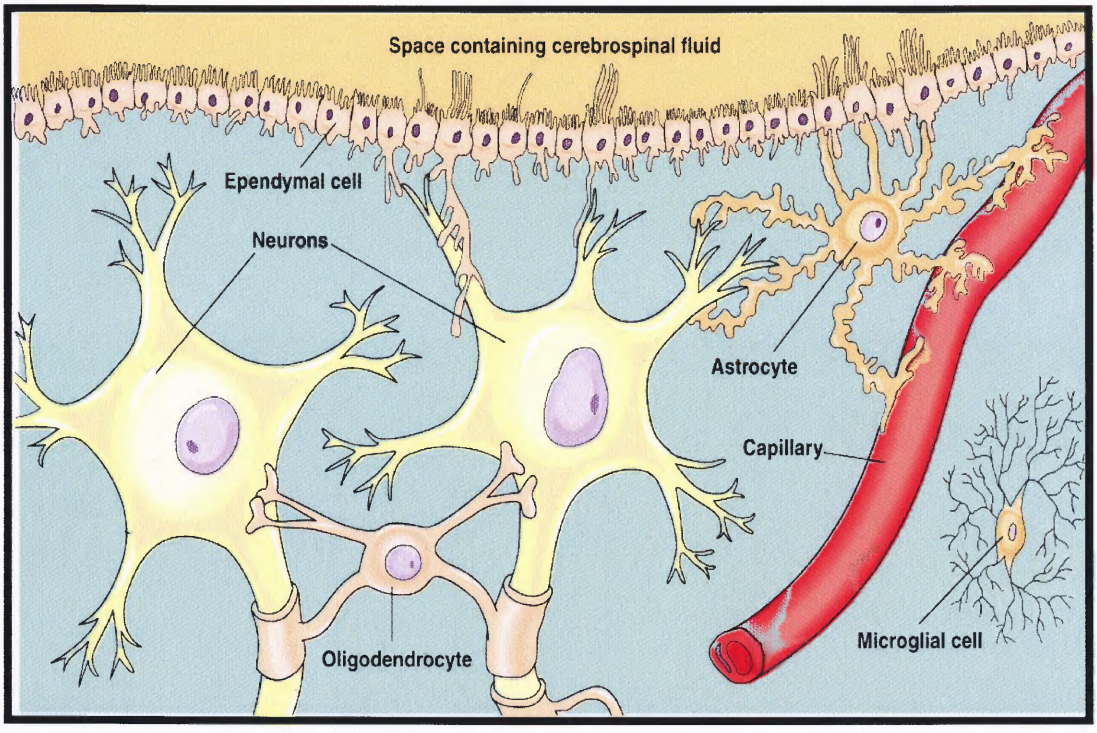

Figure 2.12 Glial-Neuron-Vascular relation.
Adapted from : Sherwood Human Physiology ,2004,. Belmont, CA: Thomson.

In summary, the interrelation between neural fibers and glial fibers create a scaffold or lattice in a special structural conformation known as a Hierarchically Structured Material. As will be explained later, among the properties of hierarchically structured material is to have a viscoelastic behavior. The neuron-glial lattice does not change their physical properties abruptly or cyclically. However, neuron and glial cells are intimately related to the brain vessels. Brain vessels, in contrast, sustain a cyclic variation of their volume during systole and diastole. The cyclic variation of the volume inside the vessels creates a change of the circumferential stress, which in turn changes the stiffness and compliance of the vessels. As the vessels increase the contained blood volume during systole, the vessels wall is distended, the circumferential stress increases, and the vessels compliance decreases. As a consequence of the brains high vascularization, the brain parenchyma compliance also decreases during systole.

2.4 Circulatory System of the Brain

Because in the brain there is not a mechanism to store energy-sources, energy supplies and oxygen have to be delivered continuously by the circulatory system to satisfy the elevated needs of the neuronal high metabolic rate. Loss of consciousness occurs in less than 15 seconds after blood flow to the brain has stopped, and irreparable damage to the brain tissue occurs within 5 minutes. About 15% of the total blood volume pumped by the heart, at rest, is directed to the brain; although the brain represents only 2% of the body weight. The total volume of blood inside the brain has been calculated as 150 cc. The cardiac out put has been calculated as 5000 cc/ min, thus approximately 750 cc are pumped each minute to the brain; amount of blood enough to replace five times the whole content of blood inside the brain. Evidently the brain has a high vascular density, and there is a tight functional relation between vessels, astrocytes and neurons.

If the brain venous drainage is impaired, an increased intracranial pressure is produced; such mechanism has been reported in some cases of Idiopathic Intracranial Hypertension where the transverse sinus is stenotic. After correction of the stenosis, the Idiopathic Intracranial Hypertension is resolved. Jugular and vertebrobasilar veins, which are responsible for draining brain blood, do not have valves; thus they depend on gravity and intra-thoracic pressure to maintain an adequate flow. Intracranial vascular congestion, as a consequence of an impaired venous drainage resulting from an increased intra-thoracic pressure, has also been documented in MRI when normal subjects are directed to produce a Valsalva maneuver. It has also been established that the pressure inside the brain is decreased when the arterial diameter is reduced by sweeping carbon dioxide out of the plasma.

The cerebral circulation is derived from two arterial systems: the internal carotid artery, and the vertebral artery. The internal carotid artery gives rise to the anterior cerebral artery and the middle cerebral artery. The anterior cerebral artery delivers blood to the anterior and basal portions of the frontal lobe, the anterior portion of the corpus callosum, and to midline structures of the frontal and parietal lobes. The middle cerebral artery irrigates the external cortex of the posterior region of the frontal lobe and the parietal and temporal lobes, and most of the occipital lobes. (Figures 2.13, 2.14)

After entering the cranium, the vertebral arteries join together forming the basilar artery, which runs in front of the pons, and ends dividing in two posterior cerebral arteries at the level of the mesencephalon. This system irrigates the brainstem, cerebellum and posterior region of the occipital lobes, mainly in the midline areas.

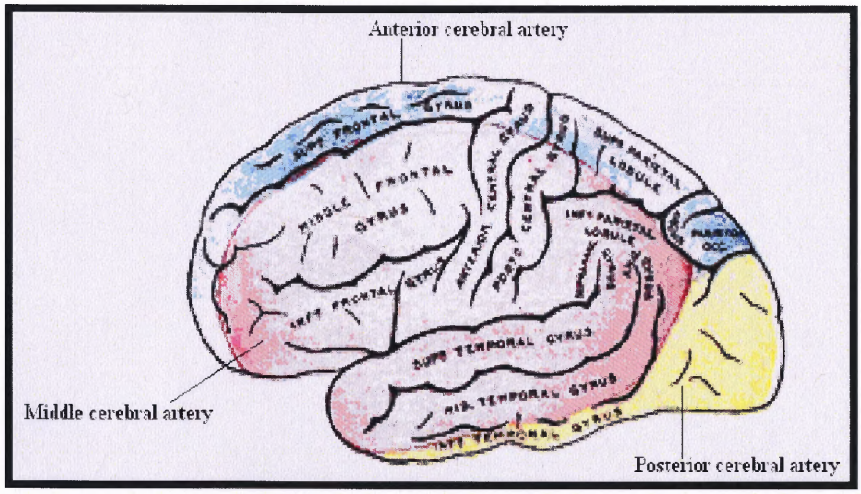

Figure 2.13 Arterial distribution. Outer surface of cerebral hemisphere, showing areas supplied by cerebral arteries.
Adapted from Gray's Anatomy, 1977. New York, NY, Random House.

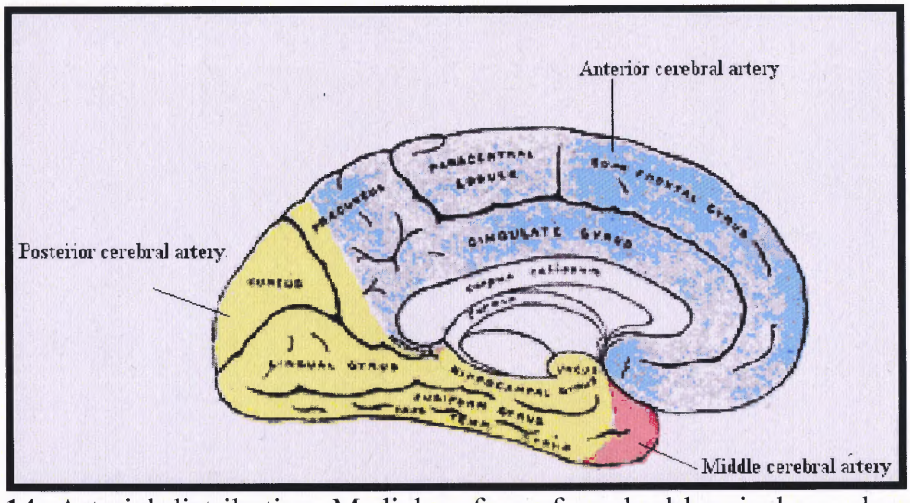

Figure 2.14 Arterial distribution. Medial surface of cerebral hemisphere, showing areas supplied by cerebral arteries.
Adapted from Gray's Anatomy, 1977. New York, NY, Random House.

The circle of Willis is the name given to an anastomotic ring formed by the two systems at the base of the brain. The main connections are done by the posterior communicating artery between the posterior cerebral artery and the internal carotid artery on each side. (Figures 2.15, 2.16)

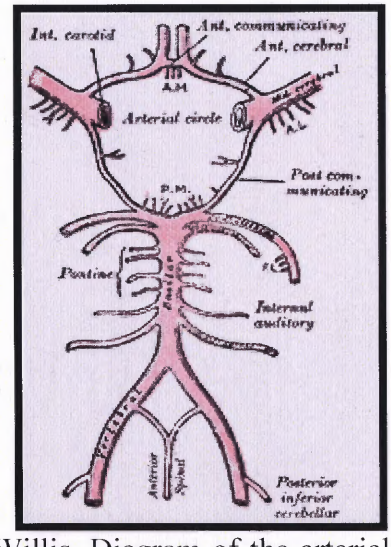

Figure 2.15 The Circle of Willis. Diagram of the arterial circulation at the base of the brain.
Adapted from Gray's Anatomy, 1977. New York, NY, Random House.

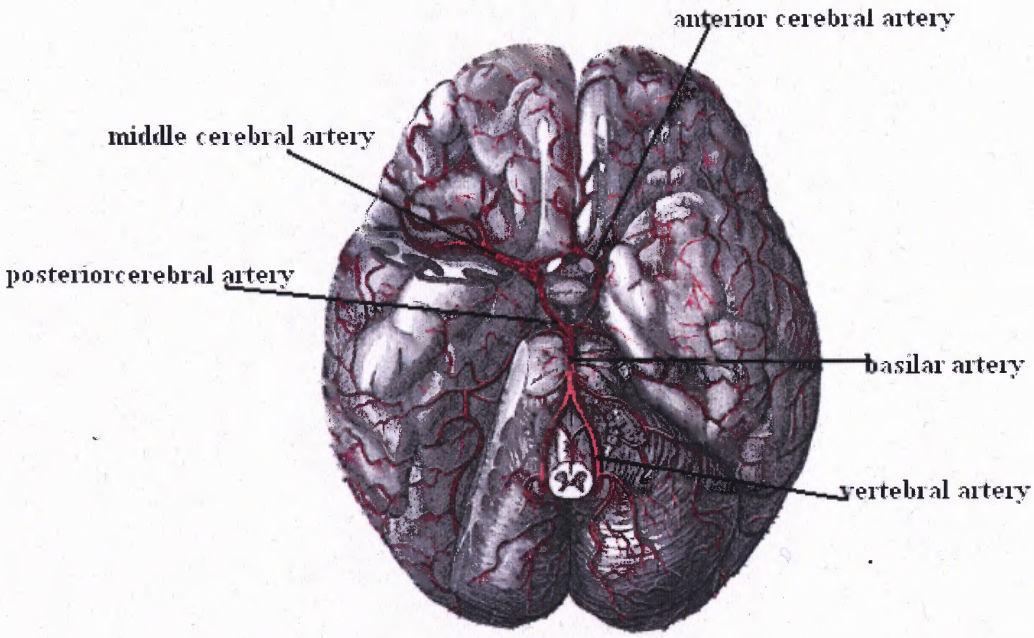

Figure 2.16 Base of the Brain Arteries. The arteries of the base of the brain. The temporal pole of the cerebrum and a portion of the cerebellar hemisphere have been removed on the right side.
Adapted from Gray's Anatomy, 1977. New York, NY, Random House.

A very dense network of capillaries has been documented in mammals. Capillaries range from a low density, found in the white matter (corpus callosum 162 capillaries/mm^2), to the high density found in cortical structures (810 capillaries/mm^2). This high capillaries presence helps explaining why the turgor of the vessels inside the brain will define the compliance. (Turner 2002, Nonaka 2002)

The venous drainage of the brain includes the veins of the brain itself, and the dural venous sinuses. Unlike systemic veins, cerebral veins have no valves and seldom accompany the corresponding cerebral arteries. (Bateman 2000, Turner 2002, Nonaka 2002)

The veins of the brain are organized into two big systems, each one of them draining a specific territory: the Deep Venous System, and the Cortical Venous System. (Andeweg 1999, Scott 2003)

The deep venous structures, buried beneath the cortex and surrounding the lateral ventricles, drain into the single midline Great Cerebral Vein (the vein of Galen), which lies beneath the posterior part of the Corpus Callosum. From here they will reach the Straight Sinus, and finally the Confluens Sinuses. The deep venous system, receives blood from subcortical areas around the ventricles and they define a territory separate from the cortical region; when visualized in an angiography, these veins clearly delineate the ventricles.

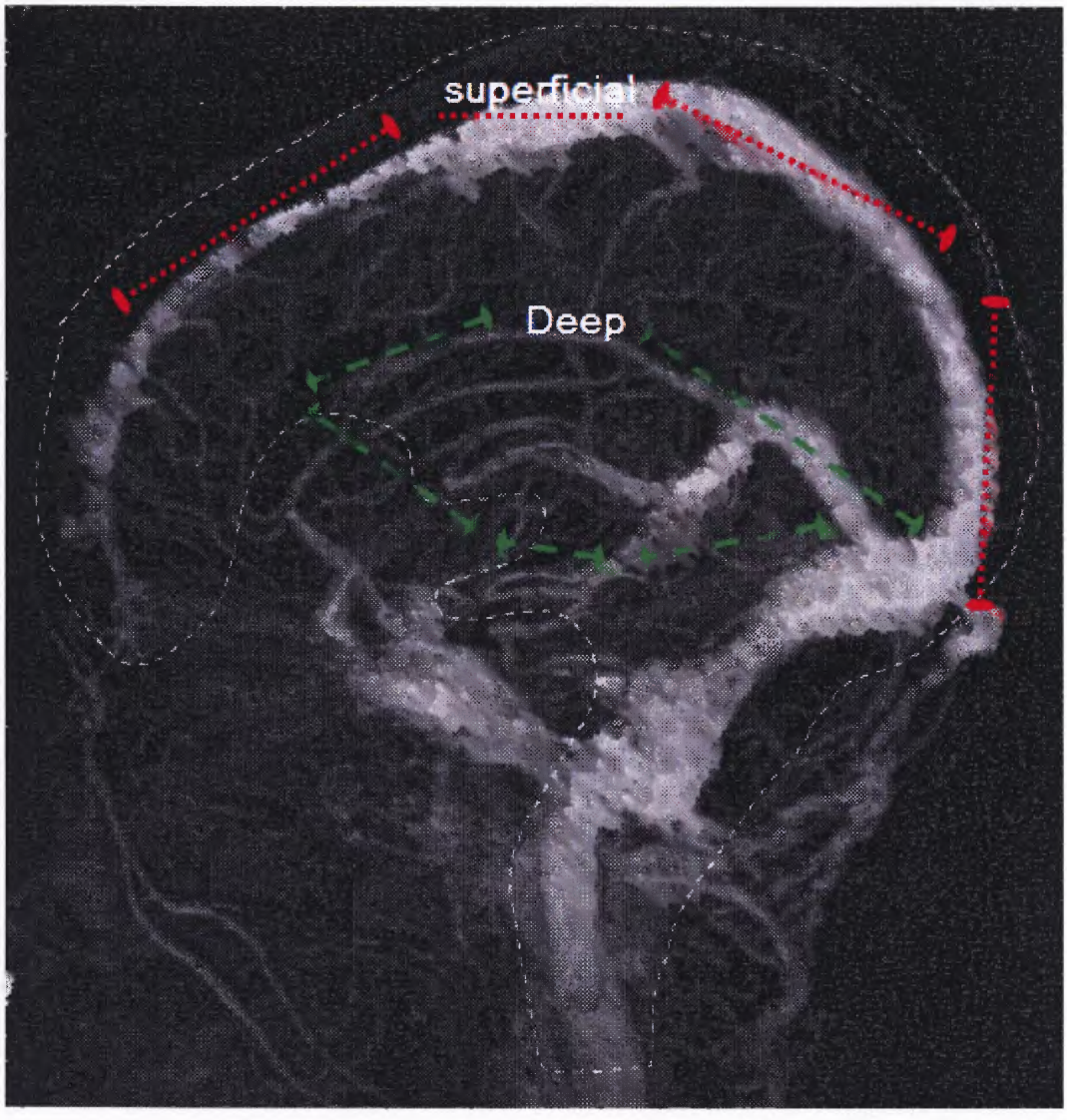

Figure 2.17 Intracranial venous system. Magnetic resonance image of a midsagittal section through the head showing venous system. Two identified venous systems: Superficial (cortical) identified by red dashed lines, and Deep identified by green dashed lines (periventricular structures).
Adapted from: Scott J.N., Farb R.I., Imaging and anatomy of the normal intracranial venous system, Neuroimag Clin N Am 13: 1–12(2003)

Venous drainage of the brain surface generally occurs into the nearest large cortical vein or sinus, from there to the Confluens Sinuses , and ultimately to the Internal Jugular Vein. The veins of the cerebral convex surfaces are divided into superior and inferior groups. The 6 to 12 superior cerebral veins run upward on the hemisphere's surface to the superior Sagittal Sinus. Most of the Inferior Cerebral Veins end in the

Superficial Middle Cerebral Vein. The Inferior Cerebral Veins that do not end in this fashion terminate in the Transverse Sinus (Figure 2.17). The cortical veins are organized in a distinctive and separate region, apart from the deep located venous system. The venous sinuses are venous channels lying between the inner and outer layers of the dura; they are called intradural (or dural) sinuses. Their tributaries come mostly from the neighboring brain substance. All sinuses ultimately drain into the internal jugular veins (Figure 2.18) via the sigmoid sinuses. Of the venous sinuses, the following are considered most important:

Superior Sagittal sinus situated in the midline between the two layers of the Falx, is considered the final collecting structure of the venous drainage from the cortical system. The Straight Sinus runs in the seam between the Falx and the Tentorium, and it receives the drainage from the deep structures of the brain. Transverse Sinuses run laterally between the two layers of the Tentorium, attached to the skull on the occipital region. Sigmoid Sinuses form S-curved continuations of the transverse sinuses running down and giving origin to the Internal Jugular Veins. Confluens Sinuses is a landmark point, situated at the midline, the most posterior region, at the margin of the Tentorium; where the two Transverse Sinuses, receive the blood drained by the Straight and Superior Sagittal Sinuses.

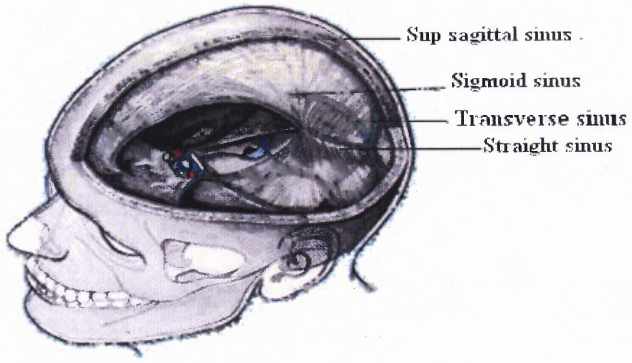

Figure 2.18 Main Venous Sinuses of the Brain
Adapted from Gray's Anatomy, 1977. New York, NY, Random House.

Brain compliance is very sensitive to the amount of blood inside of the vessels. As established by anesthesiologist and critical care physicians, if in any portion of the vascular network, arterial, capillaries, or veins, the contained blood volume is increased the brain-compliance will be reduced. Thus normally brain-compliance is permanently changing, due to the changing volume inside of the brain vasculature, during each cardiac cycle.

2.5 Viscoelastic Properties of the Brain

A thin cylindrical tube is a cylinder where the ratio between wall thickness *h* to the lumen radio *r,* is equal or less than l over 20; *h/r= 1/20* ; thus brain vessels could be approached as thin walled cylindrical tubes. In a thin walled cylindrical tube, we assume that normal stress ($\sigma_{\theta\theta}$) is uniformly distributed across the thickness (h) of the wall. By dividing the cylinder in half along its axis, a free body diagram analysis shows that the forces acting along the thickness of the wall need to be in equilibrium with the forces acting, in the opposite direction, on the surface of the vessel (Figure 2.19). Thus, the net force is computed by adding of all the forces resulting from the product of the internal pressures

(P_v), acting at each internal point, multiplied by their respective differential areas (dA). At equilibrium, this force is balanced by the opposite forces calculated by adding the product of the circumferential stresses ($\sigma_{\theta\theta}$), at each point, times their respective differential areas (dA):

$$\sum F_v = 0 \rightarrow \int p_v dA - 2\int \sigma_{\theta\theta} dA = 0 \tag{2.1}$$

Replacing and solving:

$$\mathrm{Pr}\int_0^l 2dz = 2\sigma_{\theta\theta}\int_0^l \sigma h dz \rightarrow P2rl = 2\sigma_{\theta\theta} hl \tag{2.2}$$

Form where $\sigma_{\theta\theta}$ is derived:

$$\sigma_{\theta\theta} = \frac{\mathrm{Pr}}{h} \tag{2.3}$$

Where P is the internal pressure, r is the inner radius of the cylinder, and h is the thickness of the wall of the cylinder. This relation does not imply that the increment of $\sigma_{\theta\theta}$ has to increase linearly, because the radius increment related to the increment in pressure depends exclusively on the material properties.

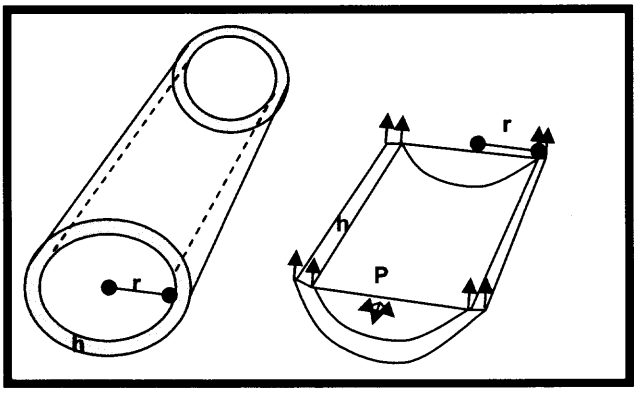

Figure 2.19 Circumferential stress illustration-σθθ- free body diagram showing equilibrium between pressure and the vessel's wall reaction force. P=pressure; r = radius; h= wall thickness.

In a similar way if we assume that an axial directed force *(f)* inside the vessel will reach equilibrium with the containing walls by:

$$-f + \int_0^{2\pi} \int_r^{r+h} \sigma_{zz} r dr d\theta = 0 \tag{2.4}$$

Solving the integral:

$$\sigma_{zz} \pi r h = f \rightarrow \sigma_{zz} = \frac{f}{\pi r h} \tag{2.5}$$

Where σ_{zz} represents the axial stress of the vessel under study.

Fluids have the characteristic of being fully deformable and, as a consequence, under shear stress molecular displacement occurs, resulting in flow. In contrast, in an elastic behavior a deformation occurs when the material is subjected to stress, and a full

recovery happens upon stress release. The viscoelastic material shares properties with both type of materials and its behavior can vary depending on the amount, frequency and timing of the loading and unloading.

Creep deformation and stress relaxation represent a characteristic behavior of viscoelastic material. If a viscoelastic material is maintained in a loaded situation, with a fixed amount of load, under constant stress, a progressive and slow deformation will appear as time goes by. This slow progressive deformation under sustained stress is referred as creep deformation. The creep deformation concept is easy to understand when the stress *(σ)* is mathematically described as a Heaviside *(H)* step function. The Heaviside *(H)* step function is equal to zero at time *(t)* less than zero, and equal to one for time greater than zero. As such, stress *(σ)* could be expressed mathematically as:

$$\sigma(t) = \sigma_0 H(t) \tag{2.6}$$

Under these conditions, the strain *(ε)* of the viscoelastic material will increase with time. Mathematically the stress/ strain relation could be represented as:

$$J(t) = \frac{\varepsilon(t)}{\sigma} \tag{2.7}$$

Where the creep compliance *(J)*, represents the ratio between the strain *(ε(t))* as a function of time, and the stress *(σ)*.

Similarly, if a sudden strain is introduced, in a viscoelastic material, and maintained constant; then a slow relaxation of the stress level is going to be observed as the molecules rearrange. If in this case we use the Heaviside function *(H)* to describe the strain behavior *(ε)*, then the relation between stress *(σ(t))* and strain*(ε)* could be expressed mathematically as:

$$\varepsilon(t) = \varepsilon_0 H(t) \tag{2.8}$$

and:

$$E = \frac{\sigma(t)}{\varepsilon} \tag{2.9}$$

where the relaxation modulus *(E)* is representing the ratio between the stress *($\sigma(t)$)* response in time to a fixed strain*(ε)*.

When a load is maintained for a certain period of time, on a viscoelastic material, a deformation occurs. When this load is suddenly removed the recovery of the original shape also occurs in a gradual fashion, and sometimes it might not be complete, or will need an "extra force" to reach the initial shape.

Brain tissue possesses viscoelastic properties. The viscoelastic properties of the brain tissue could be better understood by examining the behavior of the brain parenchyma when a benign tumor is slowly growing, and comparing the brain tissue response to a fast growing lesion (epidural hematoma). In the first case, substantial growing of the lesion could be accommodated by the brain before symptoms are present, and frequently, the symptoms are not exclusively related to increased intracranial pressure. Thus, extensive deformation of the fibers, vessels and glial cells is achieved when the load is applied for long period of time and/or in a slow and gradual manner, as in creep deformation. In contrast, when a fast increment in the intracranial volume is produced, as in a sudden bleeding, very little deformation is tolerated before a substantial increase in the intracranial pressure is observed. In addition, when a chronic collection is drained from the brain's convexity, like a chronic subdural hematoma, the cortex does not always return immediately to its original shape; frequently in elder persons it takes up to two months to return to its original shape.

If in a viscoelastic material, stress(σ) is being applied and removed in a repetitive cyclical fashion, then the corresponding strain(ε) is going to be present in a similar cyclical way but with certain specific delay after the stress(σ). If stress is varying sinusoidally with a frequency (ω) then the corresponding strain will follow in a similar sinusoidal frequency (ω), but with phase angle (φ), where (φ) represents the delayed response. Mathematically the stress (σ) could be expressed as:

$$\sigma(t) = \sigma_0 \sin(\omega t) \tag{2.10}$$

where (ω) represents the radian frequency.

The corresponding strain is:

$$\varepsilon(t) = \varepsilon_0 \sin(\omega t + \varphi) \tag{2.11}$$

Due to this lag in the strain response, every time a viscoelastic material receives a cyclical loading and unloading a hysteresis response is obtained. The amount of dissipated energy in the material is equal to the integral of the area inside the hysteresis loop. For a particular viscoelastic material a higher loading/unloading frequency will result in a more elastic behavior, while a low frequency will produce higher deformation with less energy dissipated (Figure 2.19).

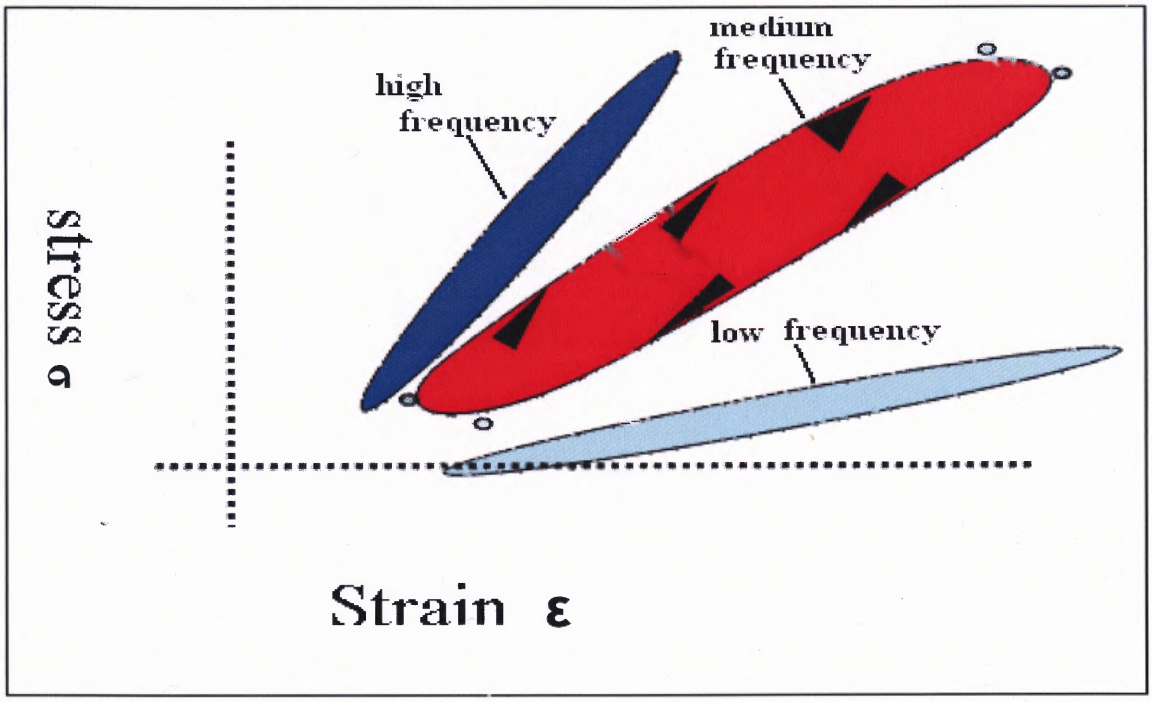

Figure 2.20 Viscoelastic Material Hysteresis Loop Frequency Dependent Behavior. At low frequency it is easy to deform. At high frequency a more stiff and elastic behavior is displayed. At intermediate frequency the amount of dissipated energy is higher due to an increased lagging of strain from stress.

Biological tissues response to loading has unique characteristics. Usually their behavior is described as viscoelastic, thus having a strong dependence in strain rate. Nevertheless, Fung described in the late 1960 a less dependent behavior of soft tissues on the strain rate. It was shown that when a soft tissue is subjected to repetitive loading/unloading cycles, the tissues will find a stable repetitive behavior during the loading with a correspondent but separate behavior during unloading. Fung coined the term pseudo-elastic to describe this behavior. The pseudo elastic behavior has been related to tissues that usually sustain a permanent cycling inside the living organism, such as arteries or lung. Experimentally, the tissue is subjected to several cycles of loading and unloading, usually between 3-10 cycles, after which the tissues seems to dissipate less

energy, become less stiff, and reaches a repeatable response. This new stable behavior suggests that a new inter-molecular dynamics has been reached.

The first Piola-Kirchhoff stress tensor *(σ)* is used to express the stress relative to the initial or reference configuration; consequently, it represents the force acting over an original oriented area. Cauchy stress tensor expresses the stress relative to the present configuration; as a consequence, it measures the force acting over current oriented area. The relation between the first Piola-Kirchhoff stress tensor *(σ),* and the resulting strain *(ε)*, denoted as stiffness, has been always a key feature when analyzing and describing any material. Due to the non-linear behavior of pseudo-elastic material it is difficult to use this relation in human tissues. Nevertheless, Y. C. Fung described a linear relation between stiffness $\delta\sigma/\delta\varepsilon$ *and* the Piola-Kirchhoff stress *(σ)*:

$$\frac{\delta\sigma}{\delta\varepsilon} = \alpha + \beta\sigma \tag{2.12}$$

Where $\acute{\alpha}$ and β are constants needed to be experimentally determined for the intercept and slope respectively. This function turns non linear stiffness into a useful tool. This relation explains how the soft tissue behaves when the stress is increased. Equation 2.12 clearly shows that an increment in the stress creates a linear increment in the stiffness of the tissue.

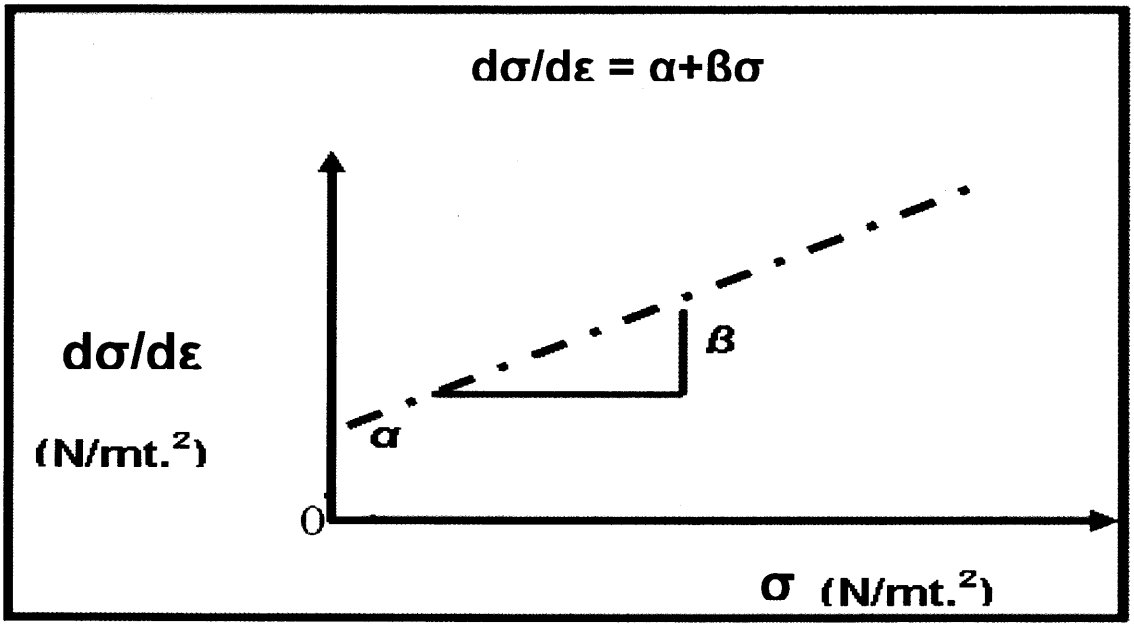

Figure 2.21 Linear relation beta (β) in pseudoelastic material between stiffness (dσ/dε) and stress (σ).
Modified from Y.C.Fung (1993)

When the brain structure is reviewed under concepts of deformation and behavior of materials, some tissue-behavior, apparently very difficult to explain, comes into clarity. The structure of the CNS is formed by a three dimensional (3D) ensemble between neurons cellular body, neurons fibers- axons and dendrites-, glial tissue – astrocyte and oligodendrocytes-, and vessels (Figure 2.12).

Based on the histological structure, a network is made by the neural fibers-axons and dendrites- running in different direction and distances. In such manner, a lattice is created by sending connections between neurons, locally, hemispherically, and interhemispherically. In addition, the network receives the contribution from the input and output fibers coming from, and going into, the peripheral nervous system. Additional lattice reinforcement between the neural fibers is created by the oligodendrocytes as they form the myelin sheath, by attaching several adjacent neurons to the same oligodendrocyte. Finally, the astrocytes, which connect on one end to the vessels and on

the other end to the neurons, also contribute to the structure by forming lattice reinforcement. From this simple description it can be easily noticed, that a multi-level lattice organization is being created. At the center, and as the back bone of this organization, remains the vasculature of the brain.. At this point, it has to be recalled the close proximity and high dependence the neurons have to the arterial system, for their normal functioning and survival. Normally, the arteries are the most firm structure inside the brain. The arterial system branches continuously in a fractal pattern. Thus, the whole brain is built around a fractal like construction, in a complex and hierarchically structured way. Notwithstanding, that each of the already mentioned elements, has at least a cell membrane, and cytoskeleton formed by proteins, glycoproteins and phospholipids; each one holding its own complex and hierarchical structure. This arrangement of the brain architecture is known in material science as a Hierarchically Structured Material.

A hierarchically structured material is one that is formed with structures that are made by parts that bear a structure themselves. Therefore, they are structures formed by structures. The hierarchical order of a structure or a material refers to (-n -) the number of levels of scale with recognized structure. Simply, the order of a hierarchically structured material refers to the number of levels of structures that form the final structure (Figure 2.22). One of the best known examples of hierarchically structured material is the Eiffel tower, were the beams are not simple beams but formed of smaller beams designed to give a better support with less mass. The Eiffel tower has been calculated to have an order of three; proteins have an order or four, while in the human brain the order of the complexity is bigger than ten. Among the properties ascribed to this type of materials are those of viscoelasticity, superplasticity (able to sustain large deformations without fracture), superior strength and toughness. (Lakes R 1993)

Traditionally, the preferred structural approach to the brain's parenchyma has been to assimilate the nervous tissue as a "sponge-like" material. This particular approximation gives more importance to the cell body than to the fibers interconnection and orientation. The "sponge-like" paradigm has diverted the vast majority of authors trying to understand the mechanical behavior of the brain tissue. (Hakim 1976, Nagashima 1987, Kaczmarek 1997, Pena 1999, Levine 1999)

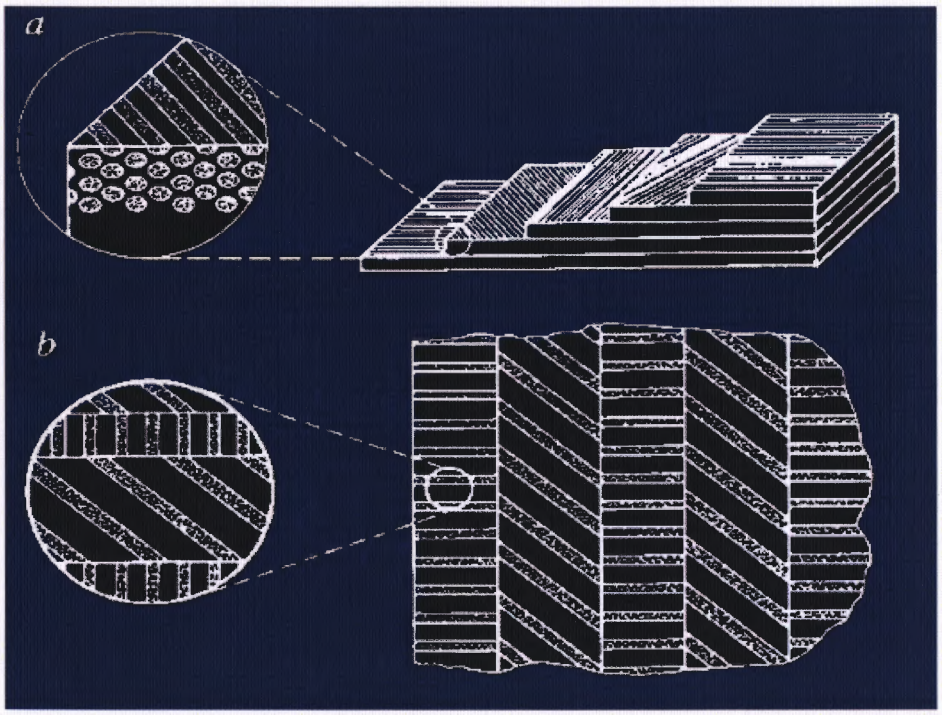

Figure 2.22 Hierarchical structure in materials hierarchical structure of order two in a practical fibrous laminate. Parallels fibres form a lamina; laminae of different orientations are stacked to form a laminate with specific anisotropy. b. Hierarchical laminate order three shown.
(Adapted from Lakes,R, Materials with Structural Hierarchy, Nature, 361(11) 511-515,1993)

It is now clear that the brain's viscoelastic properties are derived from the Hierarchical structure in which the brain is constructed. This special spatial conformation explains also why under normal circumstances the brain behaves in the elastic range. Hierarchical structure also explains the deformation that the brain parenchyma experiences when the frequency and load conditions are modified. Being the brain a

highly vascularized tissue, the behavior of the vessels mainly define the compliance of the tissue. The vessels represent a perfect example of a tissue that has a pseudo-elastic behavior. The vessels are normally preloaded in circumferential and sagittal directions; in addition they maintain a permanent loading cycle during systole and diastole at their physiological state. During systole the increment of blood volume inside the vessels produces increased loading of the vessels walls, increasing their axial stress and circumferential stress, which in turn produce increased stiffness of the vessels, resulting in a decreased compliance of the brain parenchyma. During diastole as the blood leaves the vessels, the compliance of the brain parenchyma increases.

Inflatable structures are membrane structures which require a tensile pre-stress, created by a pressure difference, to bear externally applied loads. Space inflatable structures, are currently receiving much attention by NASA. The use of space inflatable structures can potentially revolutionize the architecture and design of many large, lightweight space systems that must have extremely high packing efficiency at launch and be reliably deployed in space.

Inflatable beams are the most common representatives of the inflatable structures, they consist of a hollow cylinder, with one close end, and one fixed end where the air (fluid) is injected. The pressure of the air in its interior, translates into a force applied to the close end in the axial direction. This force creates an axial stress on the walls of the cylinder. When hold horizontally, an applied load on the surface top surface, creates a bending load on the underside, opposing the tensile stress. If the pressure inside is high enough the stress of the wall will be superior and it will not allow wrinkling. If the stress created by the weight surpasses the stress created by the pressure, then wrinkling will occur. (Figures 2.23, 2.24).(Comer, Le van, Veldman, Wielgosz)

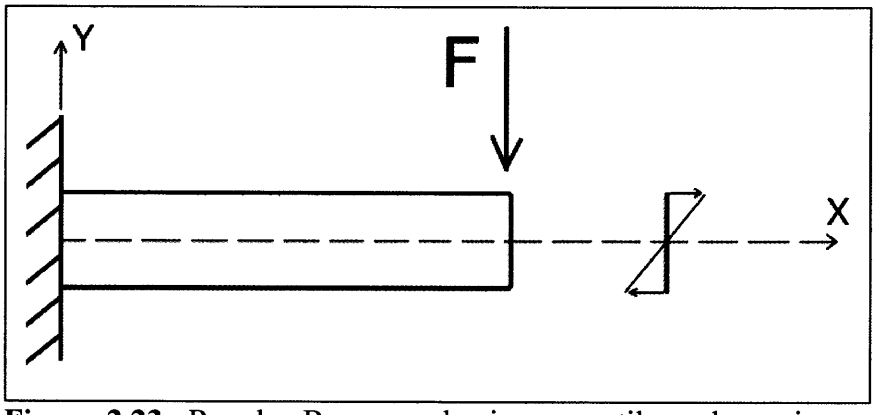

Figure 2.23 Regular Beam mechanics, a cantilever beam is generally divided in two regions divided by neutral flexion axis, one that sustains tension forces on the top, and another one that sustaining compression forces on the bottom.
Modified from: Comer, R , Levy, S.(1963), Deflections of an inflated circular cylindrical cantilever beam. A.I.A.A. Journal, 1, (7):1652-1655

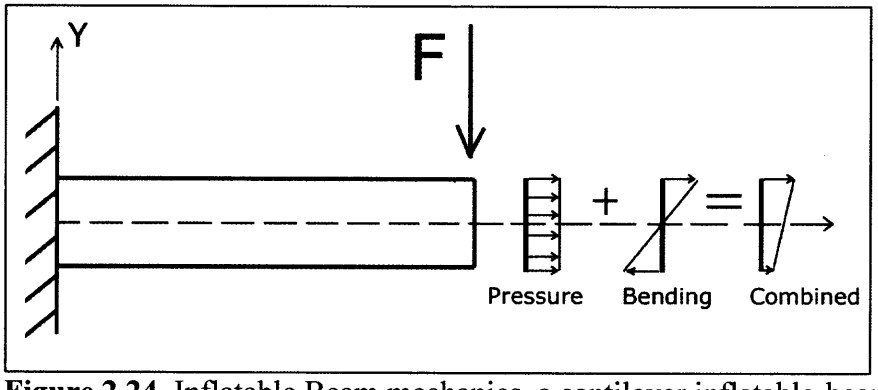

Figure 2.24 Inflatable Beam mechanics, a cantilever inflatable-beam is divided in two regions divided by neutral flexion axis, one that sustains tension forces on the top, and another one that sustaining compression forces on the bottom. In addition tension-forces resulting form the pressure acting on the walls.
Modified from: Comer, R , Levy, S.(1963), Deflections of an inflated circular cylindrical cantilever beam. A.I.A.A. Journal, 1, (7):1652-1655

In case of an open end structure, like in a vessel, the drag force is responsible for the increased tension stress on the walls of the vessel. The drag force is caused by friction of fluid current flowing over the vessel wall. The drag force is a function of vessel cross-sectional area, A, drag coefficient, C_D, external fluid density, ρ, and external flow

velocity, V. Equation 2.13 defines the drag force, F_D, on a cylindrical vessel. (Le van, Veldman, Wielgosz)

$$F_D = \frac{1}{2} C_D A \rho v^2 \qquad (2.1)$$

In medicine similar analyses have been conducted in the study of male impotence by urologists. The intracavernosal pressure has been reported as one of the most influencing factors of the penile rigidity during erection. Udelson et al. performed an engineering analysis of penile hemodynamic and structural-dynamic relationships. In this study, the major factors found to increase penile rigidity were: (1) high values of intracavernosal pressure; (2) Penile architecture; high values of penile aspect ratio and large flaccid diameter; and (3) high expandability of erectile tissue; implying the ability of the corpora to achieve its erect volume at relatively low intracavernosal pressures (Udelson et al., 1998, Udelson et al., 2000), and that:

"The relationship between buckling force and intracavernosal pressure was found to be complex but resembled an exponential-like equation". (Udelson et al., 2000)

Similar hydrodynamic concept also has been implied in cardiology; when the passive physical properties of the myocardium are determined, where it is recognized that the amount of coronary filling contributes to the stiffening the muscle. (Janicki and Weber). Recently work done by van Andel et al. on coronary arteries show a very low tolerance to deformation of the wall, with a high increment of circumferential and axial stress. (Figure 2.25). After twenty to thirty percent of strain, the arteries increase their

stress exponentially as expected in any pseudo-elastic tissue. It is worth to recall that arteries are normally in an axial and circumferential preloaded state, and are subject to cycling loading and unloading during their physiological performance; therefore complying with another characteristic of tissues with pseudo-elastic behavior.

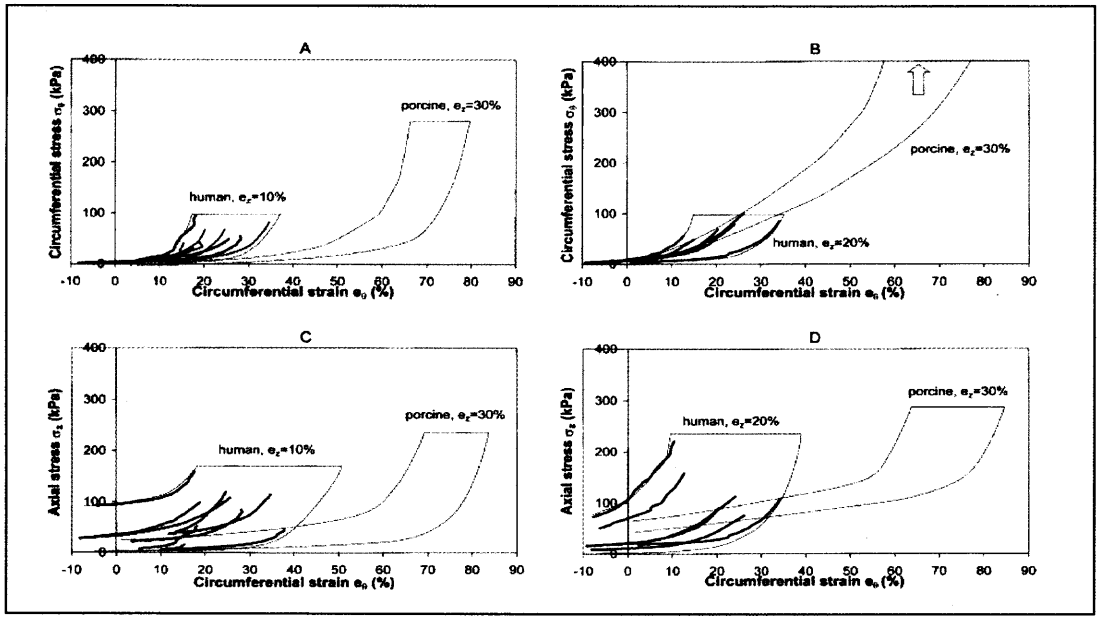

Figure 2.25 Axial and circumferential stress response to diameter increase of a human coronary artery. Note the sharp rise of the axial and circumferential stress, after a twenty percent strain.

Van Alen et al., (2003), Mechanical Properties of Porcine and Human Arteries: Implications for Coronary Anastomotic Connectors, Ann Thorac Surg;76:58–65

CHAPTER 3

NOVEL MODEL OF THE CSF DYNAMICS

A stepwise development of a computer model includes three modeling phases: conceptual modeling, mathematical modeling, and computer modeling. Conceptual modeling is the phase where the specifications of the system are established, and descriptions of the concepts to be used in later modeling phases are determined. Specification development includes determining the sequence of the events, and how they interact with each other. It also includes a description of the assumptions and simplifications of the system that are made in order to create a solid frame work for the development of the mathematical description and computer simulations that will follow. No mathematical equations are written in this phase. Only conceptual issues are considered during this phase, with an important emphasis placed on the potential factors that could affect the requirements set for modeling and simulation.

During this phase the CSF dynamics are defined as a three compartmental system, which is believed to be the simplest system that still captures the essence of CSF dynamics. The system is also characterized as a linear system for better comprehension and handling of the variables involved. The primary concepts behind the model are: vascular structures define brain compliance, the brain compliance is not necessarily homogenous, and the cyclic changes in brain compliance is what ultimately determines the distribution of CSF in the system. Important constraints are that the system has no forced directionality, as no valves are present in the system; that there is no long-standing pressure differences between the three compartments, as the system is subjected to Pascal's law, and there are no valves separating the compartments; that pressure in the

three compartments and the brain parenchyma is essentially the same, as it has been measured experimentally; the amount of CSF flow between compartment one (Ventricular compartment(Cp1)) and compartment two(Subarachnoideal compartment(Cp2)) is very little when compared to the flow between compartment two (Cp2) and compartment three (Spinal compartment(Cp3)); the amount of CSF flow between compartment two (Cp2) and compartment three (Cp3), is the same as the blood inflow occurring during a heart cycle; and the pressure in the system must stay within physiological ranges.

Mathematical modeling develops a detailed precise mathematical description of the concepts outlined in the conceptual model. It starts with a mathematical analysis of the conceptual model and ends with the formulation of the equations which are used in the next phase, computer modeling. The CSF system is described by four equations.

One steady state equation models the relationship of each compartmental volume and compartmental compliance to the whole CSF system volume and compliance. This equation is very useful in describing the CSF distribution in the three compartments whenever the CSF flow between compartments is equal to zero; an event that happens at the maximum and at the minimum volumes of each compartment.

As the system is composed of three compartments, three differential equations are used to specify the system dynamics, and two of them are independent. The third differential equation is coupled to the other two, and describes the relationship between them.

Computer Modeling traditionally entails a successive and well described process consisting of: Discretization, algorithm selection, computer programming, numerical solution, and representation of the numerical solution.

A computer model (Simulink®, Mathworks, Natick, Massachusetts) is created based on the formulas derived at the mathematical model. The process of discretization and algorithm selection is greatly facilitated as they are embedded in the algorithm used by Simulink, as the default algorithm(ODE 45) for solving differential equations. Programming in Simulink requires understanding of the potential and limitations of an icon based language; particularly acknowledging that the recollection of the results occurs simultaneously with a fixed graphical representation of the numerical solution. The computer modeling is developed in increasingly complexity. In the first version of the model, the system is represented by the least number of variables that captures and describes the essence of the CSF dynamics. Thus the first version of the model is composed of three elastic compartments with a fixed volume, and driven by a sine function representing the incoming blood volume during each heart cycle, delta blood volume. The next level of complexity is added when the sine function is replaced by a function that closely resembles the evolution in time of the blood volume inside the brain vasculature. Therefore the driving function has a more defined structure with a closer resemblance to physiological events. The next added complexity of the model is to test the impact and significance of two anatomically distinctive vascular regions found in the anatomical structure of the brain, specifically with regards to the amount and pattern of the flow between the Ventricular compartment(Cp1) and Subarachnoideal compartment(Cp2). The next added complexity acknowledges the existence of unstressed volume in compartments Cp2 and Cp3; and how the system is performing in the presence of an elastic volume, and a Unstressed volume in two of the compartments. Finally, as the mathematical analysis shows that the behavior of Cp3 is defined by the delta-blood-

volume coming into the brain vasculature, a full-constrained model is defined and implemented.

A sensitivity analysis is performed for alpha, resistance one (R1), and resistance two (R2) parameters to test the robustness of the model.

The last section of this chapter is devoted to showing the applicability of the model when analyzing altered CSF dynamics. Two important entities, Normal Pressure Hydrocephalus (NPH) and Idiopathic Intracranial Hypertension(IIH), remain without accepted physiopathology. They are explained in terms of the model, and tested by simulations done in the model.

3.1 Conceptual Model

As the anatomical structure of the ventricular system is very complex, and in an effort to better understand the system, a simplified and more comprehensible model is created. The two brain hemispheres have been lumped into one hollow sphere. The sphere walls are made of a viscoelastic substance representing the brain parenchyma, which is formed by cells and vessels. This viscoelastic material is highly vascularized. The Lateral, Third, and Fourth ventricles have been lumped into a single cavity inside of the sphere. One cylindrical communication between the interior and exterior of the hollow sphere represents the lumped resistances of the different foramens: Monroe, Luschka, Magendie; and the Sylvius Aqueduct that communicate the CSF in the interior of the brain to the Subarachnoideal space. The Subarachnoideal space is also communicated to a third compartment, the spinal compartment, via a larger foramen, the Foramen Magnum. The vessels that form part of the parenchyma sustain a cyclical variation of the amount of blood volume inside of them with each cardiac cycle. The increased volume inside the

vessels, produce an increased circumferential stress of the wall of the vessel. The increased circumferential stress produces an increment in the stiffness of the vessels itself. The increase in vessel stiffness is reflected as an increased in stiffness of the brain parenchyma. Thus during diastole the compliance increases, and during systole the compliance decreases. The sphere is submerged in the CSF, which is treated as a Newtonian fluid, with a density very similar to water. The ventricular and subarachnoideal spaces are enclosed in a rigid structure representing the cranium; the spinal compartment is located outside of the rigid structure, and is communicated to the subarachnoideal space via the Foramen Magnum. (Figure 3.1)

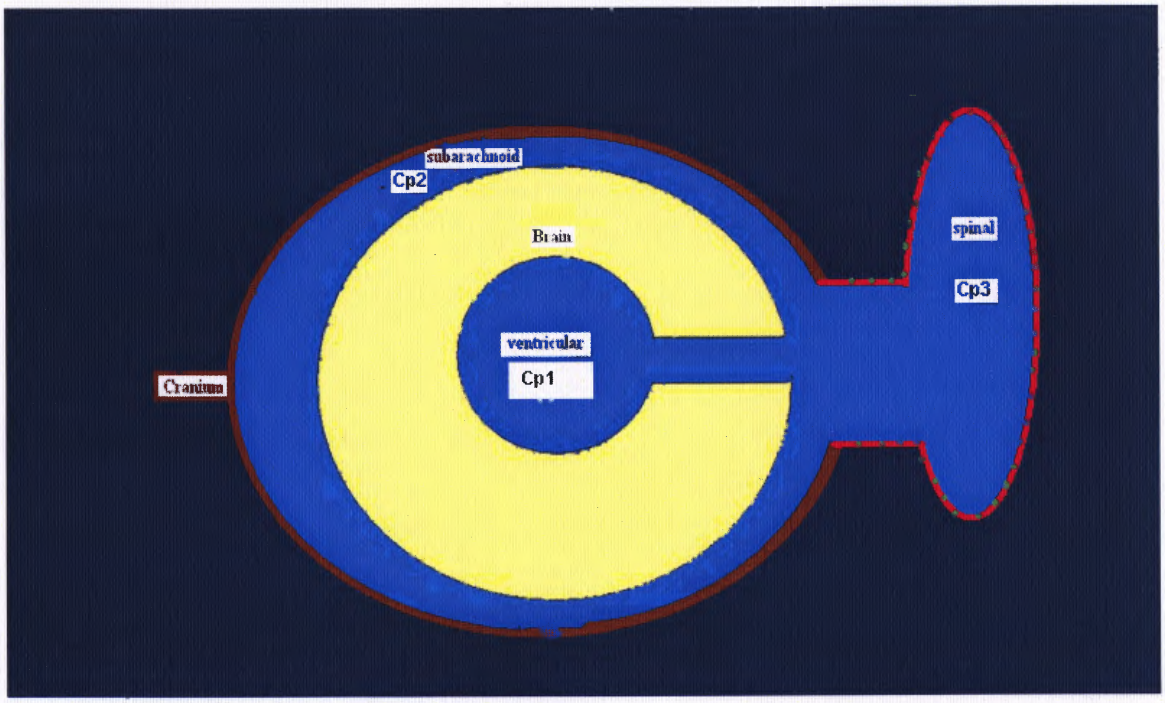

Figure 3.1 Simplified Anatomical Model of Three Compartmental System. Three compartments are distinguished; Cp1-ventricular, Cp2 Subarachnoideal, Cp3 Spinal. All are communicated unrestrictedly as no valves are present in the system. At steady state the pressures should be equal in all three compartments.

In summary the system to be modeled was simplified as a hollow sphere, constructed with a hierarchically structured material which accounts for its viscoelastic properties. This sphere is enclosed in a rigid cavity, embedded and filled with a fluid very similar to water, with a cylindrical communication between the interior and the exterior of the sphere, with no valves, and by consequence subjected to Pascal's law. The viscoelastic material sustains cyclical variation of its compliance. The brain's compliance has cyclical variation because it is dependent on the cardiac cycle. The compliance variation maintains a linear relationship with the amount of blood inside the brain vasculature.

System Characteristics:

- Hollow sphere
- Thick walls of the hollow sphere
- Viscoelastic material
- Highly vascularized
- Embedded in liquid – enclosed
- Gateway is a cylindrical communication→ in / out side of the sphere
- Same pressure in / out side (Pascal's law) of the sphere
- Same pressure in the wall of the sphere as inside and outside of the sphere
- Cyclical behavior
- Changing compliance of the viscoelastic material
- Dependent cardiac cycle
- Three compartments: Ventricular (Cp1), Subarachnoideal (Cp2), and, Spinal(Cp3).

In Figure 3.2 the importance of the cerebral vasculature is illustrated. The vessels are the only source of a mechanical force with cyclical behavior. These vessels are abundant in the brain parenchyma; a very dense network of capillaries has been documented in mammals. Capillaries range from a low density, found in the white matter (corpus callosum 162 capillaries/mm^2), to the high density found in cortical structures (810 capillaries/mm^2). Two vascular territories are well defined inside of the brain, one superficial (cortical) and one deep (ventricular).

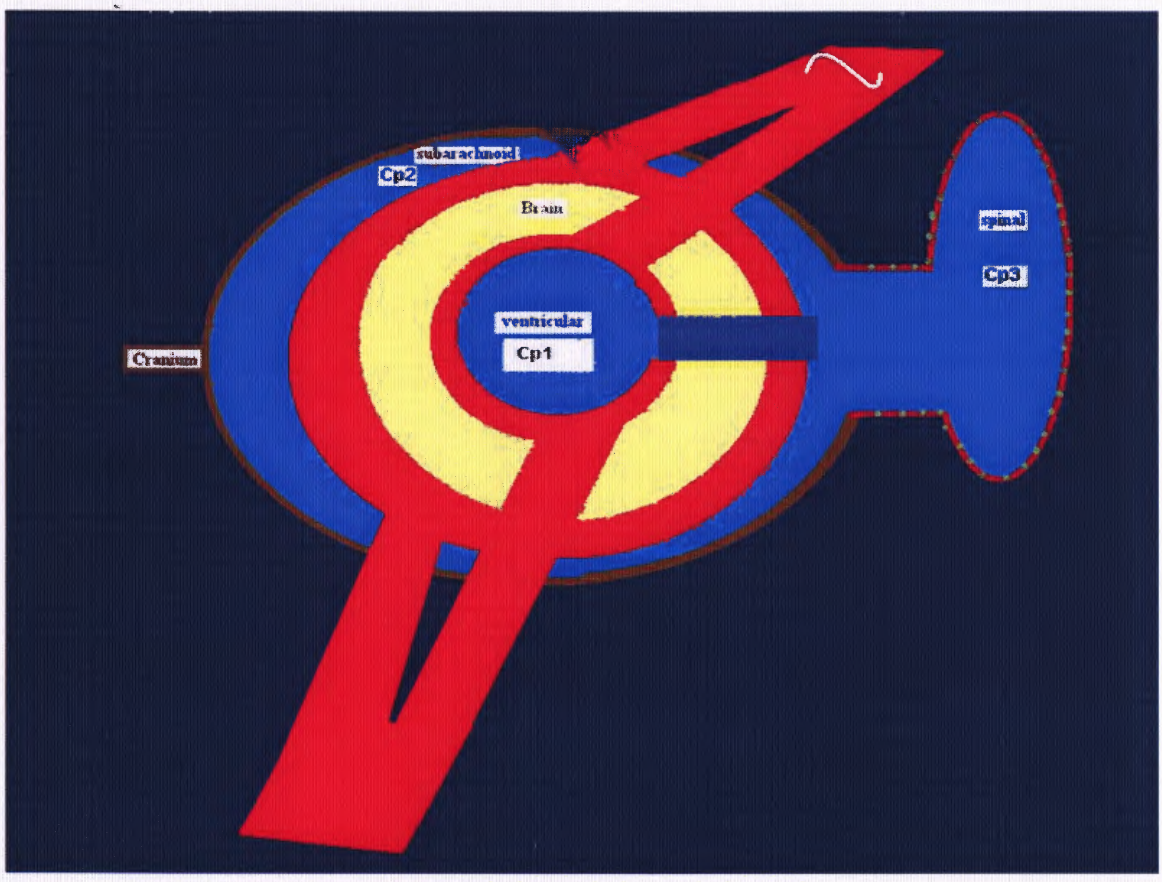

Figure 3.2 Simplified Anatomical Model of Three Compartmental System with vasculature. Two different vascular territories are displayed in this diagram. The most external vasculature corresponds to the cerebral convexity and is generally referred as cortical or superficial. The most internal vasculature surrounds the ventricular system and is usually referred as deep or periventricular. Pressures P1, P_B, and P2 have the same value, within 1 mm Hg, when measured experimentally.

The brain receives 15% of the cardiac output at rest while representing approximately 2.1 % of the body weight. With each heart systole, the blood volume entering the brain is approximately 10.5 cc per systole; 750 cc (15% of 5 lt.) of blood are pumped into the brain per minute. The high vascularization of the brain is the essence of the mechanism by which the brain forces CSF to flow.

An alternate illustration of the model is depicted in Figure 3.3. This features three compartments communicated in series: ventricular (Cp1), subarachnoideal (Cp2) and spinal (Cp3). All compartments are communicated unrestrictedly as no valves are present in the system. At steady state the pressures are equal in all three compartments. It has been documented that the pressure (P1) in the ventricular cavity (Cp1), the pressure (P2) in the subarachnoideal space (Cp2), and the pressure (PB) in the brain parenchyma are essentially equal. A difference not greater than 1 mm Hg is accepted between the ventricles and the subarachnoideal space (Penn 2005). The Ventricular compartment (Cp1), Cp2, and the walls of this compartment, are enclosed inside of a rigid case, with fixed volume, representing the cranium. Cp3 is outside of the cranium, and communicated to the Cp2 by the Foramen Magnum.

One unique feature of the system is that the pressure varies in tandem in all three cavities; increasing during systole and decreasing during diastole. The pressure variation in tandem, in all three compartments, and in the brain parenchyma, presents an obstacle to Poiseuille's equation for flow; as the pressures between different compartments do not have a measurable gradient. Still, there is a rich CSF flow between the subarachnoideal and spinal compartments, linked and dependent on the cardiac cycle; and to a lesser extent between the ventricles and the subarachnoid space.

Our first approximation of the model is to have three compartments with linear elastic behavior, with no unstressed volumes. This means that in order to have something inside of the container pressure has to be exerted on the walls of the container, and by consequence if the pressure inside of the container is zero, the container is void. Thus the compliance of the present system, in its simpler form, is calculated by the ratio between the existing volume and the existing pressure. If the pressure is maintained constant between two compartments, and the compliance varies in one of the compartments, the CSF volume will be redistributed between the compartments in accordance to the variation in compliance. Compliance is usually viewed, in mechanics and material science, as a non-varying parameter of any material. However, in living organisms this may not necessarily be the case. It has been well established that a compliance variation occurs in the myocardium during the heart cycle. The myocardium gets stiffer during systole, increasing the pressure inside the ventricle, creating a propelling force responsible of the blood ejection into the aorta. During diastole as the heart muscle relaxes the compliance increases, the pressure drops and the blood comes from the atrium into the ventricle.(Hoppensteadt and Peskin) Furthermore, in the system under study, the only plausible explanation for CSF flow is that brain compliance is varying as a function of the blood inflow during each cardiac cycle; thus this compliance variation constitutes the backbone of the model. As the compliance varies in any of the compartments, the fluid in the system is redistributed accordingly. Moreover, if only two of the three compartments present a decrement in the compliance, the redistribution will show a preferred flow towards the compartment which is not experiencing decreased compliance. A diminished compliance of the system, also explains the increment in the

pressure in the system. By decreasing the compliance in two of the three compartments, the pressure in the whole system will increase in a direct proportion.

Later in the development of the model more complex relations will be added such as an unstressed volume in Cp2 and Cp3. Also, we acknowledge that brain compliance is not a linear function, but an exponential function. Nevertheless in the normal physiological range, and as a first approximation to the system, we assume that a linear approximation is adequate.

When blood comes into the vessel a pulsation is produced as the walls of the vessel are distended. This distension of the walls creates an increased circumferential stress, $\sigma_{\theta\theta,}$ and an increased axial stress, σ_{zz}. The amount of increased stress is linearly related to an increased stiffness of the vessels. Since the brain is a highly vascularized tissue the net effect of the blood volume inflow is an increase in the stiffness of the brain parenchyma. Since the stiffness is the reciprocal of compliance, it follows that a decreased compliance is the result of the blood volume inflow. In the present model this mechanism has been incorporated by describing the effect of the incoming blood volume (v_{sv}) on compliance. The loss of compliance is directly proportional to the in-coming blood volume, by a factor alpha (α). Alpha represents the incremental effect of the delta blood volume on the circumferential and axial stresses on the walls of the brain vessels. By extension, alpha represents the effect that the incremented axial and circumferential stresses produce increasing the stiffness on the wall of the blood vessel.

The end result is a mechanism that decreases the compliance in the intracranial compartments during systole and returns to the previous values during diastole. This mechanism creates cyclical variation of the brain parenchyma compliance as a function of blood flow. As the spinal compartment does not sustain those cyclical variations, it

acts as a buffer receiving more volume of CSF during systole, and returning volume back into the intracranial compartment during diastole. The amount of CSF expelled during systole from Cp2 into Cp3, matches the amount of blood coming into the cranial cavity in order to maintain the pressure in physiological values. The increment in pressure of the CSF system is due to the diminished compliance of the brain parenchyma. The amount of CSF flowing between Ventricular compartment(Cp1) ands Cp2 is limited by a higher resistance (R1) connecting these two compartments, when compared to the resistance (R2) connecting compartments Cp2 and Cp3. Also, as Ventricular compartment(Cp1) and Cp2 experience a variation in tandem of their compliance, since the already explained mechanism influence both compartments; a minor gradient is produced between them. (Figure 3.3)

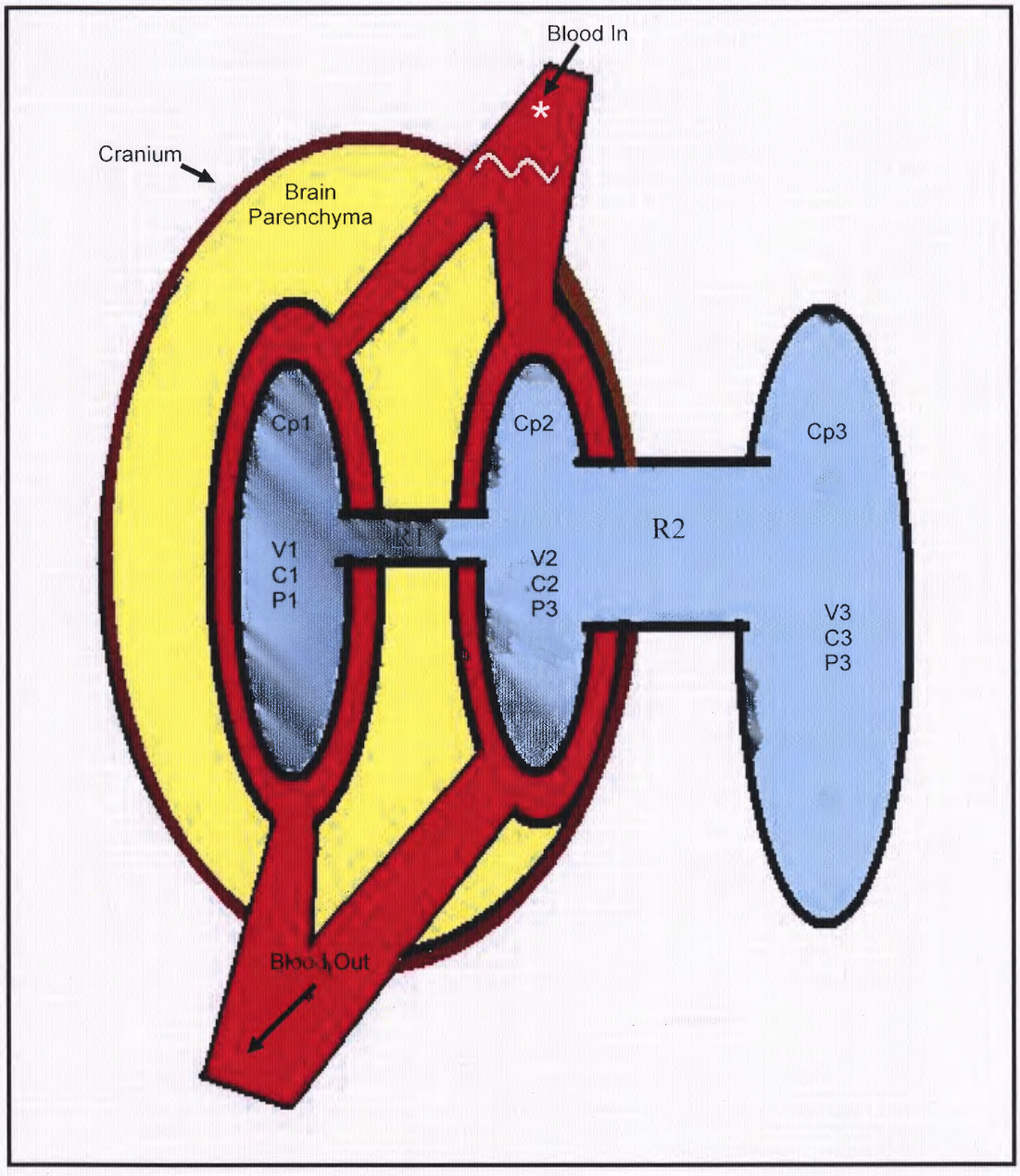

Figure 3.3 Three Compartmental Model Cp1=Ventricular; Cp2=subarachnoideal; Cp3= spinal for analysis of the system respective volumes, pressures, and compliances during the cardiac cycle. PB=Brain parenchyma. Cerebral Blood Flow (CBF) ; which produces a cyclic compliance of the brain tissue in response to the amount of blood held in the vessels. The pressures in Cp1, Cp2, and Brain Parenchyma, have the same value within a range of 1 mm Hg., when measured experimentally.(Penn et al.) V1= volume 1, C1= compliance 1, P1= pressure 1, V2= volume 2, C2= compliance 2, P2= pressure 2, V3= volume 3, C3= compliance 3, P3= pressure 3. R1= resistance 1. R2= resistance 2.

Figure 3.4 illustrates the general sequence of events in a three Compartmental Model; Cp1=Ventricular; Cp2=subarachnoideal; Cp3= spinal, during a normal cycle. Images from A to H show the changes during a complete period. Images from A to D illustrate the changes in the system produced by cardiac systole. Images from E to H illustrate the changes occurring in the system during cardiac diastole. The same nomenclature as in Figure 3.3 is maintained, though some labels have been removed for better visualization of the changes.

As blood comes in during heart systole, the vessels' diameter expands to host the incoming blood volume, an increased circumferential stress is produced in the vessels' walls; the brain parenchyma's compliance is decreased, and the CSF is expelled out of the cranium into the spinal compartment. As blood is drained, brain parenchyma's compliance increases and CSF returns into the cranium from the spinal compartment. The relation between the intracranial and the spinal compartment accounts for the vast majority of the flow dynamics in the system. However, it is also important to examine what happens between the intraventricular and subarachnoideal spaces. As blood flow comes into the vessels, the compliance in both compartments decrease in tandem; and as blood flows out of the vessels, their compliance increase in tandem. Minimal gradient is expected to build between these two compartments by this mechanism. Nevertheless as some CSF flows out of the subarachnoideal compartment into the spinal compartment, the pressure inside the subarachnoideal compartment falls, and a pressure gradient is created between the intraventricular and the subarachnoideal compartments. This gradient favors a flow between the compartments; but it should be remembered that the pressure gradient is relatively small, and depends only on the amount of fluid that has gone out of the cranium into the spine. Another factor to remember is that the resistance between the

ventricular compartment and the subarachnoideal space is higher than the resistance between the subarachnoideal compartment and the spinal compartment. These conditions make the flow coming in and out of the ventricular compartment to be relatively small, when compared to the flow that exists between the subarachnoideal (Cp2) and the spinal compartment(Cp3).

In the illustration of Figure 3.4 the sequence of events are shown. The additional volume is illustrated in Figure 3.4 A as an additional bubble on top of the vasculature. As blood-flow is coming in, an additional volume has to be accommodated inside of the vessels. As a consequence the brain compliance starts to decrease, and an equal amount of CSF is expelled from the cranial-subarachnoideal space into the spinal compartment. The increment in volume of blood coming in has to match the increment of volume in Cp3; obviously the increment in Cp3 volume has to match the combined decrement in volume on Ventricular compartment(Cp1)and Cp2. In Figure 3.4 from A to D there is a progressive increment in the blood coming in. At D the system is at the peak systolic volume; from here onwards, no more blood will come in until a new cycle starts. But even though no more blood is coming in during the cycle, the blood flow going out is permanent; thus the volume inside the vessels starts to decrease. In Figure 3.4 from E to H the sequence of events illustrate the changes happening in the system during diastole, until the lowest volume inside the vessels is achieved at "peak diastole", shown in H. Note the progression of the additional blood-volume inside the vessels illustrated as a red bubble on the right side of Ventricular compartment(Cp1) and Cp2. The change in size of Ventricular compartment (Cp1), Cp2 and Cp3 is illustrated with blue-hyphened lines, in each compartment. Note how the Cp3 increases during systole and recoils during diastole, opposite to what happens in Cp2.

Cp2 presents a more complex behavior as it interchanges volume with the Ventricular compartment (Cp1) and Cp3 simultaneously. Nevertheless, the amount of volume interchanged between the Ventricular compartment (Cp1)and Cp2 is remarkably low, when compared with the volume interchanged between Cp2 and Cp3.

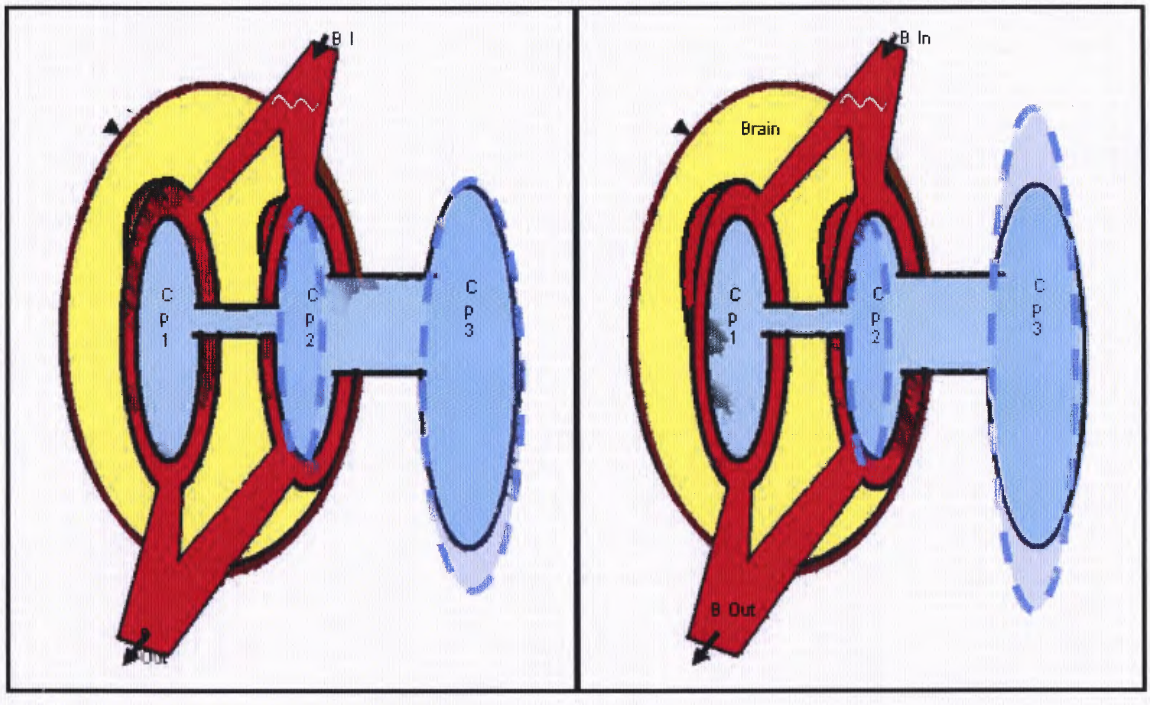

A B

Figure 3.4 Normal CSF cycle during a cardiac cycle. Three Compartmental Model Cp1=Ventricular; Cp2=subarachnoideal; Cp3= spinal. Images from A to H show the normal sequence of events in the three compartments during a normal cycle. From A to D the changes in the system produced by cardiac systole have been illustrated. From E to H the changes occurring in the system during cardiac diastole have been illustrated. The same nomenclature as in Figure 3.3 should be kept in mind; though better for visualization some labels have been removed. Additional blood volume coming in during systole has been represented as a red bubble on top of the vasculature, note how it increases in size and extension from A to D, representing increasing blood volume delivered into the brain during the heart systole.

At heart systole the blood starts coming into the brain vessels, the additional blood volume increases the circumferential stress of the vessels wall.

The additional blood volume is represented in the Figure 3.4 by a "red bubble" initially located at the left superior margin of the vessels compartment. The "red bubble" increases in size and covers more area as systole progresses, representing the amount of blood inside of the brain vasculature. As the wall of the blood vessel is distended by the additional blood, the circumferential stress increases; the vessels stiffness also increases; the brain parenchyma stiffness increases; thus the brain compliance decreases. As the brain parenchyma compliance decreases the CSF is expelled into the spinal cavity (Figure 3.4 A to D)

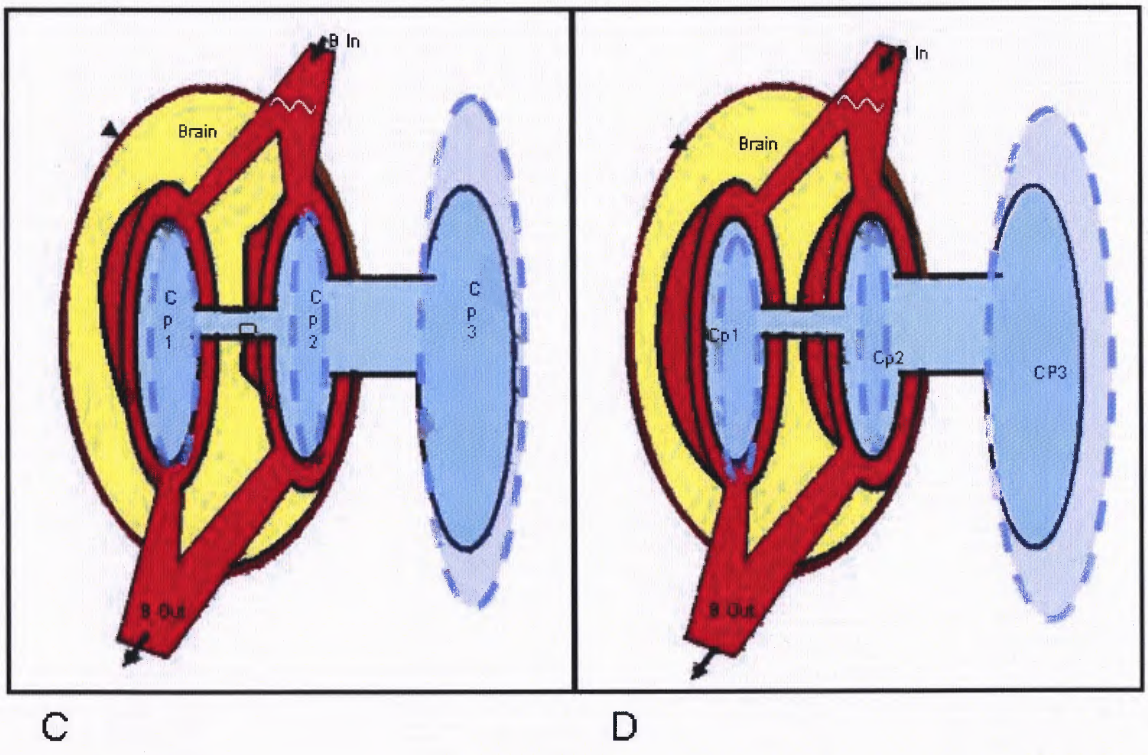

Figure 3.4 Normal CSF cycle during a cardiac cycle. Additional blood volume coming in during systole has been represented as a red bubble on top of the vasculature, note how it increases in size and extension from A to D, representing increasing blood volume delivered into the brain during the heart systole.

As systole progresses the amount of blood inside the vessels reaches its peak value, peak systole (D); at this instant the vessels' stiffness is at its maximum, and the

compliance of the brain is at its minimum. Also at this prexcise moment, the CSF flowing from the subarachnoideal compartment into the spinal canal has reached its maximum value, and is ready to change direction to go back into the cranium. When the CSF flow reverses direction, as any other mass moving in a defined direction, has to stop and then reverse its direction; this occurs at the moment where the maximum volume of Cp3 is reached (D) in "peak systole". Therefore, at peak systole CSF flow is equal to zero.

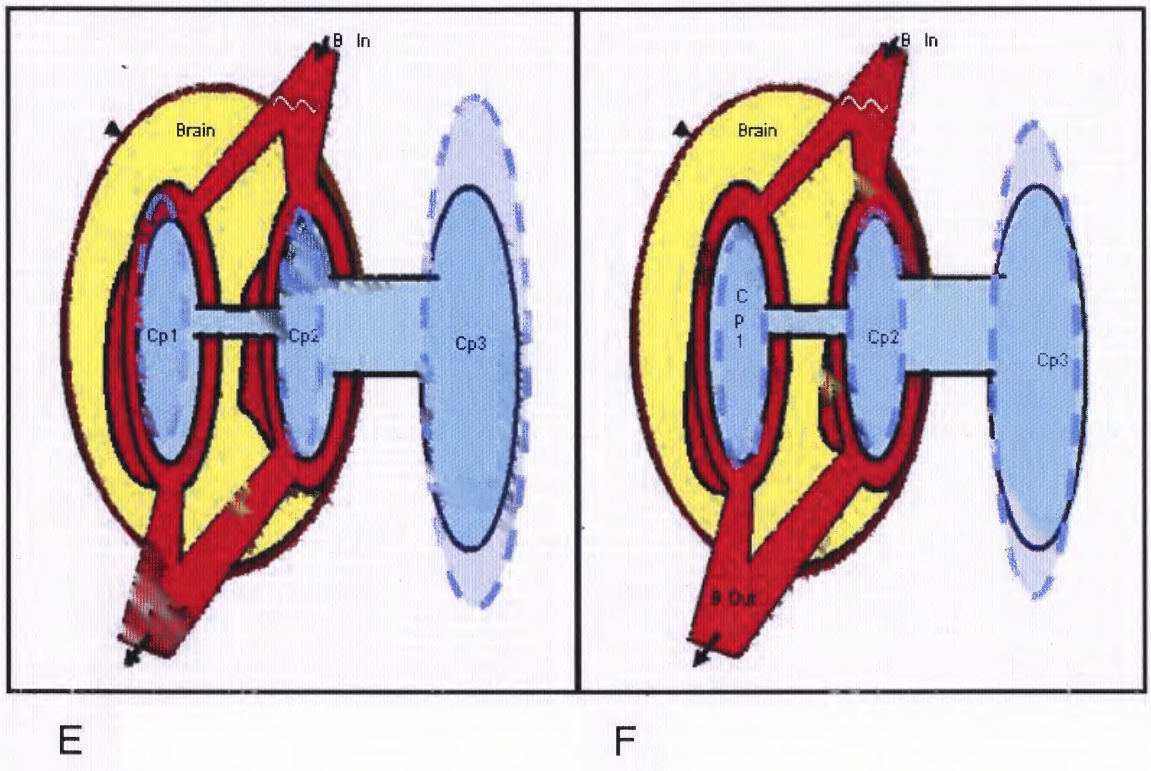

Figure 3.4 Normal CSF cycle during a cardiac cycle. Additional blood volume coming in during systole has been represented as a red bubble on top of the vasculature, note how it decreases in size and extension from E to H, representing blood volume drained from the brain by the venous system during the heart diastole.

During heart diastole, the venous drainage starts diminishing the blood content inside the brain vasculature. The vessels' walls are gradually released of the load, their circumferential stress decreases, the brain compliance increases, and the CSF starts coming back from the spinal canal into the cranium (E to H). At the end of heart diastole

the Cp3 compartment reaches its minimum volume, and is ready to start a new cycle. When a new cycle starts, CSF flow changes direction, thus at the end of diastole the CSF flow is also equal to zero (H).

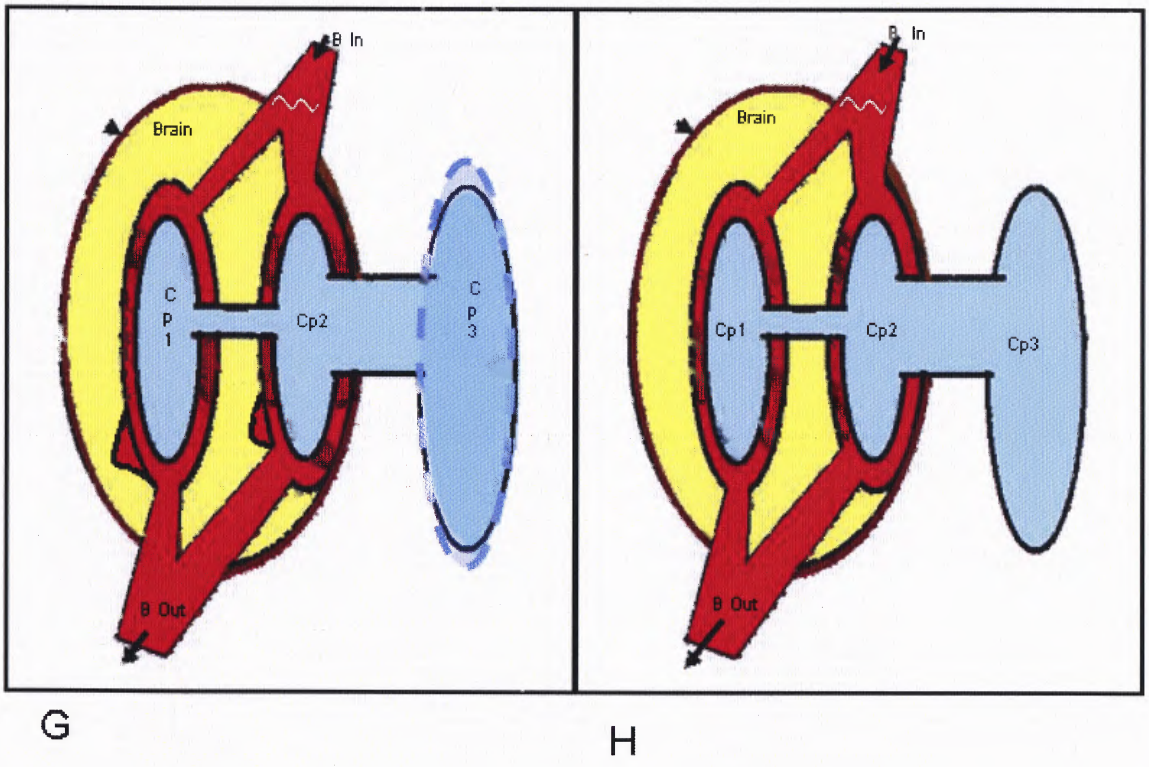

Figure 3.4 Three Compartmental Model Cp1=Ventricular; Cp2=subarachnoideal; Cp3= spinal. Images from A to H show the normal sequence of events in the three compartments during a normal cycle. From A to D the changes in the system produced by cardiac systole have been illustrated. From E to H the changes occurring in the system during cardiac diastole have been illustrated. The same nomenclature as in Figure 3.3 should be kept in mind; though better for visualization some labels have been removed.

Additional blood volume coming in during systole has been represented as a red bubble on top of the vasculature. Note how it it increases in size and extension from A to D, representing increasing blood volume delivered into the brain during the heart systole. Also note how it decreases in size and extension from E to H, representing increasing blood volume drained from the brain by the venous system during the heart diastole.

3.2 Mathematical Model

The conceptual model, previously explained, is summarized as follows: The amount of CSF volume that each compartment could hold in its interior at a certain pressure is defined by a linear compliance of the walls of each compartment. The flow between two adjacent compartments is defined by the differential pressure between them, and resistance to the flow between them. Fixed total CSF volume of the system is assumed. The fact of being embedded and filled with CSF makes the system subjected to Pascal's law; thus any change in pressure is rapidly transmitted and equilibrated trough the system. Experimental data in animals and humans show the same pressure in the subarachnoideal compartment, ventricular compartment, and in the brain parenchyma. The amount of accepted difference between the intraventricular and subarachnoideal pressures is one mm Hg; and it is due to the fact that any difference smaller than 1 mm Hg is beyond of the sensitivity of the methods utilized for the measurements (Penn 1995). A steady state analysis confirms that a final CSF volume distribution is dependent on the relation of the compliance of the specific compartment to the whole compliance of the system. In order to maintain active dynamics in the system a periodic forcing function needs to be introduced.

The initial mathematical analysis considers the principle of conservation of mass, and Poiseuille's equation for flow (mechanical equivalent of Ohm's law).

The model is constructed as mentioned by defining three distinctive compartments (Cp_i):

Ventricular: Cp_1
Subarachnoideal: Cp_2
Spinal: Cp_3

Each cavity possesses a distinct initial compliance (C_0), initial volume (V_0), and initial pressure (P_0):

$$C_{0;}\ V_{0;}\ P_0$$

Compliance of each compartment is defined as the simple linear relation between volume and pressure:

$$C_{0i} = \frac{V_{0i}}{P_{0i}} \qquad (3.1)$$
$$i = 1,2,3$$

Therefore, the pressure is:

$$P = \frac{V}{C} \qquad (3.2)$$

Assuming a fixed volume of CSF we have that the sum of the three compartments is equal to the total CSF volume (V_T):

$$V_1 + V_2 + V_3 = V_T \tag{3.3}$$

As defined earlier, the primary basis of this model relies on a compliance varying with time, dependent on the amount of blood inside the cerebral vessels (V_{sv}), with a constant of proportionality alpha (α), according to the concept developed by W.C Fung and presented in Chapter 2, Equation 2.12. When blood comes into the vessel a pulsation is produced as the walls of the vessel are distended. This distension of the walls creates an increased circumferential stress, $\sigma_{\theta\theta}$, and increased axial stress, σ_{zz}. The circumferential stress is determined by Equation 2.3. Recall:

$$\sigma_{\theta\theta} = \frac{\mathrm{Pr}}{h}$$

The axial stress is determined by Equation 2.5. Recall:

$$\sigma_{zz} = \frac{f}{\pi r h}$$

The amount of increased circumferential and axial stresses is related to an increased stiffness of the vessels in a linear fashion. As a result, the net effect of the blood volume inflow is an increase in the stiffness of the brain parenchyma. Since the stiffness is the reciprocal of compliance, it follows that a decreased compliance is the result of the increased blood volume.

In the present model this mechanism has been incorporated as a loss of compliance that is directly proportional to the incoming blood volume (V_{sv}), by a factor alpha (α). Alpha represents the decrement of compliance of the vessel's wall as a result of the additional pressure resulting from the additional blood volume held inside of the vessel. If this decrement in compliance is integrated on the whole parenchyma it will represent the entire decrement of the brain compliance per cardiac cycle, during systole.

Alpha is expressing a directly proportional relation between the amount of axial and circumferential stresses and stiffness. As compliance is the reciprocal of stiffness, the amount of delta blood volume inside the vessel will diminish the existing compliance in proportion to alpha (α), thus:

$$C_i(t) = C_0 - \alpha V_{sv} \tag{3.4}$$

Where: V_{sv} = cerebral blood volume inside the vessel

Since the vessel's compliance diminishes per unit of increasing pressure, resulting from new blood volume added during systole, alpha has units of mm Hg^{-1}. The CSF volume variation with time of each compartment is determined by the flow between the compartments. The amount of flow between two adjacent compartments is determined by the pressure difference between them, and by the resistance to the flow between the two compartments. In the present model we are interested in the Flow 1 (Q_1) where CSF comes into Cp1 from Cp2; and in the Flow 2 (Q_2) where CSF goes from Cp2 into Cp3:

Flow $_1$ (Q_1):

$$\frac{dV_1}{dt} = Q_1 \tag{3.5}$$

$$Q_1 = \frac{1}{R_1}(P_2 - P_1) \tag{3.6}$$

Flow $_2$ (Q_2):

$$\frac{dV_3}{dt} = Q_2 \tag{3.7}$$

$$Q_2 = \frac{1}{R_2}(P_2 - P_3) \tag{3.8}$$

Replacing Equation 3.4 into 3.2; Equation 3.2 into 3.6; and Equation 3.6 into 3.5 we have:

$$\frac{dV_1}{dt} = \frac{1}{R_1}\left(\frac{V_2}{(C_{02} - \alpha V_{sv})} - \frac{V_1}{(C_{01} - \alpha V_{sv})}\right) \tag{3.9}$$

Replacing Equation 3.4 into 3.2; Equation 3.2 into 3.8, and Equation 3.8 into 3.7 we have:

$$\frac{dV_3}{dt} = \frac{1}{R_2}\left(\frac{V_2}{(C_{02} - \alpha V_{sv})} - \frac{V_3}{(C_{03})}\right) \tag{3.10}$$

As a consequence of Equation 3.3 we have:

$$\frac{dV_1}{dt} + \frac{dV_2}{dt} + \frac{dV_3}{dt} = 0$$

$$\frac{dV_2}{dt} = -\frac{dV_1}{dt} - \frac{dV_3}{dt} \tag{3.11}$$

By integrating both sides of the Equation 3.11 we have the way of calculating the amount of change in volume (dV_2) in Cp2:

$$\frac{dV_2}{dt} = -\frac{dV_1}{dt} - \frac{dV_3}{dt}$$

$$\int \frac{dV_2}{dt}dt = -\int \frac{dV_1}{dt}dt - \int \frac{dV_3}{dt}dt \tag{3.12}$$

$$dV_2 = -dV_1 - dV_3$$

The final volume for each compartment will be calculated by:

$$V_{fi}(t) = V_{0i} + \int_0^T \frac{dVi}{dt} dt \qquad (3.13)$$
$$i = 1,2,3$$

Therefore to model the dynamics between the three compartments, the model is using just these three differential Equations: 3.9, 3.10, and 3.12. In this way the CSF flow between the three compartments, $\frac{dV_1}{dt}; \frac{dV_2}{dt}; \frac{dV_3}{dt}$, has been conditioned to the cerebral blood flow, Q_{sv}. Undoubtedly, the three cavities would reach equilibrium if there were not cerebral blood flow (Q_{sv}); thus no CSF flow will occur.

A cyclical variation of the CSF system has two instances per cycle where the CSF flow is equal to zero. A cyclical variation of the CSF system is characterized by two phases in each compartment: in the first phase, the volume increases and reaches a maximum value. In the second phase, the volume decreases and reaches a minimum value. At the moment where the system has reached the maximum value (just before it starts to decrease) there is no CSF flow in or out of the compartment. The same happens at the moment where the system has reached the minimum value (just before it starts to increase) there is no CSF flow in or out of the compartment. Therefore, at the instant where there is a transition from phase one into phase two (as well as when there is a transition from phase two into phase one) there is no CSF flow into or out from the compartment. Thus at those specific instances a steady state solution would occur. A steady-state solution would be of the form:

$$\frac{dV_1}{dt} = \frac{1}{R_1}\left(\frac{V_2}{C_2} - \frac{V_1}{C_1}\right) = 0 \tag{3.14}$$

$$\frac{dV_3}{dt} = \frac{1}{R_2}\left(\frac{V_2}{C_2} - \frac{V_3}{C_3}\right) = 0 \tag{3.15}$$

$$\frac{dV_2}{dt} = -\frac{dV_1}{dt} - \frac{dV_3}{dt} = 0. \tag{3.16}$$

As a consequence at steady state:

$$\frac{V_2}{C_2} = \frac{V_1}{C_1} \tag{3.17}$$

$$\frac{V_2}{C_2} = \frac{V_3}{C_3}. \tag{3.18}$$

And as the pressure through the whole system is the same:

$$\frac{V_1}{C_1} = \frac{V_2}{C_2} = \frac{V_3}{C_3} = P \tag{3.19}$$

$$P = \frac{V_T}{C_T}.$$

From Equation 3.2, the volumes could be calculated as

$$C = \frac{V}{p} \tag{3.20}$$

$$CP = V$$

Substituting Equation 3.20 into Equation 3.3:

$$V_T = V_1 + V_2 + V_3$$

$$CP = V$$

$$V_T = C_1P + C_2P + C_3P$$

$$V_T = P(C1 + C2 + C3) \tag{3.21}$$

$$P = \frac{V_T}{C1 + C2 + C3} = \frac{V_T}{C_T},$$

where

$$C_T = C_1 + C_2 + C_3 \tag{3.22}$$

V_T is the total volume, and C_T is total compliance of the system.

The pressure in the whole system P_T also maintains the relation between the entire volume , and the entire compliance of the system.

$$P_T = P = \frac{V_1}{C_1} = \frac{V_2}{C_2} = \frac{V_3}{C_3} = \frac{V_T}{C_T} \tag{3.23}$$

From Equation 3.19, it is easy to see

$$\frac{V_i}{C_i} = \frac{V_T}{C_T}$$

$$V_i = \frac{V_T C_i}{C_T} \tag{3.24}$$

$$i = 1,2,3$$

So at a hypothetical steady state or at any moment where the system dynamics reaches a point where the flow between compartments is equal to zero; the volume of

each of the compartments is determined by the ratio between the total compliance of the system and the compliance of the respective compartment of interest.

As the cranium is a rigid structure, a fixed volume is maintained. Thus any system housed inside should comply with this constraint:

$$V_1 + V_2 + V_B = V_{Cra} \tag{3.25}$$

where v_B is volume of the brain parenchyma, and V_{Cra} is the volume inside the cranium.

By subtracting Equation 3.25 from Equation 3.3 we have:

$$\begin{aligned} &(V_1 + V_2 + V_3) - (V_1 + V_2 + V_B) = V_T - V_{Cra} \\ &V_3 - V_B = V_T - V_{Cra} \end{aligned} \tag{3.26}$$

And by differentiating Equation3.26 we have,

$$\begin{aligned} &\frac{dV3}{dt} - \frac{dV_B}{dt} = 0 \\ &\frac{dV3}{dt} = \frac{dV_B}{dt} \end{aligned} \tag{3.27}$$

Thus any increment of blood volume inside of the cranium is equal to the increment of CSF in the Cp3. Therefore, Equation 3.27 represents the Monroe-Kellie theorem in this model. Also, Equation 3.27 simply explains that any blood-volume that enters into the cranium during systole, is compensated by ejecting the same amount of CSF from the cranium into the spine.

As a result of the blood flow coming in (dV_B/dt), the additional volume inside the brain parenchyma ($V_{B(t)}$), is computed by integrating dV_B/dt:

$$V_{B(t)} = \int \frac{dV_B}{dt} dt = \int \frac{dV3}{dt} dt \tag{3.28}$$

Equation 3.28 offers an easy way of calculating the volume variation of Cp3 in time.

$$V_3(t) = V_{3(0)} + \int \frac{dV_3}{dt} = V_{3(0)} + \int \frac{dV_B}{dt} = V_{3(0)} + V_{B(t)} \tag{3.29}$$

Rearranging the terms of Equations 3.9 and 3.10, which define the system, we have

$$\frac{dV_1}{dt} = \frac{1}{R_1}\left(\frac{V_2}{(C_2(t))} - \frac{V_1}{(C_1(t))}\right) \tag{3.30}$$

$$\frac{dV_3}{dt} = \frac{1}{R_2}\left(\frac{V_2}{(C_2(t))} - \frac{V_3}{(C_3)}\right). \tag{3.31}$$

From Equation 3.3, we could substitute V_2 in Equation 3.30

$$\frac{dV_1}{dt} = \frac{1}{R_1}\left(\frac{V_T - V_1 - V_3}{(C_2(t))} - \frac{V_1}{(C_1(t))}\right). \tag{3.32}$$

From Equation 3.3, we could substitute V_2 in Equation 3.31

$$\frac{dV_3}{dt} = \frac{1}{R_2}\left(\frac{V_T - V_1 - V_3}{(C_2(t))} - \frac{V_3}{(C_3)}\right). \tag{3.33}$$

As the system is defined by two differential Equations they can be solved simultaneously:

$$\frac{dV_1}{dt} = \frac{1}{R_1}\left(\frac{V_T}{(C_2(t))} - \frac{V_1}{(C_2(t))} - \frac{V_1}{(C_1(t))} - \frac{V_3}{(C_2(t))}\right)$$

$$\frac{dV_3}{dt} = \frac{1}{R_2}\left(\frac{V_T}{(C_2(t))} - \frac{V_1}{(C_2(t))} - \frac{V_3}{(C_2(t))} - \frac{V_3}{(C_3)}\right). \tag{3.34}$$

Rearranging terms we have

$$\frac{dV_1}{dt} = \left(\frac{V_T}{R_1(C_2(t))}\right) - \left(\frac{V_1}{R_1}\left(\frac{1}{(C_2(t))} + \frac{1}{(C_1(t))}\right) - \frac{V_3}{R_1(C_2(t))}\right)$$

$$\frac{dV_3}{dt} = \left(\frac{V_T}{R_2(C_2(t))}\right) - \left(\frac{V_1}{R_2(C_2(t))} - \frac{V_3}{R_2}\left(\frac{1}{(C_2(t))} + \frac{1}{(C_3)}\right)\right). \tag{3.35}$$

By writing the Equations in a matrix notation

$$\begin{pmatrix} \frac{dV_1}{dt} \\ \frac{dV_3}{dt} \end{pmatrix} = \begin{pmatrix} \frac{V_T}{R_1(C_2(t))} \\ \frac{V_T}{R2(C_2(t))} \end{pmatrix} - \begin{pmatrix} \left(\frac{1}{R_1(C_2(t))} + \frac{1}{R_1(C_1(t))}\right) & \frac{1}{R_1(C_2(t))} \\ \frac{1}{R_2(C_2(t))} & \frac{1}{R_2(C_2(t))} + \frac{1}{(C_3)} \end{pmatrix} \begin{pmatrix} V_1 \\ V_3 \end{pmatrix} \tag{3.36}$$

But from Equation 3.27, the matrix can be simplified to

$$\begin{pmatrix} \frac{dV_1}{dt} \\ \frac{dV_3}{dt} \end{pmatrix} = \begin{pmatrix} \frac{V_T}{R_1(C_2(t))} \\ \frac{dV_B}{dt} \end{pmatrix} - \begin{pmatrix} \left(\frac{1}{R_1(C_2(t))} + \frac{1}{R_1(C_1(t))}\right) & \frac{1}{R_1(C_2(t))} \\ 0 & 0 \end{pmatrix} \begin{pmatrix} V_1 \\ V_3 \end{pmatrix} \tag{3.37}$$

From Equation 3.38 the system is now reduced to a single differential Equation:

$$\frac{dV_1}{dt} = \frac{V_T}{R_1(C_2(t))} - \left(\frac{V_1}{R_1(C_2(t))} + \frac{V_1}{R_1(C_1(t))} \right) - \frac{V_3}{R_1(C_2(t))} \quad \text{or}$$

$$\frac{dV_1}{dt} = \frac{V_T}{R_1(C_2(t))} - \frac{V_3}{R_1(C_2(t))} - \left(\frac{V_1}{R_1(C_2(t))} + \frac{V_1}{R_1(C_1(t))} \right). \tag{3.38}$$

Since v_3, behavior in time, is already known from Equation3.29, and substituting Equation 3.29 into Equation 3.39, we therefore have

$$\frac{dV_1}{dt} = \frac{V_T}{R_1(C_2(t))} - \frac{V_{3(0)} + V_B(t)}{R_1(C_2(t))} - \left(\frac{V_1}{R_1(C_2(t))} + \frac{V_1}{R_1(C_1(t))} \right) \tag{3.39}$$

Rearranging terms, Equation 3.40 becomes

$$\frac{dV_1}{dt} = \frac{V_T - V_{3(0)} - V_B(t)}{R_1(C_2(t))} - V_1 \left(\frac{1}{R_1(C_2(t))} + \frac{1}{R_1(C_1(t))} \right) \tag{3.40}$$

3.3 Computer Model

A computerized model (Simulink®) was developed, in accordance to the previously exposed hypothesis. The introduced forcing function is representing the integral of the cerebral blood flow, which is changing the amount of blood inside the vessels, and by consequence changing the circumferential and axial stresses of the intracranial vessels. A sine wave was elected as an initial forcing function; later in the development of the model the forcing signal is replaced by a function that emulates the blood flow coming from the heart. This wave representing the incoming blood in turn introduces a cyclical change of the compliance of the intracranial compartments of the system, producing an oscillatory CSF flow. In agreement to the anatomy, two different venous drainage territories, with two different circulatory times are modeled: one superficial draining the cortex, and another deep draining the periventricular area. As it is not subjected to cyclical changes in its compliance, the spinal compartment performs a buffer function for the system .

When parameters within physiological ranges are introduced, the resulting CSF flow adequately resembles those flows documented by phase contrast cine-MRI.

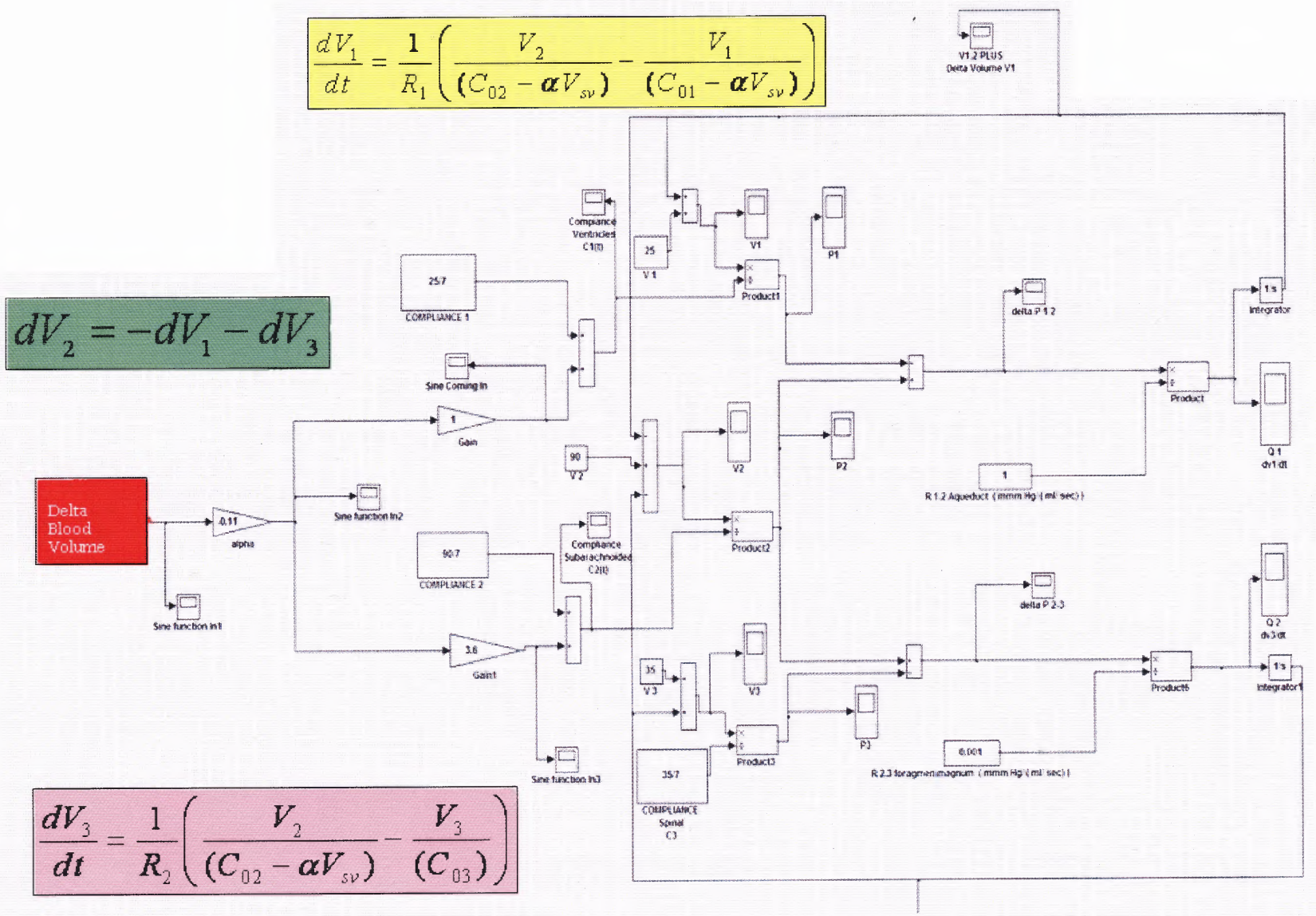

Figure 3.5 Sine driven model.

3.3.1 Sine Driven Model

Taking into consideration the just mentioned concepts, the first computer model was generated by placing into interaction three differential equations derived in the previous section; Equation3.9, Equation 3.10, and Equation 3.12 . Each equation defines flow for each one of the compartments of interest. The first compartment (Cp1) represents the ventricular system. The second compartment (Cp2) represents the intra-cranial subarachnoideal space. The third compartment (Cp3) represents the spinal compartment. Using Simulink ® (Mathworks, Natick, Massachusetts), the equations were initially implemented as if the system has reached equilibrium; then an oscillatory function was introduced to drive the system periodically.

The use of a periodic oscillatory function is mandatory to simulate the cerebral delta-blood volume (*Vsv*), which in turn modulates the compliance in the system, as formulated in Equation 3.4. The first model uses a sine function for these purposes. For convenience a one hertz frequency sine function is selected as it closely resembles the frequency of a healthy heart at rest.

The model is considered to represent the normal CSF dynamics if certain limits are maintained during the simulation:

a) Maintain the CSF pressure in physiological ranges. Normally the intracranial pressure is less than fifteen millimeters of mercury (15 mm Hg). , and not less than five millimeters of mercury (5 mm Hg).

b) Expel ten cubic centimeters (10 cc) of CSF from the intra-cranial subarachnoideal space into the spinal compartment, during each cardiac cycle. As ten cubic centimeters of blood enter the cranial cavity,

approximately the same amount of CSF leaves the cranial cavity, thus the Monroe-Kelly doctrine is respected.

c) Maintain a peak-to-peak pressure difference of less than one millimeter of mercury (1 mm Hg) between the ventricular and subarachnoideal compartments. As it has been established that "transmantle pressure" is less than 1 mm Hg.

d) Allow a very small variation of the ventricular system during the each cycle. A normal variation is considered less than two cubic centimeters (2 cc) of CSF.

This model consists of three independent compartments, Cp1 - Cp2- Cp3, and two communicating ducts, R1 and R2, between them. As stated earlier the Ventricular compartment (Cp1) and Cp2 are connected by a duct, which gives a resistance (R1) to the flow between the two of them. Similarly, compartments Cp2 and Cp3 are connected by a duct, which gives resistance (R2) to the flow between the two of them.

The CSF system is considered a closed system, which entails no volume variation. The total CSF is set at 150 cc.; being distributed as follows: Cp1 Ventricular compartment 25 cc, Cp2 Intra-cranial Subarachnoideal compartment 90 cc, and, Cp3 spinal compartment 35 cc. The initial pressure is set at a mid value of 7 mm Hg. Thus the compliance for each compartment follows the simple relation of Equation 3.1. Recall:

$$C_{0i} = \frac{V_{0i}}{P_{0i}}$$
$$i = 1,2,3$$

Therefore, the initial compliance (C_{01}) for Ventricular compartment(Cp1) is set to 25/7, the initial compliance (C_{02}) for Cp2 is set to 90/7, and the initial compliance (C_{03}) for Cp3 is set to 35/7.

Initial rough approximations of 1 mmHg-sec/cc for R1, and of 0.001 mmHg-sec/cc for R2, were selected by taking into consideration the calculated diameter of each duct. The R1 resistance is a lumped resistance representing the sum of the resistances from several anatomic structures. Each one of these structures, independently offer resistance to the CSF flow from inside of the brain to the intra-cranial subarachnoideal space. They are located at the junction between the two compartments and consist of five foramens or orifices (two Orifices of Monroe, two Orifices of Luschka and one orifice of Magendie) and a narrow duct, the Sylvius Aqueduct. Each of the orifices has a diameter of approximately 2 mm. The Sylvius Aqueduct is a narrow duct that communicates between the third and the fourth ventricles. It has a dimension of approximately 3.5 mm in diameter and an approximate length of 17.5 mm. The approximate cross sectional area is 9.6211 $mm^{2.}$

The R2 resistance represents the resistance to the flow at the junction of the intra-cranial subarachnoideal space and the spinal subarachnoideal space, essentially occurring at the Foramen Magnum. As suggested by its name, it has a large diameter of approximately 35 mm.; with a correspondent cross sectional area of 962.11 mm^2. In the interior of the foramen magnum runs the nervous tissue at its transition from medulla into spinal cord, with an approximately diameter of 25 mm.; thus rendering a cross sectional area of 490.87 mm^2. The effective area for CSF flow at the Foramen Magnum level is the one corresponding to the difference between the cross sectional areas of the Foramen Magnum(962.11 mm^2) and of the nervous tissue at the level of the cranio-cervical junction (490.87 mm^2). In consequence the effective area at the level of the foramen magnum is calculated to be 471.23 mm^2. The resistance to flow is proportional to the fourth power of the radius, while the area is proportional to the second power of the

radius. This will give us a resistance ratio between R2/R1 of $(471.23)^2/(9.62)^2$, which is a ratio of 2399, around three orders of magnitude.

Alpha represents the decrement of compliance, reciprocal of increment in stiffness, of the vessels' wall as a result of the additional blood volume held inside of the vessel during each cardiac cycle. If this decrement in compliance is integrated on the whole parenchyma it will be representing the whole decrement of the brain compliance per cardiac cycle, as a consequence of the cerebral blood flow coming inside of the brain vessels. As vessel's compliance diminishes per unit of increasing pressure, resulting from new blood volume added during systole, alpha has units of mm Hg^{-1}, and alpha (α) times delta-volume (V_{sv}) is equal to delta-compliance (C_δ) which has units of

$$\alpha V_{sv} = \frac{cc}{(\text{mm Hg})} = C_\delta .$$

In the present model this mechanism has been incorporated by describing the effect of the incoming blood volume on compliance; as a loss of compliance that is directly proportional to the in-coming blood volume, by a factor alpha (α), as explained in Equation 3.4. Recall:

$$ci(t) = ci_0 - \alpha v_B$$
$$i = 1,2$$

It is important to recall that the first model is just the starting point, and that further complexity will be gradually introduced to help us improve both the understanding of CSF dynamics, and the computer model.

After running the simulation on the first model, as shown in Figure 3.6, the volume (V1) of the first compartment (Cp1) varies from 23.88 cc to 23.72 cc, with a difference of 0.16 cc of CSF per cycle. The volume (V2) of the second compartment

(Cp2) varies from 91.12 cc to 80.79 cc, with a difference of 10.33 cc of CSF per cycle. The volume (V3) of the third compartment (Cp3) varies from 35 cc to 45.4 cc, with a difference of 10.4 cc of CSF per cycle. When comparing the graphs corresponding to volumes V2 and V3, it is easy to appreciate the mirror image between these two curves; it also becomes apparent how the spinal compartment (Cp3) behaves as a reservoir or a buffer for the volume that is expelled from the cranial cavity. As normally happens, the vast amount of CSF flow occurs between Cp2 and Cp3.

As shown in Figure 3.7, the pressure P1 in Ventricular compartment(Cp1) settles to a very stable condition oscillating between 6.67 and 9.6 mms Hg. Pressures P2 and P3 in Cp2 and Cp3 maintain a very stable oscillation between 7.06 and 9.08 mm Hg.; thus the pressure in all the system is maintained below 15 mm Hg. Also note that peak to peak pressure difference between Ventricular compartment(Cp1) and Cp2 is 0.52 mm Hg, which is a difference of less than 1 mm Hg.

This first approach fulfills the previously expressed needed criteria for acceptance as representative of the CSF dynamics.

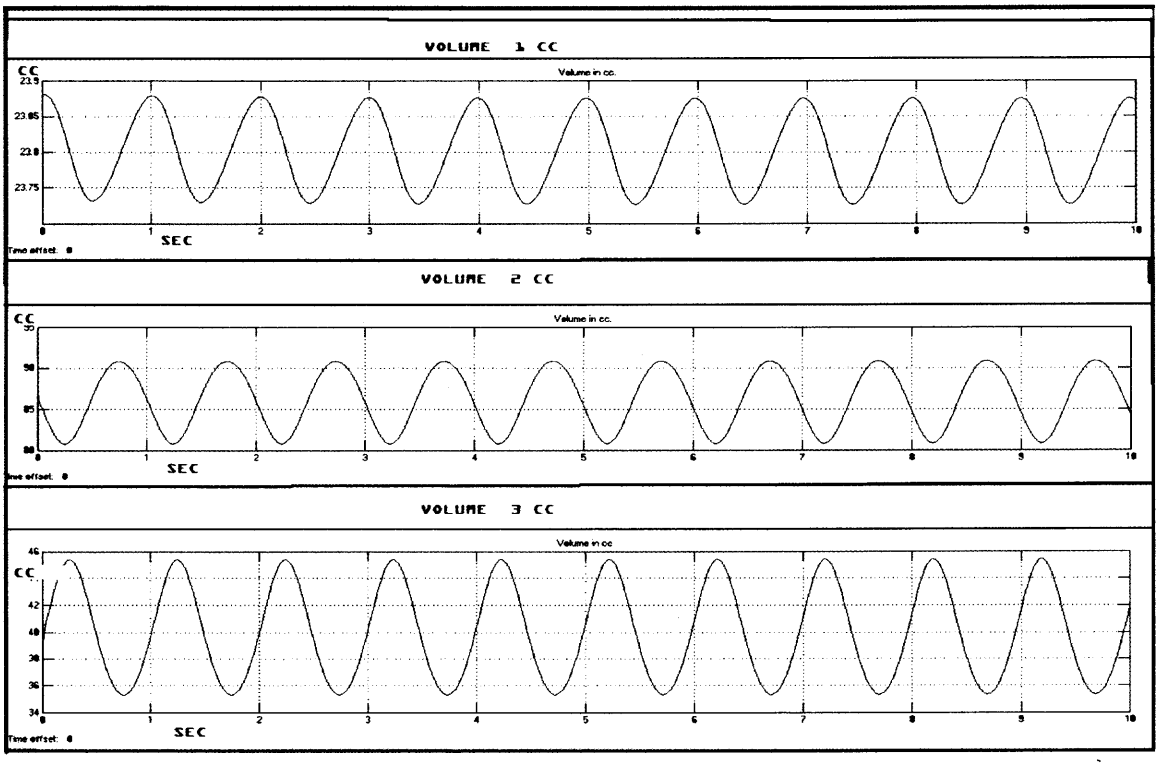

Figure 3.6 Sine driven model; behavior in time of the volume in cc of each compartment.

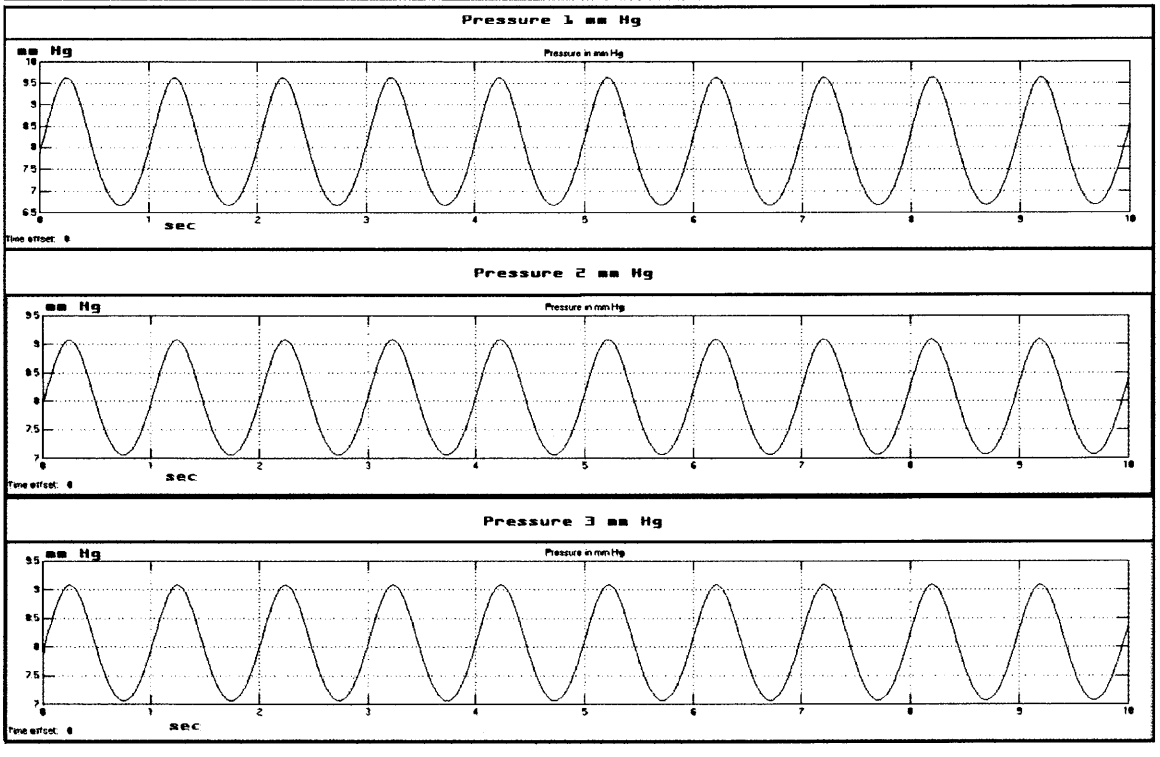

Figure 3.7 Sine driven model; behavior in time of the pressure in mm Hg of each compartment.

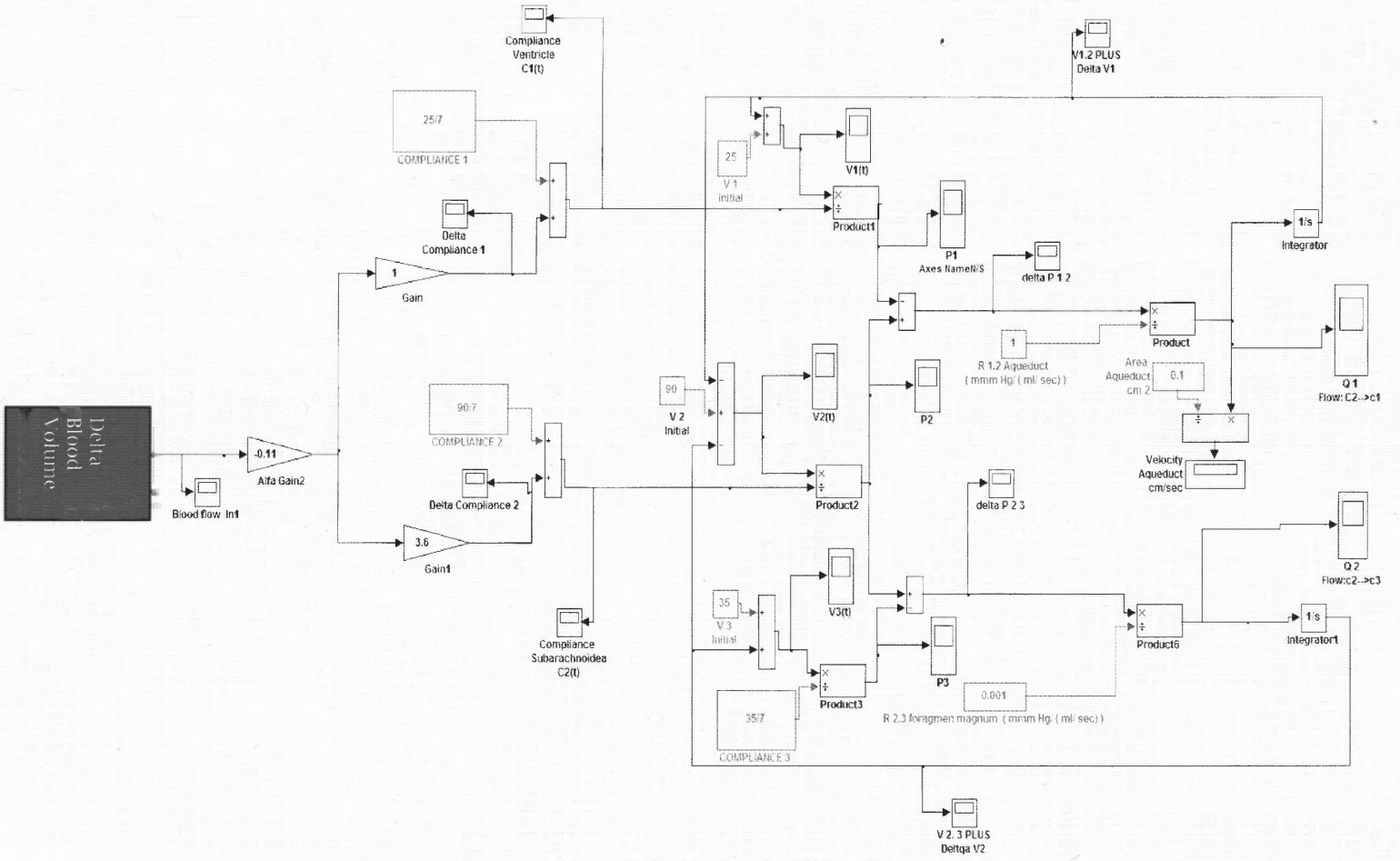

Figure 3.8 Delta blood-volume driven model.

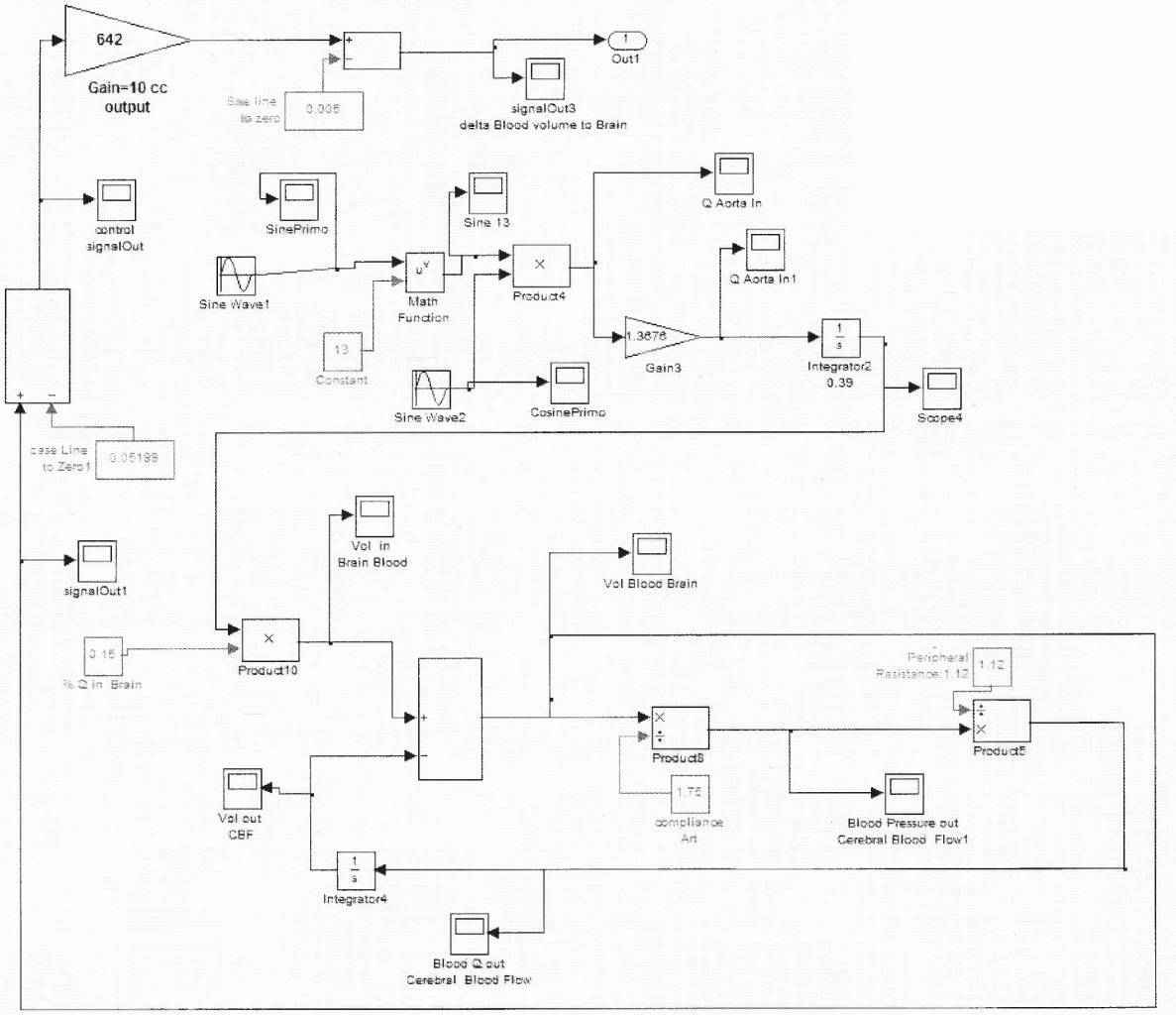

Figure 3.9 Delta blood-volume function.

3.3.2 Cerebral Delta Blood-Volume Function

The model is improved by replacing the sine driving function by a continuous function describing the blood volume variation in time, during a cardiac cycle. The sine function in the model was replaced by a function described by Stevens et al., who uses the Fourier series to mimic the cardiac output. Stevens et al described a periodic differentiable function that adequately represents the cardiac output by multiplying the thirteen power of a sine function by a cosine function with a fixed phase angle:

$$Q = (\sin^{13}(\omega t))(\cos(\omega t + \varphi))$$

The incoming cerebral blood volume per cardiac cycle is obtained by taking fifteen percent of the cardiac output, and integrating it in time. Pressure inside the vessel is computed by dividing the incoming volume by compliance. When this pressure is divided by the vascular resistance a mathematical function of the cerebral blood flowing-out is obtained. By integrating this signal, the volume-out is obtained; which in turn is subtracted from the volume-in giving the amount of volume present at every moment in the cerebral vasculature. The cerebral delta-blood volume sub-function is presented in Figure 3.9. Several conditions have to be matched by this calculated cerebral blood flow to meet real events. The cerebral delta-blood volume waveform is illustrated in the Figure 3.10.

First, the total cerebral delta blood-volume per heart beat has to be fifteen percent of the cardiac stroke volume. Being the cardiac stroke volume roughly seventy cubic centimeters, the calculated fifteen percent is equal to ten and a half cubic centimeters. That means that a signal representing the additional volume present inside the vessels should have a peak volume of 10 cc. Second, this function has a period of approximately eight hundred milliseconds (0.8 sec.), resembling the normal heart cycle period. Third, in

the normal blood flow during the first third of the period the blood is being injected into the vascular system from the heart; meanwhile during the other two thirds of the period the blood is flowing against the peripheral resistance propelled by the force normally stored in the arterial walls. Fourth, peak volume should be achieved by the end of the first third of the period. Fifth, the flow should decay exponentially. Sixth, by the end of the period the volume-inside the vasculature should come back to the value at the beginning of the period.

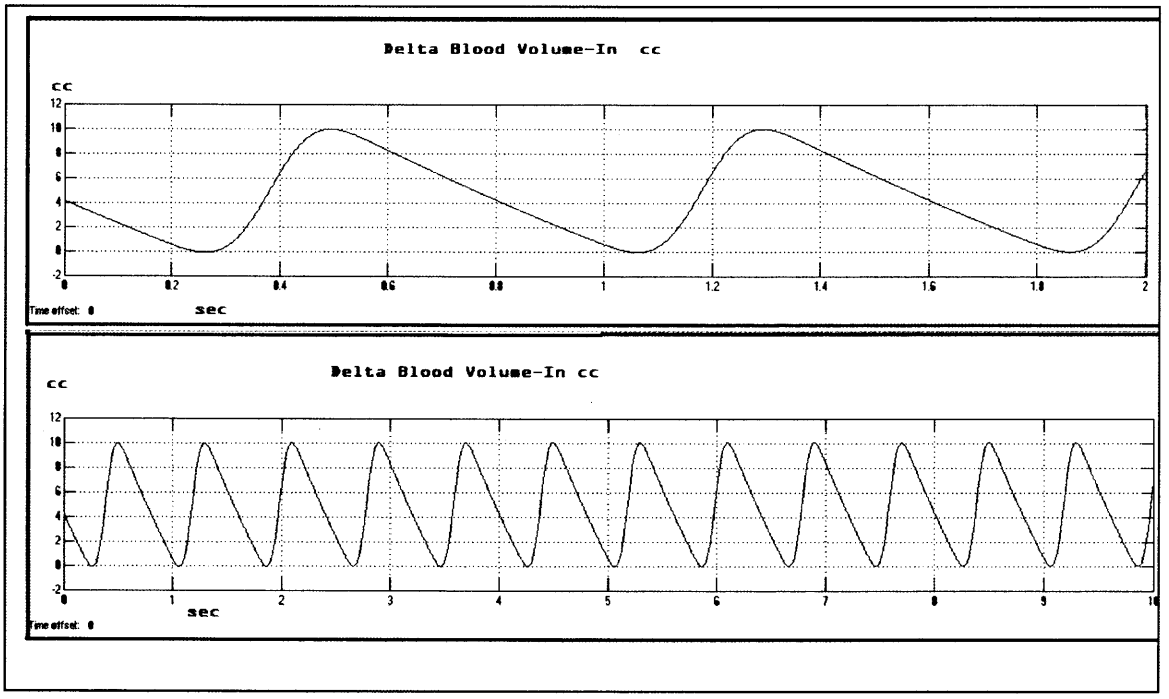

Figure 3.10 Cerebral delta blood-volume signal. The upper image is a close up of the inferior image for a detailed examination of systole (1/3) and diastole (2/3) duration during the period.

After running the Delta blood-volume driven model, as shown in Figure 3.11, the volume (V1) of the first compartment (Ventricular compartment(Cp1)) varies from 23.92 cc to 23.81 cc, with a difference of 0.11 cc of CSF per cycle. The volume (V2) of the second compartment (Cp2) varies from 91.18 cc to 80.69 cc, with a difference of 9.49 cc

of CSF per cycle. The volume (V3) of the third compartment (Cp3) varies from 35 cc to 45.42 cc, with a difference of 10.42 cc of CSF per cycle.

As shown in Figure 3.12, the pressure P1 in Ventricular compartment(Cp1) settles to a very stable condition oscillating between 6.67 and 9.6 mms Hg. Pressures P2 and P3 in Cp2 and Cp3 maintain a very stable oscillation between 7.06 and 9.08 mm Hg.; thus the pressure in all the system is maintained below 15 mm Hg. Also note that peak to peak pressure difference between Ventricular compartment(Cp1) and Cp2 is 0.52 mm Hg, which is a difference of less than 1 mm Hg.

After introducing the function for cerebral blood volume, the model behavior still represents the normal CSF dynamics, fulfilling all the required boundaries to consider it a representative model of CSF dynamics.

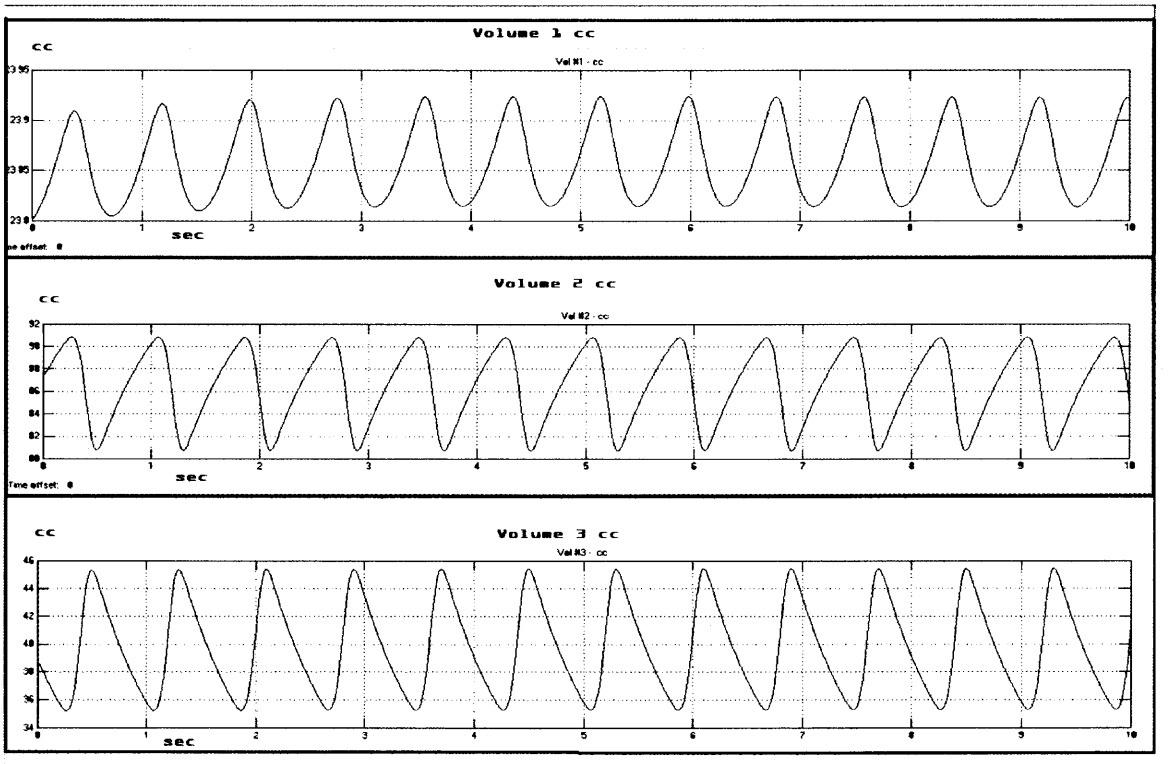

Figure 3.11 Volume behavior in cc. from the three compartments after introducing Cerebral Blood flow signal.

While in the previous model the sinusoidal wave allows an appreciation of the general behavior, the introduction of a different wave permits a more distinctive analysis of the influence of the heart systole in the CSF dynamics.

After introducing the signal representing cerebral blood flow, the signal shape in the CSF graphs changes reflecting the pattern generated by the heart. Pattern which is easy to follow in the volume and pressure curves. This pattern provides a better way to analyze how each compartment is influenced by heart systole, and how it returns back to its previous state. Thus the signal has a sharp rise, caused by the blood coming in, and a slower decrease as the blood flows out by venous drainage during each heart cycle. These two distinctive regions in the wave shape permits to well-define whether the heart systole influences certain compartment by increasing or decreasing its volume. As shown in Figure 3.11 the volume waves of Cp3 and Cp2, are mirror images, presenting an increment in Cp3 and a decrement in Cp2 as systole takes place. In Ventricular compartment(Cp1) there is a lag in the volume response to the influence of systole and a complex response, that will be analyzed in the next section, with an initial volume increment followed by a volume decrement during systole.

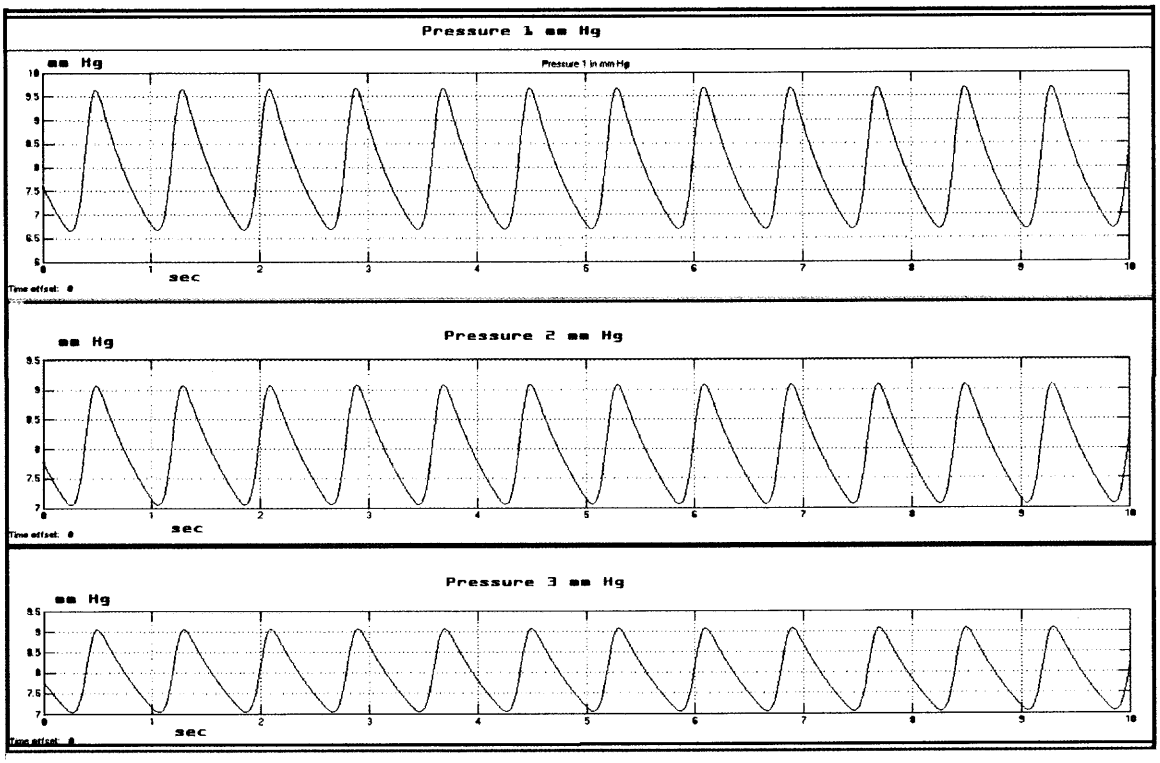

Figure 3.12 Pressure behavior in mm. Hg from the three compartments after introducing Cerebral Blood flow signal.

The blood-volume new waveform also allows comparing the timing and behavior of pressure in each compartment; as is shown in Figure 3.12. Normally they are synchronized, but as we will discuss later in the next two sections they can become unsynchronized.

It is evident in the Cp2 into Ventricular compartment(Cp1) flow waveform, as well as in the Cp2 into Cp3 flow waveform, the influence in shape and timing produced by the in-coming cerebral blood flow. As shown in Figure 3.13, there are at least four different CSF flow stages which are matched to the CSF flow documented by Naidich with phase-contrast cine MRI. Taken at 200 milliseconds intervals the wave forms corresponding to, and labeled as "Flow C2→C1"; and labeled as "Flow C2→C3" are divided in four stages per each cycle.

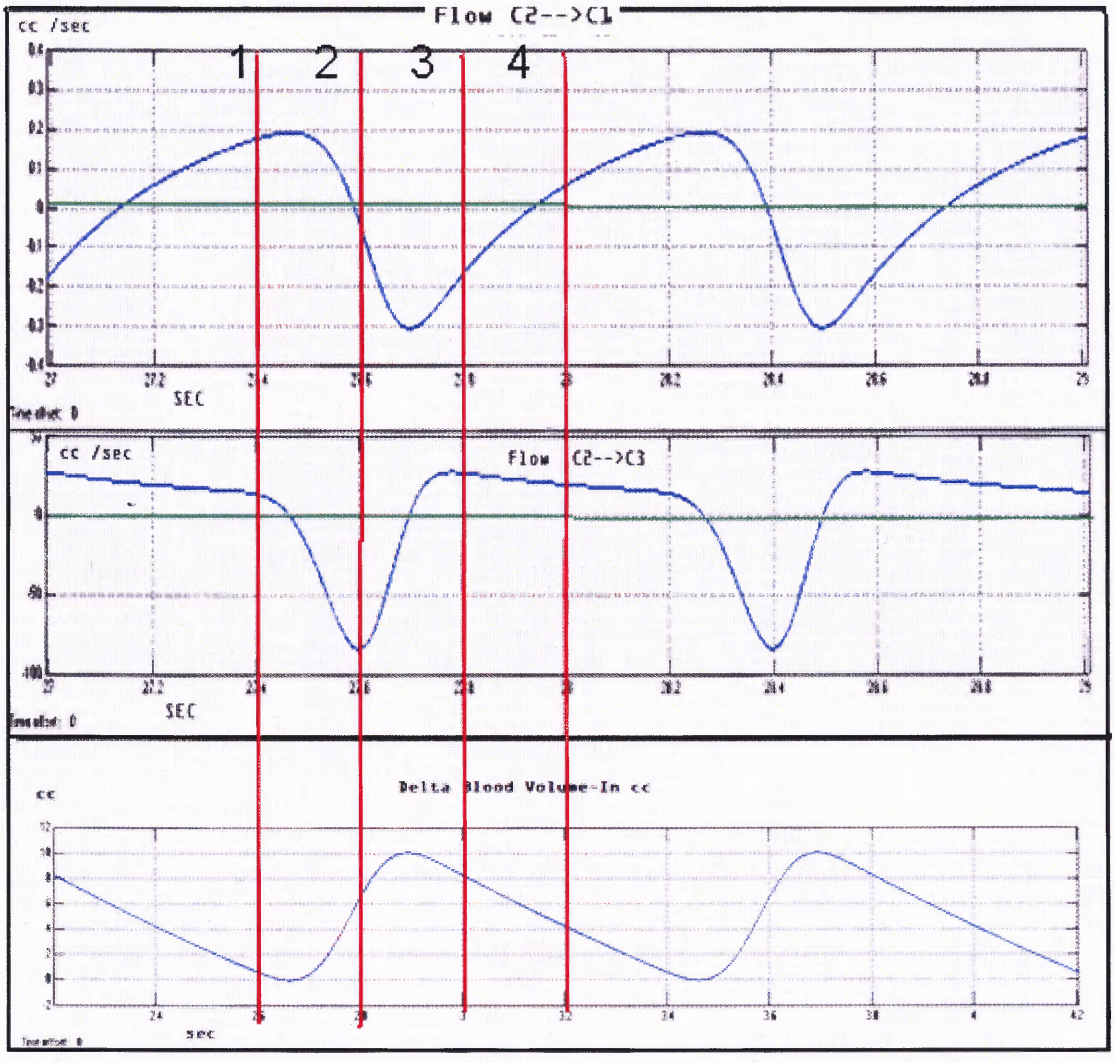

Figure 3.13 Showing the four stages of the CSF flow during a cycle, in relation with the delta-cerebral blood volume. Note the green line divides positive values showing cephalic direction, from negative values showing caudal direction.

Stage 1: At the end of diastole the CSF in the ventricular Cp1, Subarachnoideal Cp2, and Spinal Cp3 compartments is flowing cephalic.

Stage 2: At the initial systole CSF in Ventricular compartment(Cp1) still runs cephalic, while CSF flow in Cp2 and Cp3 rapidly turns direction going caudally.

Stage 3: As the systole progresses the flow in all the compartments is directed caudally. At the end of this stage the CSF in Cp2 and Cp3 compartments is flowing cephalic, while CSF in Ventricular compartment(Cp1) is still flowing caudally.

Stage 4: The first milliseconds of this stage resembles the end of previous stage where CSF in Cp2 and Cp3 compartments is flowing cephalic, while CSF in Ventricular compartment(Cp1) is still flowing caudally. At the end of this stage, CSF in Ventricular compartment(Cp1) changes direction going cephalic, and setting all the conditions to start a new cycle at stage 1.

Note that a green line divides the zero crossing, where the positive value denotes cephalic direction and the negative value denotes caudal direction of the CSF flow. This information is summarized in Table 3.1; comparing the results from the model, of normal CSF oscillations, during the cardiac cycle; with the data from Table 2.2, in chapter four, where the results from the studies done by Naidich with Phase Contrast Cine MRI were collected. In Table 3.1, a column on the right has been added corresponding to the stage analyzed in Figure 3.13.

Table 3.1 Normal CSF Oscillations during a Cardiac Cycle. Nolte Column on the Right, Each Stage Corresponds with the Stages Shown on Figure 3.13

MRI Stage	Compartment	Cephalic	Caudal	Slow Down	Changing Direction	Model Stage
1	Ventricular	↑↑				1
	Subarachnoideal	↑↑				
	Spinal	↑↑				
2	Ventricular	↑↑				1→2
	Subarachnoideal	↑↑				
	Spinal		↓↓			
3	Ventricular	↑↑				2
	Subarachnoideal		↓↓			
	Spinal		↓↓			
4	Ventricular				↓↑	2 (end)
	Subarachnoideal		↓↓			
	Spinal		↓↓			
5	Ventricular		↓↓			3
	Subarachnoideal		↓↓			
	Spinal			↓		
6	Ventricular		↓↓			3
	Subarachnoideal			↓		
	Spinal				↓↑	
7	Ventricular			↓		4
	Subarachnoideal	↑↑				
	Spinal	↑↑				
8	Ventricular				↓↑	4
	Subarachnoideal	↑↑				
	Spinal	↑↑				

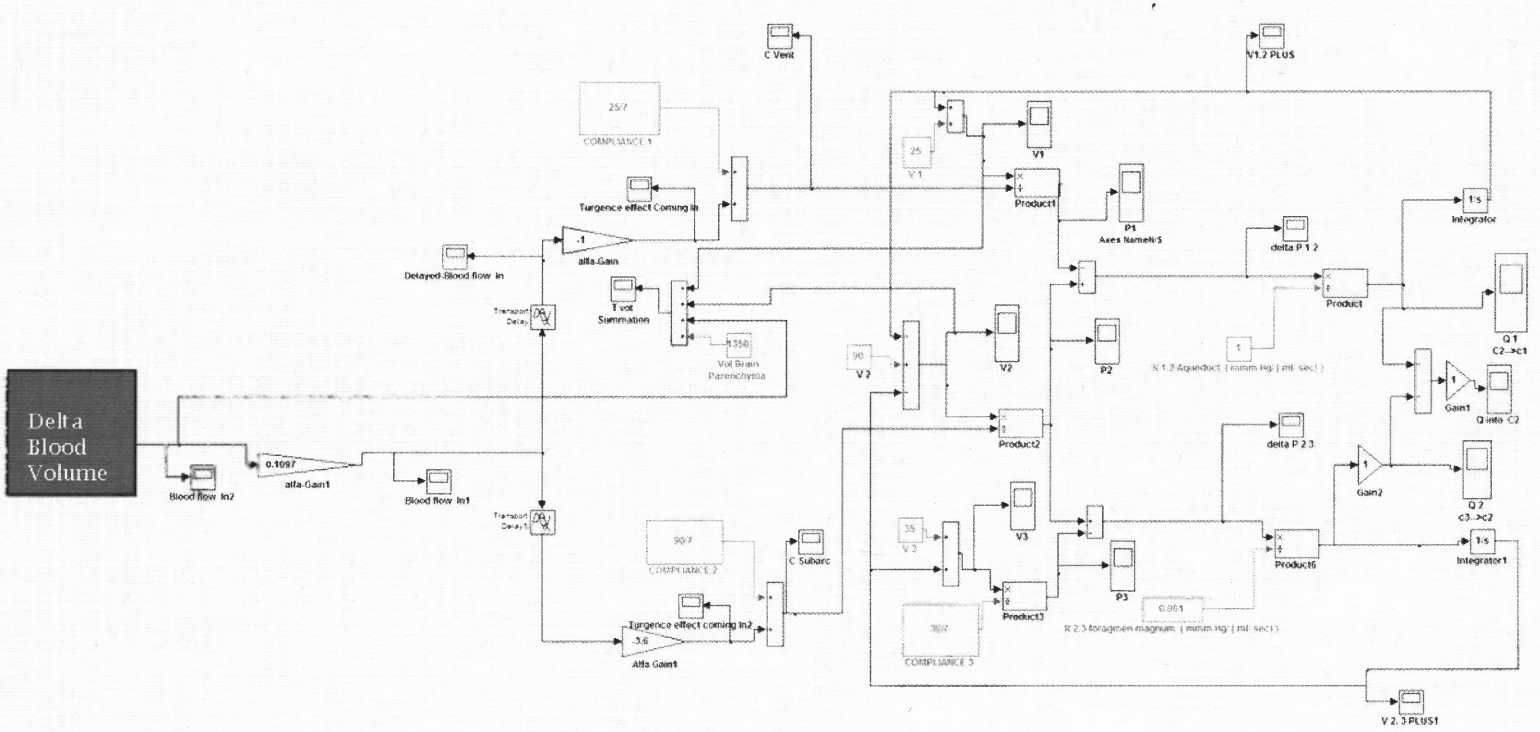

Figure 3.14 Delta blood-volume driven with variable delay

3.3.3 Importance of Two Vascular Territories. In the third model it is important to examine the effect of the two venous vascular territories in the brain. For this purpose a delay was first introduced into the blood flow coming into the ventricular walls, thus representing the lag described in the deep venous circulation around the ventricles.

Initially the phase shift was set to zero, and then gradually was incremented in intervals of 200 msec. until a whole period of 800 msec was covered. As previously stated, the closest anatomical parallel to the duct between Ventricular compartment(Cp1) and Cp2 is the Sylviu's Aqueduct (SA); a structure that has been studied with great interest for many years. One of the actual debated topics is the normal CSF flow profile through the aqueduct. This interest is probably related to the long time and still prevalent assumption that altered SA CSF circulation, mainly aqueduct stenosis, is the cause of communicating Hydrocephalus. Notwithstanding the clarifications already made of the lumped elements in R2, this model results will first be compared with some published data.

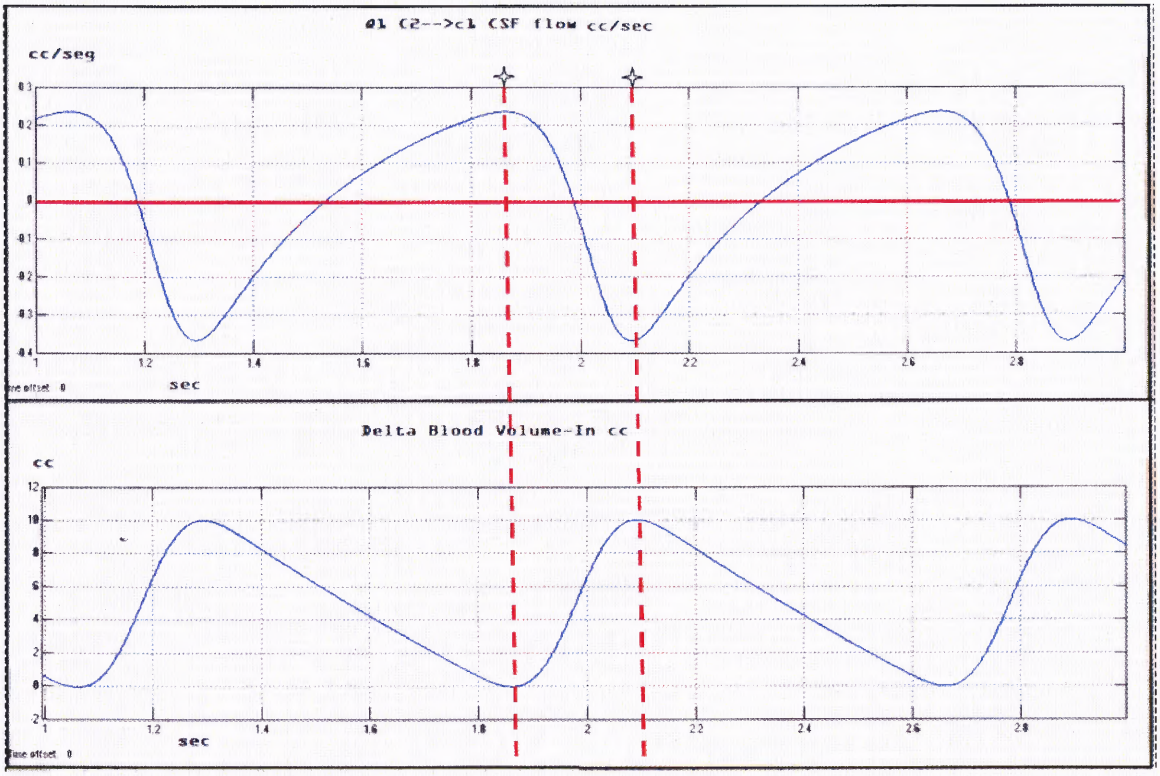

Figure 3.15 Showing relationship between the Ventricular compartment(Cp1) -Cp2 flow (figure on the top) and the Cerebral Blood Volume (figure on the bottom). Systole: Space limited by stars.

As illustrated by Naidich et al. using phase-contrast cine MRI, during the normal cycle at the end of heart diastole all the CSF flow is directing cephalic. As systole comes in, there is a documented lag in time for the flow at the Sylvius Aqueduct to change direction into caudal. As a result, when phase contrast cine MRI is used to correlate the direction of CSF flow with the heart cycle, CSF flow initially appears going cephalic, and then it shifts its direction going caudally during the cardiac systole. As shown in Figure 3.15 the model reproduces this CSF dynamics through the aqueduct. During the first portion of the systole while the CSF is being pumped from Cp2 into Ventricular compartment(Cp1), the flow through the aqueduct is directed cephalic. After approximately 10 msec. the flow changes going in the opposite direction, and

maintaining this direction into nearly half of the heart diastole. Finally the CSF changes again going in the cephalic direction until the mid portion of systole.

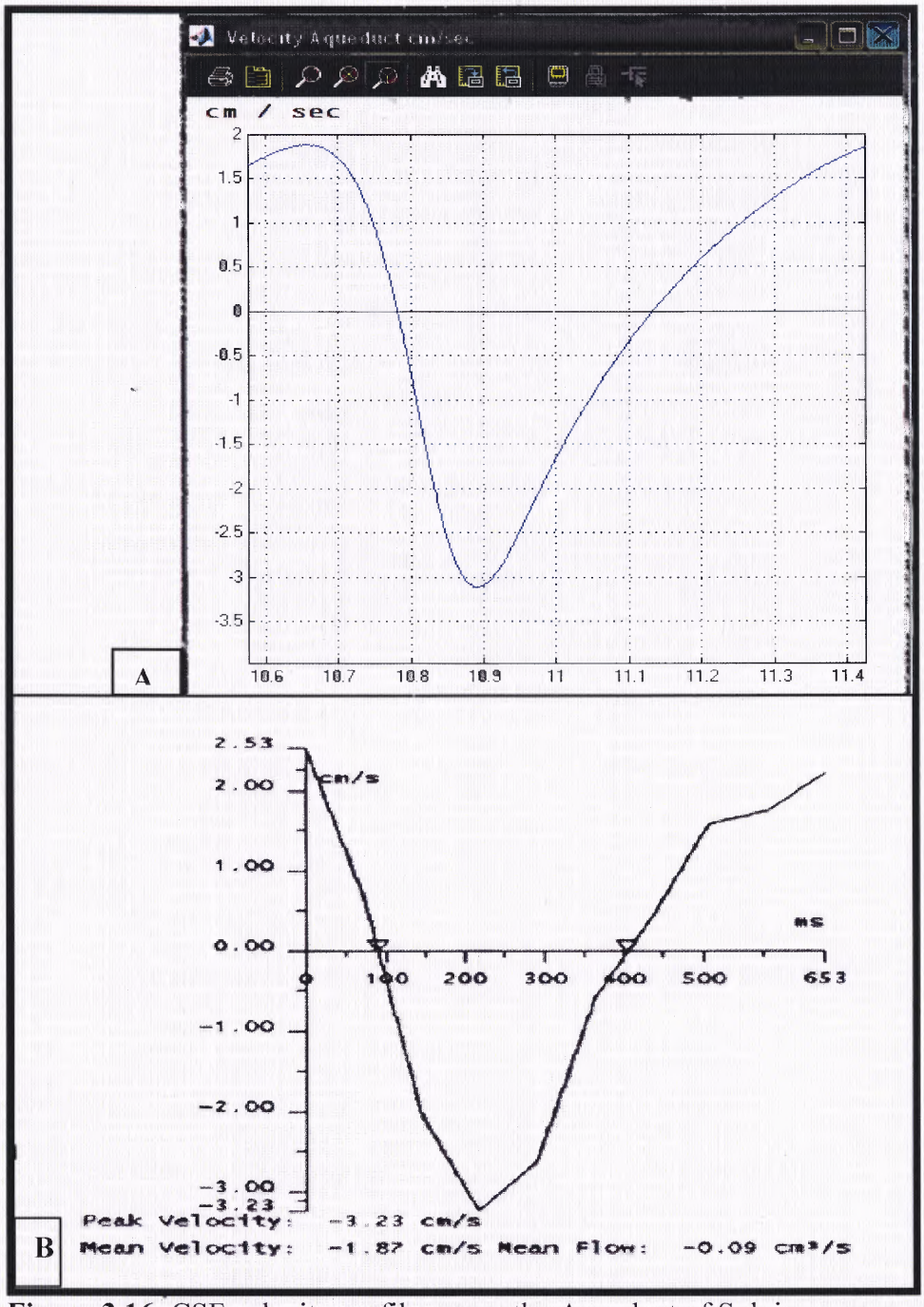

Figure 3.16 CSF velocity profile across the Aqueduct of Sylvius compared to the profile across Ventricular compartment(Cp1) and Cp2 in the model. The inferior graph (B) is taken from Phase contrast Cine MRI in a normal patient (Bateman et al. 2005), compared to the graph (A) on top from the model. Velocity in cm/sec. Note matching, shape, values and period.

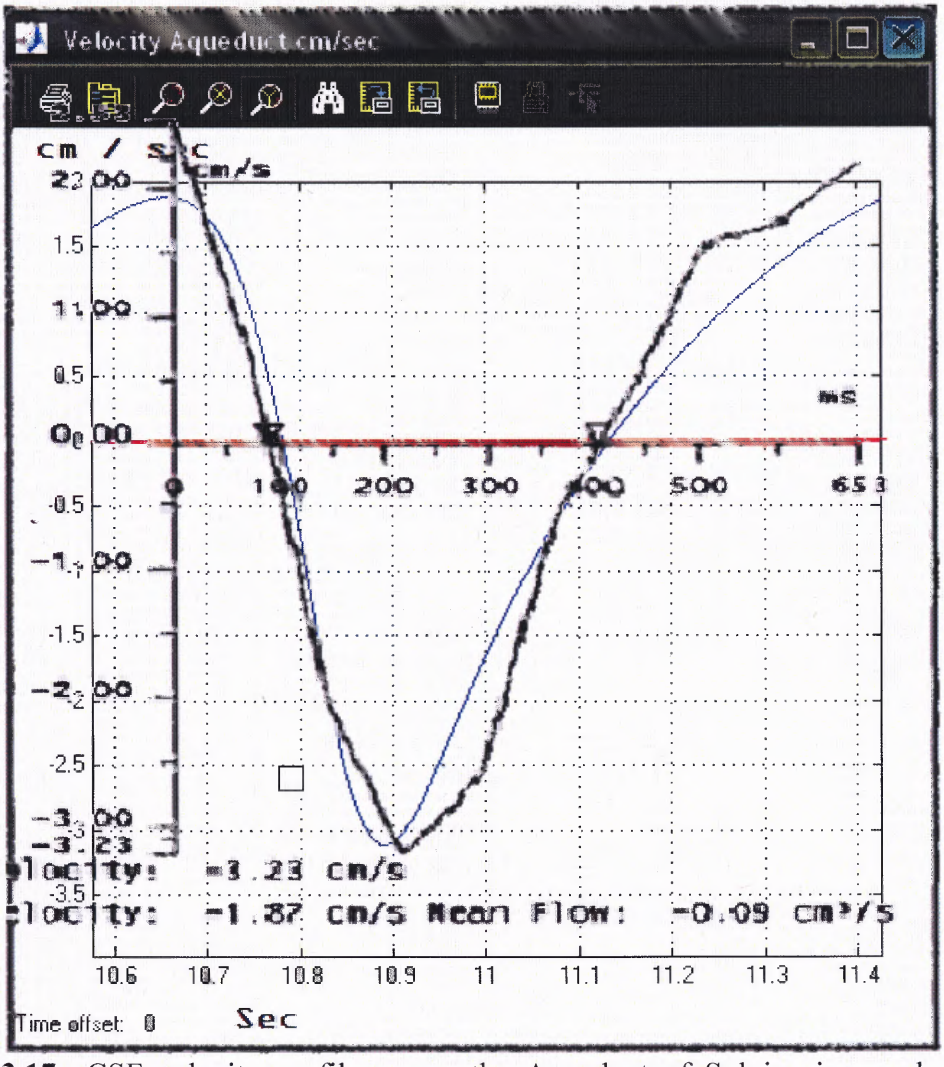

Figure 3.17 CSF velocity profile across the Aqueduct of Sylvius imposed over the profile across CSF velocity between Cp1 and Cp2 in the model. The graph taken from Phase contrast Cine MRI in a normal patient (Bateman 2005), is imposed over the graph from the model. Velocities in cm/sec. scales have identical intervals, to allow comparison between graphs. Note matching, shape, values and period.

It is also of interest to review certain published data with respect to the AS. CSF circulation, and compare them to the model. As shown in Figures 3.16 and 3.17 the velocity of the CSF through the aqueduct has a unique shape, determined by the changing delta pressure between Ventricular compartment(Cp1) and Cp2. The peak velocities have been calculated by several authors, and range from approximately. +2 cms/sec to approximately -3.23 cms/sec.; the plus sign denotes cephalic direction and the minus sign denotes caudal direction. Compared to the data obtained by Bateman et al. (2005) with

the ones obtained in the model a nearly perfect matching in values and shape are obtained.

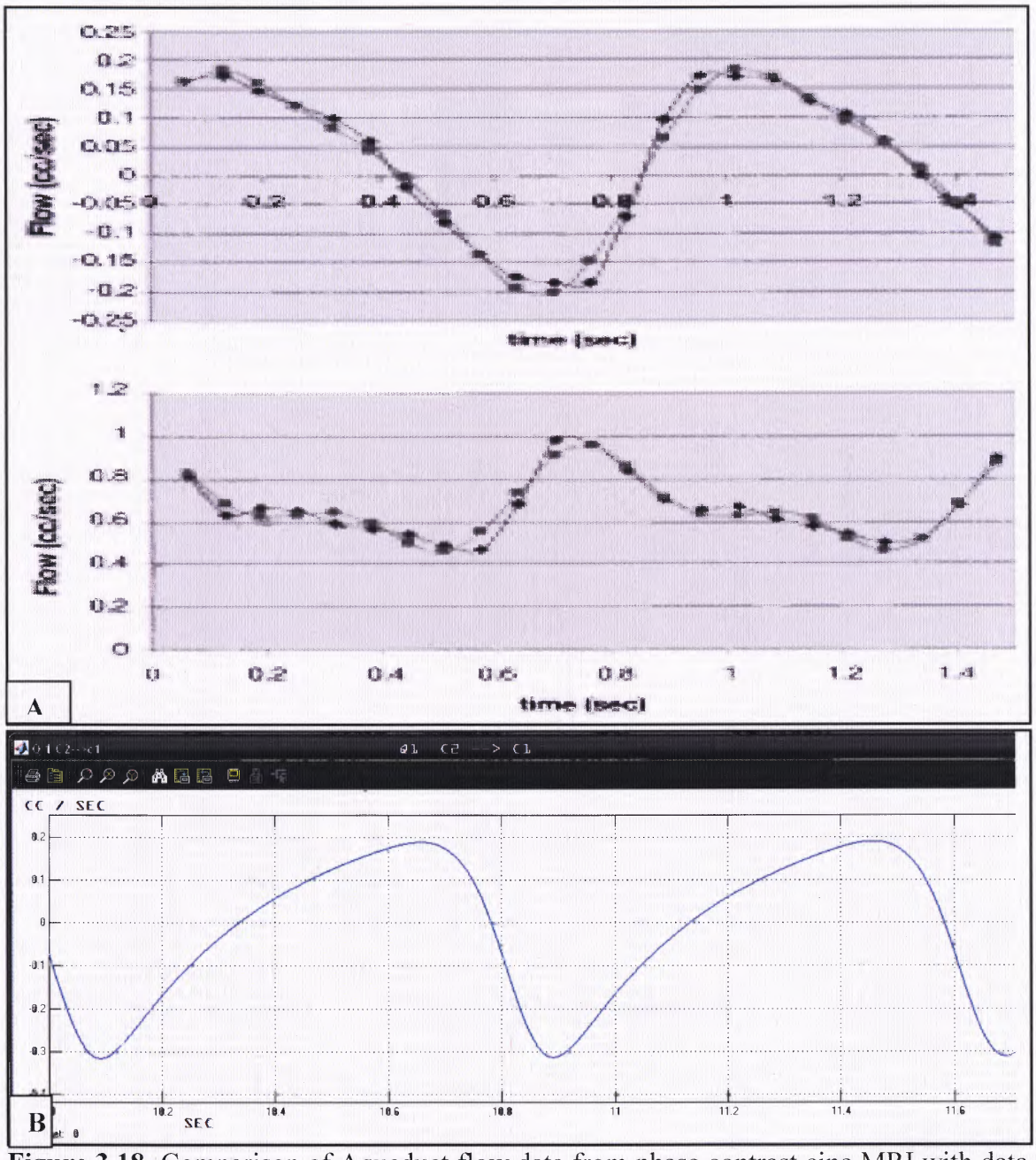

Figure 3.18 Comparison of Aqueduct flow data from phase contrast cine MRI with data obtained by the model. A) Shows data obtained by Wagshul et al. (2006), of Aqueduct CSF flow (up), in relation to carotid arterial blood flow (below). B) Flow data obtained in the model in cc/seg.

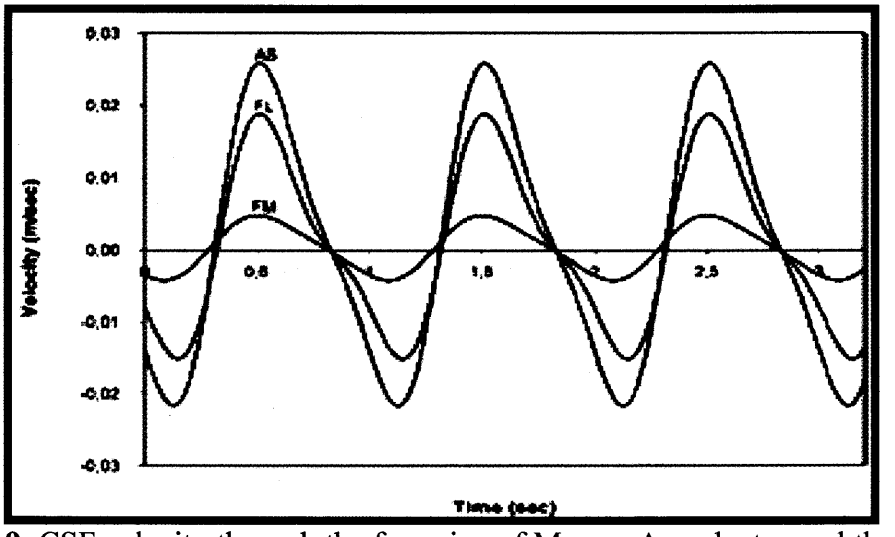

Figure 3.19 CSF velocity through the foramina of Monro, Aqueductus and the foramina of Magendie. Data collected on dogs.
Modified from Linninger, Penn at al 2005.

Also matching values of flow are obtained when compared to studies done by different independent authors, as is demonstrated in Figure 3.18. If the diameter of the aqueduct is calculated at 0.35 cms, the conversion between flow and velocity is obtained by multiplying the velocity by cross sectional area. In this case the area is equal to 0.1 cms^2, a factor that matches perfectly the three obtained data. Diameter anatomical dimensions of the Aqueduct of Sylvius (AS) 0.35 cm., peak velocity of the CSF across the AS 3.23 cm/sec, and flow across the AS 0.2 cc/sec. These results confirm once more the validity of the model.

Even though great expectations were given to the possible influence on the system of the delay in the signal representing the incoming blood flow, it was not possible to determine any significant change in the volume , or pressure dynamics of any compartment of the system when different delays were introduced. Never the less, the shape and peak-values for the CSF flow between Ventricular compartment(Cp1) and Cp2 were diverse when 3 different delays were introduced each 0.2 sec, starting at the initial no delay through a whole period (0.8 sec) at the intervals: 0.2 sec, 0.4 sec., and 0.6 sec.

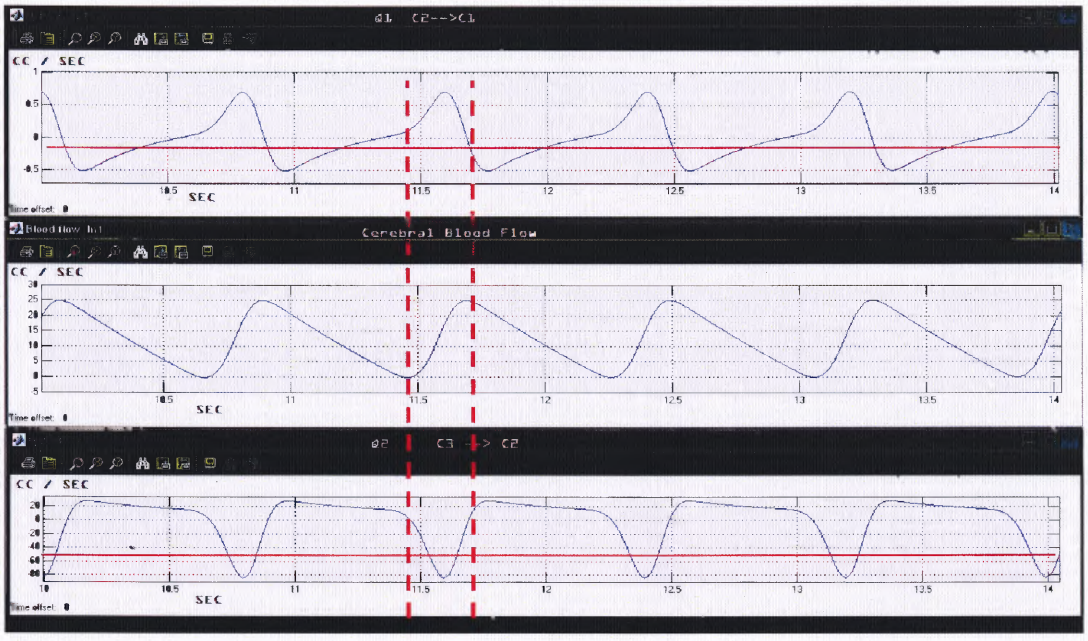

Figure 3.20 Showing the effect on the first component of the wave shape at 0.2 sec input delay of the cerebral blood flow signal to Ventricular compartment(Cp1). Note the direction of the CSF is now cephalic during the whole systole.

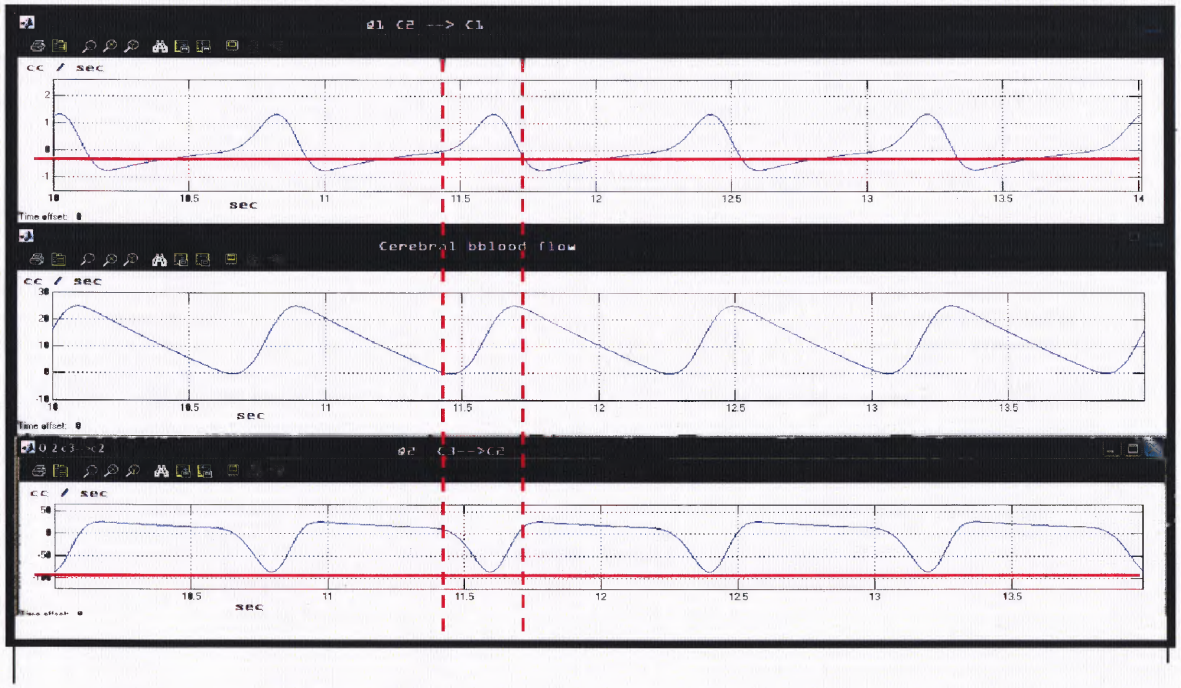

Figure 3.21 Showing the effect on the first component of the wave shape at 0.4 sec input delay of the cerebral blood flow signal to Ventricular compartment(Cp1). Note the direction of the CSF is now cephalic during the whole systole and that zero crossing , denoting change in CSF direction occurs at the beginning of heart systole.

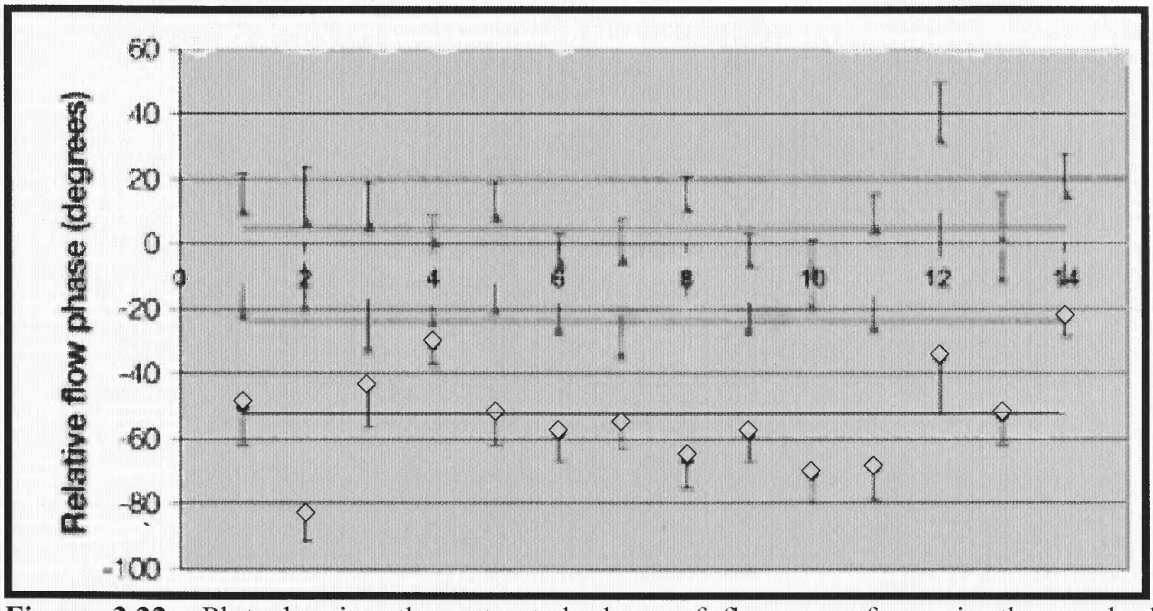

Figure 3.22 Plot showing the extracted phase of flow waveforms in the cerebral aqueduct (blue diamond), in the prepontine (PP) cistern (square), and at the level of C-2 (triangle), calculated relative to the average phase in the CAs, shown for 14 study participants.

This unexpected result is explained when reviewing data published by Egnor et al. as shown in Figure 3.22 where the phase lag of the CSF aqueduct flow wave form was calculated with respect to the blood pressure wave. As it is clearly seen great variation is observed (diamonds in the picture) in the phase shift from fourteen normal subjects. Thus once more the model confirms its dynamic behavior with published data. In this case there are not any consequences in volume distribution when the phasic relation between the aqueductal CSF flow and the cerebral blood flow varies. The model is flexible enough to provide a way of creating different shifts in the timing between the CSF flow and cerebral blood flow.

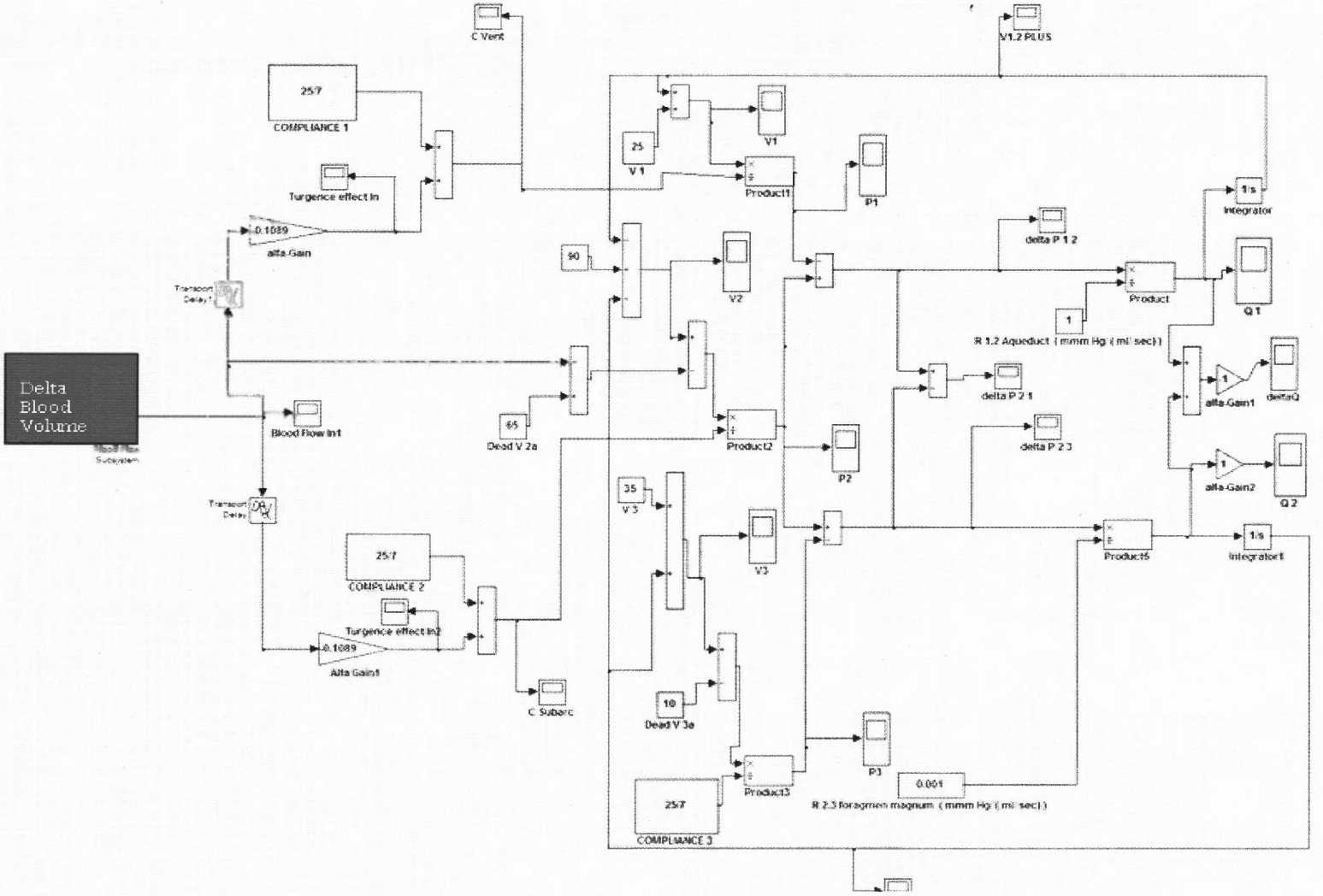

Figure 3.23 Unstressed volume model.

3.3.4 Introduction of Unstressed Volume

The concept of Unstressed volume is taken into consideration. A Unstressed volume is the one that is stored inside of a compartment with zero pressure. As the lateral and third ventricles will collapse if all the CSF is drained; these cavities are considered as having unstressed volume. In contrast the subarachnoideal space is enclosed between the pia matter beneath and the arachnoid membrane above. The arachnoid membrane is closely adjoined to the dura matter. The dura matter is adherent to the cranial cavity. The cranial cavity which is inelastic does not collapse when the CSF is drained. Thus we consider in this model that the cranial cavity forms part of the walls of the sub-arachnoid compartment, and as a consequence unstressed volume should be taken into consideration. A similar situation is encountered in the spinal subarachnoid space in which the dural sac does not totally-collapse when the CSF is drained. So it was found appropriate to include a dead-space in the spinal compartment too. The advantage of including dead space, in the model, is to model the compliance of the three cavities in a more unified way. Unstressed volume was not introduced in the Ventricular compartment(Cp1). Unstressed volume in the amount of 65 cc was introduced in the Cp2, and a Unstressed volume of 10 cc was introduced in the Cp3 compartment. Thus the compliance was unified to 25/7 cc/ mm Hg in all three compartments.

After the introduction of unstressed volume, the model performs adequately within the expected ranges. Nevertheless, unstressed volume is important to maintain a unified compliance in every compartment of the system. Even though, the introduction of the Unstressed volume did not alter significately the model behavior, it provided a more balanced and more unified behavior of the pressures in the three compartments.

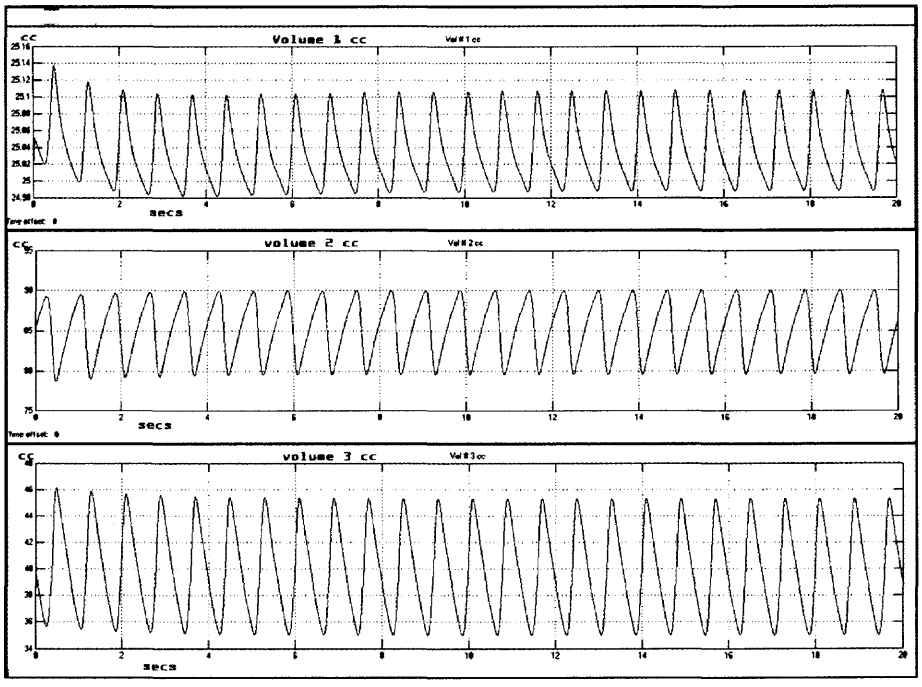

Figure 3.24 Volumes in the three compartments after introducing unstressed volume in the model. The system dynamics is still preserved.

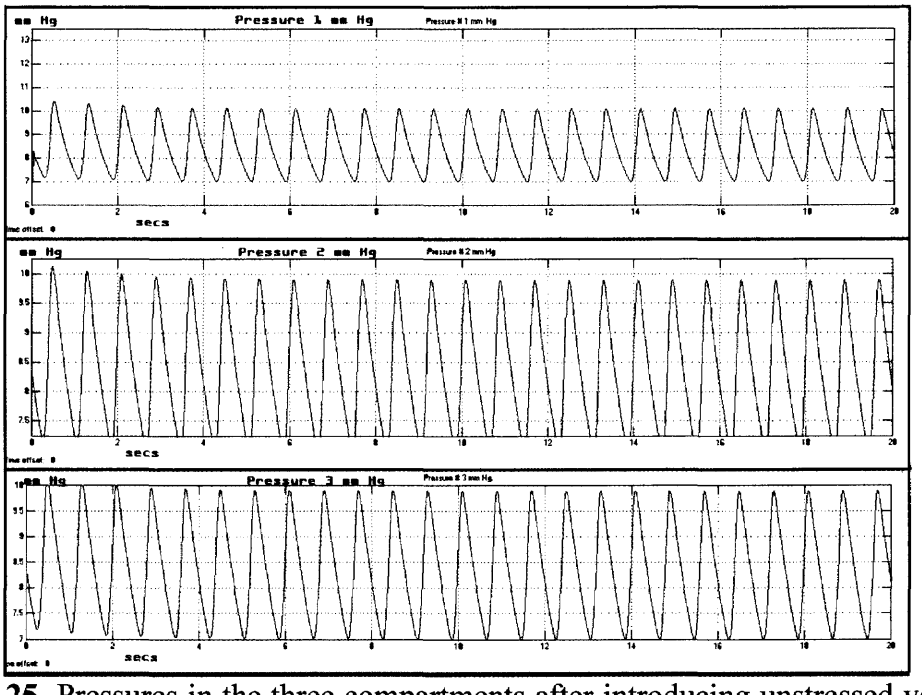

Figure 3.25 Pressures in the three compartments after introducing unstressed volume in the model. The system dynamics is still preserved.

Unstressed Volume with Several Blood Flow Signal Delays. Since the arrival of the phase contrast cine MRI for the study of CSF dynamics, the morphology and characteristics of the aqueduct flow has caught the attention of nearly every author. Even though a number of studies have been published, no one has reached a firm and valid conclusion. As compliance of each compartment in grand part dictates the behavior of the system; then by varying the relation and timing of the compliance variation in Ventricular compartment(Cp1) and Cp2, the flow dynamics between these two compartments should vary. Based on the anatomic and physiologic studies that determine two different vascular compartments in the brain; time delay between Ventricular compartment(Cp1) and Cp2 was introduced again, in the Unstressed volume model. Several different delays in timing of the incoming delta blood–volume flow to Ventricular compartment(Cp1) were introduced, and the system response was evaluated.

Several delta blood-volume delays were introduced in Ventricular compartment(Cp1); starting from 0.02 sec, with increasing intervals of 0.02 sec, until 0.08 sec was reached; and then intervals of 0.2 sec were introduced until 0.8 sec of delay was reached. The system response to every one of the different delays is illustrated in the same graph, in Figure3.26. As expected the CSF flow profile between Ventricular compartment(Cp1) and Cp2 is influenced by the timing of the incoming blood flow. As shown in Figure 3.26; the amount of CSF interchanged between Ventricular compartment(Cp1) and Cp2 varies with each of the blood-flow delays introduced in Ventricular compartment(Cp1). Note in the Figure 3.26 the different amount of CSF flowing in and out of Ventricular compartment(Cp1). In the case of least variation the volume varies between 25.01 and 25.02 cc; while in the greatest variation V1 varies from 24.7 to 25.4 cc. V1 volume variation seems very different in each case, since a variation

of 0.7 cc is at least one order of magnitude greater than a variation of 0.01cc. Nevertheless, when the variation is evaluated in respect to the amount of CSF hold inside of the ventricular system, the difference in variation seems to loose importance; as no one will argue that 25.02 cc is not very different from 25.4 cc., or 24.6 cc of CSF. Also, due to technical constraints in sensitivity of MRI, it is not easy to quantify these small differences in real experiments.

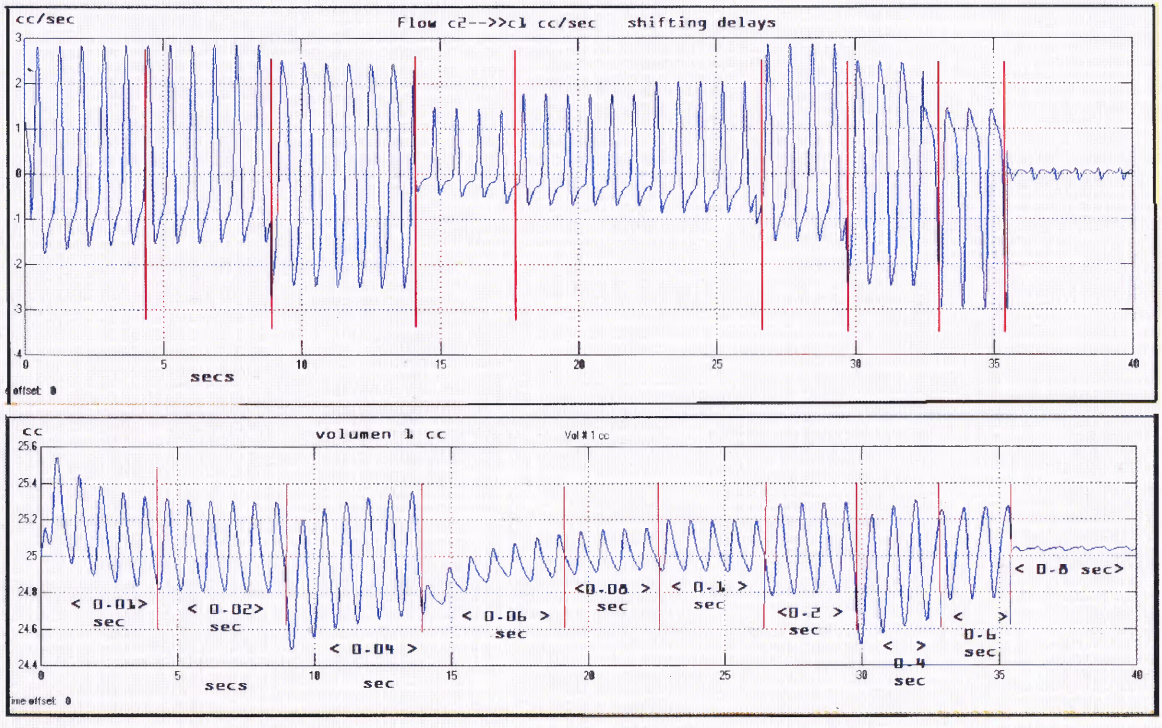

Figure 3.26 Volume and Flow response to several times delays in the incoming blood flow signal into Ventricular compartment(Cp1). in the none-stressed volume model.

When Figure 3.26 is examined, it is relatively easy to recognize the varying response in the amount of flow, and consequently in volume to the different introduced delays. It is tricky though, to recognize the changes in the wave form , and profile; including the peak flow and peak velocity; both of which has been widely studied in nearly every publication done with phase contrast cine MRI.

In order to facilitate the visualization of the waves a series of close-up figures of each time delay have been included. Delays included in Figure 3.27 correspond to: A: 0.8. sec, B:0.6 sec , C:0.4sec, D:0.2 sec, E:0.1 sec, F0.08 sec, G:0.06 sec, H0.04sec, and I:0.02 sec. After evaluating the series of changes, in morphology and dimension of the wave, it is clear that it is not possible to draw any significant conclusion by the simple analysis of the wave form; as it is pretended by several authors. The CSF flow changes need to be analyzed in reference to the changes in compliance in each compartment, and how they occur in time, to probably achieve any conclusion.

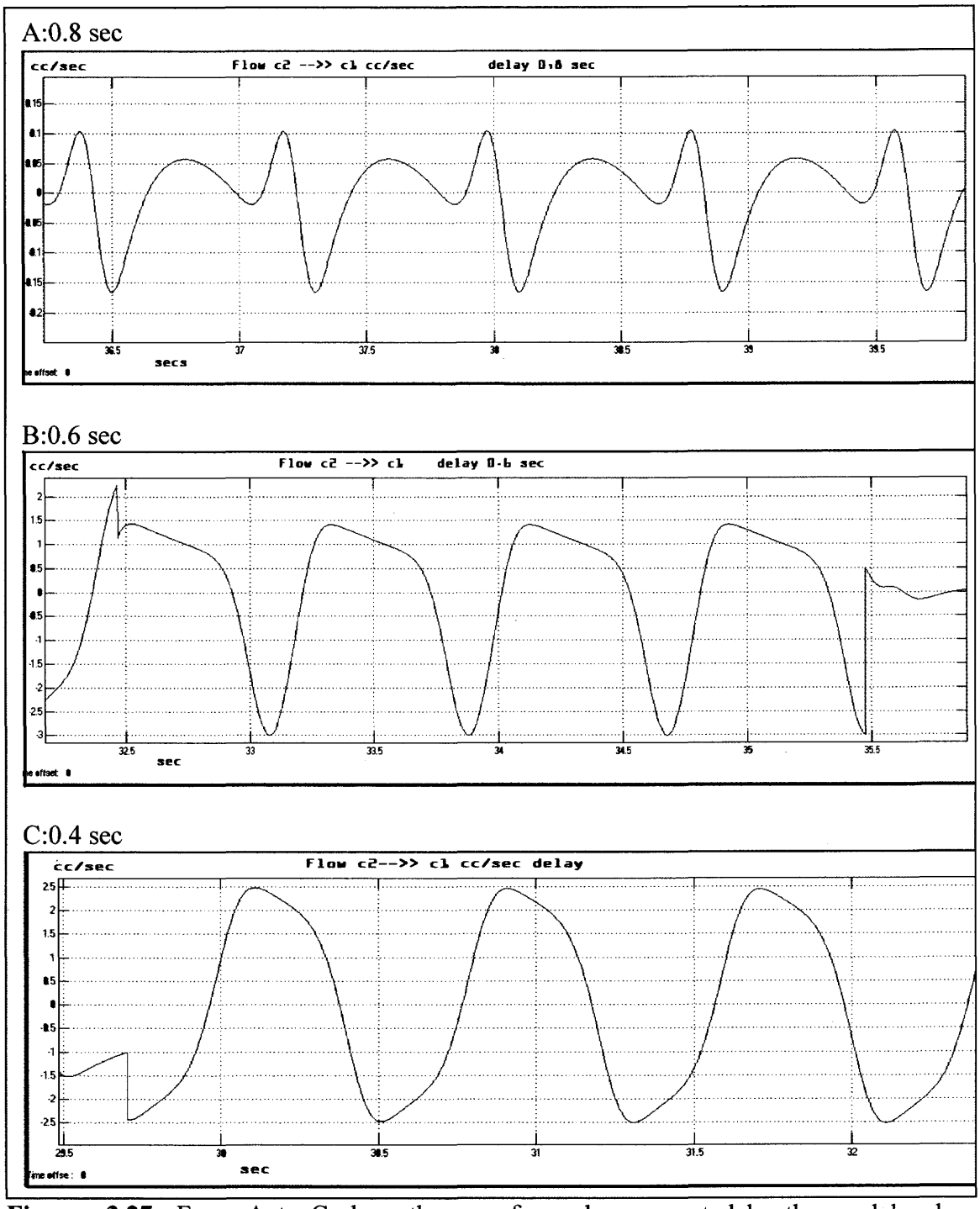

Figure 3.27 From A to C show the waveform shapes created by the model, when different delays were introduced.

D;0.2 sec

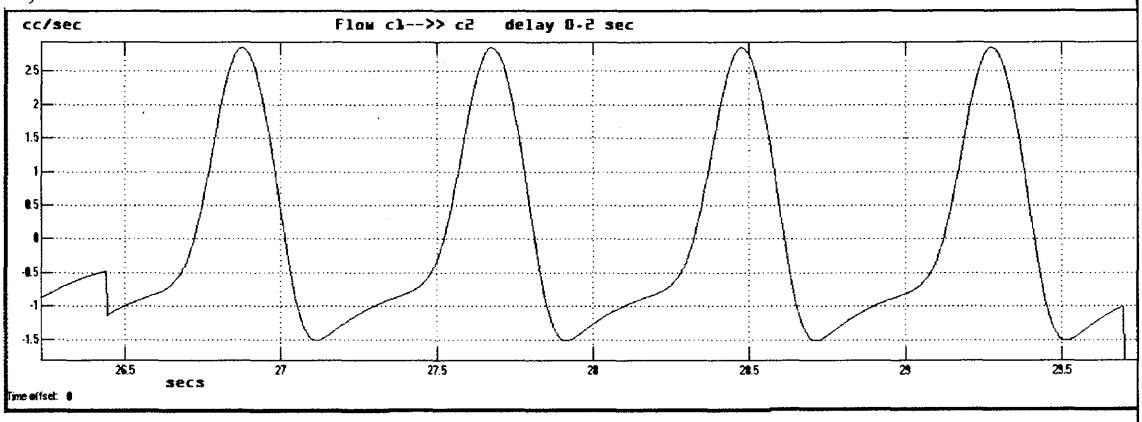

E:0.1sec

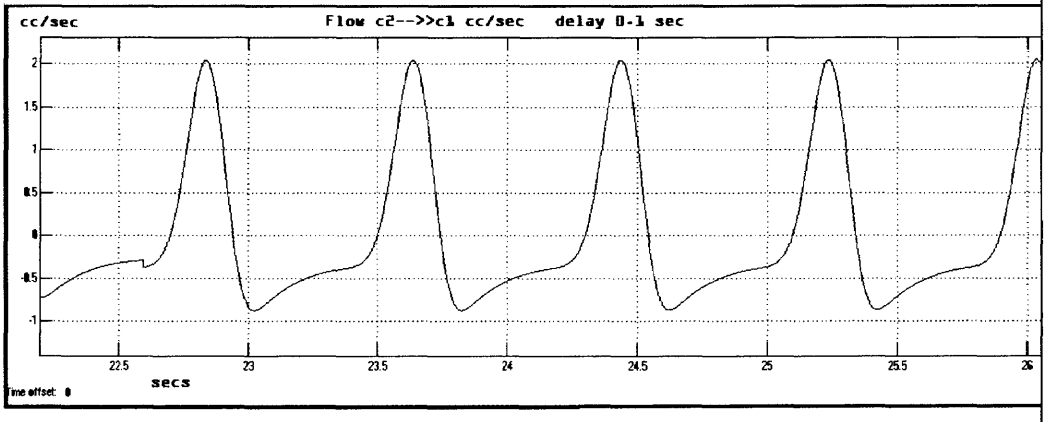

F:0.08 sec

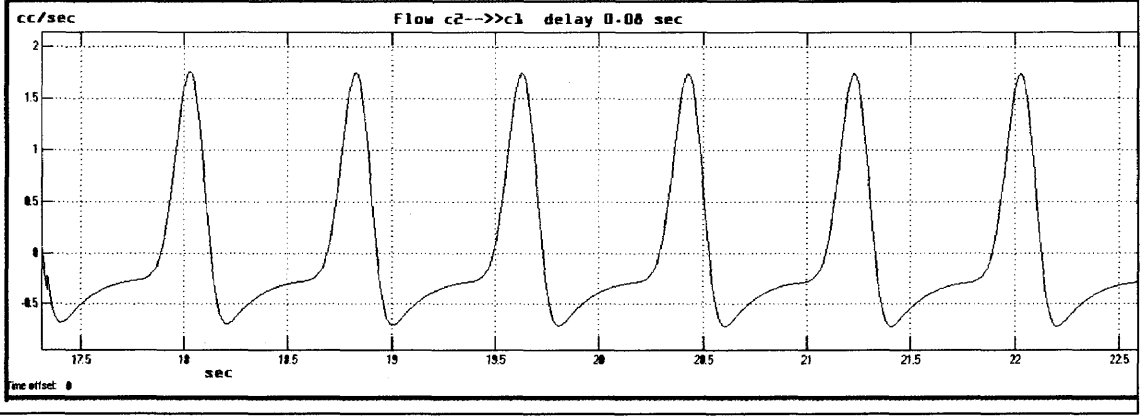

Figure 3.28 From D to F show the waveform shapes created by the model, when different delays were introduced.

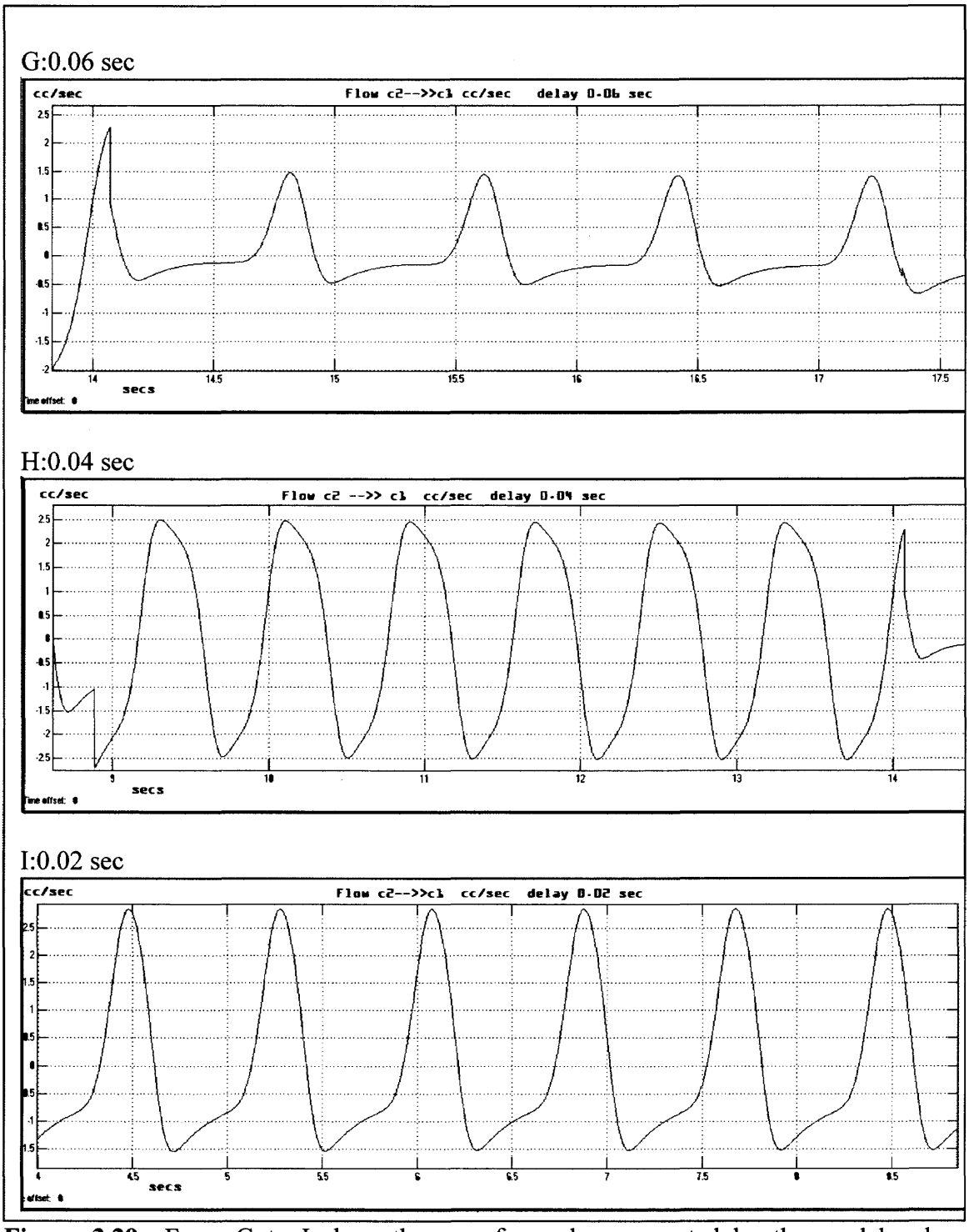

Figure 3.29 From G to I show the waveform shapes created by the model, when different delays were introduced.

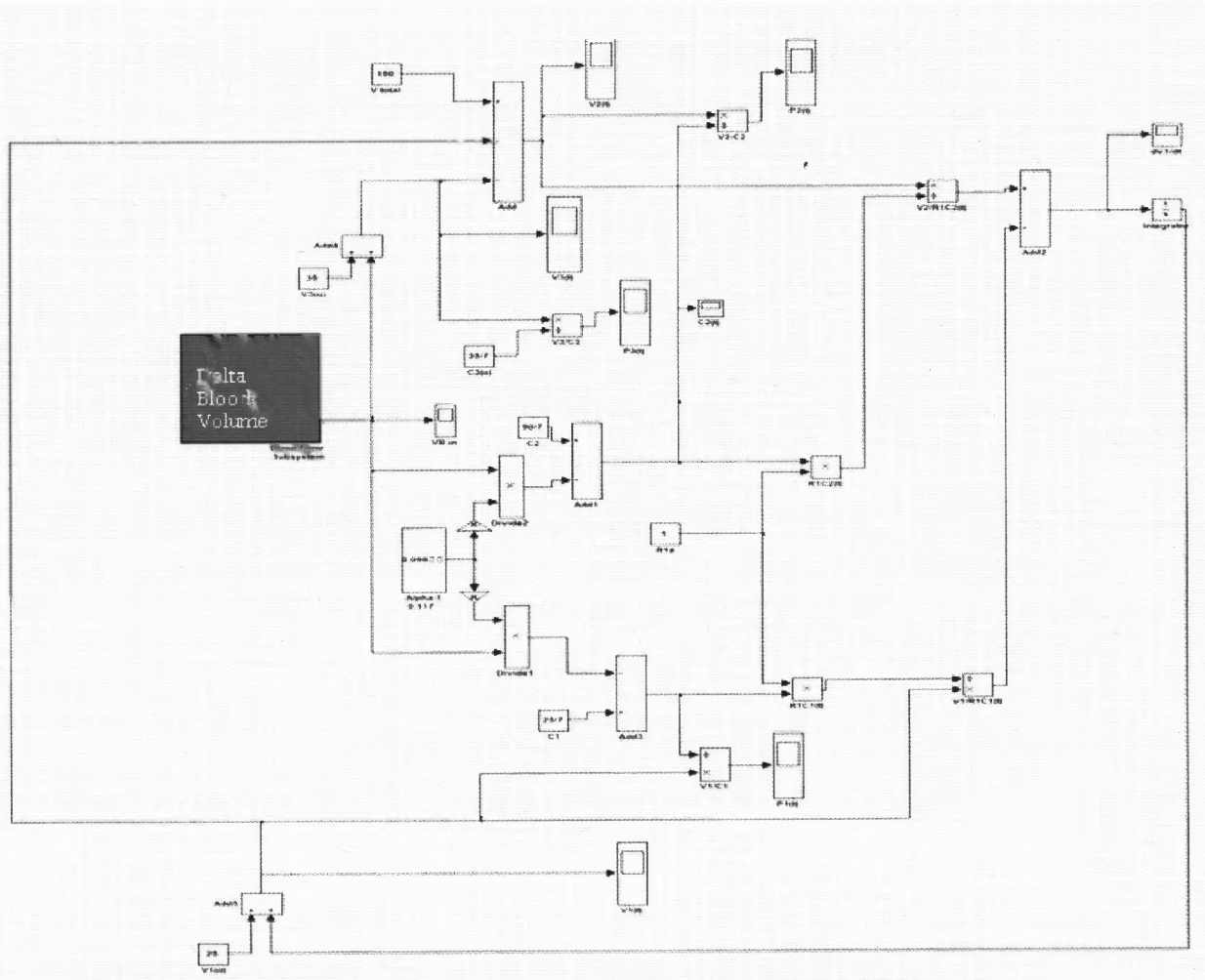

$$\frac{dV_1}{dt} = \frac{V_T}{R_1(C_2(t))} - \frac{V_{3(0)} + V_B(t)}{R_1(C_2(t))} - \left(\frac{V_1}{R_1(C_2(t))} + \frac{V_1}{R_1(C_1(t))} \right)$$

Figure 3.30 Full-constrained model.

3.3.5 Full Constrained Model

When the model takes into consideration that the amount of CSF to be expelled into the spinal compartment, has to be equal to the delta blood- volume coming into the cranium, for the intracranial pressures to be within physiological ranges; and this constraint is enforced in the model, it is considered a full-constrained model. Mathematically it was described in Equation 3.40:

$$\frac{dv_1}{dt} = \frac{v_T - v3_{(0)} - v_B(t)}{R_1(C_2(t))} - v1\left(\frac{1}{R_1(C_2(t))} + \frac{1}{R_1(C_1(t))}\right)$$

A computerized model (Simulink®) developed for this Equation was tested and compared to the previous models.

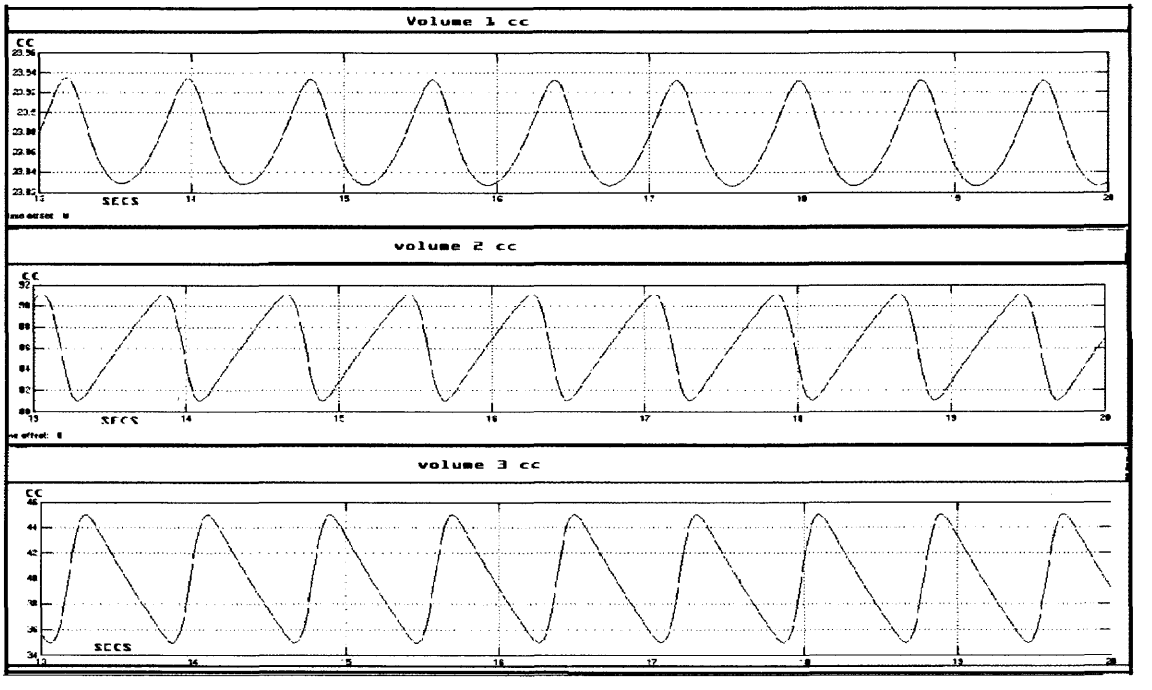

Figure 3.31 Full constrained model, behavior in time of the volume in cc of each compartment.

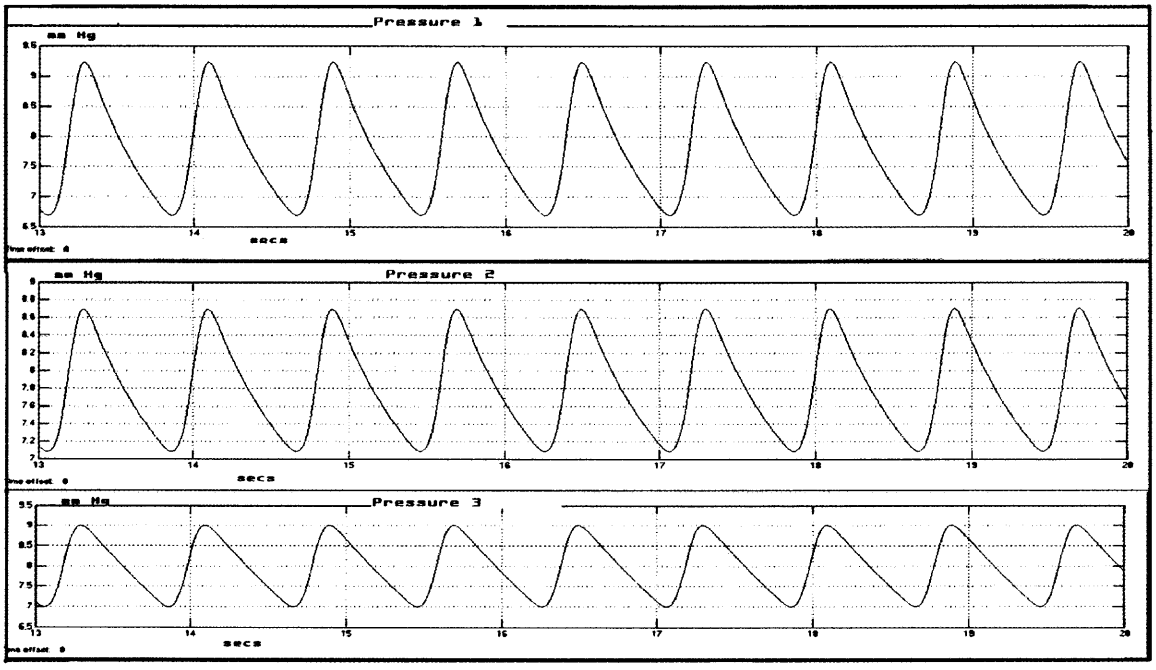

Figure 3.32 Full-constrained model; behavior in time of the pressure in mm Hg of each compartment.

After running the full-constrained model, as shown in Figure 3.31, the volume (V1) of the first compartment (Ventricular compartment(Cp1)) varies from 23.83 cc to 23.93 cc, with a difference of 0.10 cc of CSF per cycle. The volume (V2) of the second compartment (Cp2) varies from 91 cc to 81 cc, with a difference of 10 cc of CSF. The volume (V3) of the third compartment (Cp3) varies from 35 cc to 45 cc, with a difference of 10 cc of CSF. When comparing the graphs corresponding to volumes V1, V2 and V3, with those from previous models, no difference could be appreciated. As normally happens, the msajority of CSF flow occurs between Cp2 and Cp3.

As shown in Figure3.32, the pressure P1 in Ventricular compartment(Cp1) settles to a very stable condition oscillating between 6.8 and 9.3 mms Hg. Pressures P2 and P3 in Cp2 and Cp3 maintain a very stable oscillation between 7 and 9 mm Hg.; thus the pressure in all the system is maintained within physiological ranges, below 15 mm Hg.

Also note that peak to peak pressure difference between Ventricular compartment(Cp1) and Cp2 is less than 1 mm Hg.

The full-constrained model fulfills the previously expressed needed criteria for acceptance as representative of the normal CSF dynamics. The full-constrained model fully describes the normal CSF dynamics as it has forced CSF to exit from the cranial cavity (Cp2) in an equal amount to the blood volume coming into the brain. The resistance between the intraventricular and subarachnoideal spaces still defines the velocity at which the CSF is traveling between these two compartments.

3.4 Sensitivity Analysis of the Model

When modeling any complex system, it is not unusual to find different published values for certain specific parameters of the model; or sometimes it could be very difficult to measure directly or indirectly a parameter with a great level of accuracy. Some other times a new parameter is introduced, and by consequence no one has measured such parameter in the system of interest. Also, in the real world some parameter values change in time. These sets of possibilities create a certain amount of uncertainty in the model, uncertainty that could be of two types; stochastic and epistemic. Stochastic or aleatory uncertainty refers to non-controllable or non-deterministic variables; usually they are a result of the system interacting with the environment. They are frequently referred in the literature as irreducible, inherent or stochastic. Epistemic uncertainty refers to the ones that arise for the lack of knowledge of a system; these ones are also referred as reducible, subjective or cognitive. Epistemic uncertainties can frequently be calculated from other measured parameters; or once they have been identified, they could be measured in a direct or indirect way during further

experimentation. Consequently when building a model, the modeler has certain level of uncertainty, and when choosing parameters values, is compelled to choose estimates.

Sensitivity analysis helps building confidence in the model, as it helps the modeler to estimate what level of accuracy is necessary for a parameter to make the model useful and valid by comparing the changes in outcome of the system as the chosen parameter is varying.

In the present CSF dynamics model a new concept is introduced, alpha parameter, relating the loss in the parenchymal compliance as a function of the increment of delta blood-volume inside of the vessels. Alpha could be calculated from existing parameters, Equation A-1 Appendix 1, thus it constitutes an epistemic uncertainty. Therefore, it is important to perform a sensitivity analysis to the alpha parameter in the system. Two sets of sensitivity analysis were performed. One set was performed for the sine driven model; and another set was performed for the full-constrained model.

After determining the value alpha, used in the simulation of the sine driven model, which was the same used in the full-constrained model, a stepwise decrement of one percent of its value was implemented until a total ten percent decrement was achieved. Also, a stepwise increment of one percent of its value was implemented until a total ten percent increment was achieved. The system response was recorded for each of the variations. The parameters chosen to evaluate the impact of alpha in the model were, C1, C2, V1, V2, V3, P1, P2, and P3.

The results are shown in the figures on Appendix Two, Extended Sensitivity Analysis .Sine driven model figures are labeled as "Non-Constrained Model", while full-constrained model are labeled as "Constrained Model". As the events are regulated by the

cardiac cycle, each figure shows a maximum value in red, and a minimum value in blue per cycle.

The results for the sensitivity analysis for the sine driven model showed an overall 11 percent variation of C1 is observed when a 20% variation of alpha is introduce; while an overall 8 percent variation of C2 is observed when a 20% variation of alpha is introduce.

An overall change in volume one of 1.16 %, while the change in volume two was of 3.7 %, corresponding to a 20% alpha variation..

Since Volume three is a crucial value, and the main difference between the non-constraint and the fully constraint model, it is shown with a fine grid to facilitate a more careful analysis. Figure 3.33 shows an overall change in volume three of 5.4 %, corresponding to a 20% alpha variation.

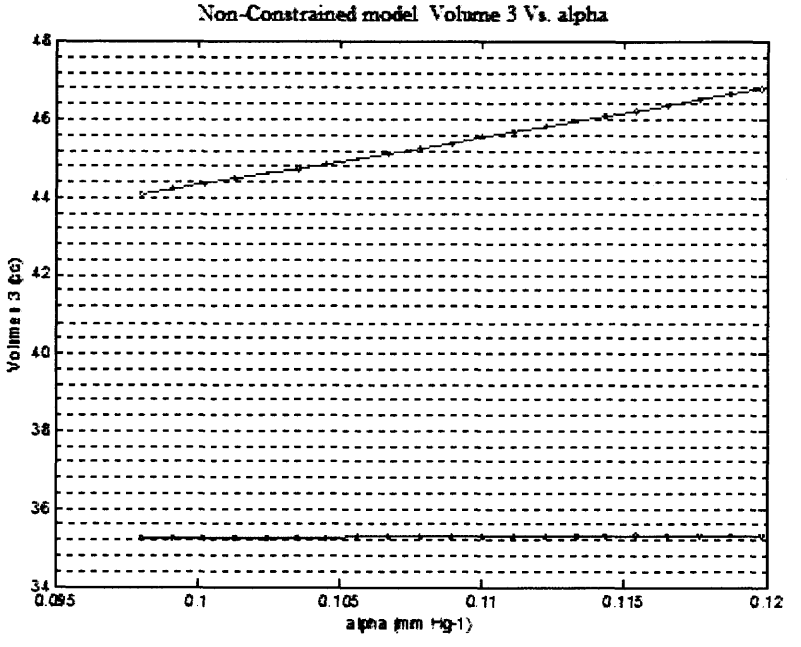

Figure 3.33 Sine driven model; behavior of Volume 3 as alpha is changed.

The sensitivity analysis shows an adequate behavior of the sine driven model, computing volumes for the three compartments within physiological ranges; even when the alpha parameter was varied between a plus or minus ten percent, for an overall twenty percent alpha variation. The volume changes vary between a 1% to a 5.4%, which is considered a very little variation.

An overall change in pressure one (P1) of 6 % was observed; while the change in pressure two, and in pressure three (P2, P3) was of 6.4 %, when a 20% alpha variation was introduced.

As significant changes in behavior of the system did not occur when alpha parameter was changed, we can have a good confidence on the alpha parameter in the sine driven model. The change of alpha parameter values also demonstrate a robust model as the structure of the system maintains its dynamics within physiological limits, with out a strong dependence on the parameter value. These results show that it is the structure of the system, and not the parameter values, which has most influence on the behavior of the system.

Results from sensitivity analysis of the full-constrained model showed an overall 11 percent variation; while an overall 8 percent variation of C2 was observed when a 20% variation of alpha was introduced.

An overall change in volume one of 0.05 % was observed, corresponding to a 20% alpha variation. No change in volume two and volume three was observed when a 20% alpha variation is introduced (Figure 3.34). This fixed volume, insensitive to alpha variation, is the obvious result of the constraint introduced; because the volume variation in compartment two and compartment three is defined exclusively by the blood volume coming in.

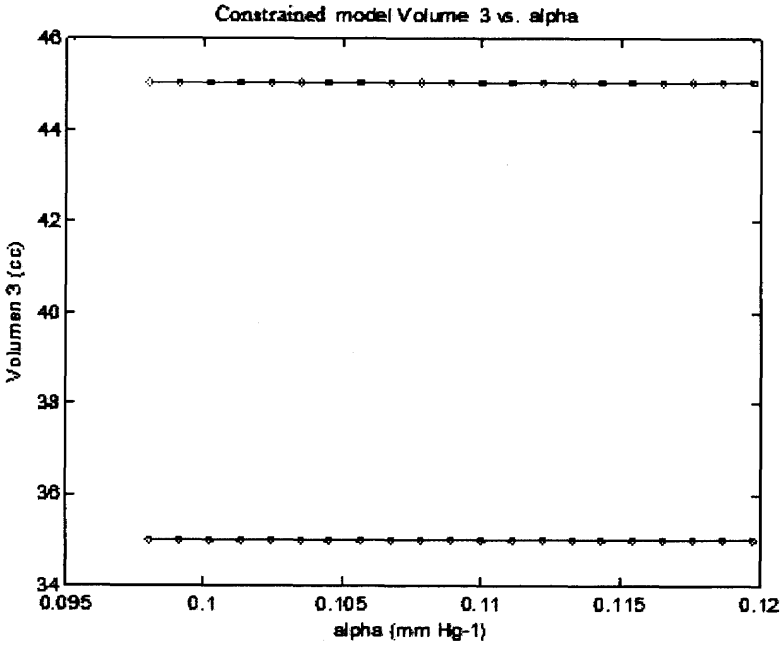

Figure 3.34 Full-constrained model; behavior of volume 3 as alpha is changed.

An overall change in pressure one of 9 %, and of 8.4 % in pressure two, were observed corresponding to a 20% alpha variation. No change in pressure three, corresponding to a 20% alpha variation. The pressure variation in the full-constrained model is maintained in the normal physiological range during the 20% alpha variation.

The constrained model proves to behave in a very robust manner describing the normal CSF dynamics. The variation of the alpha parameter is well tolerated by the model.

Two resistances, R1 and R2, are important parameters of the model which also have been calculated from anatomical references. Therefore is important to perform sensibility analysis on both of them.

After determining the value of R1, used in the simulation of the Sine Driven Model, which was the same used in the Full-Constrained Model, a stepwise decrement of

one percent of its value was implemented until a total ten percent decrement was achieved. Also, a stepwise increment of one percent of its value was implemented until a total ten percent increment was achieved. The system response was recorded for each of the variations. The parameters chosen to evaluate the impact of alpha were, C1, C2, V1, V2, V3, P1, P2, and P3. The results are shown in the set of figures below, sine-driven model figures are labeled as "Sine Driven Model", while constrained model figures are labeled as "Constrained Model". As the events are regulated by the cardiac cycle, each figure shows a maximum value in red, and a minimum value in blue, per cycle.

The sensitivity analysis shows that when R1 is modified practically no change is noted in the system response. V1 is the only parameter that displays a small change in response to R1 variation of less than one percent, from a value of 23.88 cc to a value of 23.87 cc. As practically no changes in behavior of the system occur when R1 parameter was changed, we can have a good confidence on the R1 parameter in the sine driven model. The change of R1 parameter values also demonstrate a robust model as the structure of the system maintains its dynamics within physiological limits, with out a strong dependence on the parameter value. These results show that it is the structure of the system, and not the parameter values, which has most influence on the behavior of the system.

The sensitivity analysis shows that when R1 is modified in the Full-Constrained model practically no change is noted in the system response. V1 is the only parameter that displays a small change in response to R1 variation of less than one percent, from a value of 23.98 cc to a value of 23.97 cc. As practically no changes in behavior of the system occur when R1 parameter was changed, we can have a good confidence on the R1 parameter in the full-constrained model. The change of R1 parameter values also

demonstrate a robust model as the structure of the system maintains its dynamics within physiological limits, with out a strong dependence on the parameter value. These results show that it is the structure of the system, and not the parameter values, which has most influence on the behavior of the system.

The sensitivity analysis shows that when R2 is modified in the sine driven model, practically no change is noted in the system response. As practically no changes in behavior of the system occur when R2 parameter was changed, we can have a good confidence on the R2 parameter in the sine driven model. The change of R2 parameter values also demonstrate a robust model as the structure of the system maintains its dynamics within physiological limits, with out a strong dependence on the parameter value. These results show that it is the structure of the system, and not the parameter values, which has most influence on the behavior of the system.

3.5 Model Applicability To Pathological States

Normal Pressure Hydrocephalus (NPH) and Idiopathic Intracranial Hypertension (IIH) are two pathological entities that have puzzled the neurological world for a long time because there is not a cohesive explanation on how the nervous system has been altered in both cases. The model here developed, constitutes a formidable tool to explore and explain the physiopathology of both entities; therefore providing new avenues for further research that will hopefully help to disclose the etiology of these two entities. The next section will review the relation of the model with these two entities, as an example of the future applicability of the model.

Normal Pressure Hydrocephalus (NPH) is characterized by a triad: altered gait, altered sphincter control, and memory loss. Hakim and Adams in 1964, were the first to

describe a group of elderly patients that developed dementia associated with a characteristic "magnetic walking", and loss of sphincter control. Imaging studies of these patients revealed ventricle enlargement, suggestive of communicating hydrocephalus. When lumbar puncture was performed, a normal intracranial pressure was found, and surprisingly some of the patients seem to alleviate their symptoms when CSF was drained. If CSF was permanently diverted by a shunt, a group of patients continue improving until they regain full function. If not shunted the patients will fall back into dementia, loss of sphincter control and altered walking. Initial enthusiasm on the diagnosis of this new syndrome was blurred by a difficult selection of patients; and a complicated differential diagnosis with other causes of dementia associated to ventricular enlargement such as Alzheimer's disease; and subcortical ischemic brain disease particularly lacunar states and Binswanger's disease. To ensure better results after shunting, and to justify the surgery in elderly patients, better selection criteria have been eagerly sought with still unsuccessful results. Numerous studies on selection criteria based on ventricular size , MRI indices, and absorption/impedance indices have been published but none has proved to provide better selection. The assumed pathophisiology is still based on the concept of an altered CSF bulk flow from the production site to the absorption site. As no obstruction is visualized on the imaging studies, it is assumed that somewhere along the CSF pathway there is an obstruction to the flow, or that there is a diminished absorption of the CSF; thus accumulation of CSF will occur; and as a consequence ventricle enlargement will follow. The ventricular enlargement will produce a deformation of the neural fibers that when compressed and elongated will not function properly, and consequently will originate the symptoms. When these patients are shunted,

the ventricles regain their structure, the fibers go back to their original state, the symptoms relapse, and the patient will be cured.

Some problems are still encountered after shunting even in successfully responding patients. If excessive drainage is performed subdural collections are formed; but if the drainage is insufficient the ventricles would remain enlarged and a partial recovery could be the final outcome. So it was recommended to maintain a close follow-up of the ventricular size shown in the MRI, and to correlate it with the clinical out come; if the ventricles seem to decrease too much after shunting it is advantageous to increase the pressure of the draining system; thus a variable pressure shunting system was developed.

The physiopathology, diagnostic criteria, selection criteria for surgery and expected outcome are still under discussion; even more some authors have even questioned the existence of the entity per se.

Most of the authors still try to find a way of quantifying the increased impedance, or decreased absorption of CSF. Pertinent to physiopathology, some authors have hypothesized that an increase in the venous sines impedance will diminished the absorption of CSF, at the level of the Arachnoid Villi. Other authors have hypothesized partial blocking of the CSF pathways along the basal cisterns, or at the convexity due to scar tissue formation after inflammatory processes. Both of these groups agreed that to explain the development of NPH, there should exist a silent period of high pressure that will enlarge the ventricles, will deform the fibers and will produce hydrocephalus; followed by a symptomatic period of enlarged ventricles with normal pressure hydrocephalus. During the first period a transmantle pressure gradient between the interior and exterior of the brain is the "only plausible explanation" for a ventricle

dilation to occur. Nevertheless, no one has been able to show the existence of these periods. Recently, some reports from experimental and clinical data, have shown the inexistence of the transmantle pressure gradient.

The CSF model here developed provides a novel mechanism, based on altered brain-compliance, to explain the appearance of dilated ventricles, associated to diminished intracranial-subarachnoideal space, and normal intracranial pressure.

If the ventricular compartment compliance is increased independently from the rest of the compartments, a new redistribution of the CSF-volumes will occur in such a way that the ventricular volume will increase, and the subarachnoideal and spinal compartmental volumes will decrease.

To illustrate this effect on the CSF dynamics, three simulations were run with an increased ventricular compliance (C1). The first simulation was carried with the sine-driven model, the second was carried with the model driven by blood-volume-signal which also incorporates the Unstressed volume concept, and the third simulation was run in the full-constrained model.

The purpose of running in these three different versions of the model was to compare the behavior of each one, and to evaluate if there was gathered any additional information, or on the contrary if any information was lost in each case.

As shown in the mathematical analysis, the ratio between the whole system compliance (C_T) and the compliance of each compartment (C_i) is what ultimately dictate the final volume of each compartment (Cp_i). When the flow, dv_i/dt, between two compartments is equal to zero the volume of each compartment is calculated by Equation 3.24. Recall:

$$\frac{v_i}{C_i} = \frac{v_T}{C_T}$$

$$v_i = \frac{v_T C_i}{C_T}$$

$$i = 1,2,3$$

Having each compartment a cycling behavior there are two instances in this cycle hwere the flow is equal to zero. The first one happens when the volume achieves its maximum value; just before it starts to decrease there is an instant in which the flow is equal to zero. At the transition, between the flow coming in and the flow coming out, there is a zero flow. A similar situation happens at the lowest value of the volume. For this reason the volume dimension at maximum value and at minimum value is determined by the ratio between the specific compartment compliance, and the whole system compliance, as defined by Equation 3.24. It is logical to deduce that in between the maximum and minimum values, the compliances ratio is also an important determinant of the final volume of each compartment.

Table 3.2 Sine Driven Model Simulation with C1=40/7 cc/mm Hg

Sine Driven Model		
C1 Compliance	25 / 7	40 / 7
V1 max	23.8340	36.9446
V2 max	91.9000	81.4227
V3 max	45.3316	40.8019
	0	0
V1 min	23.4090	36.8919
V2 min	81.0226	72.2755
V3 min	34.6000	31.6636
	0	0
P1 max	9.6117	8.0023
P2 max	9.0669	8.1610
P3 max	9.0663	8.1604
	0	0
P1 min	6.5845	6.4596
P2 min	7.0692	6.3324
P3 min	6.9200	6.3327
	0	0

Sine Driven Model simulation with C1=40/7 cc/mm Hg. By increasing the compliance in Ventricular compartment(Cp1) to 40/7 cc/mm Hg the CSF volumes change as expected. As shown in Figure 3.35, there is volume increment in compartment Ventricular compartment(Cp1) from 23.40 cc to 36.94 cc; associated to a decrement in the other two compartments. Cp2 maximum value changes from 91.9 cc to 81.42 cc, while Cp 3 maximum value changes from 45.33 cc to 40.80 cc. Surprisingly, the new minimum value for Cp2 is 72.27 cc, while for Cp3 the new lower value is 31.66 cc. Even though V3 did not meet the value needed to fully comply with Monroe-Kelly theorem, a difference of at least 10 cc of CSF volume between V3-max and V3-min, the difference in this case was of 9.14 cc, failing to evacuate 0.86 cc per cycle. If it is taken into consideration that the approximate value of brain volume is around 1.500 cc, and that the CSF volume is approximate 150 cc, rendering a total approximate intracranial volume of

1650 cc; then 0.86 cc represent 0.05 percent of the total intracranial volume. If the total CSF coming out of the cranium is not enough, then some brain parenchyma could be forced out of the cranium into spinal canal. Actually, it has been documented that the brain moves inside the cranium in a caudal direction during heart systole. This missing CSF volume could also be interpreted as the amount of nervous tissue that comes out of the cranium into the spinal canal. With a diameter of 2.5 cms, the spinal cord at the cervico-medullary junction has an area of approximate 4.90 cm^2; thus to account for 0.86 cc to fully comply with the model boundaries, it is necessary to for the medulla to move 0.175 cm in caudal direction; displacement that lies in the inside of the measured displacement of the pons in caudal direction during heart systole.

In the same way, a lower pressure in the system is predicted as the whole system compliance has been increased. This expected pressure value is confirmed in the corresponding pressures graphs, Figure 3.36. While P1 varies between 6.5 and 8.0 mm Hg, P2 and P3 vary between 6.3 and 8.2 mm Hg.; both pressure values still remain inside the physiological range.

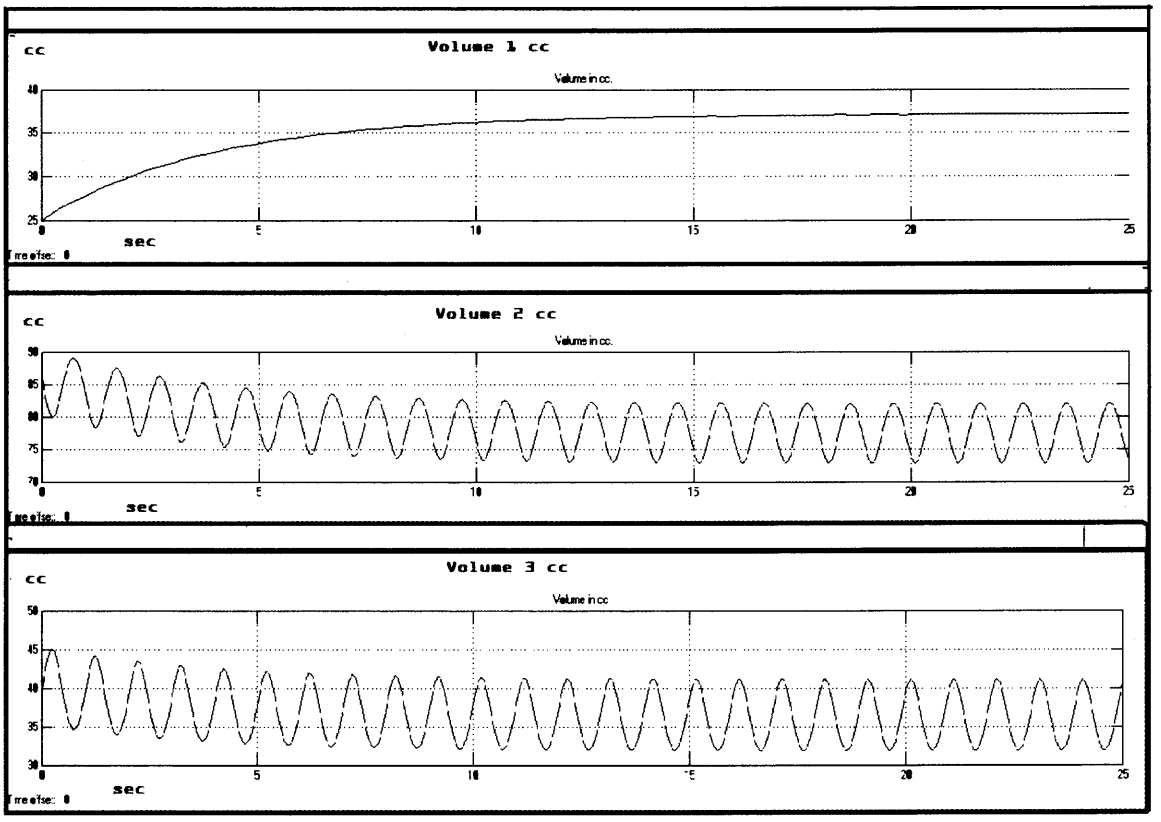

Figure 3.35 Sine driven model; behavior in time of the volume in cc of each compartment, after increasing Ventricular compartment(Cp1) compliance C1 to 40/7.

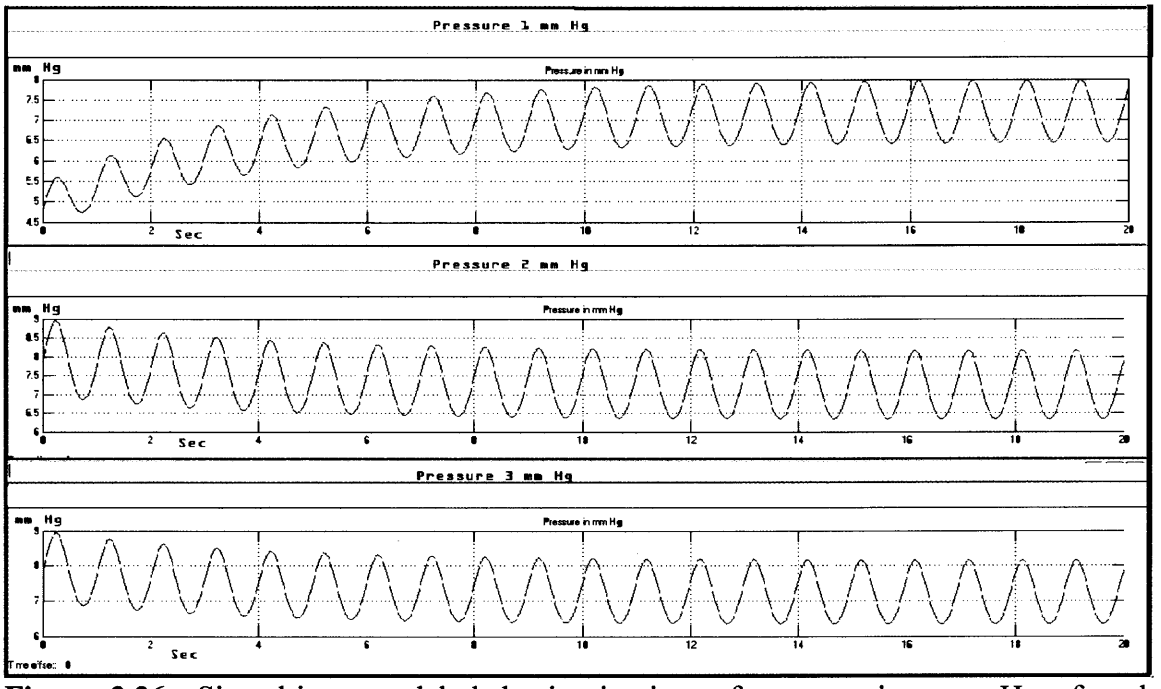

Figure 3.36 Sine driven model; behavior in time of pressure in mm Hg of each compartment, after increasing Ventricular compartment(Cp1) compliance C1 to 40/7.

The most accepted hydrocephalus animal-model is created by the insertion of a kaolin suspension into the Cisterna Magna. Kaolin produces an inflammatory reaction of the meninges, followed by extensive formation of glial scar-tissue. After a few days, hydrocephalus develops. A blocked CSF flow pathway, due to the new scar tissue in the brain convexity, has been interpreted as the responsible mechanism for hydrocephalus. In addition, there have been published anecdotal reports trying to correlate patients with communicating hydrocephalus with previous meningeal inflammatory process such as subarachnoid hemorrhage and meningitis, suggesting a parallel situation to the experimental model.

Nevertheless, it is good to remember that any resolution of an inflammatory process conveys the formation of scar tissue; which in turn diminishes the compliance of the original tissue. Therefore, an alternate explanation could be that a decreased C2 compliance, associated with an increased C1 compliance, will produce a more dramatic change in the distribution of the CSF volumes in the system; originating the changes seen in NPH.

In an effort to depict the mentioned scenario, the model compliances were changed by decreasing C2 and increasing C1.

Table 3.3 Sine Driven Model Simulation of NPH

Sine Driven Model		
C1 Compliance	25 / 7	40 / 7
C2 Compliance	90/7	75/7
V1 max	23.8340	41.6399
V2 max	91.9000	73.9320
V3 max	45.3316	47.4938
	0	0
V1 min	23.4090	41.5043
V2 min	81.0226	60.9281
V3 min	34.6000	35.025
	0	0
P1 max	9.6117	9.0108
P2 max	9.0669	9.4996
P3 max	9.0663	9.4988
	0	0
P1 min	6.5845	7.2738
P2 min	7.0692	6.9000
P3 min	6.9200	6.9005
	0	0

Sinus Driven Model simulation with C1=40/7 cc/mmHg, and C2=75/7 cc/mmHg. If the compliances are changed again the volume distribution should follow the changes. By setting C1= 40/7, C2= 75/7, C3= 35/7; the following results are achieved. V1 shifts again to an oscillatory value between 41.6 and 41.5 cc. V2 shifts to an oscillatory value between 73.9 and 60.9 cc, and V3 shifts to an oscillatory value between 47.49 and 35 cc, as in Figures 3.37 and 3.38.

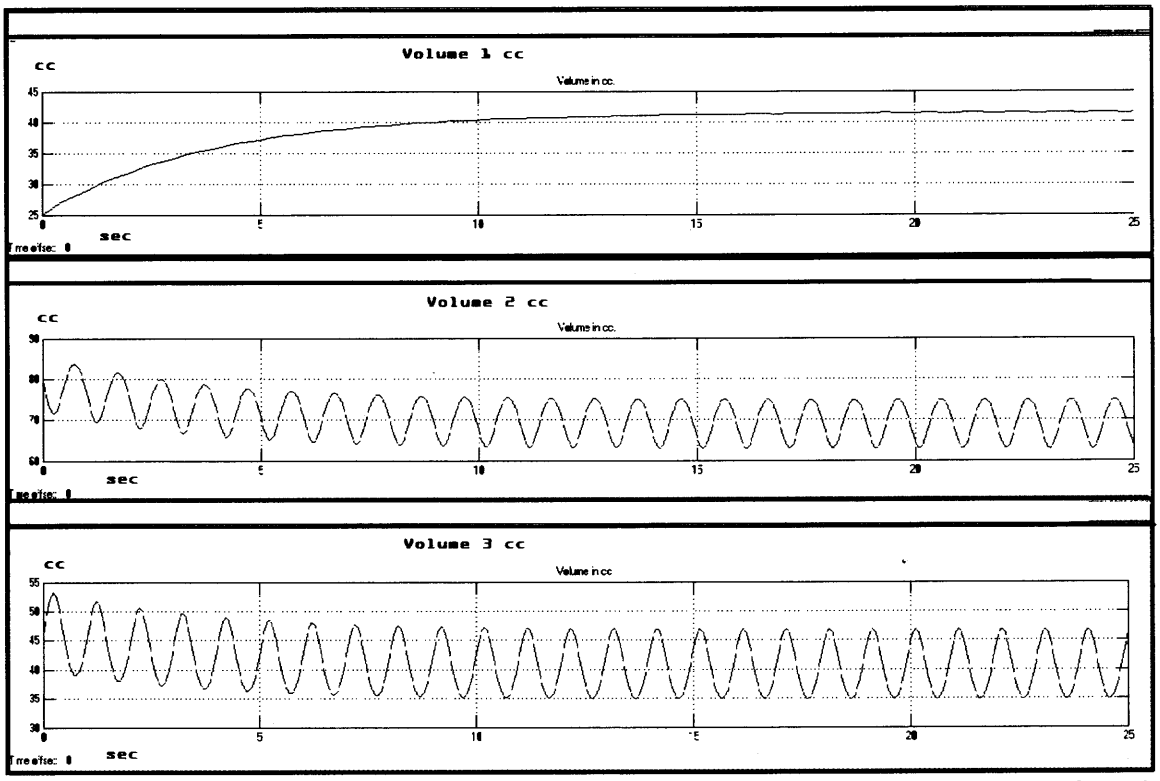

Figure 3.37 Sine driven model; behavior in time of the volume in cc of each compartment, after increasing Ventricular compartment(Cp1) compliance C1 to 40/7, and decreasing compliance C2 to 75/7.

Restoring the initial value of the total system compliance (C_T) brings back the pressures in the system to their original values. P1 is readjusted to values between 7.2 and 9 mm Hg; while P2 and P3 values are adjusted between 9.4 and 6.9 mm Hg.

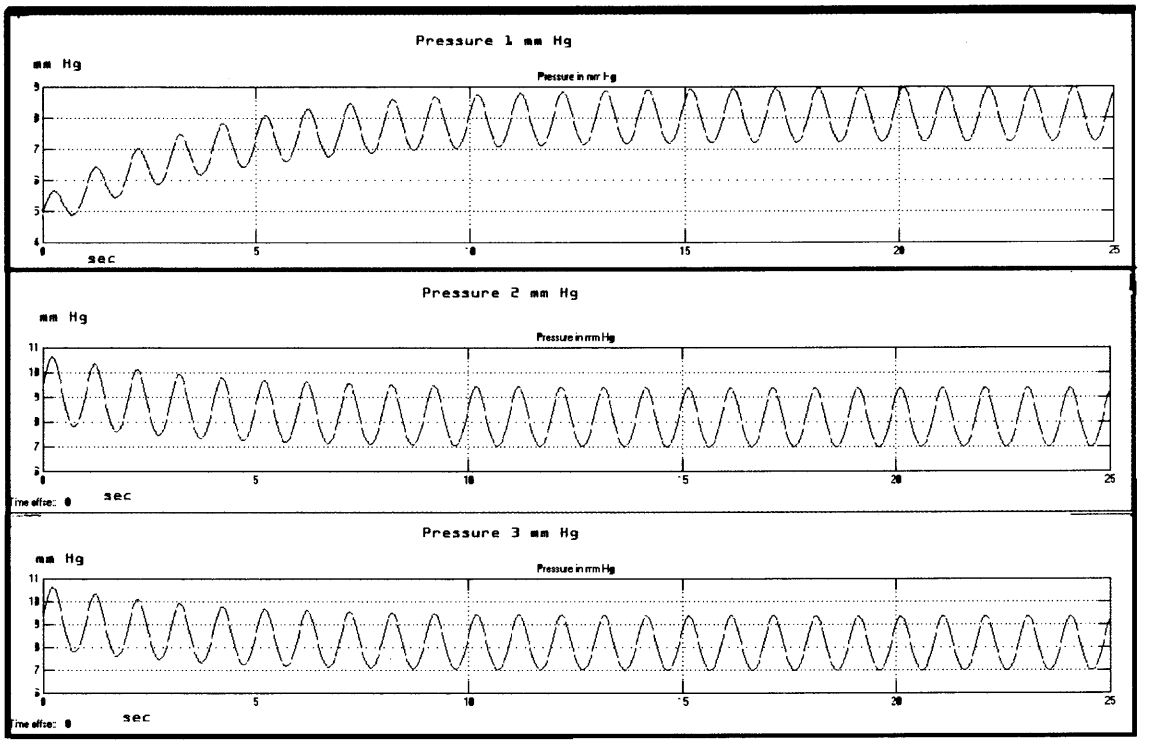

Figure 3.38 Sine driven model; behavior in time of the pressure in mm Hg of each compartment after increasing Ventricular compartment(Cp1) compliance C1 to 40/7, and decreasing compliance C2 to 75/7.

Table 3.4 Blood-Volume Driving Signal Model and Unstressed Volume Simulation of NPH.

Blood-Volume Driving Signal Model and Unstressed Volume		
C1 Compliance	25 / 7	35/7
C2 Compliance	25/7	15/7
V1 max	25.8007	37.1429
V2 max	89.9227	79.2939
V3 max	44.9499	46.5600
	0	0
V1 min	25.1511	36.9441
V2 min	79.7247	66.4140
V3 min	34.6001	33.7012
	0	0
P1 max	10.0607	9.3124
P2 max	9.7873	10.2386
P3 max	9.7860	10.2368
	0	0
P1 min	7.0430	7.3944
P2 min	6.8873	6.6355
P3 min	6.8880	6.6363
	0	0

Unstressed Volume and Blood-Volume Driving Signal Model with C1=35/7 cc/mmHg, and C2=15/7 cc/mmHg. By setting C1= 35/7, C2= 15/7, C3= 25/7; the following results are achieved. V1 shifts again to an oscillatory value between 37.14 and 36.9 cc. V2 shifts to an oscillatory value between 79.29 and 66.41cc, and V3 shifts to an oscillatory value between 46.5 and 33.7 cc., Figure 3.39.

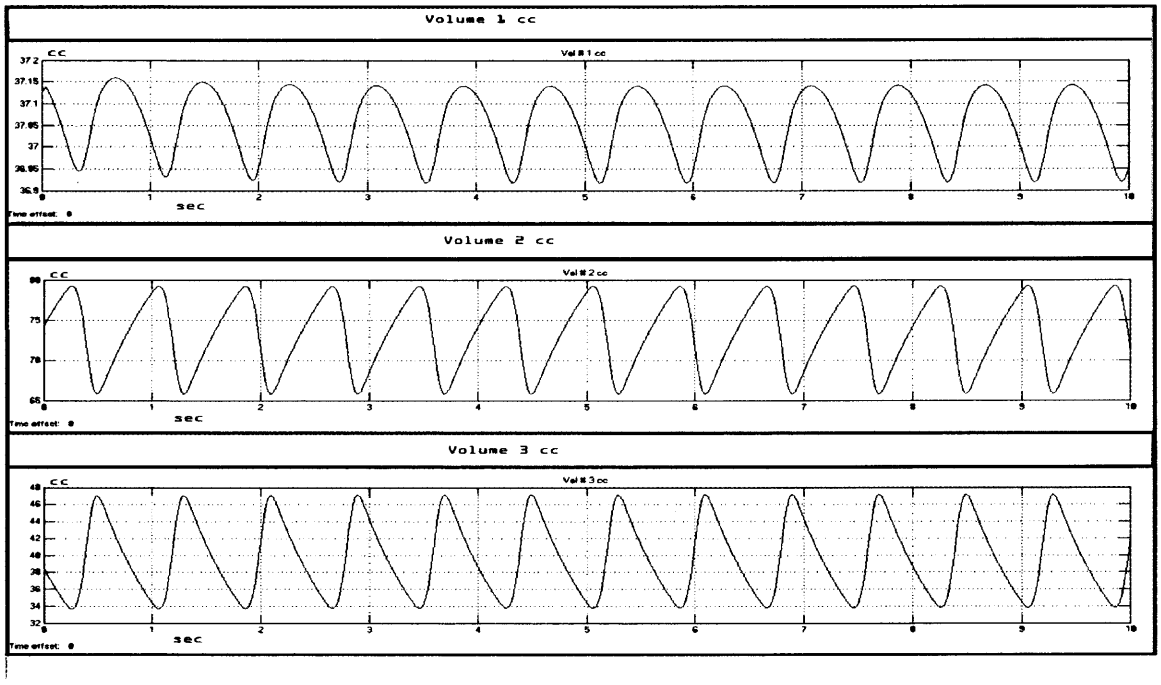

Figure 3.39 Delta blood-volume driven and Unstressed volume model, behavior in time of volume in cc of each compartment after increasing Ventricular compartment(Cp1) compliance C1 to 35/7, and decreasing compliance C2 to 15/7.

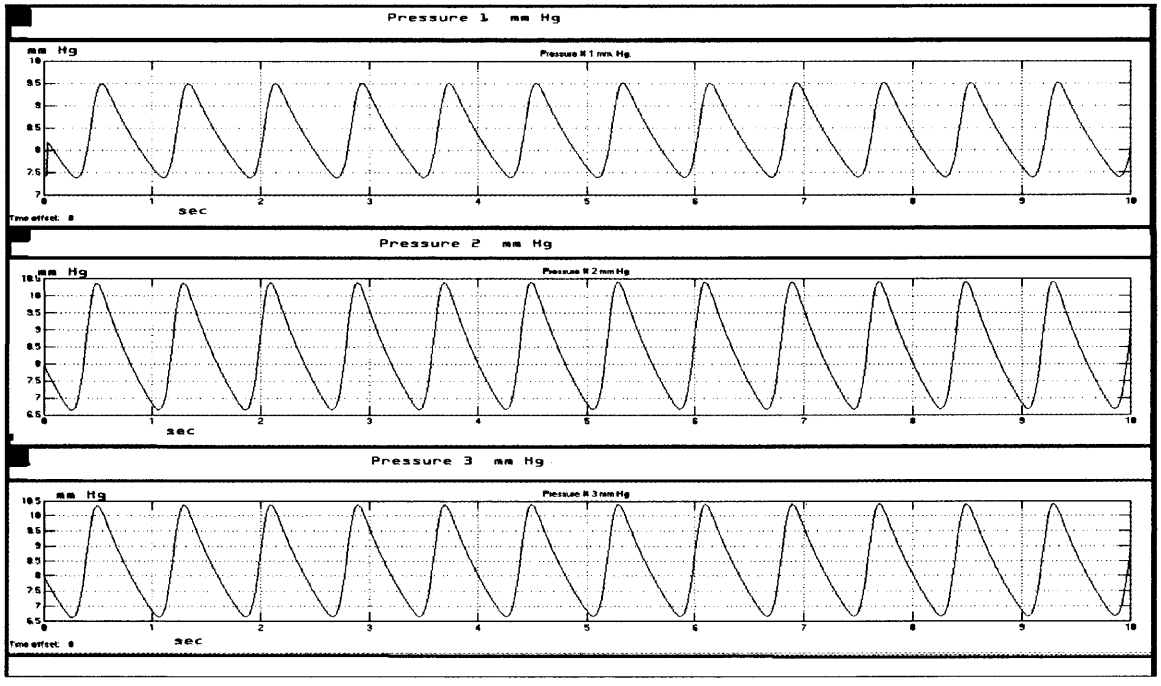

Figure 3.40 Delta blood-volume driven and Unstressed volume model; behavior in time of the pressure in mm Hg of each compartment after increasing Ventricular compartment(Cp1) compliance C1 to 35/7, and decreasing compliance C2 to 15/7.

P1 value oscillates between 7.5 and 9.5 mm Hg; while P2 and P3 values are adjusted between 10.5 and 6.7 mm Hg; peak to peak maximum pressure difference between Ventricular compartment(Cp1) and Cp2 reaches the set limit of 1 mm Hg. in the established limits between them. Figure 3.40

Table 3.5 Full-Constrained Model Simulation of NPH

Full-Constrained Model		
C1 Compliance	25 / 7	40 / 7
C2 Compliance	90/7	75/7
V1 max	23.8340	40.7322
V2 max	91.9000	74.4320
V3 max	45.3316	45
	0	0
V1 min	23.4090	40.6701
V2 min	81.0226	64.2918
V3 min	34.6000	35
	0	0
P1 max	9.6117	9.0108
P2 max	9.0669	9.4996
P3 max	9.0663	9.4988
	0	0
P1 min	6.5845	7.2738
P2 min	7.0692	6.9000
P3 min	6.9200	6.9005
	0	0

Full Constrained Model. C1 = 40/7 cc/mm Hg; C2 = 75/7 cc/mm Hg. When C1, initial compliance of the ventricular compartment is incremented to a value of 40/7 cc/mm Hg; and C2, initial compliance of the subarachnoideal compartment is decremented to a value of 75/7 cc/mm Hg; then steady state volume in V1 reaches 40. 7 cc., with a very little variation of about plus or minus (+/-) 0.05 cc during the cycle. Meanwhile the volume in Cp2 is reduced to a range between 74.4 cc and 64.29 cc, during

the cycle. Figure 3.41 show the changes in this case, generated by the model that represent the volume changes in a mild case of hydrocephalus.

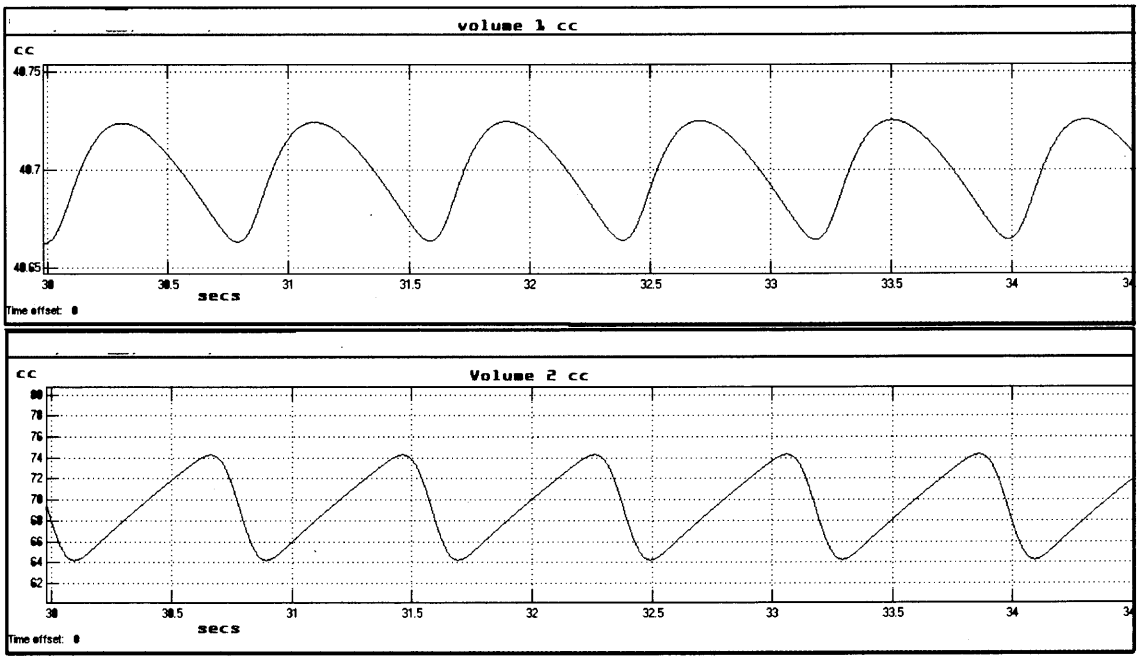

Figure 3.41 Full-constrained model; behavior in time of the Volumes V1 and V2 in cc, after C1 was raised to 40/7 cc/mmHg, and C2 was lowered to75/7 cc/mm Hg. Close up showing a very close oscillation of V1 around 40.7 cc; and a V2 oscillating between 64 cc and 74 cc.

The Cp3 volume, V3, behaves very normally not being affected by any changes in any of the intracranial compliances; and V3 varies between 45 cc and 35 cc during the cycle. A shown in every case the increment in C1 produces a shift of CSF volumes hat resembles NPH; more over the condition was easier to identify when the increment in C1 is associated with a decrement of C2.

Idiopathic Intracranial Hypertension (IIH), is an entity that has received numerous names through history(Pseudotumor Cerebri, Benign Intracranial

Hypertension), as a consequence of the still undefined pathophysiology and ethiology. It is characteristic of this syndrome to present a severely increased intracranial hypertension, associated to severe papilledema, and distinctive slit ventricles, with non apparent cause or explanation. Several conditions have been associated to IIH , though none of them has to be present for the diagnosis, the list include but are not restricted to the intake of: Non-steroidal anti-inflammatory drugs (NSAIDs) , Tetracycline , Nalidixic acid , Lithium , Steroids (starting or stopping them) , Obesity , Vitamin A (too much or too little) ,Cushing's disease , Hypoparathyroidism , Hypothyroidism ,etc. The IIH syndrome frequently leads to blindness if untreated, could present occasional spontaneous remissions, or remains in a chronic condition for several years. Treatment frequently involves CSF shunting, or optic's nerve dural-cuff decompression.

According to the model here developed, the physiopatholgy of this syndrome could be explained in terms of a decreased compliance of the intracranial compartments, Ventricular compartment(Cp1) and Cp2. As a consequence the total system compliance is reduced, the intracranial pressure will increase, and the CSF volume inside of both compartments will be reduced.

One of the most rare, but also one of the more comprehensible examples of this syndrome is the one caused by a stenosis of the transverse sinus. When a transverse sinus stenosis is documented by angiography as the cause of the IIH syndrome, it is corrected by placement of a stent; usually with complete restoration of the venous drainage, and complete remission of the symptoms.

The first IIH simulation was carried out in the sine-driven model. To model the above explained syndrome, the driving function baseline is shifted (biased) to a higher

value, thus resembling the effect produced by an increased peripheral resistance to the blood drainage.

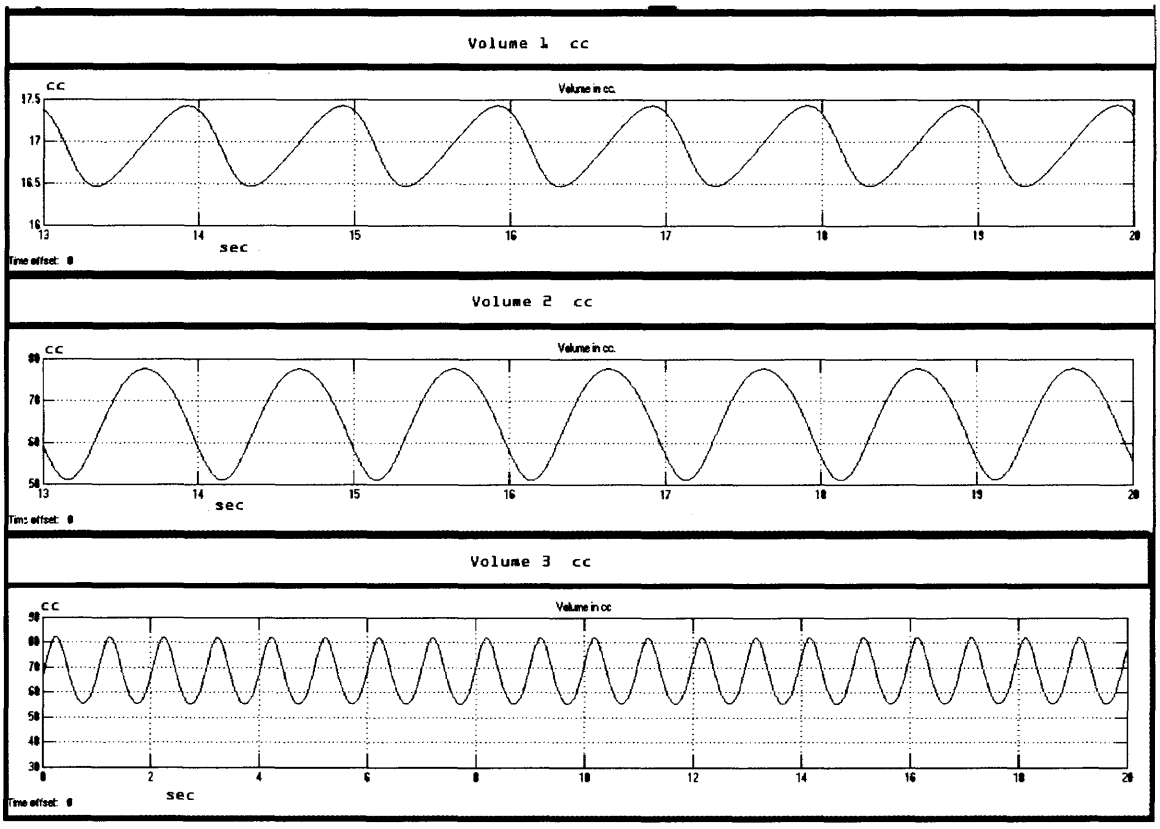

Figure 3.42 Sine driven model; behavior in time of the volume in cc of each compartment, after introducing a baseline bias of 4, simulating IIH secondary to Transverse Sinus stenosis.

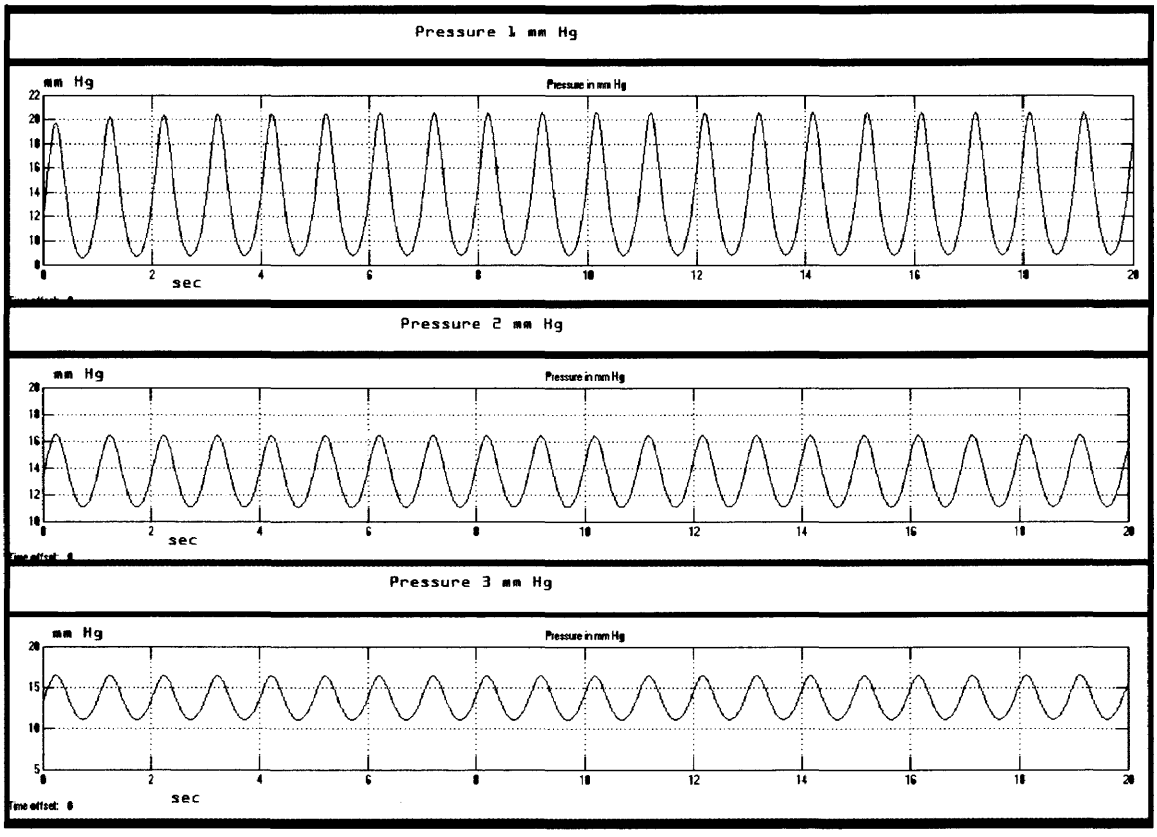

Figure 3.43 Sine driven model; behavior in time of the pressure in mm Hg of each compartment, after introducing a baseline bias of four, simulating IIH secondary to Transverse Sinus stenosis.

When the venous drainage is obstructed the amount of blood inside the vasculature builds-up, and the permanent congestion maintains an incremented load on the vasculature wall. This incremented load produces a less compliant vessel, and by consequence there is less complaint brain parenchyma. It is manifested clinically as an increased intra-cranial pressure, associated to a diminished amount of CSF volume in Ventricular compartment(Cp1) and Cp2.

Table 3.6 IIH in the Sine-Driven Model Simulation, with Biased Baseline as Equivalent of Increased Peripheral Resistance

Sine Driven Model		
Baseline-Bias	0	4
V1 max	23.8340	17.4283
V2 max	91.9000	77.6078
V3 max	45.3316	82.5220
	0	0
V1 min	23.4090	16.4659
V2 min	81.0226	51.0261
V3 min	34.6000	34.6000
	0	0
P1 max	9.6117	20.5766
P2 max	9.0669	19.5565
P3 max	9.0663	16.5044
	0	0
P1 min	6.5845	8.6131
P2 min	7.0692	11.0755
P3 min	6.9200	6.9200
	0	0

The results in Table 3.5, and Figures 3.42 and 3.43 clearly show an increased intracranial pressure associated to a diminished ventricular and subarachnoideal CSF volume; both are distinctive changes of IIH. The simulation carried on the sine driven model resembles the altered CSF dynamics in IIH.

The second simulation was carried out by directly increasing the peripheral resistance of the blood-volume driving function; which is a direct resemblance of the pathology described in the transverse sinus stenosis.

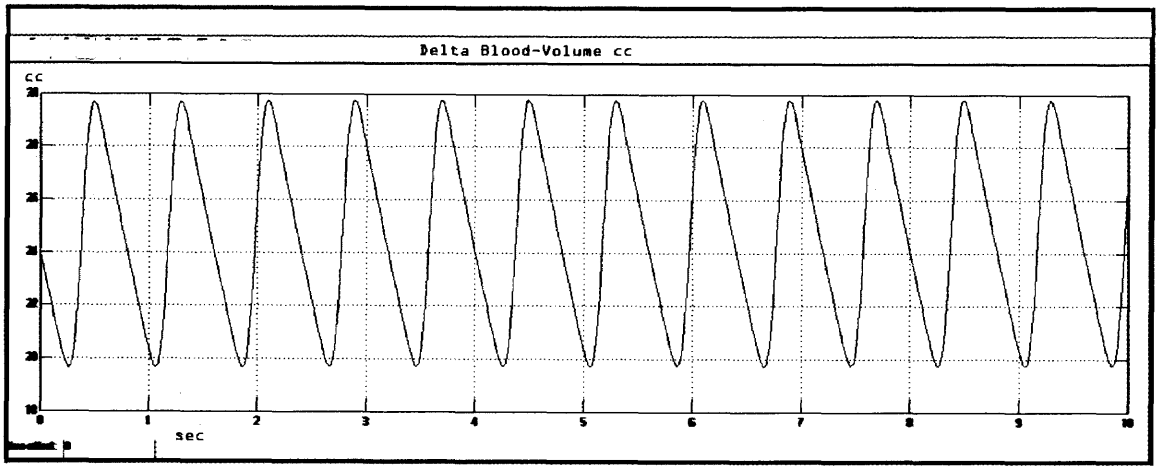

Figure 3.44 Delta Blood-Volume function after the increment of the peripheral resistance was introduced simulating Transverse Sinus stenosis.

After incrementing the peripheral resistance simulating Transverse Sinus stenosis, the Delta Blood-Volume function changes its baseline, but preserves the morphology and the amplitude of the wave. Thus 10 cc of blood volume are injected during systole, but the baseline is not zero anymore. The base line is shifted to 20 cc, as a consequence the delta blood-volume function now oscillates between 20 cc and 30 cc during the heart cycle (Figure 3.44). Consequently, there is a permanent congestion of the vasculature, producing a diminished compliance of the brain tissue. Clinically it is manifested as Increased Intracranial Hypertension, associated to decreased intracranial CSF volume.

Table 3.7 IIH Simulation in the Blood-Volume Driving Signal Model and Unstressed Volume Model by Increasing Peripheral Resistance

Blood-Volume Driving Signal Model and Unstressed Volume		
Blood Flow Peripheral Resistance	1.12 mm Hg-sec/cc	1.7 mm Hg-sec/cc
V1 max	25.8007	17.8579
V2 max	89.9227	67.6000
V3 max	44.9499	86.2965
	0	0
V1 min	25.1511	16.2962
V2 min	79.7247	46.5956
V3 min	34.6001	62.0000
	0	0
P1 max	10.0607	32.2148
P2 max	9.7873	21.3829
P3 max	9.7860	21.3630
	0	0
P1 min	7.0430	11.0876
P2 min	6.8873	15.0299
P3 min	6.8880	14.8700
	0	0

Table 3.6, and Figures 3.45 and 3.46 show the results of the simulation very consistent with the finding in patients with IIH. Increase intracranial pressure at ranges that represent real threatening not only to the Optic's Nerve, but also for all the brain's perfusion.

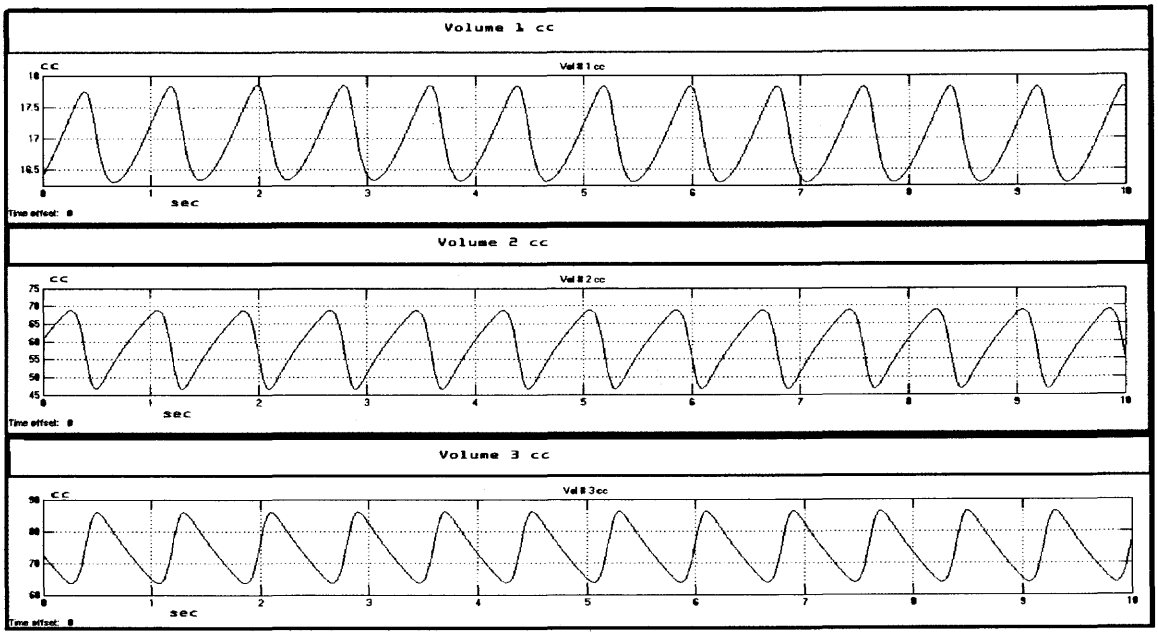

Figure 3.45 CSF Compartmental volumes after incrementing the peripheral resistance in the Delta Blood-Volume driving function simulating Transverse Sinus stenosis.

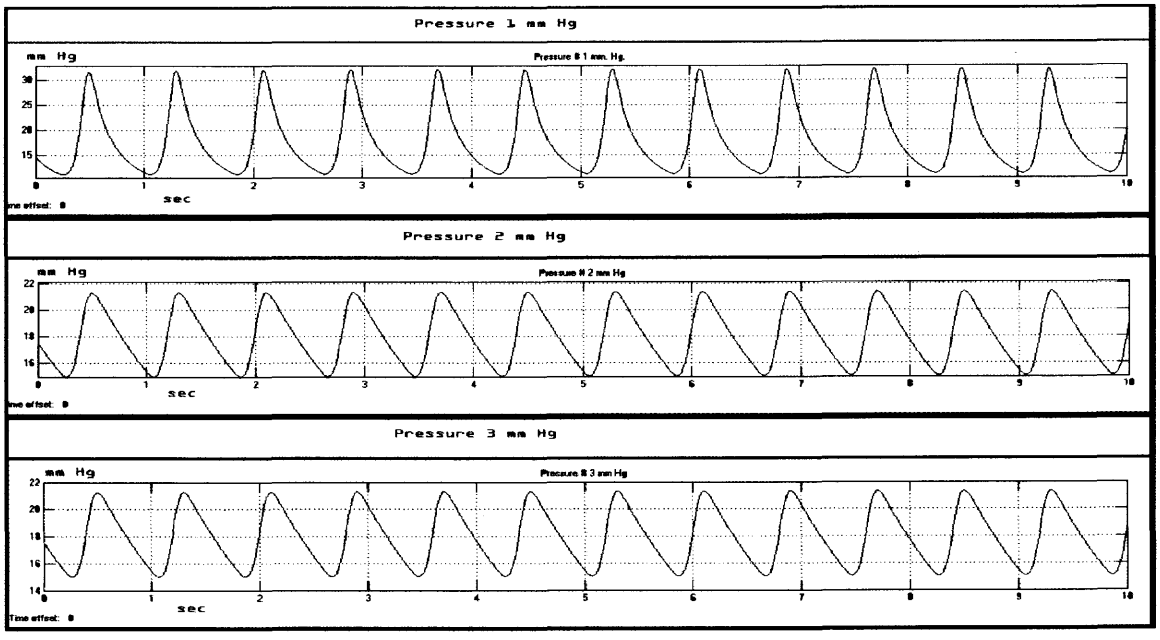

Figure 3.46 CSF Compartmental pressures after incrementing the peripheral resistance in the Delta Blood-Volume driving function simulating Transverse Sinus stenosis.

The third simulation was carried out in the full-constrained model, again by directly increasing the peripheral resistance of the blood-volume driving function; which is a direct resemblance of the pathology described in the transverse sinus stenosis.

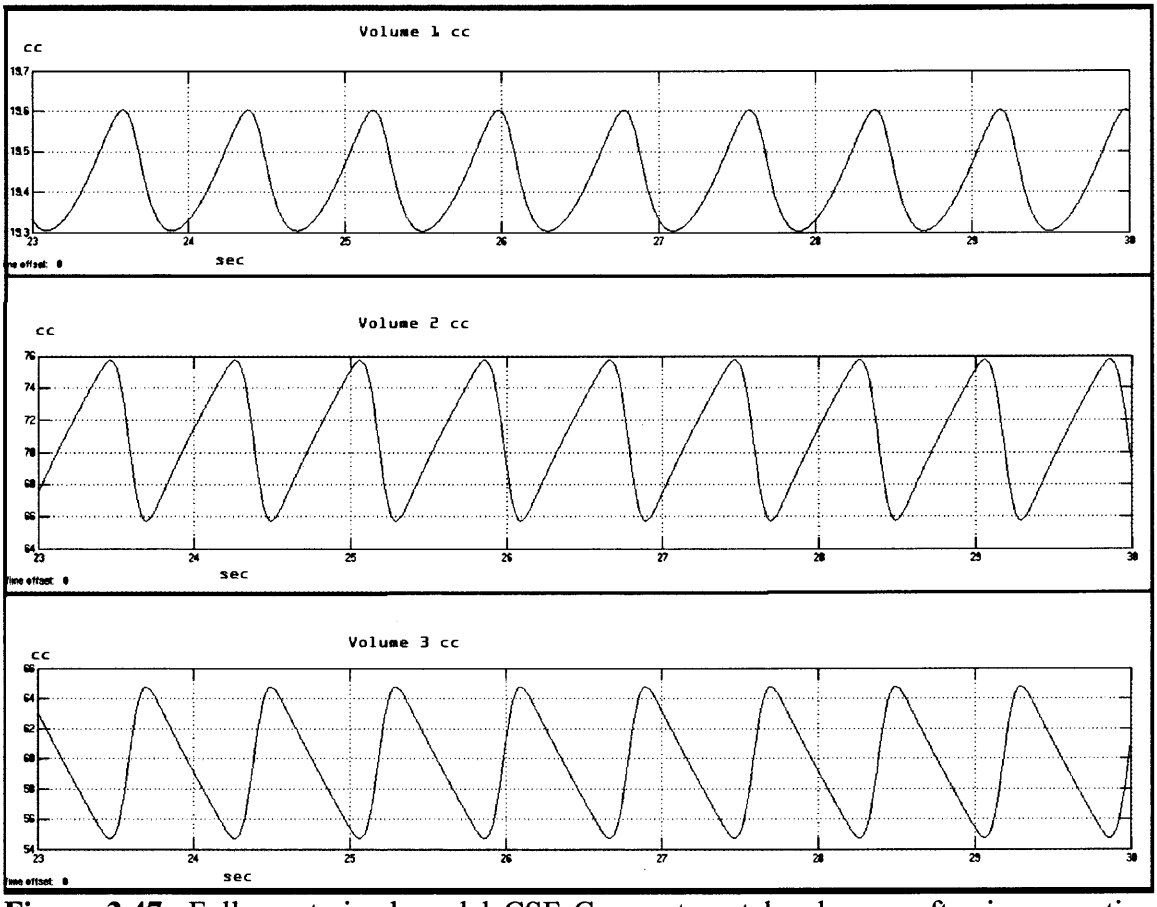

Figure 3.47 Full-constrained model CSF Compartmental volumes, after incrementing the peripheral resistance in the Delta Blood-Volume driving function simulating Transverse Sinus stenosis.

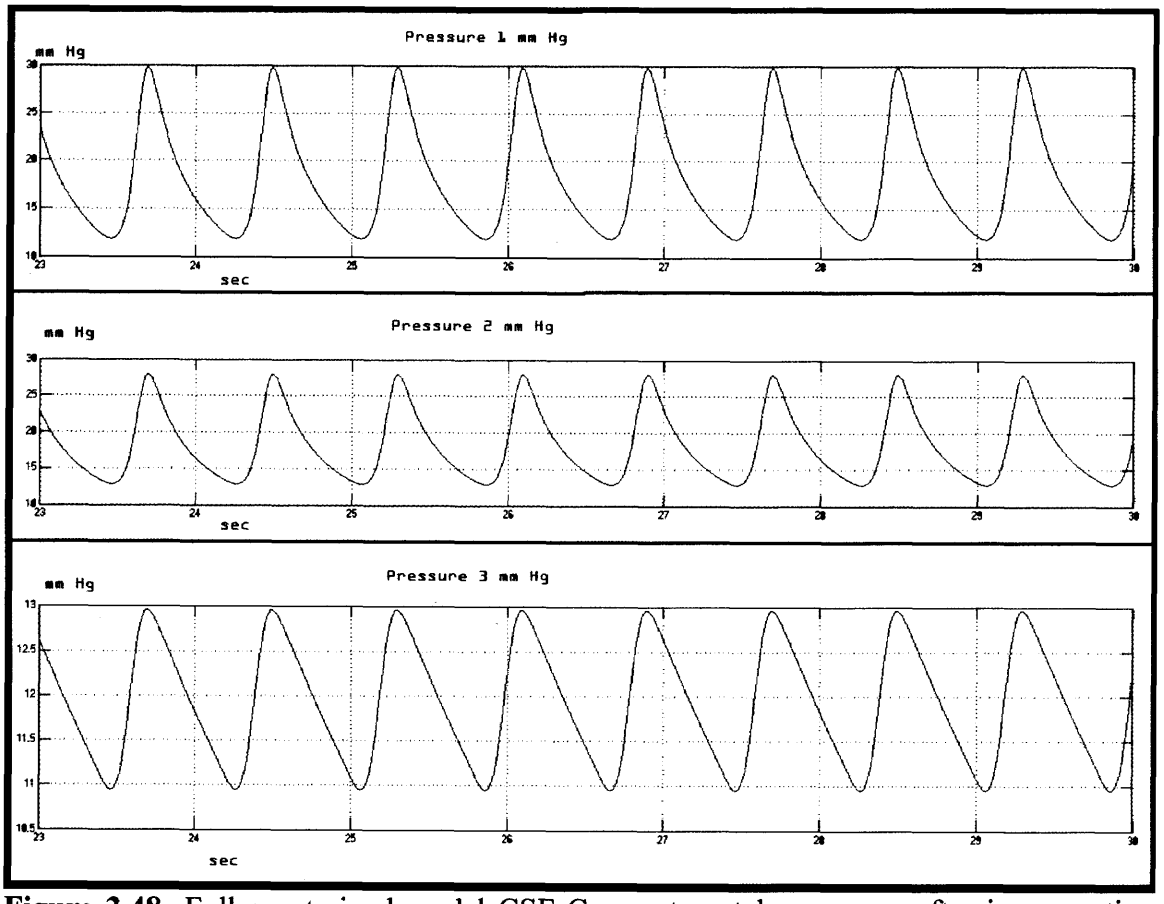

Figure 3.48 Full-constrained model CSF Compartmental pressures, after incrementing the peripheral resistance in the Delta Blood-Volume driving function simulating Transverse Sinus stenosis.

Careful evaluation of the pressure graph in Figure 3.48 reveals two independent behaviors. P1 and P2 behave independently from P3. The range in P1 and P2 are consistent with the findings in IIH, a very high intracranial pressure. Meanwhile, P3 maintains a normal pressure, situation difficult to explain as there are no valves between Cp2 and Cp3. Therefore, as the R2 resistance is very low, it is expected a fast transmission of the pressure between compartments Ventricular compartment(Cp1) and Cp2; which is nt happening.

Table 3.8 IIH Simulation in the Full-Constrained Model by Directly Increasing the Peripheral Resistance

Full-Constrained Model		
Blood flow Peripheral Resistance	1.12 mm Hg-sec/cc	1.7 mm Hg-sec/cc
V1 max	23.8340	19.6861
V2 max	91.9000	75.9126
V3 max	45.3316	64.7645
	0	0
V1 min	23.4090	19.3117
V2 min	81.0226	65.8519
V3 min	34.6000	54.4736
	0	0
P1 max	9.6117	29.7656
P2 max	9.0669	27.9070
P3 max	9.0663	12.9529
	0	0
P1 min	6.5845	11.7941
P2 min	7.0692	12.6797
P3 min	6.9200	10.8947
	0	0

Interestingly, all the three simulations resemble the syndrome. In every case the CSF volume in Ventricular compartment(Cp1) and Cp2 are reduced; and the intracranial pressure increases dramatically to levels that could damage the optic nerve.

The only interesting difference between the three models is that in the full-constrained model P3 does not behave as expected. In the full-constrained model P3 varies between 11 mm Hg and 13 mm Hg, reflecting the fully constrained system; but failing to represent the changes in the system under the pathological circumstances.

Thus, a full-constrained model is a very good model to represent the normal CSF dynamics; but it could fail under certain circumstances to fully represent altered CSF dynamics.

CHAPTER 4

DISCUSSION

Walter Dandy's studies established the landmarks for the study in hydrocephalus, and by generalization, the underlying laws of CSF dynamics. Even though never proved, assumptions of bulk flow from the plexus choroideus to arrachnoid villi became the prevalent concepts derived from his studies. The concept of balanced production and absorption as the primary regulation of CSF volume and distribution is another prevalent concept from his studies. Both of these assumptions have constituted the frame of reference for nearly all the approaches to the study of CSF flow. The few attempts to deviate from this line of thought have not created a cohesive explanation on CSF flow dynamics, which could replace the existing paradigm.(Dandy 1919)

Since the description of normal pressure hydrocephalus by Hakim, and further attempts to characterize the brain parenchyma as a "sponge-like" structure, numerous authors have approached the study of the physical characteristics of the brain, and its relationship with CSF dynamics in the same way. Thus, numerous studies begin by modeling the brain as a porous material, and frequently use the Equations used in civil engineering for the study of soil.(Hakim S 1976, Johnston 2000, Meier 2002)

The purpose of this research is to find an alternate explanation of the accepted mechanism for cerebro-spinal fluid (CSF) bulk flow resultant from its production and absorption. In essence, this study directly challenges the previously explained hypothesis by assuming a fixed volume system, where no absorption or secretion of CSF is present. In a simpler statement, this study is intended to answer the following question: If the

formation / absorption of CSF does not explain the CSF flow, what alternative mechanism could be responsible?

In an effort to better understand CSF dynamics a computational model has been created based on the concept of a dynamic variation of the bulk properties of the brain parenchyma. This model focuses on cyclic changes in the compliance of brain parenchyma during each heart cycle, and its relation to the CSF flow. Our hypothesis is that cyclical variation of blood volume, which causes intermittent engorgement of the cerebral vasculature, will lead to a cyclical variation in the stress of the walls of the brain vessels. An increase in the vessels' wall stress produces a stiffer vessel. As the blood comes in, the increased stress of the brain vessels' walls produces an increment of the stiffness of the brain parenchyma, which means that brain compliance is reduced. When the blood is drained by the venous system the vessels' walls are released from load, and the brain compliance increases. The cyclical variation of the volume-pressure relation of the ventricular and subarachnoid spaces dictates the CSF flow dynamics between the two compartments, and the spinal compartment. The compliance variation of brain parenchyma moves CSF much like the cyclic variation of the heart volume-pressure relation pumps blood out from cardiac ventricles.

During each cardiac cycle the entering blood decreases the brain parenchyma compliance, squeezing the CSF out from the cranial cavity into the spinal compartment. As the venous drainage proceeds, the CSF refluxes into the cranial cavity. Inside the cranium there is a complex dynamic flow of CSF between the intra-ventricular and subarachnoid space. This intracranial dynamic is dictated mainly by a relation between the arterial blood flow coming in, and the venous drainage in two different

compartments, one superficial and one deep. CSF circulation has a complex pattern that has been documented by several authors with phase-contrast cine MRI.

Taking into consideration that there does not exist inside the brain a contractile element, which can impart a propelling force to the CSF circulation, our model provides a suitable explanation for the CSF circulation. The present model resembles the CSF dynamics coupled with the cardiac cycle, and offers a flexible model for studying both normal and altered CSF dynamics. Future work will extend the model to pathological entities like Communicating Hydrocephalus.

Several models have been published in an attempt to understand both normal and abnormal CSF circulation. For over two decades numerous models have been created in an attempt to explain the behavior of the CSF. Every model published before 2001 is based on the assumption that the CSF dynamics is governed by a relation between the production of CSF by the plexus choroideus, and absorption of CSF at the arachnoid Villi. (Guinane) Thus the emphasis focuses on modeling the production, and the absorption; as well as the response of the cerebral tissue to the pressure caused by the existing CSF. As a consequence, these models always include some representation of the rate of CSF volume (dv/dt) change , as a function of the difference between the formation rate $I_f(t)$ and the absorption rate $I_a(t)$

$$\frac{dv}{dt} = I_f(t) - I_a(t) \tag{4.1}$$

This concept was obviously linked to the controlling function of the absorption rate, which was modeled as a simple pressure difference between the subarachnoid

compartment and the superior sagittal sinus , where the CSF will enter into the blood stream. Thus:

$$I_a(t) = \frac{1}{R}(P(t) - Pss) \tag{4.2}$$

where P(t) is the intracranial pressure, Pss is the venous pressure at the superior sagittal sinus, and R is the resistance at the arachnoid villi to the flow of CSF.

Next, the concept of brain compliance was incorporated into the model, as the relation between volume (V) and pressure (P)

$$C = \frac{V}{P} \tag{4.3}$$

When substituting Equations 4.3 and 4.2 into Equation 4.1, and rearranging terms, the following first order differential equation was obtained:

$$C\frac{dp}{dt} + \frac{P(t)}{R} = I_f(t) + \frac{Pss}{R} \tag{4.4}$$

This has been regarded as the paramount dogma, and by consequence the starting point of modeling the CSF dynamics.

As the obtained models did not give a full representation of the system, additional refinements were added as including a non linear compliance of the brain. Marmarou introduced in 1978 the concept of a non linear compliance in the form:

$$\frac{dv}{dp} = \frac{1}{kP^1} \tag{4.5}$$

Where k = constant, and P^1 is a reference pressure for a reference volume V^1. This first order differential equation has a solution:

$$P(V) = P^1 e^{k(v-v^1)} \tag{4.6}$$

Still with no adequate results, the literature has recently started to deviate into a number of different approaches. Nagashima, followed by some others (Pena,Czonyka), attempted modeling the brain parenchyma and its relationship with CSF dynamics using finite element analysis. This approach has faced the shortcoming of not having a reliable and unified figure for the bulk properties of the brain tissue; which is a fact that becomes very understandable if the literature published by neuro-anesthesiologists and intensive care physicians is examined. Their concept is not of a fixed, static compliance of the brain. Physicians are aware of the dynamic characteristic of the brain compliance. The dynamics of brain compliance relies on the vessels' wall dynamics; which in turn is responsive to a variety of procedures. Anesthesiologists and intensive care physicians are interested in manipulating the vessels diameter in order to increase the compliance and by consequence decrease the intracranial pressure. Various engineering studies ignore this fact, and attempt to measure the compliance in tissue extracted from the brain or in dead animals where no vessels regulation is present. Also, some engineering studies have quantified the bulk properties of the brain by directly measuring the tissue in living animals with out quantifying the amount of arterial PCO_2, one of the most potent and recognized determinants of the brain vessels' diameters. Other studies have approached the quantification of the brain physical properties by a direct "repetitive contact" of the cortex surface, not taking into consideration the inflammatory response elicited by such

technique. All these factors have contributed to equivocal and non uniform figures when calculating the brain bulk properties. As a result, the approach of the finite element method has a limited use until the brain physical properties are better categorized and understood.

With the contribution of the phase-contrast cine MRI, the evidence of the lack of consistency in the accepted paradigm of CSF has been increasing. Thus several attempts to explain and model the forces contributing to the CSF flow have been published; though none of them has received wide acceptance. Egnor et al. have proposed a "resonant harmonic oscillator" based on an electric equivalent with no clear explanation of the elements intervening in the model. Greitz gives great importance to a "piston action" of the brain pumping the CSF into the spine, as a consequence of the arterial dilation during systole. Nevertheless this piston action does not explain the complex nature of the movement and the phase lag in the CSF response to heart-systole in separate regions of the brain, as evidenced by Naidich et al. It is important to say that Greitz major contribution is highlighting the importance and predominance of the CSF pulsatile flow, in his MRI studies. He also documented the close relationship between the amount of CSF expelled from the cranial into the spinal cavity, and the amount of blood entering the cerebral vessels. Bering believes the CSF movement could be explained by pulsating forces derived from and communicated by the choroid plexus at the moment of the CSF formation in the interior of the ventricles. Bhadelia emphasizes the importance, and the impact of the altered venous drainage in the behavior of the CSF dynamics. Czonika calls attention to altered vascularization in certain patients with altered CSF dynamics.

The hypothesis of this research reinforces the importance of the pulsatile flow and introduces several novel concepts. The most important event in CSF dynamics is the

flow occurring between the intracranial and spinal compartments, and not the bulk flow caused by production/absorption. While the calculated rate of formation of CSF is 0.35 ml/ min, which give us an approximated 0.005 cc per cycle, the flow between the intracranial and the spinal compartments has an average normal value of 10 cc/ cycle. Thus the amount of CSF flowing back and forward inside / outside the cranium in each cycle is considerably larger, and should be the one explaining the CSF dynamics.

The brain compliance is not a static value; it changes in a cyclic way. The only oscillating mechanical force inside the brain is derived from the blood flow, which in turn originates from the cardiac cycle. The compliance cycle in the brain is dependent on the cardiac cycle. The brain's tissue compliance is inversely proportional to the stress in the wall of the vessels. As a consequence during systole the compliance diminishes, and during diastole the compliance increases. The relation between arterial cerebral blood - influx- and cerebral venous drainage- efflux- is a critical determinant of the compliance cycle. The compliance in the spinal compartment does not sustain this critical variation. Thus the spinal compartment acts as a buffer for the CSF pulsatile flow in and out of the cranium. The pulsatile flow is modeled better as a cyclic redistribution of CSF volumes between the different CSF compartments. The intracranial variation in compliance could explain the CSF circulation between the intracranial and spinal compartments. There exist at least two important CSF compartmental regions related to two distinctive venous territories: the superficial or cortical, and the deep or periventricular region. These territories maintain a balance, during the compliance cycle by engorging and draining in a synchronized way. Altered balance could result in redistribution of the compartmental volumes.

The CSF flow has a complex pattern formed by at least four different stages per each period. This CSF complex pattern, documented by phase contrast cine MRI, is well explained by the compliance cycle of the brain tissue. CSF flow is explained by two coupled cycles; the cardiac cycle and the compliance cycle of the brain's tissue. Altered states of the CSF flow, not fully understood at the present, could be readily explained in view of this mechanism. The model presented here captures in a simplified form the essential components, and their relation to explain the normal CSF flow. Three components are essential to the adequate model performance. Brain compliance, cerebral blood flow and relative dimensions between the foramen magnum (R2) and the intraventricular CSF pathways represented by the Sylvius aqueduct(R1). If these parameters are maintained in physiological values, the model performance is solid and consistent. Furthermore, introducing the concept of a cycling compliance of the brain tissue, dependent on the vessels stiffness, establishes a coupling mechanism between the cerebral blood flow and the CSF flow. This mechanism is a better explanation for the missing transfer function between blood pressure and intracranial pressure.

In medicine and engineering interest is usually driven towards solving existing problems. Regularly these are very complex problems addressed by scientists across geography and generations. The concept here presented, like many complexities that arise in the search for an answer, helps to review the problem from a different perspective, and discloses a new path towards solving the problem. Further research should be implemented to confirm the model; primarily the concept of compliance variation during the cardiac cycle should be calculated from MRI measurements. Secondly the compliance variation should be measured in patients with normal pressure hydrocephalus. Alperin et al. have described a technique for calculating the brain elastance in patients with

traumatic brain injury; adapting and implementing their technique would be very useful for calculating the compliance in normal subjects and in patients in which altered CSF dynamics.

Undoubtedly, studying hydrocephalus has created a big interest in the physiology of CSF, which is the focus of the present study. For a long time the approach has been directed to prove an unbalanced production/ absorption of the CSF. Nevertheless a bulk flow between the production site and the absorption site was never proved to be the dominant trait of CSF dynamics. Recently this accepted explanation has been questioned, though there is not any other existing coherent and consistent explanation. Since the introduction of phase contrast cine- MRI for the study of CSF in living organism, specially human beings, numerous data has been collected that have increased the amount of uncertainties more than solving the puzzle. The present study takes those data, analyzes them in context of physics and engineering, and gives a suitable response explaining the mechanism involved in the movement of CSF.

4.1 Conclusion

As a summary, the results of the present work introduce the following novel concepts:

- The brain is built as a hierarchically structured material from where its viscoelastic properties are derived.
- The amount of blood present inside of the brain vessels determines the compliance of the brain parenchyma.
- There is a cyclic variation of the compliance of the brain tissue as a resultant of the blood flow, and by extension of the cardiac cycle.
- The CSF dynamics could be adequately represented by three compartments: ventricular, subarachnoideal and spinal.
- The normal oscillatory flow characteristics of the CSF could be better understood in terms of compliance, than in terms of the relation between production/absorption of CSF.
- A more cohesive explanation of diverse pathologies of the CSF dynamics (communicating hydrocephalus, increased intracranial hypertension) could be explained in terms of altered compliance of one or several of the cited compartments.
- A clearer understanding of the normal and abnormal CSF dynamics, could lead to wiser decision making, thus improving patients' treatment.
- More accurate shunting devices could be developed if there is a better understanding of the normal and abnormal CSF dynamics.
- The present model is a starting point, validated by existing published data from humans' MRI. Further funding should be sought to continue the research of this promising field.

APPENDIX 1

ALPHA PARAMETER CALCULATION

Alpha represents the decrement of compliance, reciprocal of increment in stiffness, of the vessels' wall as a resultant of the additional blood volume hold inside of the vessel during each cardiac cycle. As delta blood volume is hold inside the brain vasculature , pressure increases, with a consequent increment in axial and circumferential stress, resulting in a decreased compliance of the vessels ; and by extension a decreased compliance of the brain tissue. If this decrement in compliance is integrated on the whole parenchyma it will be representing the whole decrement of the brain compliance per cardiac cycle, as a consequence of the cerebral blood flow coming inside of the brain vessels, during systole. In the present model this mechanism has been incorporated as a loss of compliance that is directly proportional to the incoming blood volume (v_{sv}), by a factor alpha (α). Alpha represents the decrement of compliance of the vessel's wall as a resultant of the additional pressure resulting form the additional blood volume held inside of the vessel.

Thus alpha has units of mm Hg $^{-1}$, as explained in equation 3.4. Recall:

$$ci(t) = ci_0 - \alpha v_B$$
$$i = 1,2$$

Alpha is easy to calculate by first subtracting equation 3.25 from equation 3.3, which gives equation 3.26. Recall:

$$v3 - vB = Vcra - Vcsf$$

then by differentiating the expression we have equation 3.27. Recall:

$$\frac{dv3}{dt} - \frac{dvB}{dt} = 0$$
$$\frac{dv3}{dt} = \frac{dvB}{dt}$$

This means that any amount of blood coming into the cranium during each cardiac cycle has to be compensated by an equal amount of CSF coming out of the cranium into the spinal compartment.

Then Alpha is calculated from the equation 3.31. Recall:

$$\frac{dv3}{dt} = \frac{1}{R2}\left(\frac{v2(t)}{c2(t)} - \frac{v3(t)}{c3}\right)$$

and as c2(t) could be replaced by equation 3.4. Recall:

$$c2(t) = c2_0 - \alpha v_B$$

From equation 3.10, the following relation is established:

$$\frac{dvB}{dt} = \frac{dv3}{dt} = \frac{1}{R2}\left(\frac{v2(t)}{c2_0 - \alpha v_B} - \frac{v3(t)}{c3}\right)$$

$$\left(\frac{R2dvB}{dt} + \frac{v3(t)}{c3}\right)\frac{1}{v2(t)} = \frac{1}{c2_0 - \alpha v_B}$$

$$\left(\frac{dt}{R2dvB} + \frac{c3}{v3(t)}\right)v2(t) = c2_0 - \alpha v_B$$

$$\left(\frac{v2(t)dt}{R2dvB} + \frac{v2(t)c3}{v3(t)}\right) = c2_0 - \alpha v_B$$

$$\alpha v_B = c2_0 - \left(\frac{v2(t)dt}{R2dvB} + \frac{v2(t)c3}{v3(t)}\right)$$

$$\alpha = \frac{1}{v_B}\left(c2_0 - \frac{v2(t)dt}{R2dvB} - \frac{v2(t)c3}{v3(t)}\right)$$

At the end of systole when all the blood flowing-in is already inside of the vessels, just before the slope of the volume curve on time changes direction, thus the slope is equal to zero, we have the following situation:

$$\frac{dv3}{dt} = \frac{1}{R2}\left(\frac{v2(t)}{c2_0 - \alpha v_B} - \frac{v3(t)}{c3}\right) = \frac{dvB}{dt}$$

$$\frac{dv3}{dt} = \frac{1}{R2}\left(\frac{v2(t)}{c2_0 - \alpha v_B} - \frac{v3(t)}{c3}\right) = \frac{dvB}{dt} = 0$$

which makes possible to calculate alpha value:

$$\frac{1}{R2}\left(\frac{v2(t)}{c2_0-\alpha v_B}-\frac{v3(t)}{c3}\right)=0$$

$$\frac{v2(t)}{c2_0-\alpha v_B}-\frac{v3(t)}{c3}=0$$

$$\frac{v2(t)}{c2_0-\alpha v_B}=\frac{v3(t)}{c3}$$

$$\frac{v2(t)c3}{v3(t)}=c2_0-\alpha v_B$$

$$\alpha v_B=c2_0-\frac{v2(t)c3}{v3(t)}$$

$$\alpha=\left(c2_0-\frac{v2(t)c3}{v3(t)}\right)\frac{1}{v_B}$$

At these precise instant several values are known, that when substituted in the Equation (1.7) give the value of alpha:

v2=80, v3=45, $c2_0$=90/7, c3=5, vb=10.

$$\alpha=\left(c2_0-\frac{v2(t)c3}{v3(t)}\right)\frac{1}{v_B}$$

=

$$\alpha=\left(\frac{90}{7}-\frac{80*5}{45}\right)\frac{1}{10}$$

$$\alpha=0.3968$$

Alpha could also be computed by calculating the difference between Cp2 compliance at the end of the diastole, and Cp2 compliance at the end of systole. Thus Delta compliance (δc) is

$$\delta c = c_d - c_s$$

$$c = \frac{v}{P}$$

$$c_d = \frac{90}{p_d} = \frac{90}{7}$$

$$c_s = \frac{80}{p_s} = \frac{80}{9}$$

where C_d is compliance at end of diastole and C_S is compliance at end systole, Pd is pressure at end of diastole , and Ps is pressure at end systole.

The difference between the two compliances is caused by the effect of the blood volume that had just come in during the initial portion of systole, until it reaches end systole.

$$\delta c = c_d - c_s$$

$$\delta c = \frac{90}{7} - \frac{80}{9} = 3.9683$$

So delta compliance(δc) is the amount of decrement in compliance from systole to diastole, which in turn is equal to the amount of blood volume coming during systole times alpha.

$$\delta c = \alpha v_B$$

$$\frac{\delta c}{v_B} = \alpha$$

$$\alpha = \frac{3.9683}{10} = 0.39683$$

In the first generation model C1 compliance is set at 25/70, while the C2 compliance is set at 90/7. Thus there is a ratio of C2/ C1, 90/25, of 3.6. It could be interpreted as discrepancy in the original size, and surface of each compartment, which also implies that compliance should vary in the same proportion during the systole. As a consequence alpha for C1 should be 1.1 mm Hg^{-1}, and alpha for C2 it should scaled by 3.6 times greater, to a value of 3.9 mm Hg^{-1}.

APPENDIX 2

EXTENDED SENSITIVITY ANALYSIS OF THE MODEL

When modeling any complex system, it is not unusual to find different published values for certain specific parameter of the model; or sometimes it could be very difficult to measure directly or indirectly a parameter with a great level of accuracy. Some other times a new parameter is introduced, and by consequence no one has measured such parameter in the system of interest. Also, in the real world some parameter values change in time. These sets of possibilities create certain amount of uncertainty in the model. Uncertainty that could be of two types; stochastic and epistemic. Stochastic or aleatory uncertainty refers to non-controllable or non-deterministic variables; usually they are a result of the system interacting with the environment. They are frequently referred in the literature as irreducible, inherent or stochastic. Epistemic uncertainty refers to the ones that arise for the lack of knowledge of a system; these ones are also referred as reducible, subjective or cognitive. Epistemic uncertainties can frequently be calculated from other measured parameters; or once they have been identified, they could be measured in a direct or indirect way during further experimentation. Consequently when building a model, the modeler has certain level of uncertainty, and when choosing parameters values he is compelled to choose estimates.

Sensitivity analysis helps building confidence in the model, as it helps the modeler to estimate what level of accuracy is necessary for a parameter to make the model useful and valid by comparing the changes in outcome of the system as the chosen parameter is varying.

In the present CSF dynamics model a new concept is introduced, alpha parameter, relating the loss in the parenchymal compliance as a function of the increment of delta blood-volume inside of the vessels. Alpha could be calculated from existing parameters, Equation A-1 Appendix 1, thus it constitutes an epistemic uncertainty. Therefore, it is important to perform a sensitivity analysis to the alpha parameter in the system. Two sets of sensitivity analysis were performed. One set was performed for the sine driven model; and another set was performed for the full-constrained model.

After determining the value alpha, used in the simulation of the sine driven model, which was the same used in the full-constrained model, a stepwise decrement of one percent of its value was implemented until a total ten percent decrement was achieved. Also, a stepwise increment of one percent of its value was implemented until a total ten percent increment was achieved. The system response was recorded for each of the variations. The parameters chosen to evaluate the impact of alpha in the model were, C1, C2, V1, V2, V3, P1, P2, and P3. The results are shown in the figures below, sine driven model figures are labeled as "Non-Constrained Model", while full-constrained model are labeled as "Constrained Model". As the events are regulated by the cardiac cycle, each figure shows a maximum value in red, and a minimum value in blue per cycle.

The results for the sensitivity analysis for the sine driven model are shown on Figures A2.1, and A2.2. An overall 11 percent variation of C1 is observed when a 20% variation of alpha is introduce; while an overall 8 percent variation of C2 is observed when a 20% variation of alpha is introduce

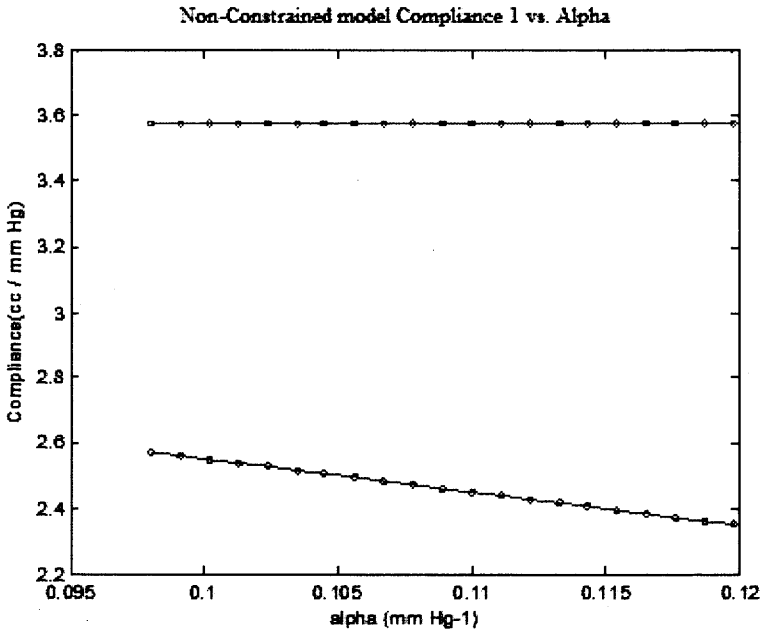

Figure A2.1 Sine driven model; behavior of compliance 1 as alpha is changed.

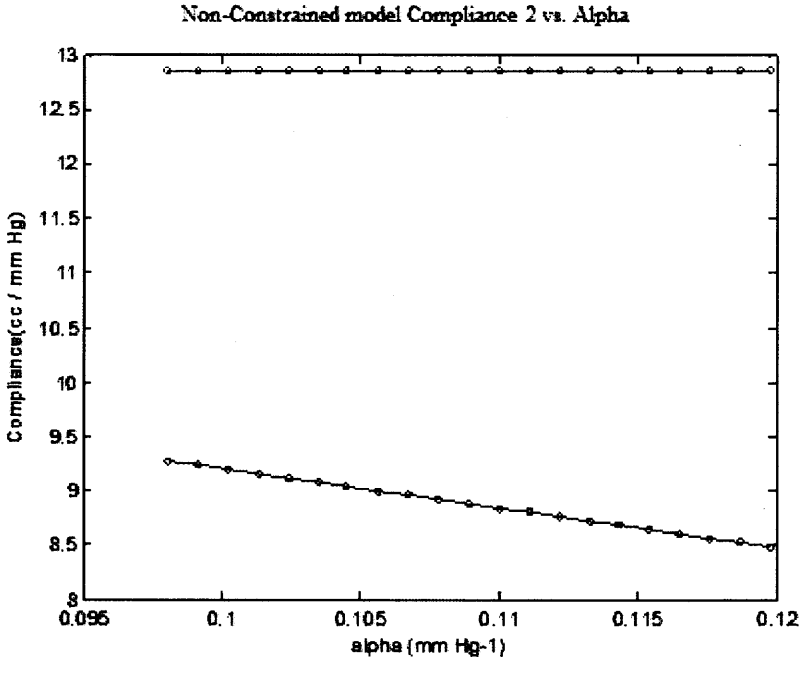

Figure A2.2 Sine driven model; behavior of compliance 2 as alpha is changed.

Figure A2.3 shows an overall change in volume one of 1.16 %, corresponding to a 20% alpha variation. Figure A2.4 shows an overall change in volume two of 3.7 %, corresponding to a 20% alpha variation..

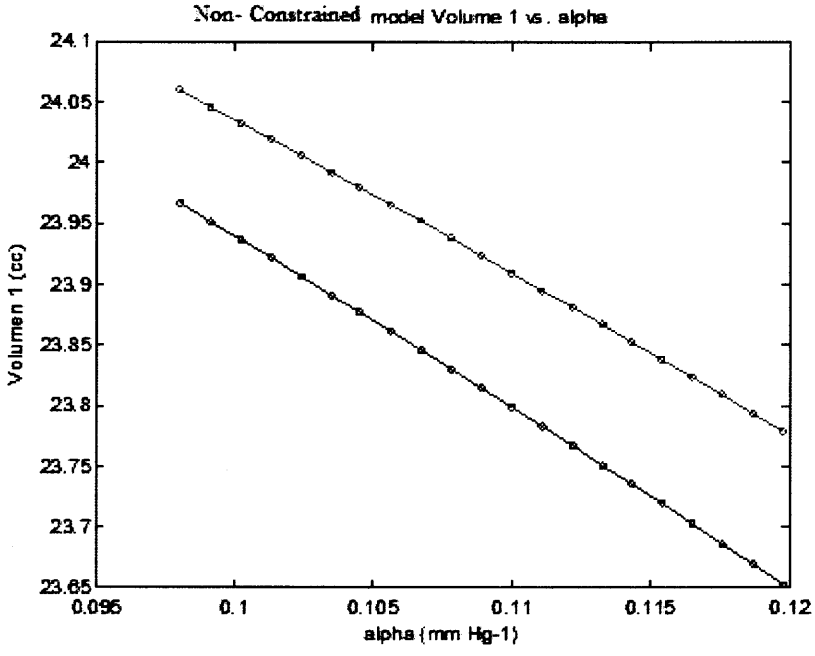

Figure A2.3 Sine driven model; behavior of Volume 1 as alpha is changed.

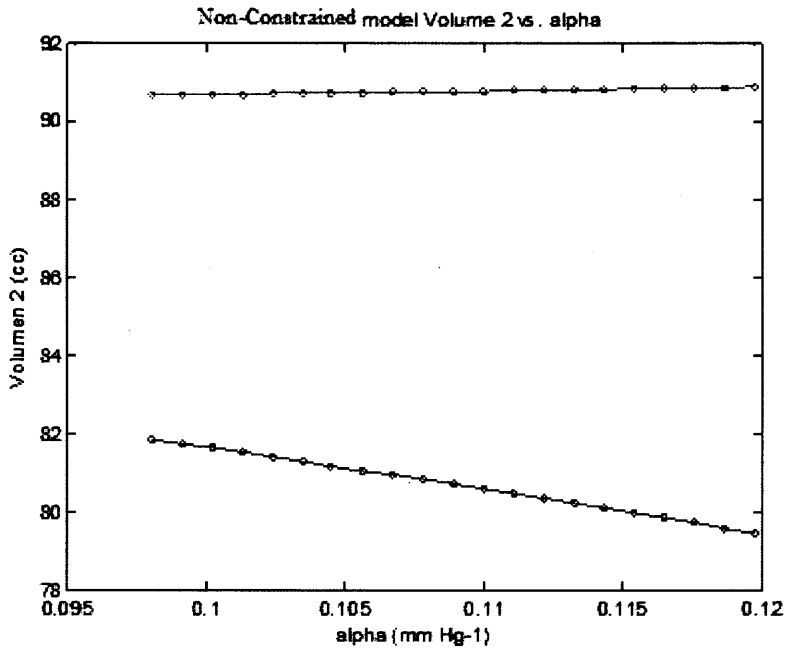

Figure A2.4 Sine driven model; behavior of Volume 2 as alpha is changed.

Being Volume three a crucial value, and the main difference between the non-constraint and the fully constraint model, it is shown with a fine grid to facilitate a more careful analysis. Figure A2.5 shows an overall change in volume three of 5.4 %, corresponding to a 20% alpha variation

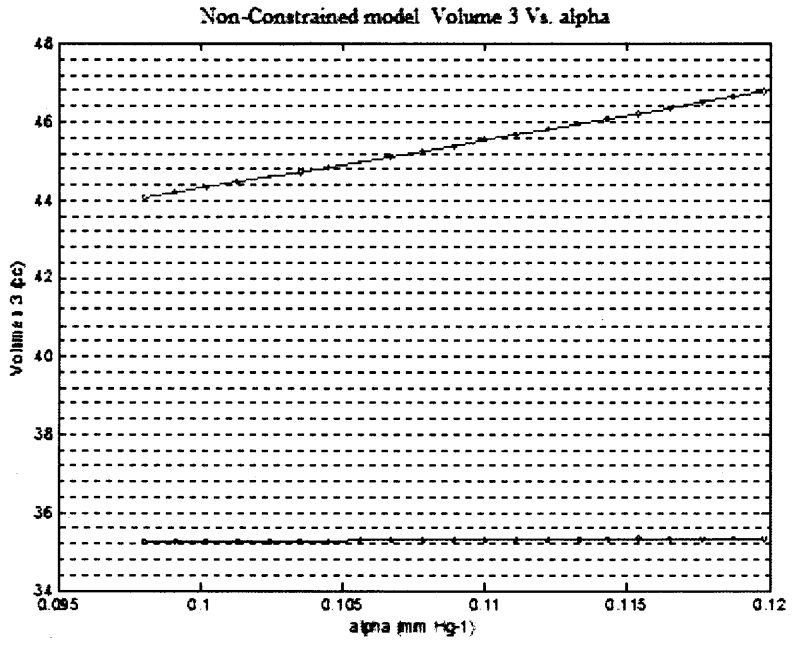

Figure A2.5 Sine driven model; behavior of Volume 3 as alpha is changed.

The sensitivity analysis shows an adequate behavior of the model, computing volumes for the three compartments within physiological ranges; even when the alpha parameter was varied between a plus or minus ten percent, for an overall twenty percent alpha variation. The volume changes vary between a 1% to a 5.4%, which is considered a very little variation.

Figure A2.6 shows an overall change in pressure one (P1) of 6 %, corresponding to a 20% alpha variation. Figures A2.7, and A2.8 show an overall change in pressure two, and in pressure three (P2, P3) of 6.4 %, corresponding to a 20% alpha variation.

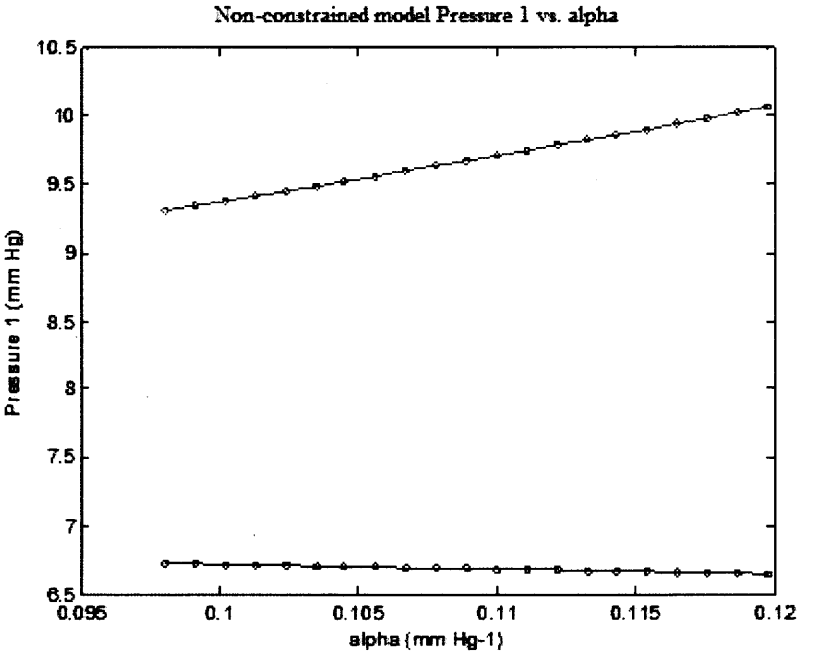

Figure A2.6 Sine driven model; behavior of Pressure 1 as alpha is changed.

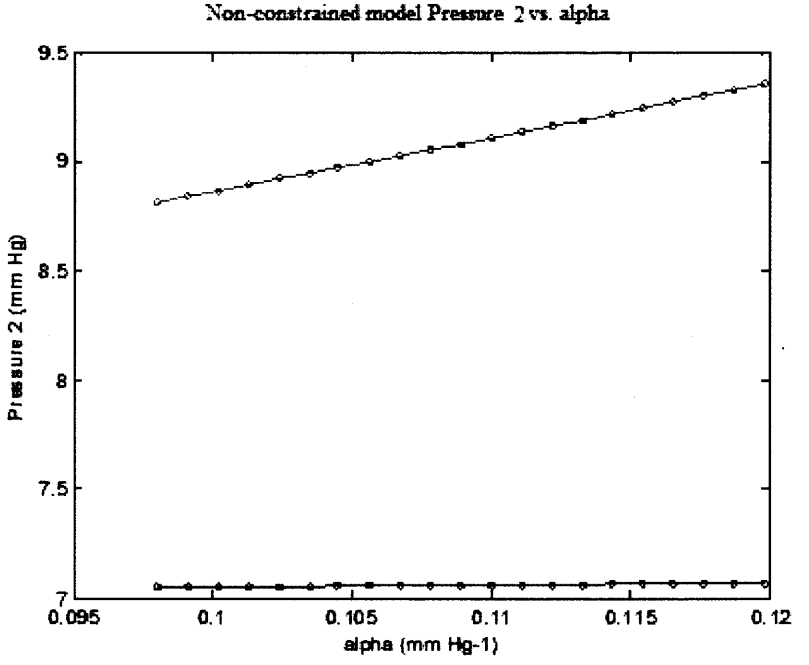

Figure A2.7 Sine driven model; behavior of Pressure 2 as alpha is changed.

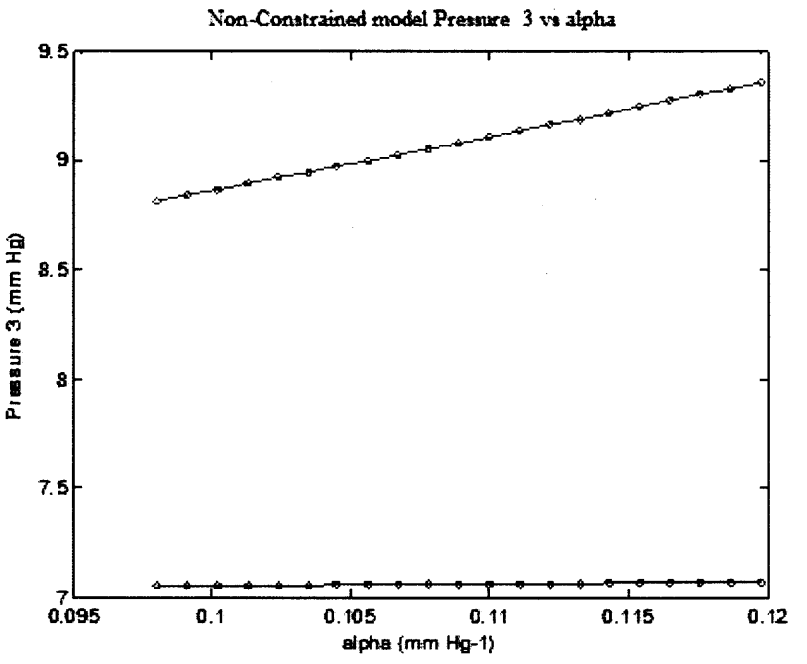

Figure A2.8 Sine driven model; behavior of Pressure 3 as alpha is changed.

As significant changes in behavior of the system did not occur when alpha parameter was changed, we can have a good confidence on the alpha parameter in the sine driven model. The change of alpha parameter values also demonstrate a robust model as the structure of the system maintains its dynamics within physiological limits, with out a strong dependence on the parameter value. These results show that it is the structure of the system, and not the parameter values, which has most influence on the behavior of the system.

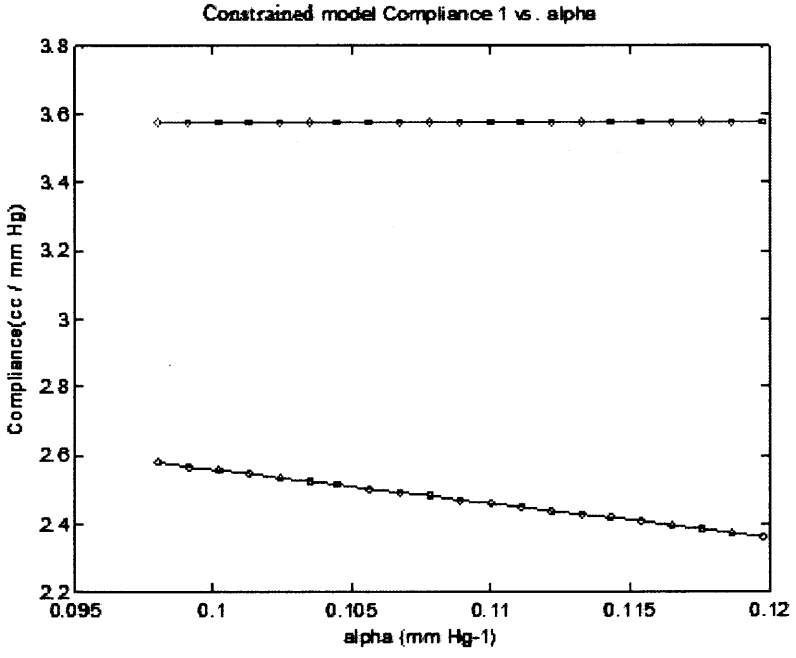

Figure A2. 9 Full-constrained model; behavior of compliance 1 as alpha is changed.

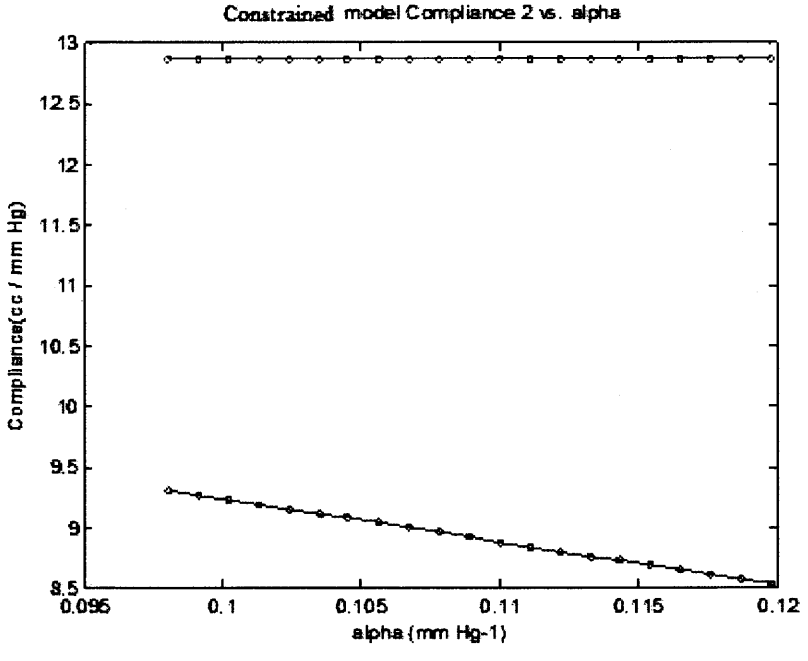

Figure A2.10 Full-constrained model; behavior of compliance 2 as alpha is changed.

Results from sensitivity analysis of the full-constrained model are illustrated on Figures A2.9 and following. As shown on Figures A2.9 and A2.10 , an overall 11 percent variation of C1 is observed when a 20% variation of alpha is introduce; while an overall 8 percent variation of C2 is observed when a 20% variation of alpha is introduced.

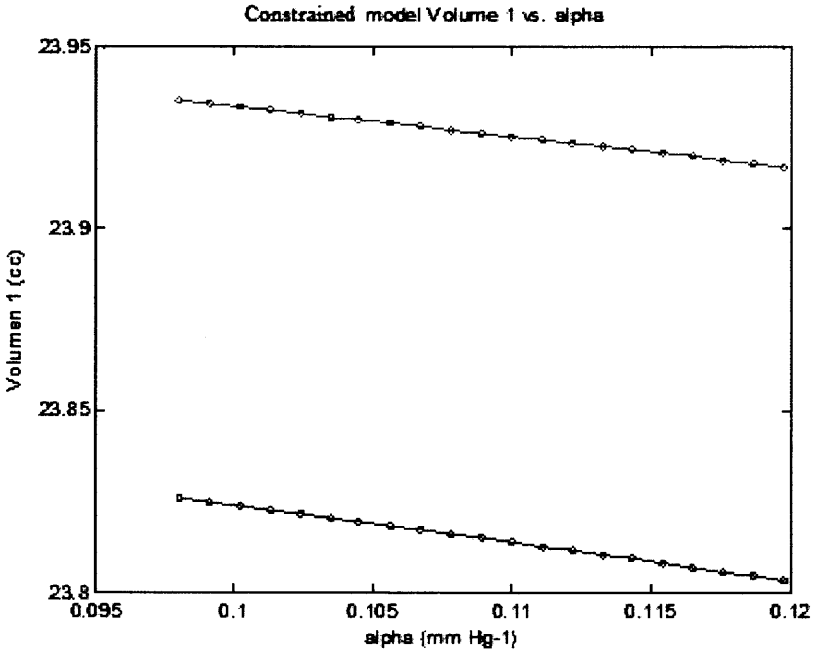

Figure A2.11 Full-constrained model; behavior of volume 1 as alpha is changed.

Figure A2.11 shows an overall change in volume one of 0.05 %, corresponding to a 20% alpha variation. Figure A2.12 and Figure A2.13 show no change in volume two and volume three when a 20% alpha variation is introduced. This fixed volume, insensitive to alpha variation, is the obvious result of the constraint introduced; because the volume variation in compartment two and compartment three is defined exclusively by the blood volume coming in.

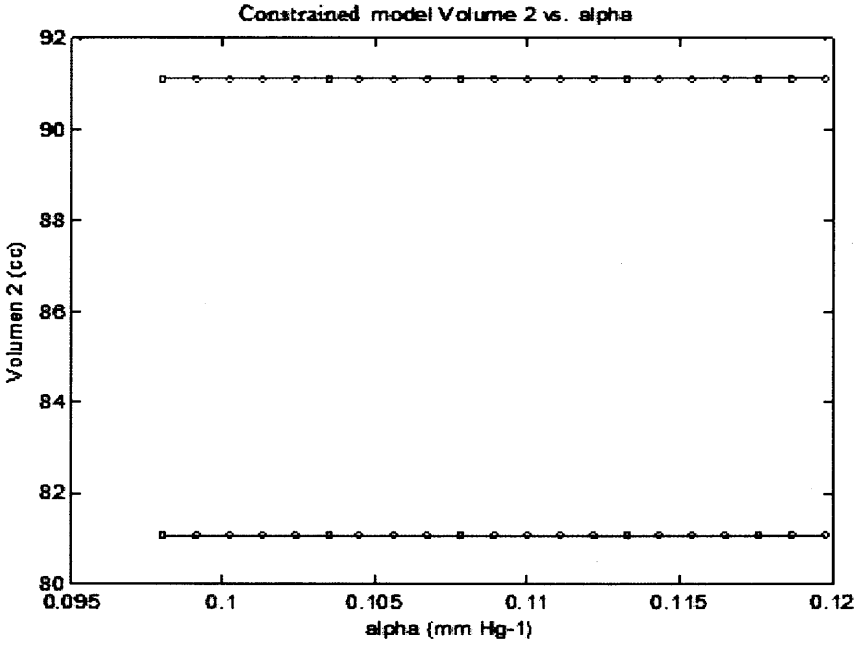

Figure A2.12 Full-constrained model; behavior of volume 2 as alpha is changed.

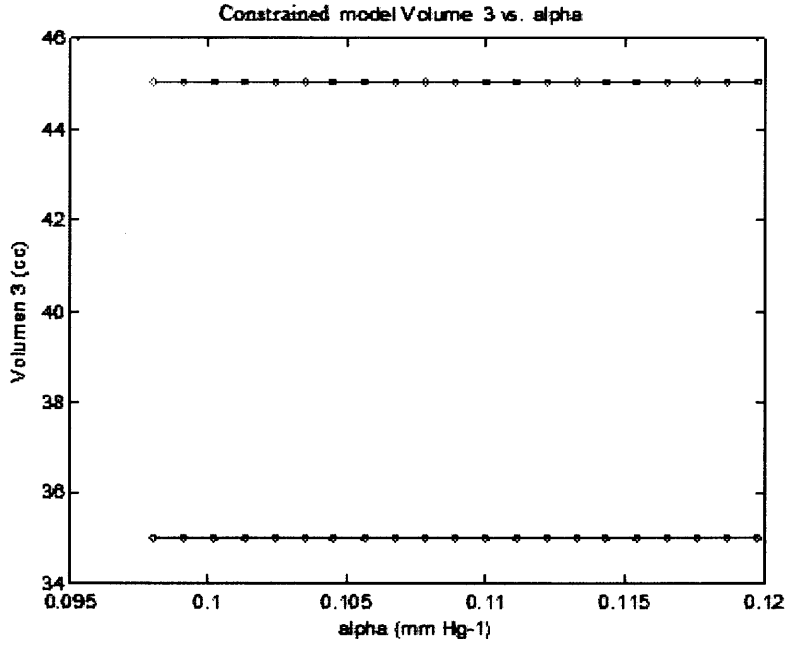

Figure A2.13 Full-constrained model; behavior of volume 3 as alpha is changed.

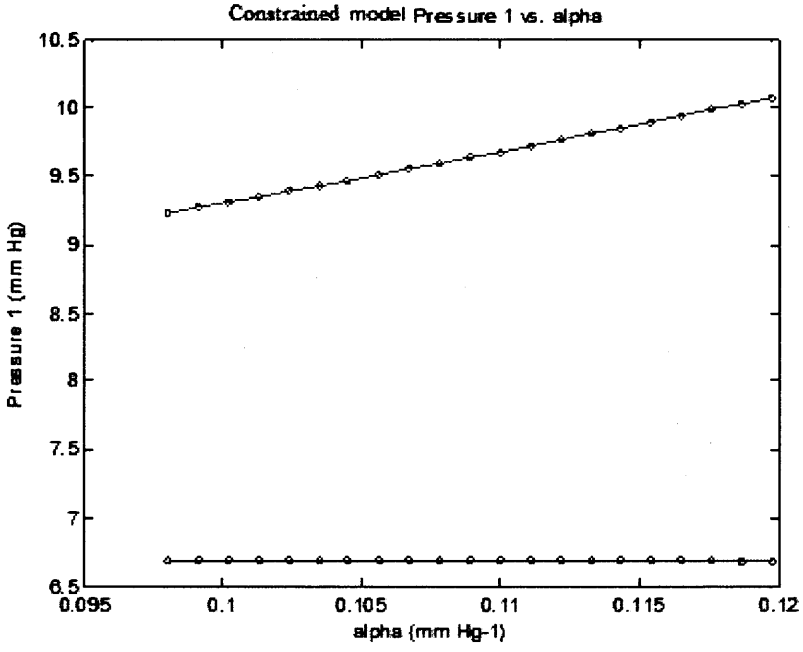

Figure A2.14 Full-constrained model; behavior of Pressure 1 as alpha is changed.

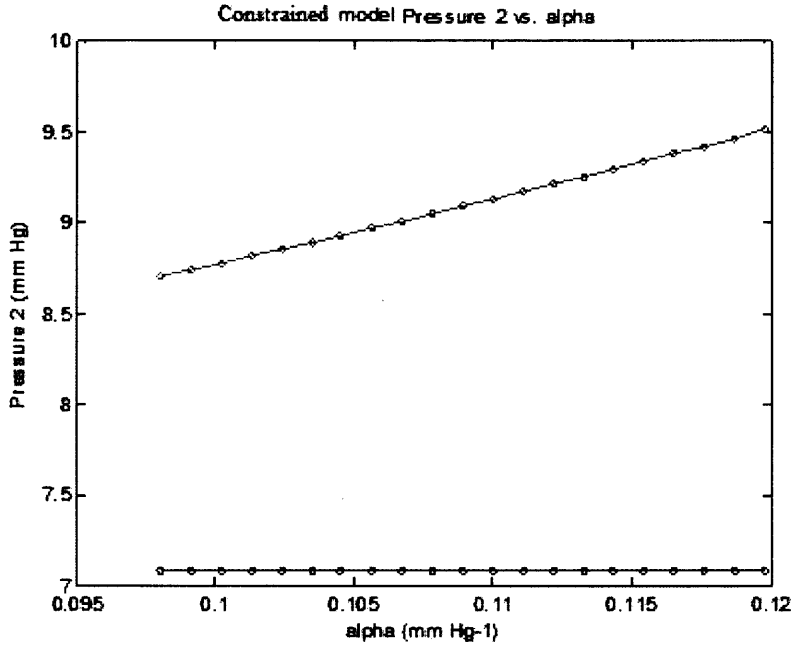

Figure A2.15 Full-constrained model; behavior of Pressure 2 as alpha is changed.

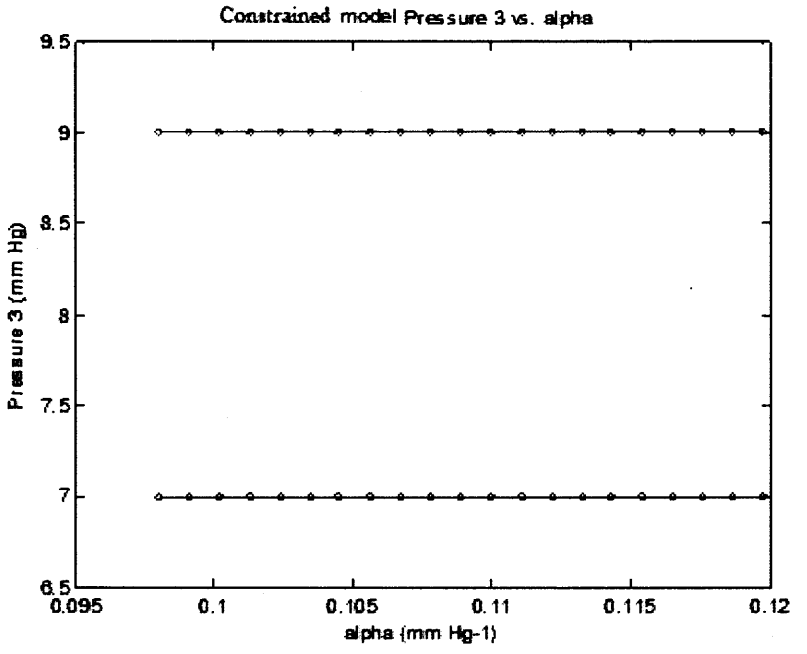

Figure A2.16 Full-constrained model; behavior of Pressure 3 as alpha is changed.

Figure A2.14 shows an overall change in pressure one of 9 %, corresponding to a 20% alpha variation. Figure A2.15 shows an overall change in pressure two of 8.4 %, corresponding to a 20% alpha variation. Figure A2.16 shows no change in pressure three, corresponding to a 20% alpha variation. The pressure variation in the full-constrained model is maintained in the normal physiological range during the 20% alpha variation.

The constraint model proves to behave in a very robust manner describing the normal CSF dynamics. The variation of the alpha parameter is well tolerated by the model.

Two resistances, R1 and R2, are important parameters of the model which also have been calculated from anatomical references. Therefore is important to perform sensibility analysis on both of them.

After determining the value of R1, used in the simulation of the Sine Driven Model, which was the same used in the Full-Constrained Model, a stepwise decrement of

one percent of its value was implemented until a total ten percent decrement was achieved. Also, a stepwise increment of one percent of its value was implemented until a total ten percent increment was achieved. The system response was recorded for each of the variations. The parameters chosen to evaluate the impact of alpha were, C1, C2, V1, V2, V3, P1, P2, and P3. The results are shown in the set of figures below, sine-driven model figures are labeled as "Sine Driven Model", while constrained model figures are labeled as "Constrained Model". As the events are regulated by the cardiac cycle, each figure shows a maximum value in red, and a minimum value in blue, per cycle.

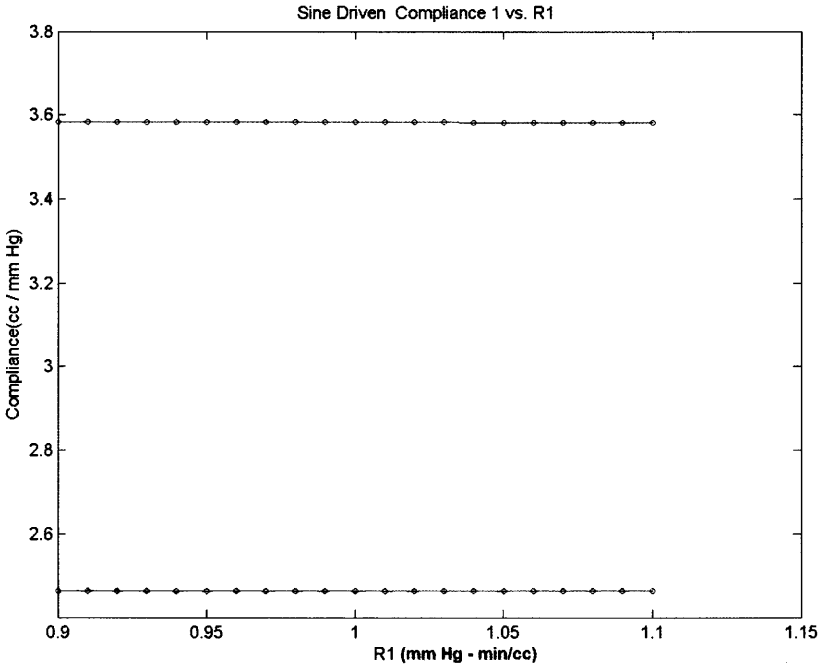

Figure A2.17 Sine driven model; behavior of C1 as R1 is changed.

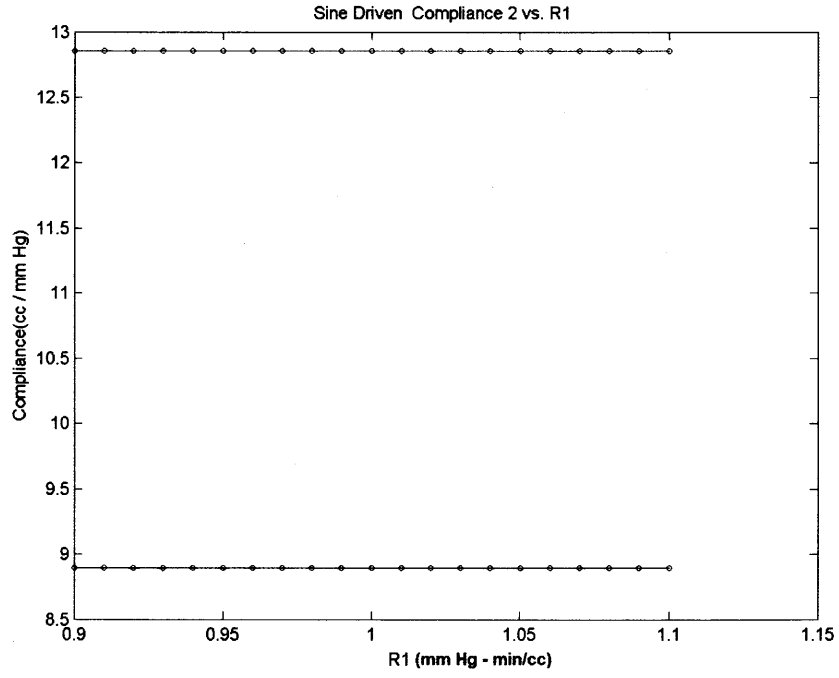

Figure A2.18 Sine driven model; behavior of C2 as R1 is changed.

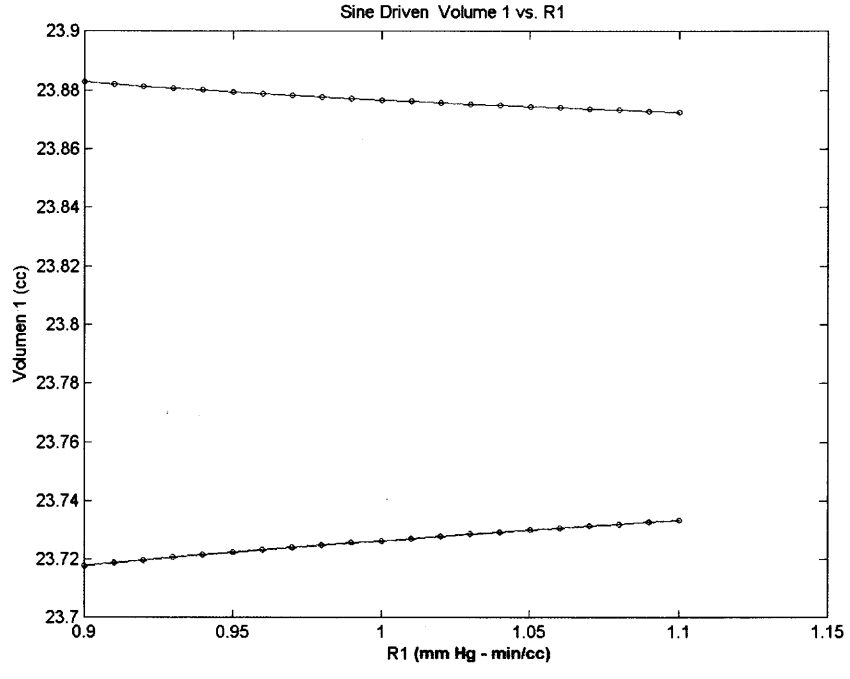

Figure A2. 19 Sine driven model; behavior of V1 as R1 is changed..

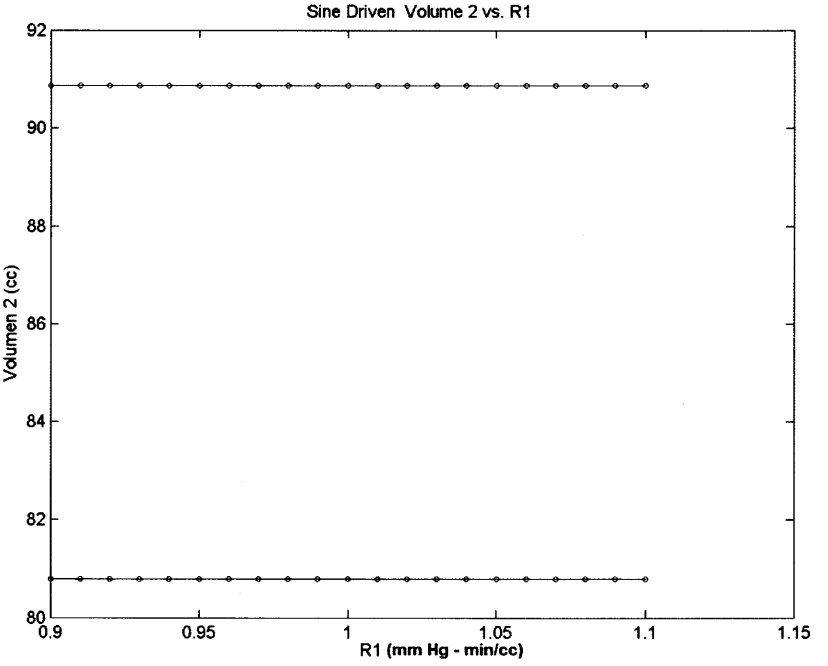

Figure A2. 20 Sine driven model; behavior of V2 as R1 is changed.

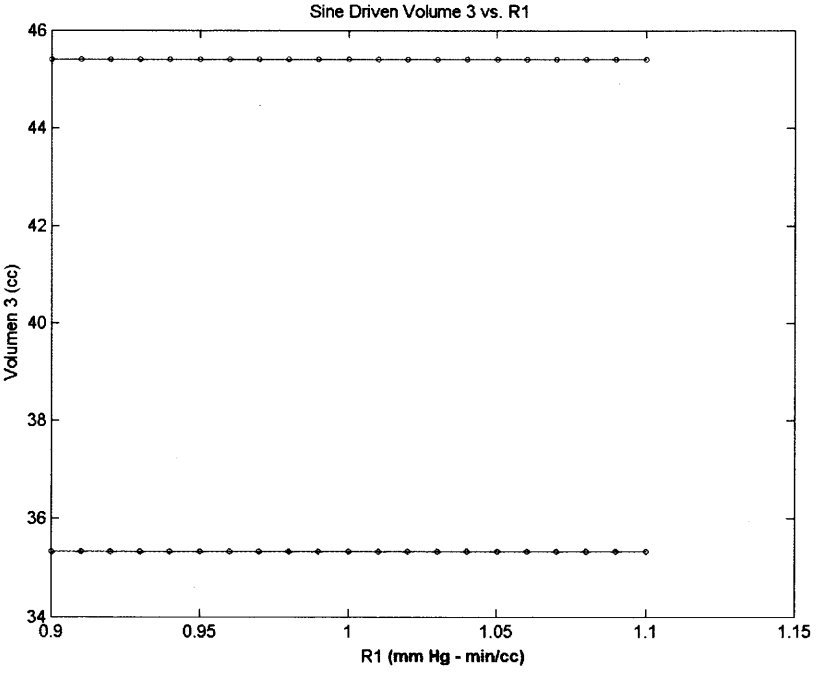

Figure A2.21 Sine driven model; behavior of V3 as R1 is changed.

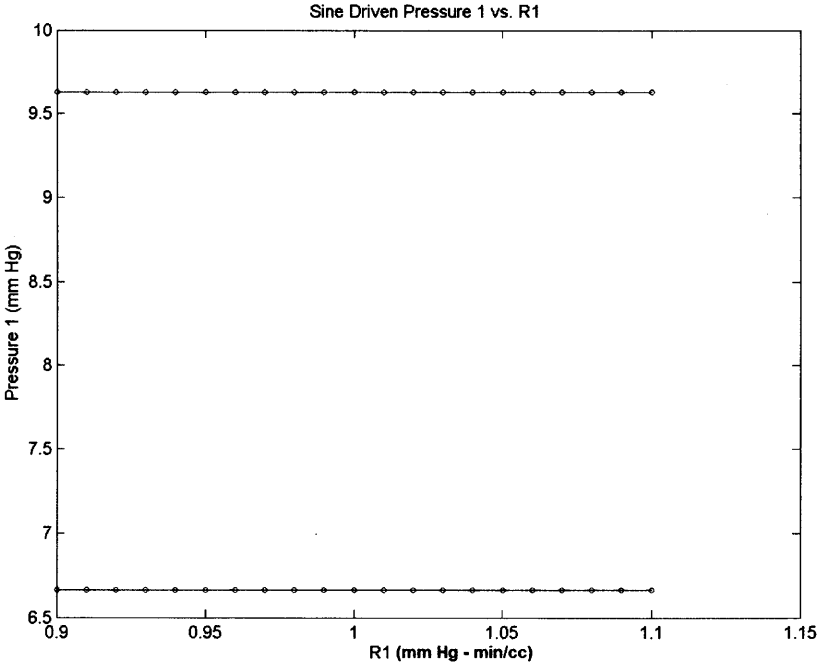

Figure A2. 22 Sine driven model; behavior of P1 as R1 is changed.

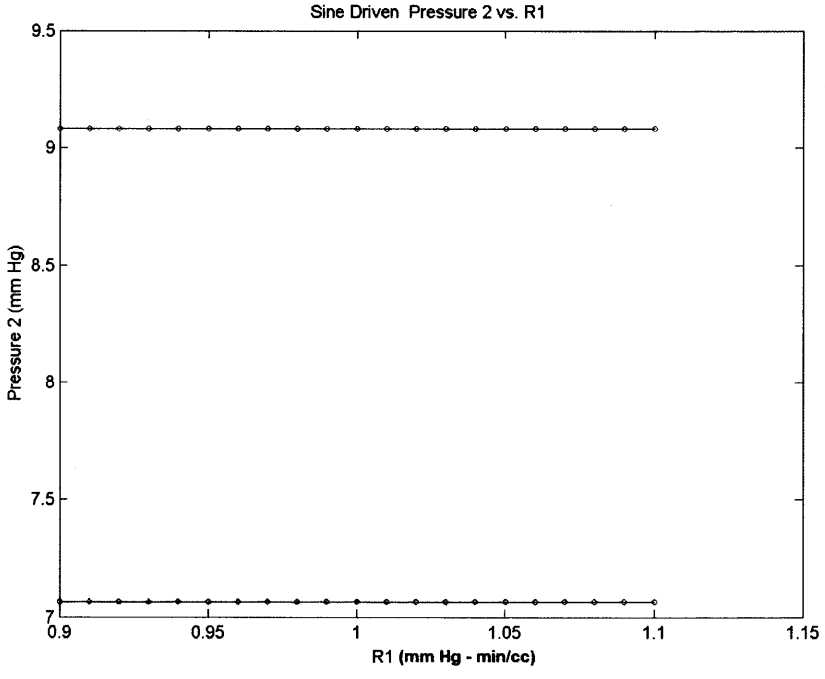

\

Figure A2.23 Sine driven model; behavior of P2 as R1 is changed.

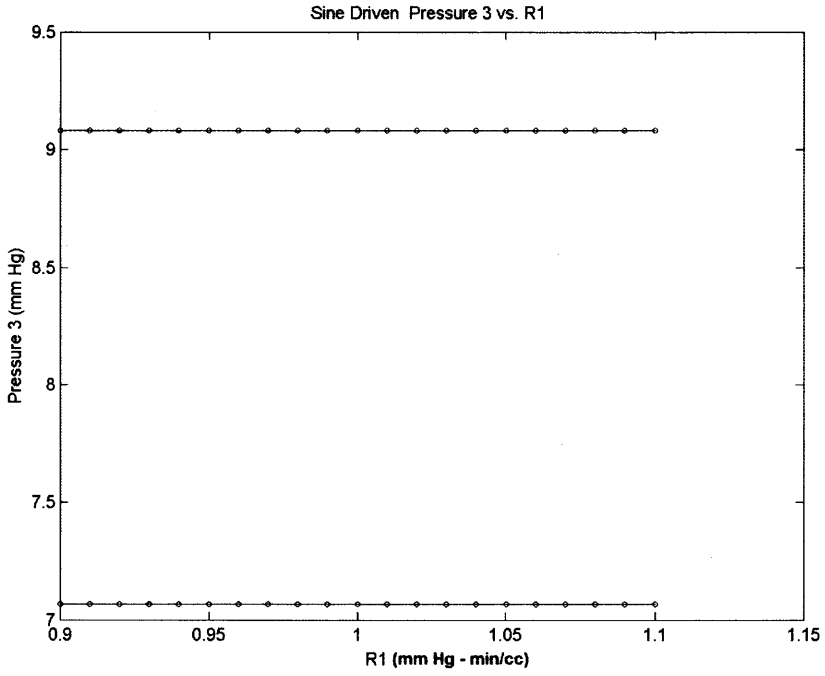

Figure A2.24 Sine driven model; behavior of P3 as R1 is changed.

The sensitivity analysis shows that when R1 is modified practically no change is noted in the system response. V1 is the only parameter that displays a small change in response to R1 variation of less than one percent, from a value of 23.88 cc to a value of 23.87 cc. As practically no changes in behavior of the system occur when R1 parameter was changed, we can have a good confidence on the R1 parameter in the sine driven model. The change of R1 parameter values also demonstrate a robust model as the structure of the system maintains its dynamics within physiological limits, with out a strong dependence on the parameter value. These results show that it is the structure of the system, and not the parameter values, which has most influence on the behavior of the system.

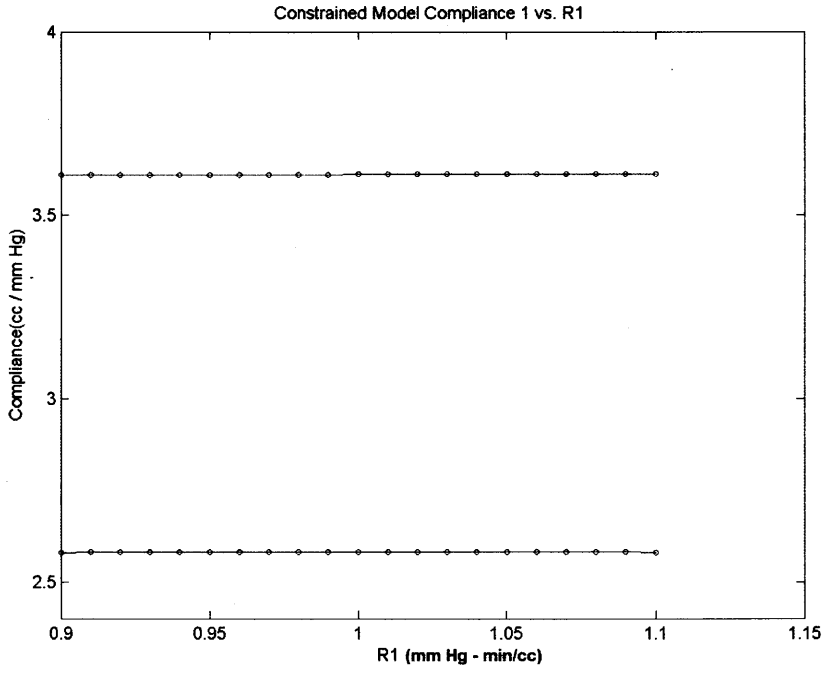

Figure A2.25 Full-constrained model; behavior of C1 as R1 is changed.

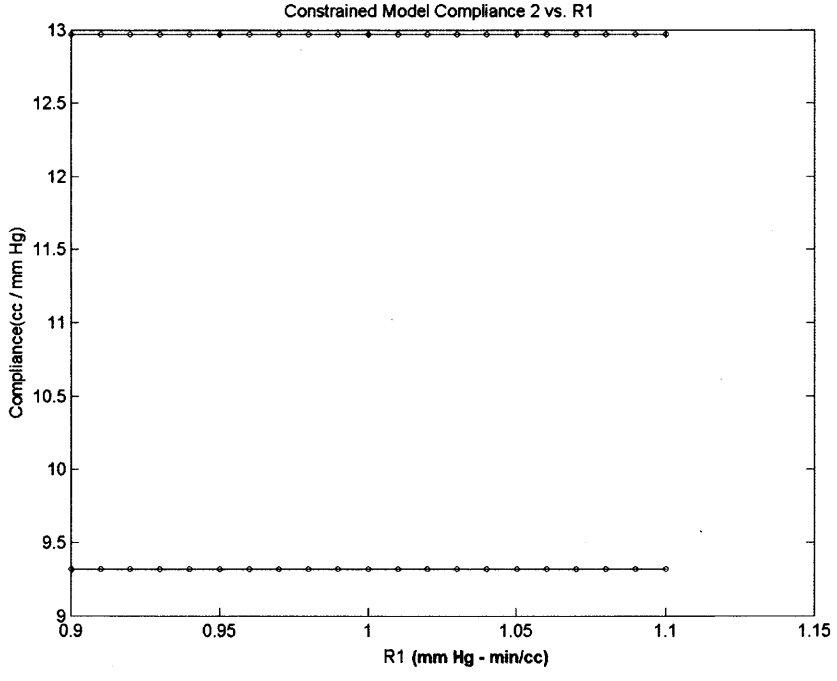

Figure A2.26 Full-constrained model; behavior of P3 as R1 is changed.

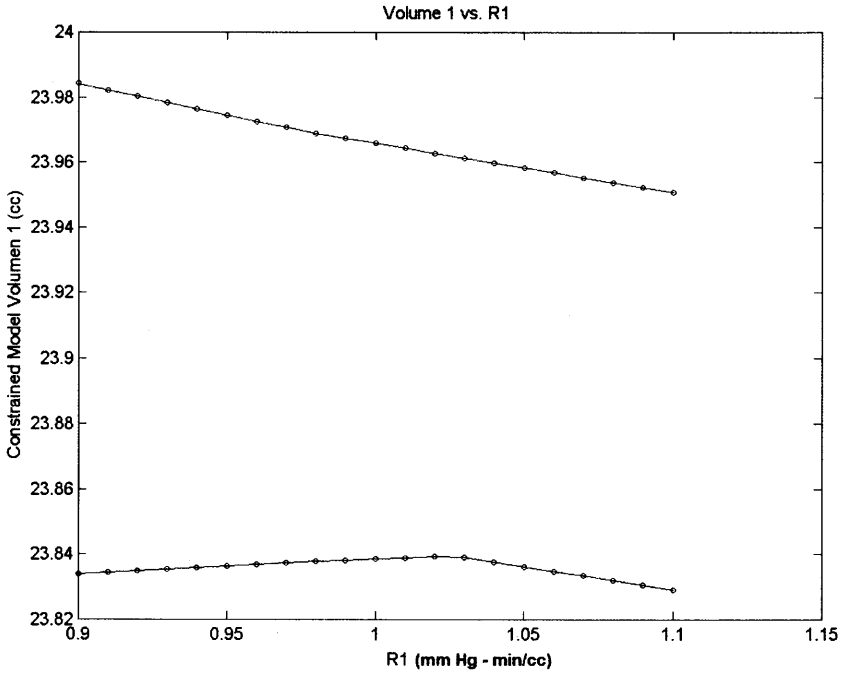

Figure A2.27 Full-constrained model; behavior of V1 as R1 is changed.

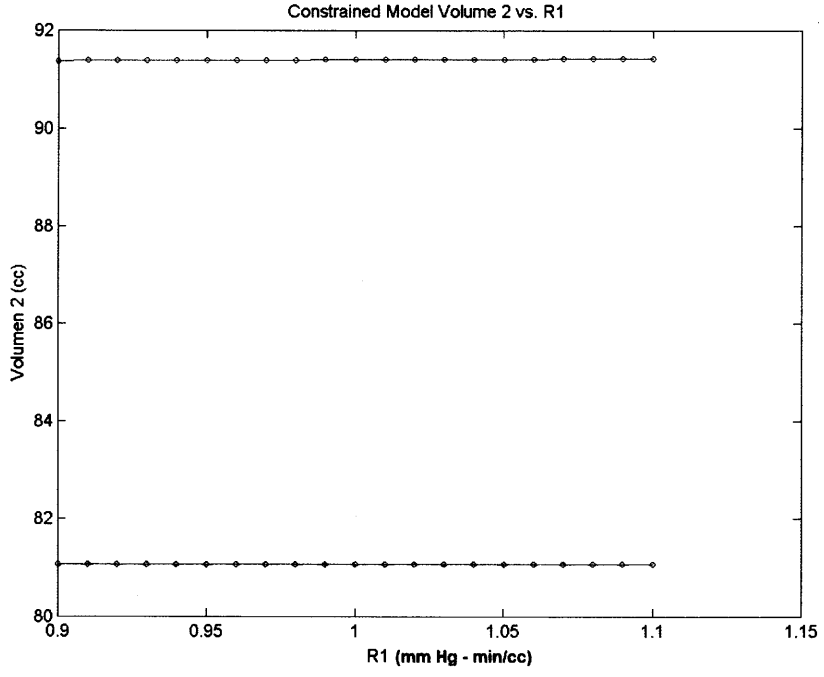

Figure A2.28 Full-constrained model; behavior of V2 as R1 is changed.

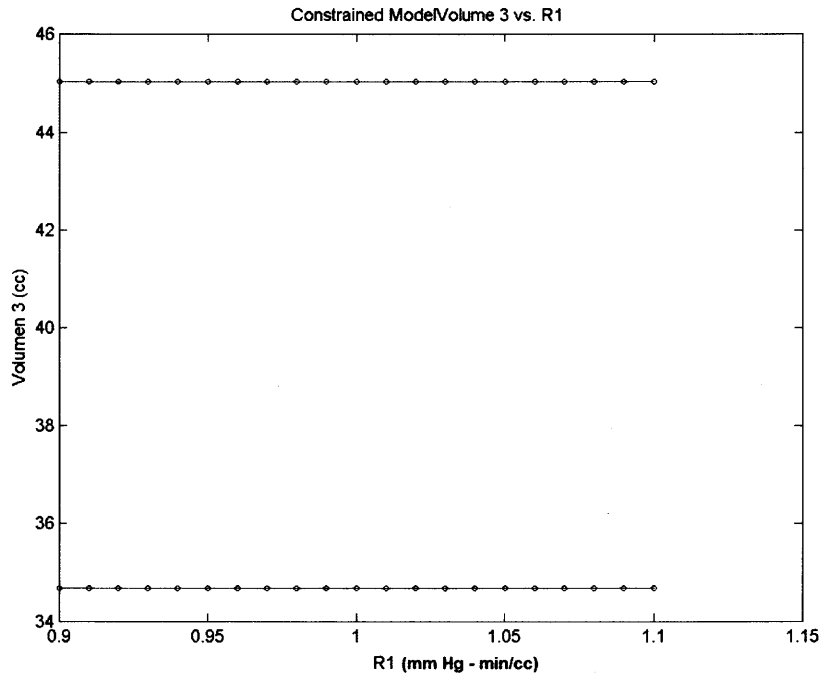

Figure A2.29 Full-constrained model; behavior of P3 as R1 is changed.

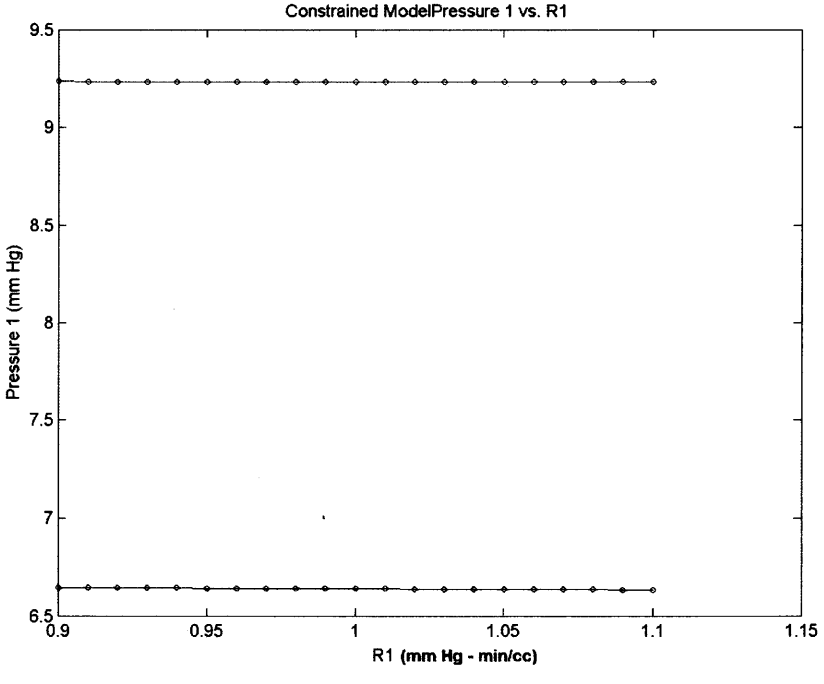

Figure A2.30 Full-constrained model; behavior of P1 as R1 is changed.

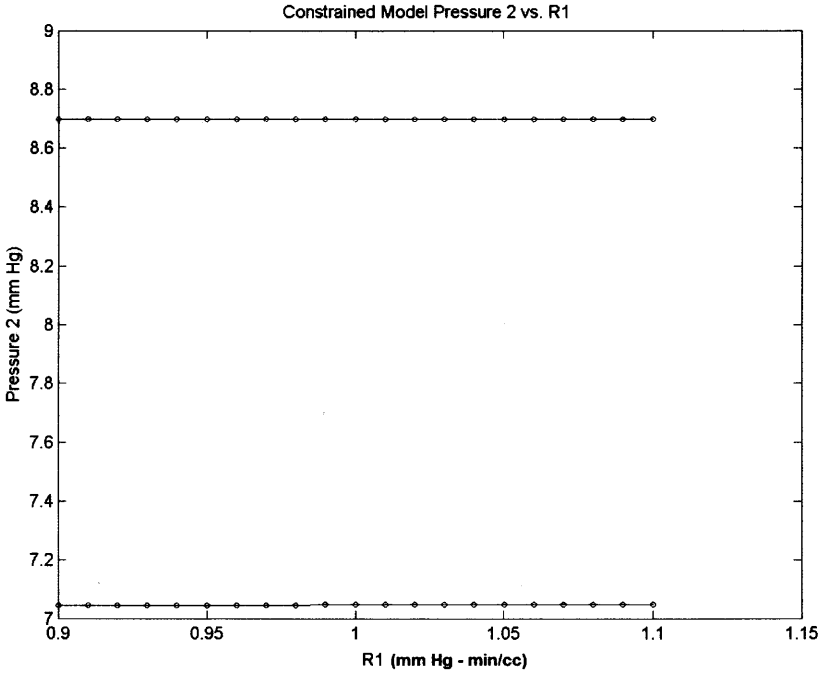

Figure A2.31 Full-constrained model; behavior of P2 as R1 is changed.

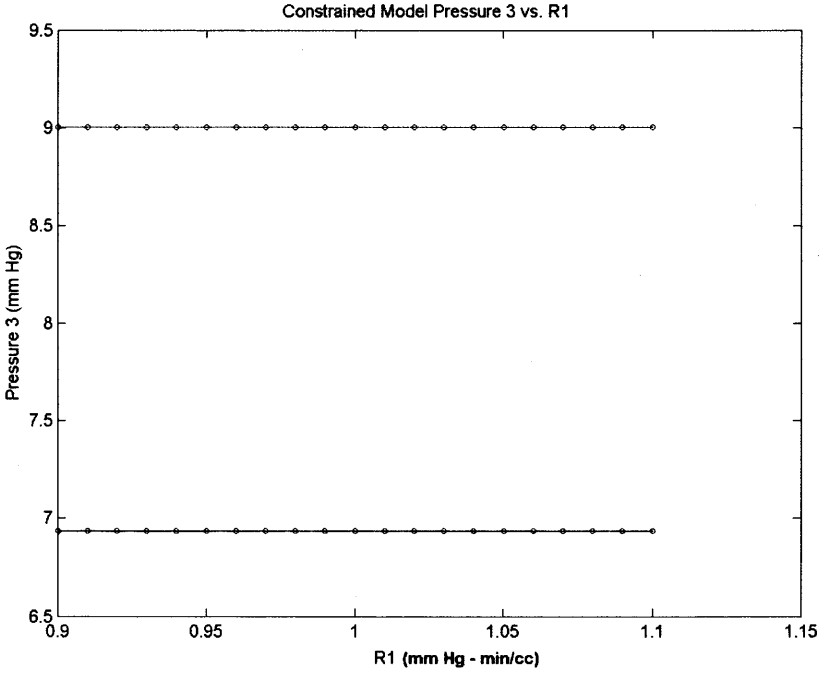

Figure A2. 32 Full-constrained model; behavior of P3 as R1 is changed.

The sensitivity analysis shows that when R1 is modified practically no change is noted in the system response. V1 is the only parameter that displays a small change in response to R1 variation of less than one percent, from a value of 23.98 cc to a value of 23.97 cc. As practically no changes in behavior of the system occur when R1 parameter was changed, we can have a good confidence on the R1 parameter in the full-constrained model. The change of R1 parameter values also demonstrate a robust model as the structure of the system maintains its dynamics within physiological limits, with out a strong dependence on the parameter value. These results show that it is the structure of the system, and not the parameter values, which has most influence on the behavior of the system.

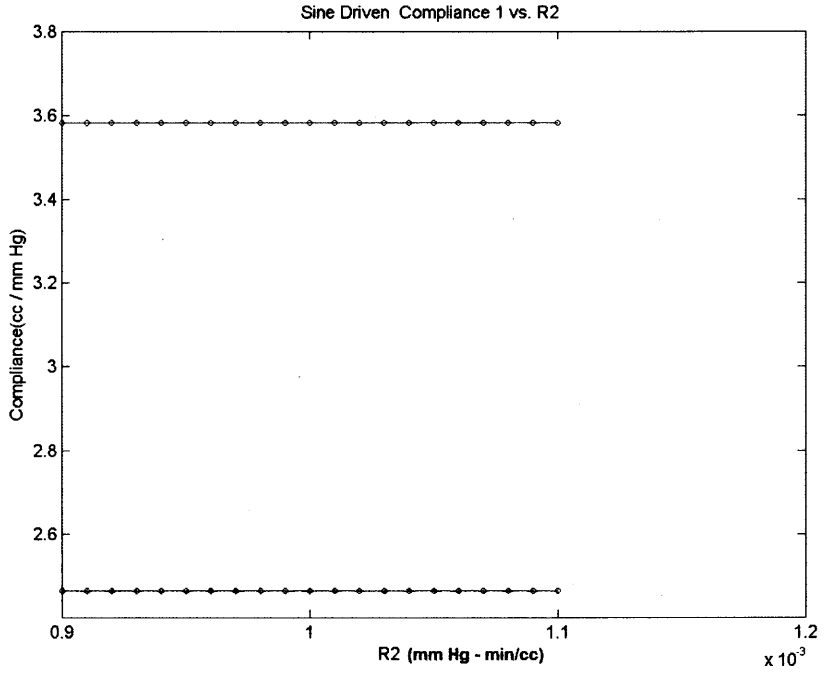

Figure A2.33 Sine driven model; behavior of C1 as R2 is changed.

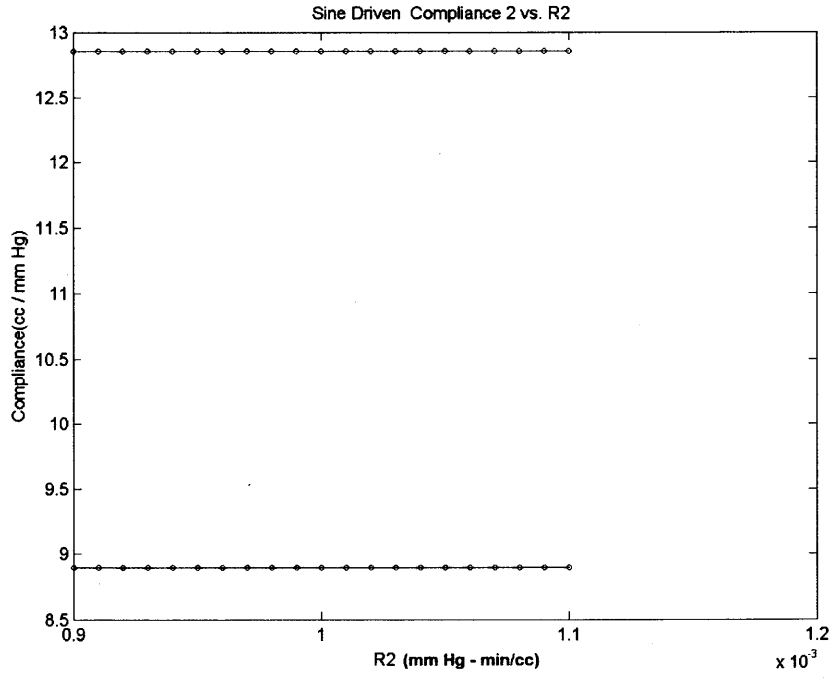

Figure A2.34 Sine driven model; behavior of C2 as R2 is changed.

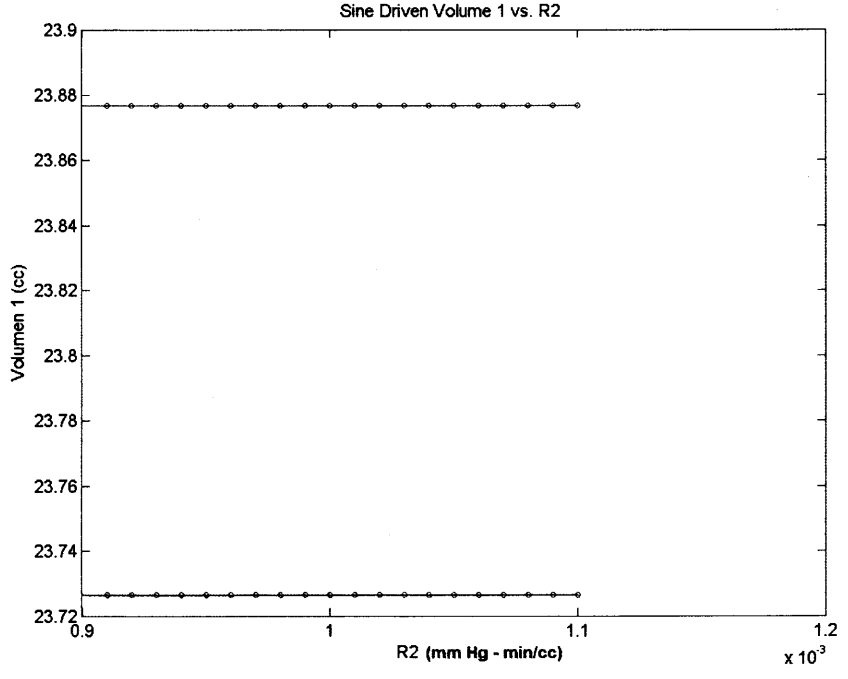

Figure A2.35 Sine driven model; behavior of V1 as R2 is changed.

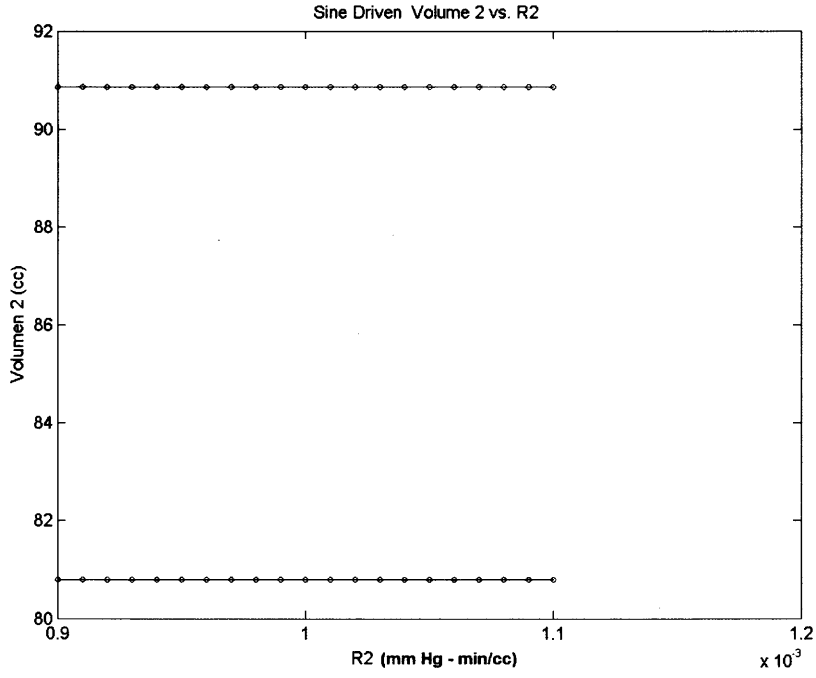

Figure A2.36 Sine driven model; behavior of V2 as R2 is changed.

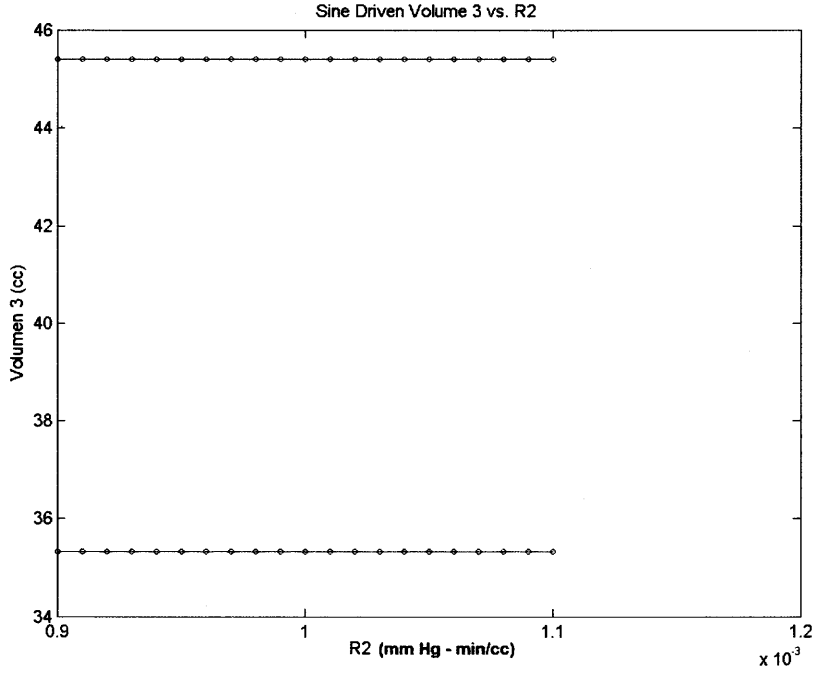

Figure A2.37 Sine driven model; behavior of V3 as R2 is changed.

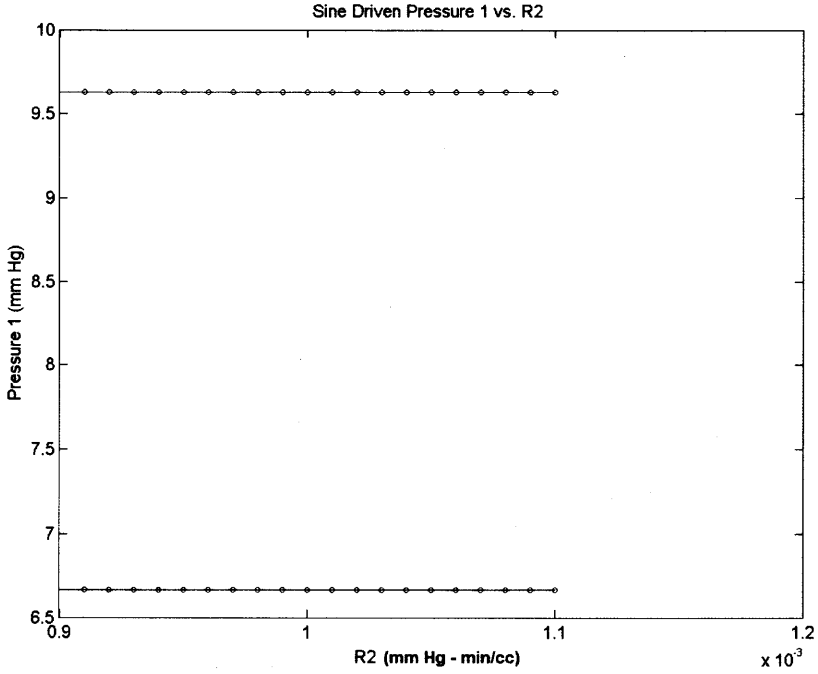

Figure A2.38 Sine driven model; behavior of P1 as R2 is changed.

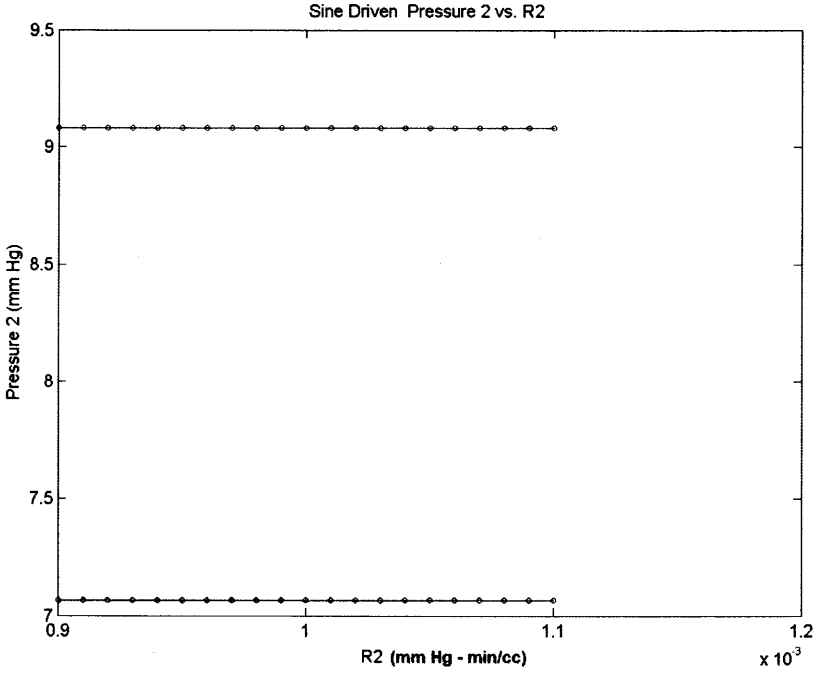

Figure A2.39 Sine driven model; behavior of P2 as R2 is changed.

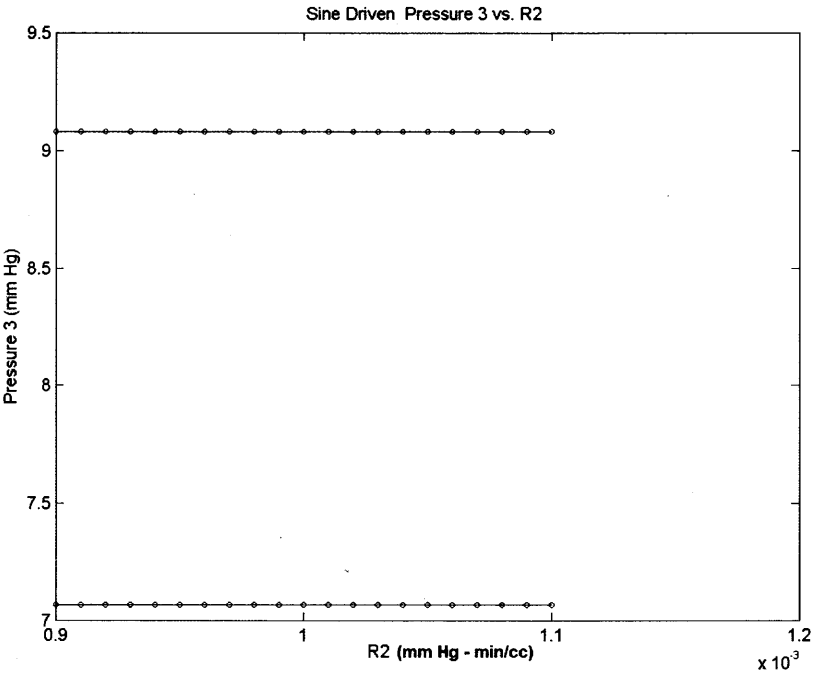

Figure A2.40 Sine driven model; behavior of P3 as R2 is changed.

The sensitivity analysis shows that when R2 is modified practically no change is noted in the system response. As practically no changes in behavior of the system occur when R2 parameter was changed, we can have a good confidence on the R2 parameter in the sine driven model. The change of R2 parameter values also demonstrate a robust model as the structure of the system maintains its dynamics within physiological limits, with out a strong dependence on the parameter value. These results show that it is the structure of the system, and not the parameter values, which has most influence on the behavior of the system.

APPENDIX 3

RESISTANCE ONE AND RESISTANCE TWO EXTREME VALUES

The R1 resistance is a lumped resistance representing the sum of the resistances from several anatomic structures. Each one of these structures, independently offer resistance to the CSF flow from inside of the brain to the intra-cranial subarachnoideal space. They are located at the junction between two compartments and consist of five foramens or orifices (two Orifices of Monroe, two Orifices of Luschka and one orifice of Magendie) and a narrow duct, the Sylvius Aqueduct. Each of the orifices has a diameter of approximately 2 mm. The Sylvius Aqueduct is a narrow duct that communicates between the third and the fourth ventricles. It has a dimension of approximately 3.5 mm in diameter and an approximate length of 17.5 mm. The approximate cross sectional area is 10 mm^2.

The R2 resistance represents the resistance to the flow at the junction of the intra-cranial subarachnoideal space and the spinal subarachnoideal space, essentially occurring at the Foramen Magnum. As suggested by its name, it has a large diameter of approximately 35 mm.; with a correspondent cross sectional area of 962.12 mm^2. In the interior of the foramen magnum runs the nervous tissue at its transition from medulla into spinal cord, with an approximately diameter of 25 mm.; thus rendering a cross sectional area of 490.87 mm^2. In consequence the effective area of the foramen magnum is calculated to be 471.23 mm^2. The resistance to flow is proportional to the fourth power of the radius, while the area is proportional to the second power of the radius. This will give us a resistance ratio between R1/R2 of $(66.75)^2/1$, which is a ratio of 4455. If the resistances of the five orifices are taken into consideration, R1 could increase by several

orders of magnitude. Furthermore, the system is not receiving just one impulse on one end that forces the fluid through the whole set of ventricular compartments. As the brain tissue compliance diminishes around each one of these ventricular compartments during each cardiac cycle, each of these compartments receives an effective compression, which in turn facilitates the fluid inside to flow into the next compartment. Thus the final result of the contributing resistance of each orifice and contributing loss to the system, as well as the effective compression force added in each compartment to the system, are very difficult to calculate if not impossible. These anatomical and physiological constraints not only lead to a series of unknowns; but also generate a number of very interesting questions like: what would be the system behavior at different values for each one of the R1 and R2 resistance? Are both resistances defining the system behavior equally? Which portion of the system behavior is being defined by R1? Which portion of the system behavior is being defined by R2? Inside which limits of R1 and R2 does the system still behaves as expected?

In an effort to gain more information and insight, several simulations were run under different values for the resistances. Compliances are maintained at a set value; C1 is fixed at 25/7, C2 at 90/7, and C3 at 35/7.

First the R1 resistance was fixed at 10 mmHg-sec/cc, and several values were given to R2, and the response of the system was carefully documented.

Case #1: R1= 10 mmHg-sec/cc R2= 0.0001 mmHg-sec/cc.

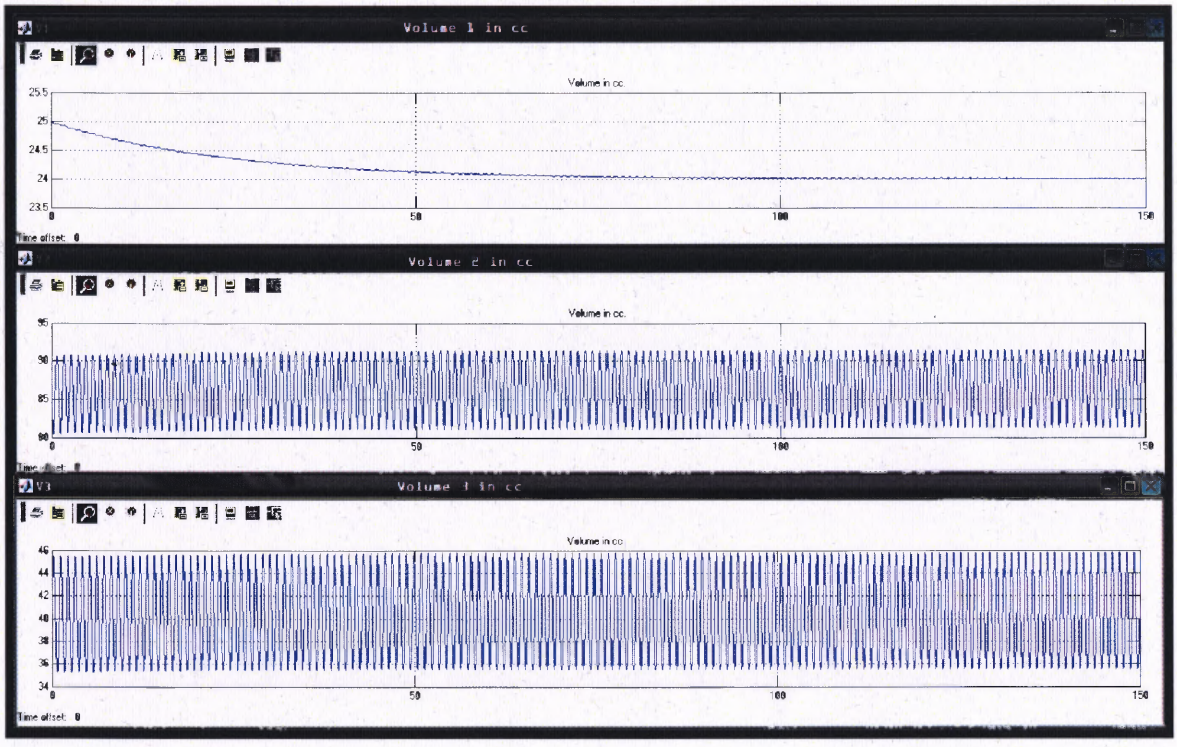

Figure A3.1 Sine driven model; behavior in time of the volume in cc of each compartment. R1 = 10 R2= 0.0001.

After approximately 100 sec. the system reaches equilibrium. The final Cp1 volume requires approximately. 100 sec to reach an equilibrium; meanwhile Cp2 and Cp3 achieve a faster equilibrium, related to the minor value of resistance between them. (Figure A3.1)

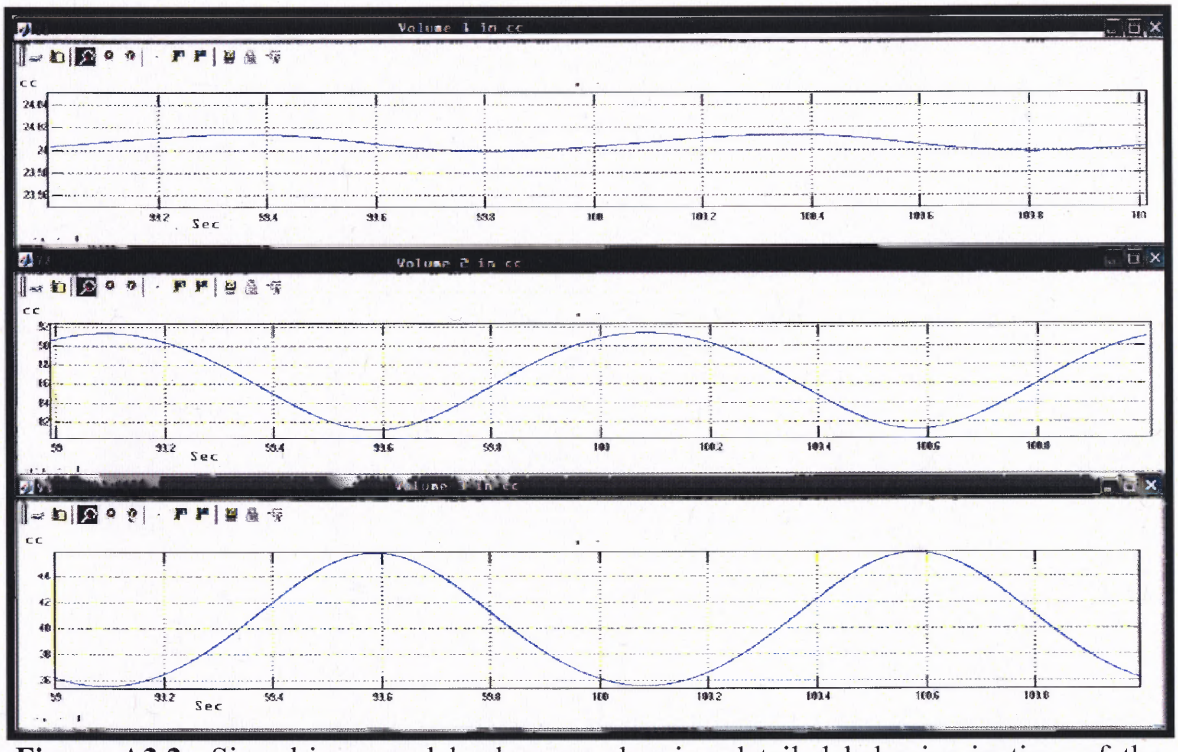

Figure A3.2 Sine driven model; close up showing detailed behavior in time of the volume in cc of each compartment. R1= 10 mmHg-sec/cc R2= 0.0001 mmHg-sec/cc.

At a close up (see figure A3.2) it is easy to observe that the volume exchange from the intracranial to spinal compartment is still more than 10 cc; as could be seen in the graph corresponding to V3- spinal compartment volume; thus fulfilling the requiredcondition of expelling at least 10 cc of CSF from the cranial cavity into the spinal compartment. The volume variation of Cp1 is approximately of 0.02 cc, fulfilling another required condition.

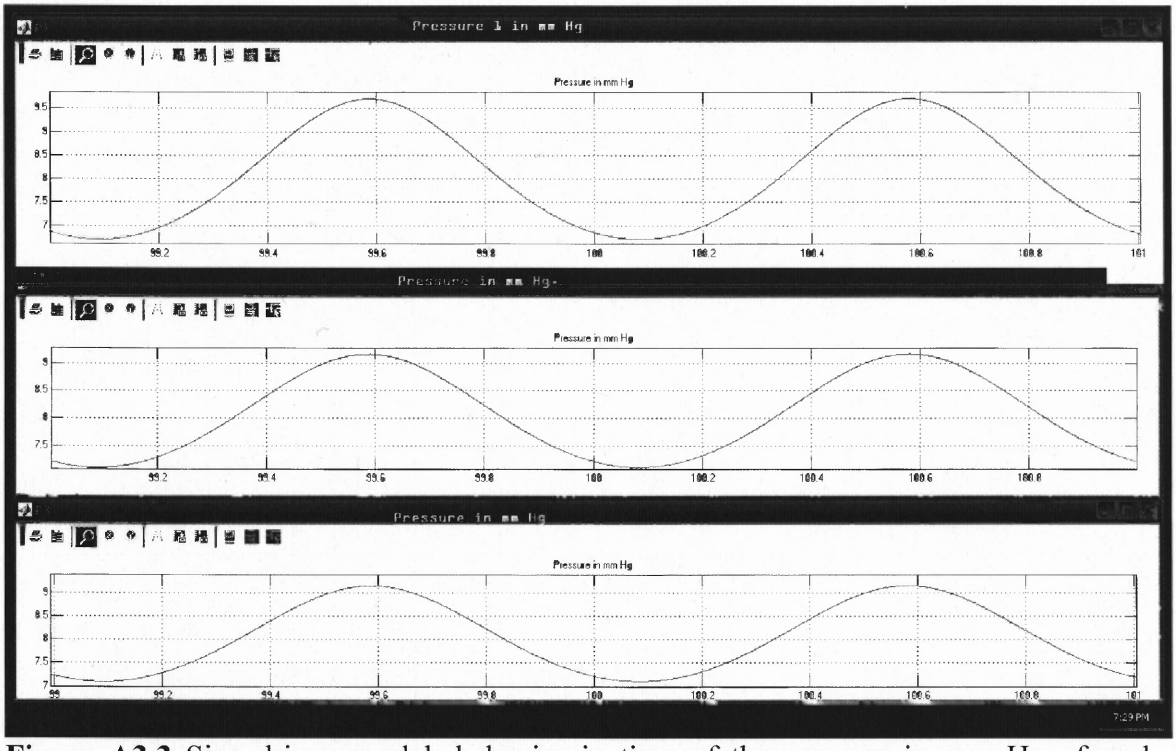

Figure A3.3 Sine driven model; behavior in time of the pressure in mm Hg of each compartment. R1= 10 mmHg-sec/cc R2= 0.0001 mmHg-sec/cc.

After approximately 50 sec pressure stabilizes in the desired physiological range in all three compartments. The overall variations in the three compartments reside between 9.5 and 7 mm Hg., fulfilling thecondition on maintaining the pressure under 15 mm Hg.(see figure A3.3)

Equally important is that the peak pressure difference between Cp1 and Cp2 is less than 1 mm Hg, fulfilling the last required condition for the system to be considered as representative of CSF dynamics.

Case #2: R1= 10 mmHg-sec/cc R2= 0.001 mmHg-sec/cc . By increasing one order of magnitude the resistance in R2, there is no appreciable change in the systems dynamics. All the specified and needed conditions (boundaries) are still met to consider the model as representative of the system. (see figures A3.4 and A3.5)

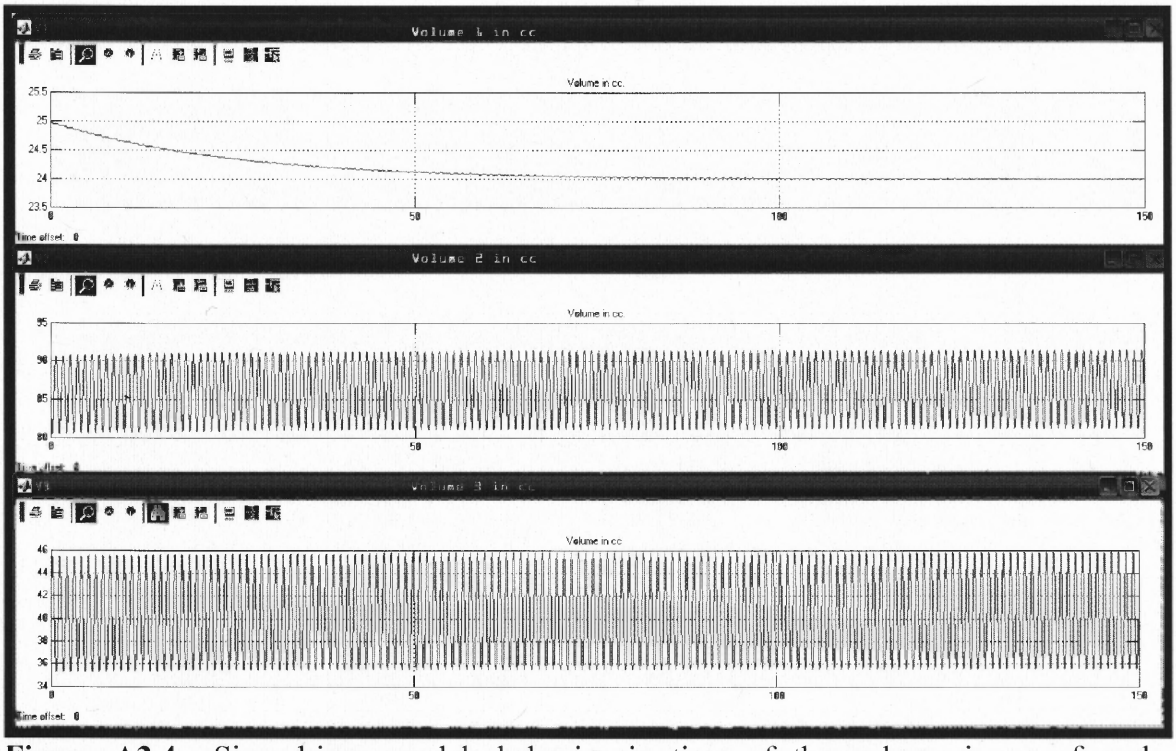

Figure A3.4 Sine driven model; behavior in time of the volume in cc of each compartment. R1= 10 mmHg-sec/cc R2= 0.001 mmHg-sec/cc.

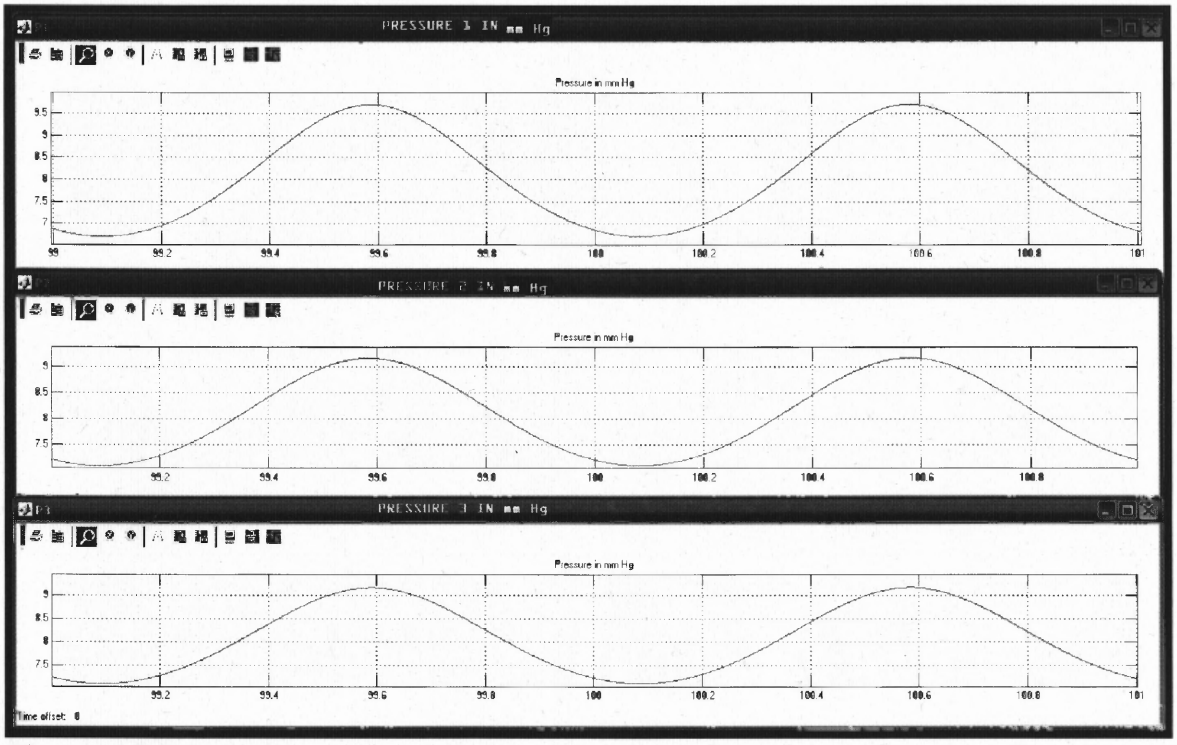

Figure A3.5 Sine driven model; behavior in time of the pressure in mm Hg of each compartment. R1= 10 mmHg-sec/cc R2= 0.001 mmHg-sec/cc.

Case #3: R1= 10 mmHg-sec/cc R2= 0.01 mmHg-sec/cc. By increasing two orders of magnitude the resistance in R2, there is no appreciable change in the systems dynamics. All the specified and needed conditions (boundaries) are still met to consider the model as representative of the system (see Figures A3.6, A3.7 and A3.8).

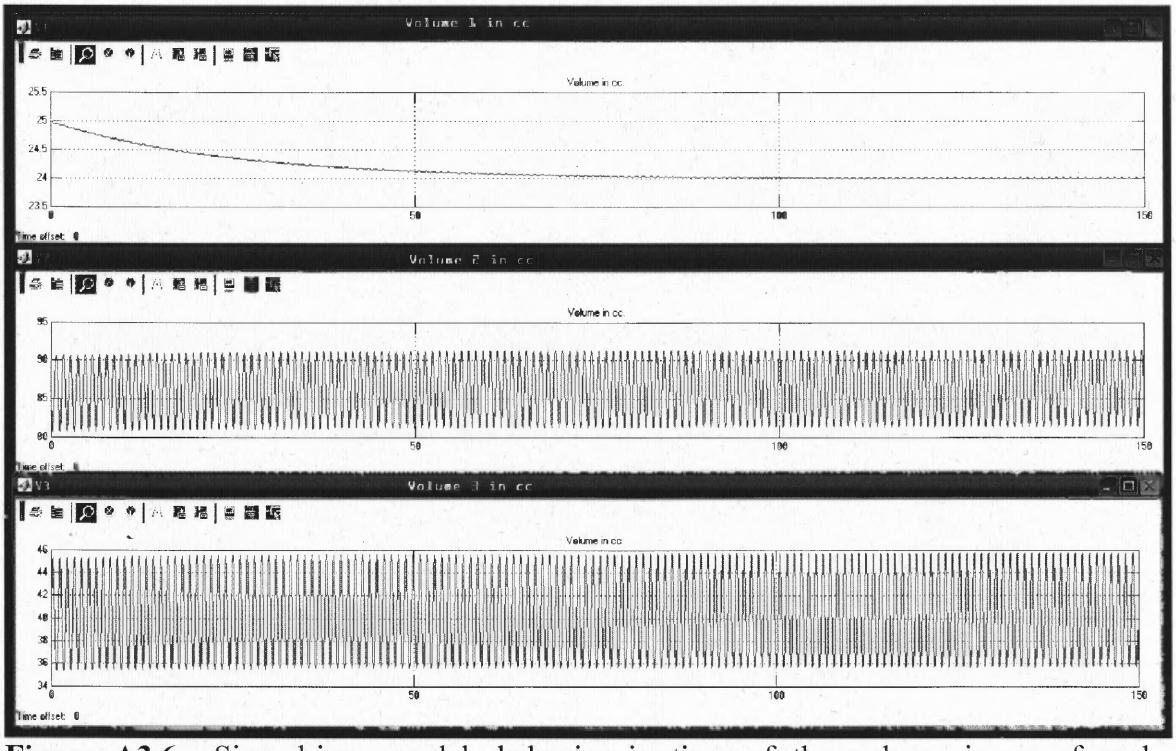

Figure A3.6 Sine driven model; behavior in time of the volume in cc of each compartment. R1= 10 mmHg-sec/cc R2= 0.01 mmHg-sec/cc.

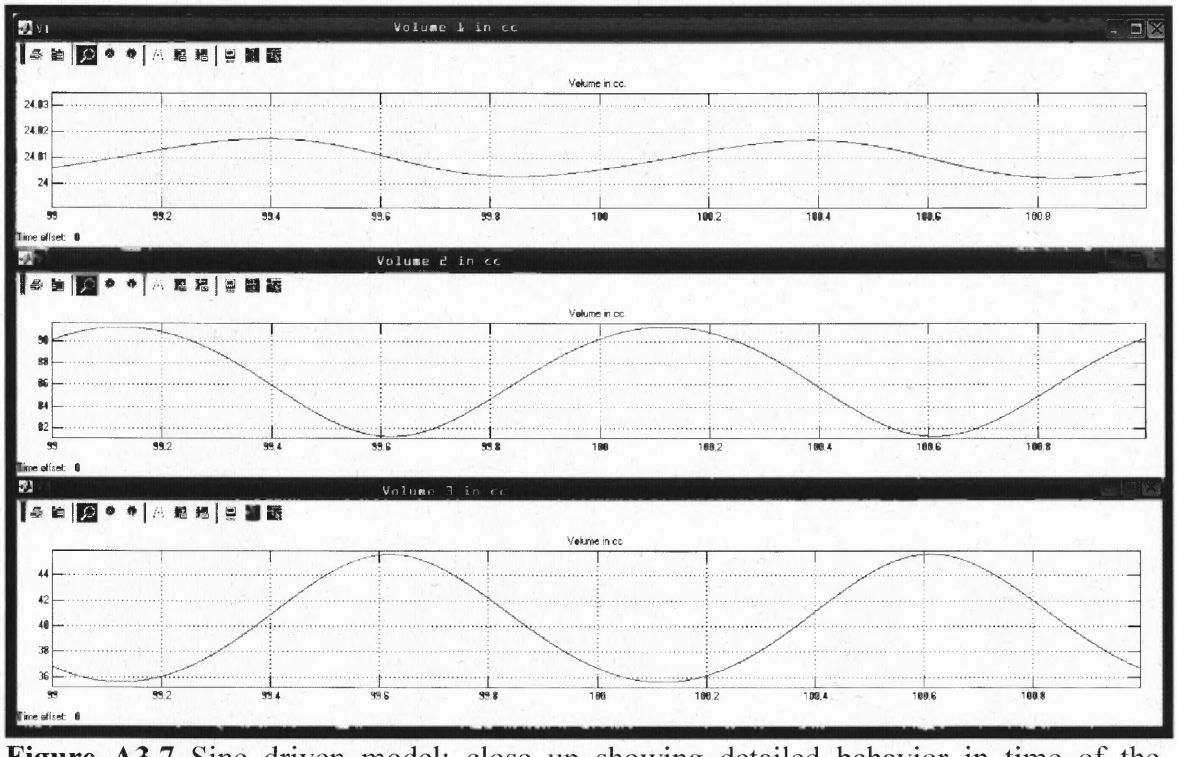

Figure A3.7 Sine driven model; close up showing detailed behavior in time of the volume in cc of each compartment. R1= 10 mmHg-sec/cc R2= 0.01 mmHg-sec/cc.

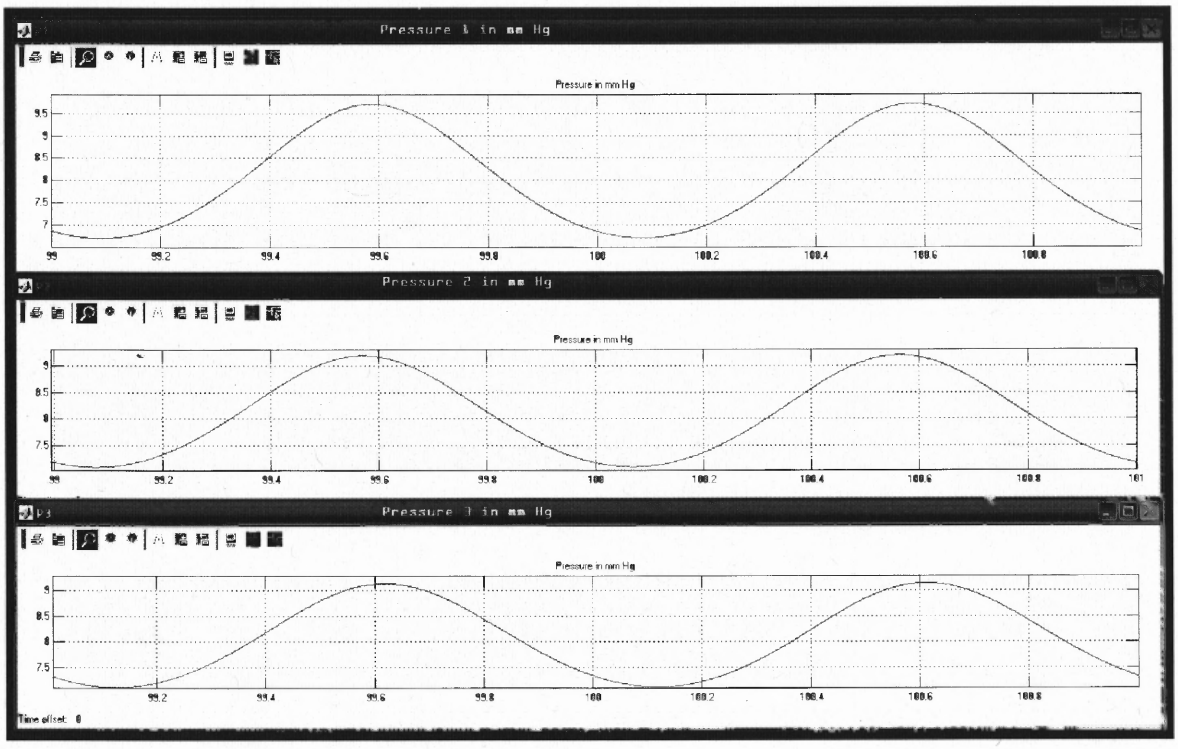

Figure A3.8 Sine driven model; behavior in time of the pressure in mm Hg of each compartment. R1= 10 mmHg-sec/cc R2= 0.01 mmHg-sec/cc.

Case #4 R1= 10 mmHg-sec/cc R2= 0.1 mmHg-sec/cc : When the resistance increases by three orders of magnitude, the model can no longer represent normal CSF dynamics.(see figures A3.9 and A3.10)

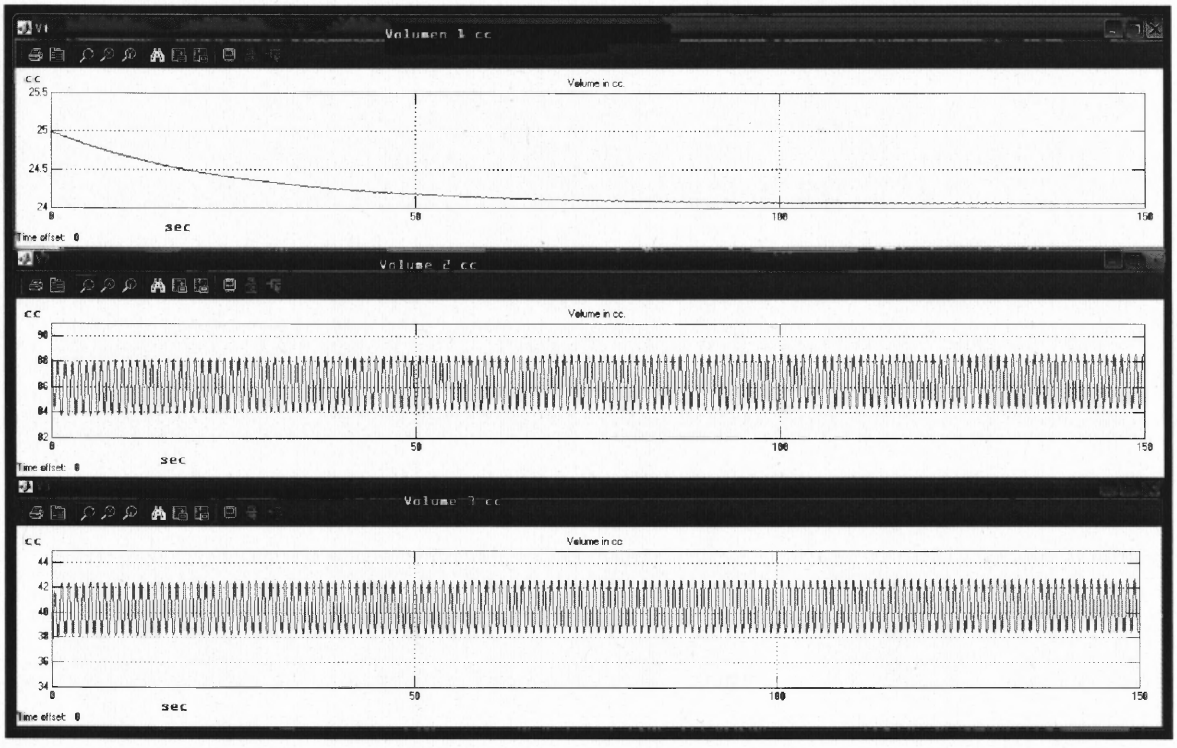

Figure A3.9 Sine driven model; behavior in time of the volume in cc of each compartment. R1= 10 mmHg-sec/cc R2= 0.1 mmHg-sec/cc.

The model is not considered representative of the normal CSF dynamics as it fails to maintain the second necessary boundary condition:

> b) Expel ten cubic centimeters (10 cc) of CSF of the intra-cranial subarachnoideal space into the spinal compartment, during each cardiac cycle. As ten cubic centimeters of blood enter the cranial cavity, approximately the same amount of CSF leaves the cranial cavity, thus the Monroe-Kelly doctrine is respected.

In this case the amount of exchange between Cp2 and Cp3 is about 5 cc CSF.

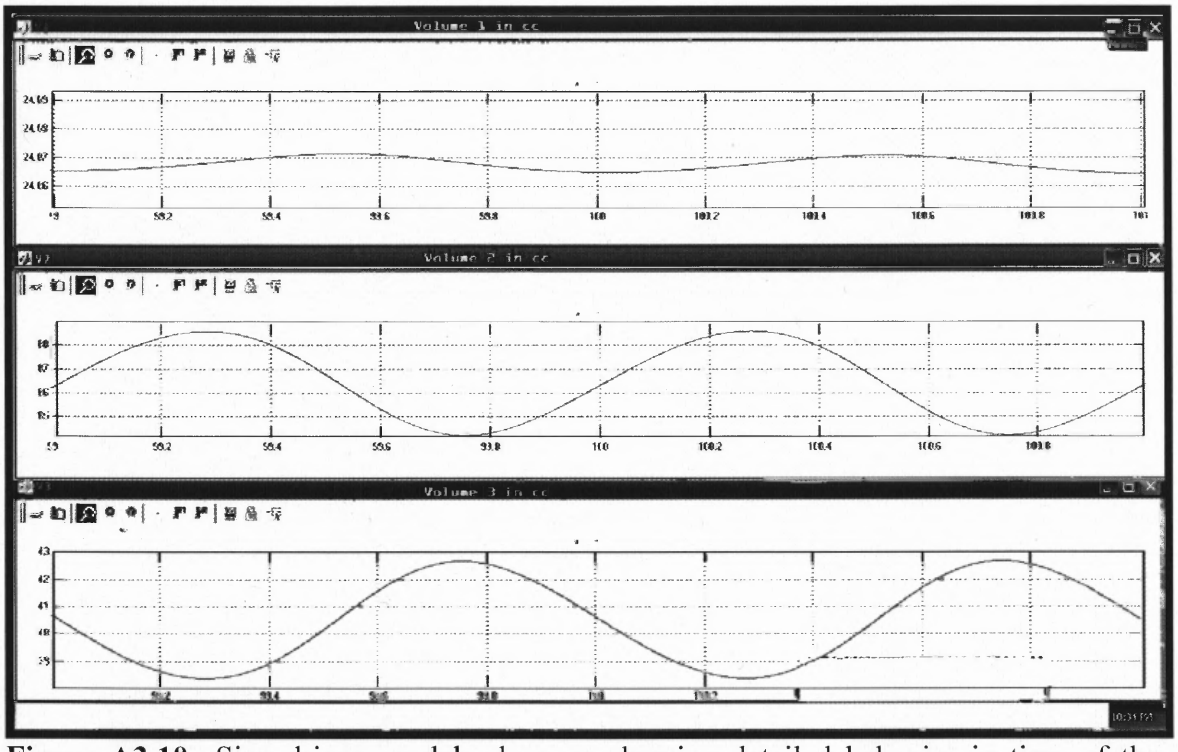

Figure A3.10 Sine driven model; close up showing detailed behavior in time of the volume in cc of each compartment. R1= 10 mmHg-sec/cc R2= 0.1 mmHg-sec/cc.

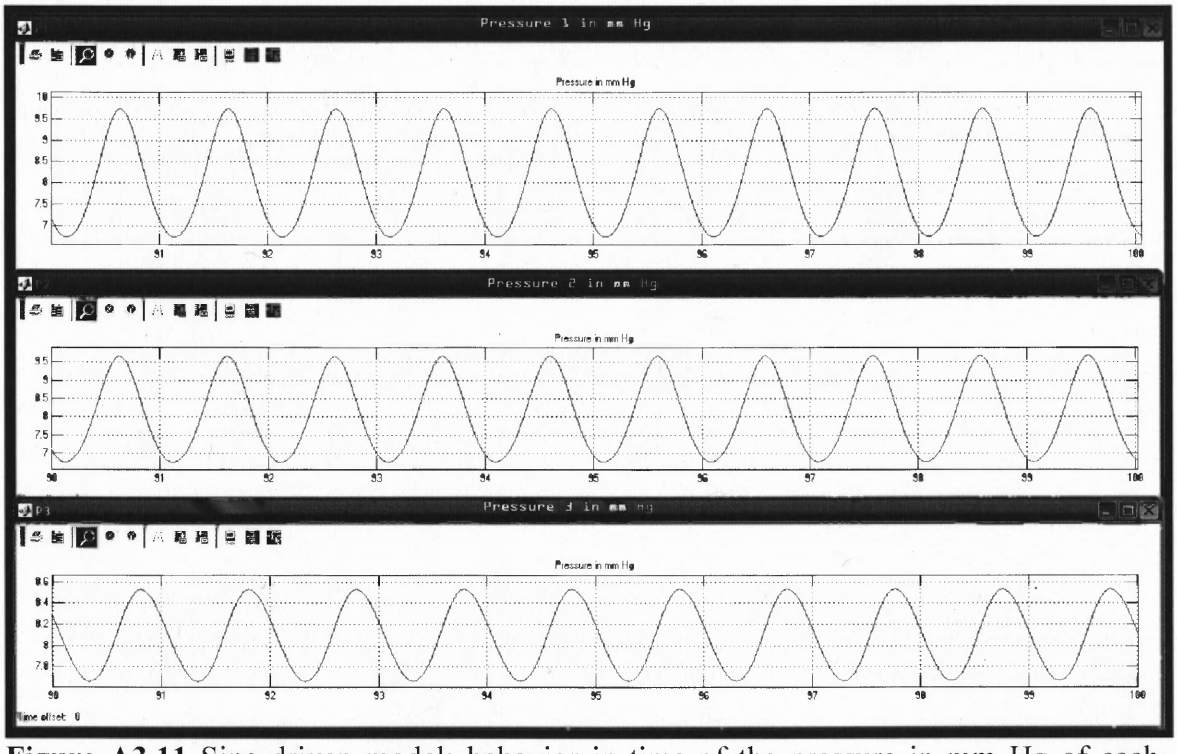

Figure A3.11 Sine driven model; behavior in time of the pressure in mm Hg of each compartment. R1= 10 mmHg-sec/cc R2= 0.01 mmHg-sec/cc.

The intracranial pressure rises but is still within normal ranges. Interestingly the pressure in the spinal compartment behaves differently than the intracranial compartment pressure. The increased resistance at R2 does not allow to fully transmitting the increment in the intracranial pressure caused by the diminishing compliance during each cycle.

Case #5:R1= 100 mmHg-sec/cc R2= 0.0001 mmHg-sec/cc. Starting from this case it will be introduced a higher R1 resistance. This relatively high R1 resistance makes the system spend a comparatively long time to reach equilibrium, approximately 1200 sec. Nevertheless, as shown in the present V1 graph, the final value meets the same value achieved by V1 in the first simulation. (see figures 3.12; 3.13; A3.14)

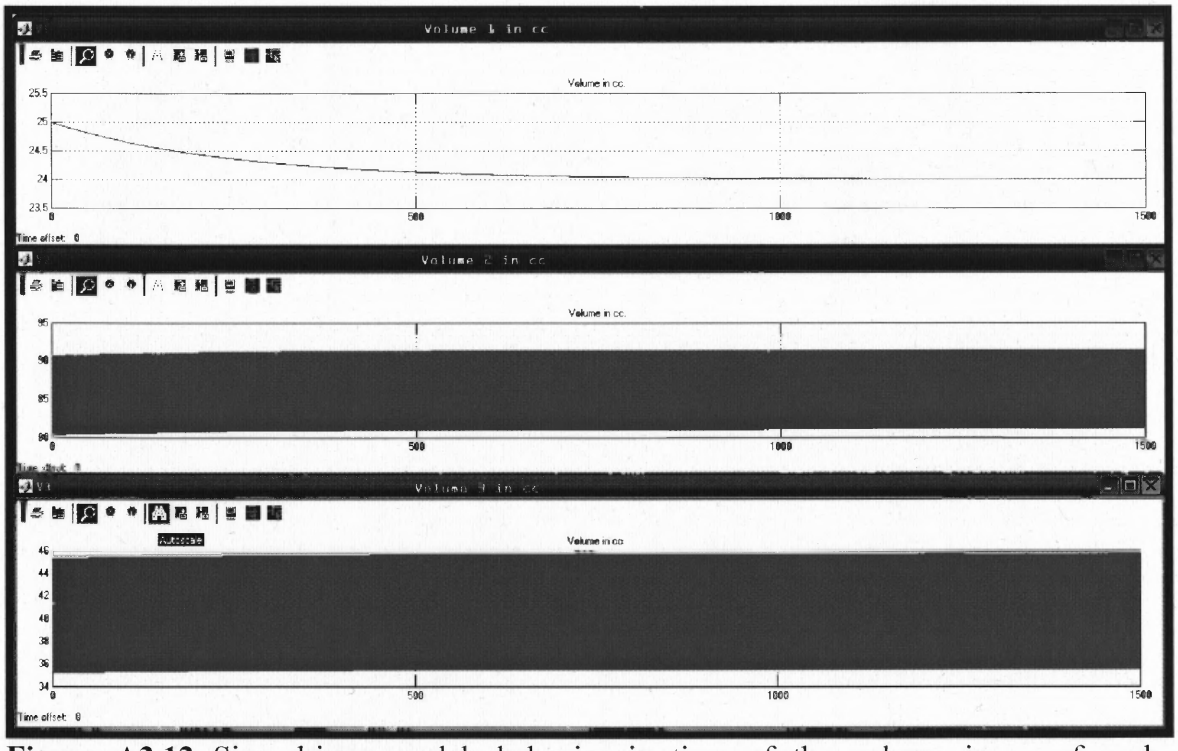

Figure A3.12 Sine driven model; behavior in time of the volume in cc of each compartment. R1= 100 mmHg-sec/cc R2= 0.0001 mmHg-sec/cc.

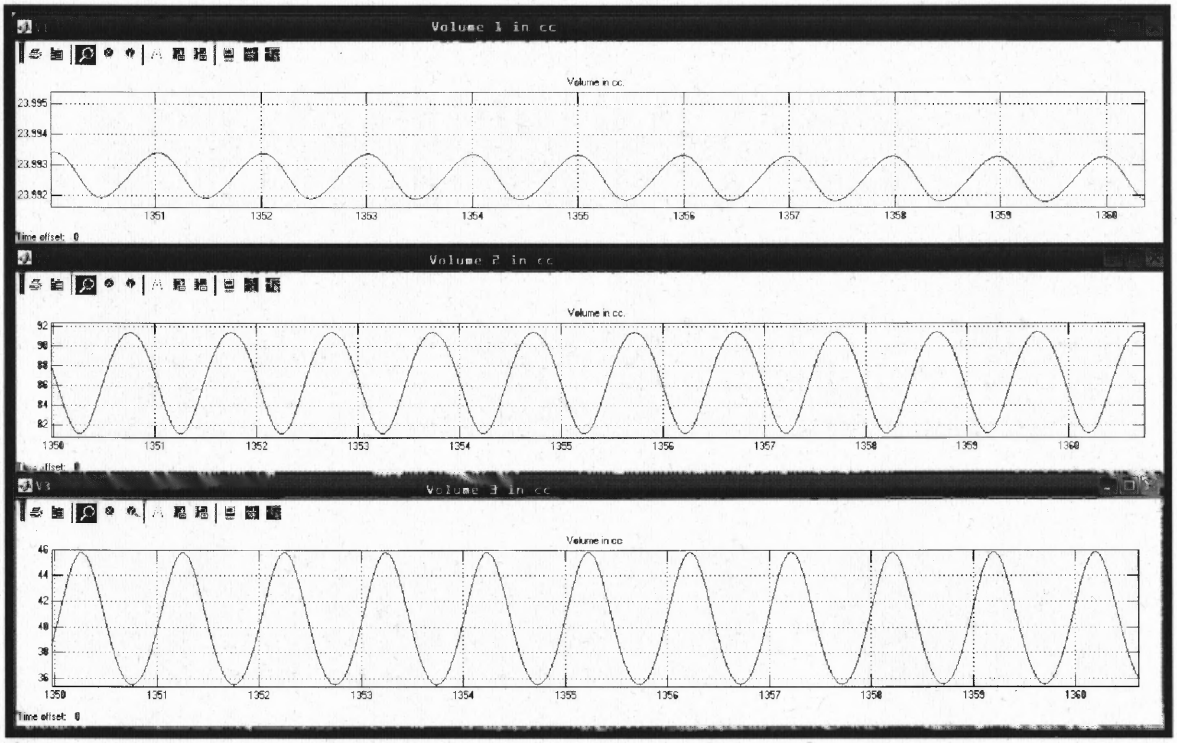

Figure A3.13 Sine driven model; behavior in time of the volume in cc of each compartment. R1= 100 mmHg-sec/cc R2= 0.0001 mmHg-sec/cc.

Interestingly, the pressures get leveled quite early in the system, at the first five seconds every compartment has their equilibrium pressure. P1 varies between 6.8 and 9.5 mm Hg., while P2 and P3 vary between 7 and 9 mm Hg.

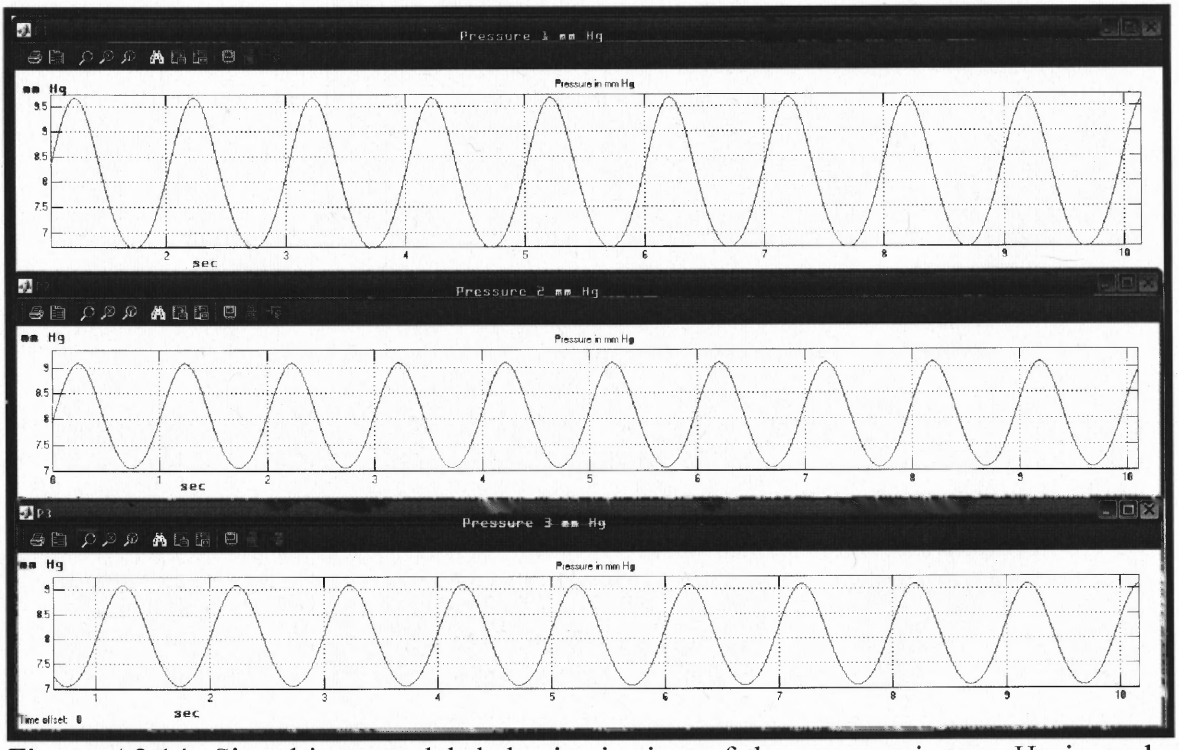

Figure A3.14 Sine driven model; behavior in time of the pressure in mm Hg in each compartment. R1= 100 mmHg-sec/cc R2= 0.0001 mmHg-sec/cc.

Case #6: R1= 100 mmHg-sec/cc R2= 0.001 mmHg-sec/cc Virtually, no difference is seen in the system behavior when the previous values of R1(100 mmHg-sec/cc) and R2(0.0001 mmHg-sec/cc) are replace by and the actual values for R1(100 mmHg-sec/cc) and R2(0.001 mmHg-sec/cc) .(see figure A3.15.)

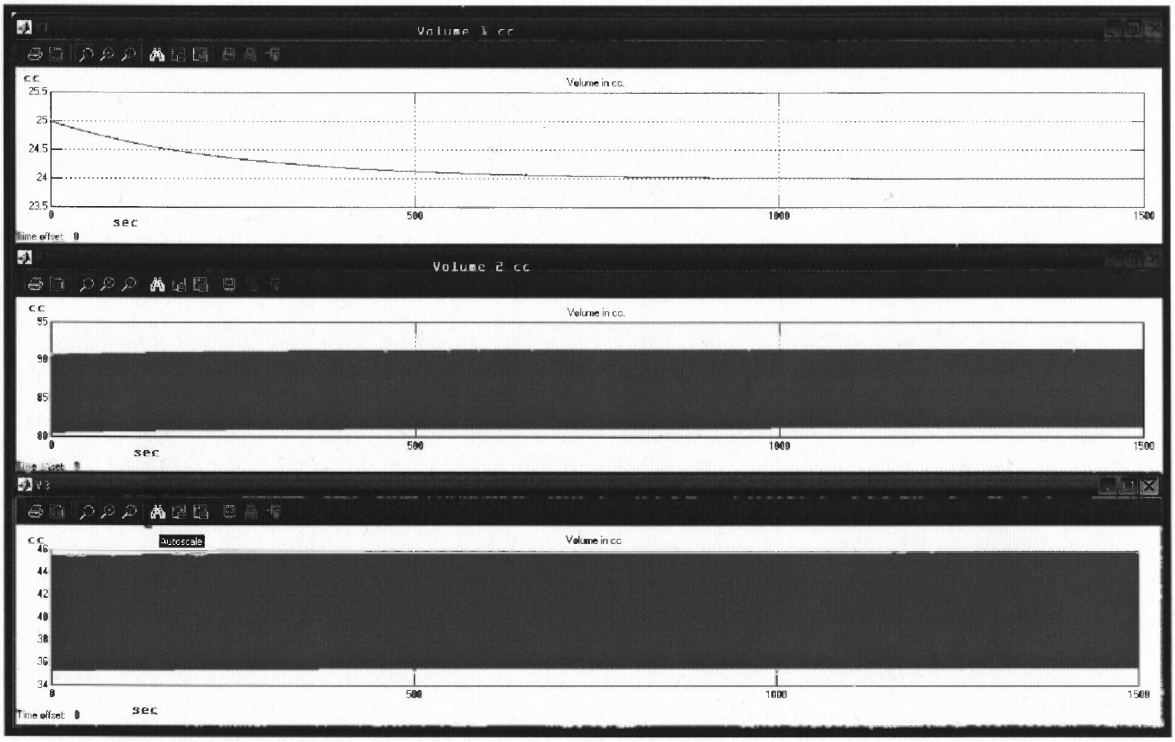

Figure A3.15 Sine driven model; behavior in time of the volume in cc of each compartment. R1= 100 mmHg-sec/cc R2= 0.001 mmHg-sec/cc.

Case #7: R1= 100 mmHg-sec/cc R2= 0.01 mmHg-sec/cc. Again no significant difference is found between the present and previous simulation **(see figures A3.16, A3.17, A3.18).**

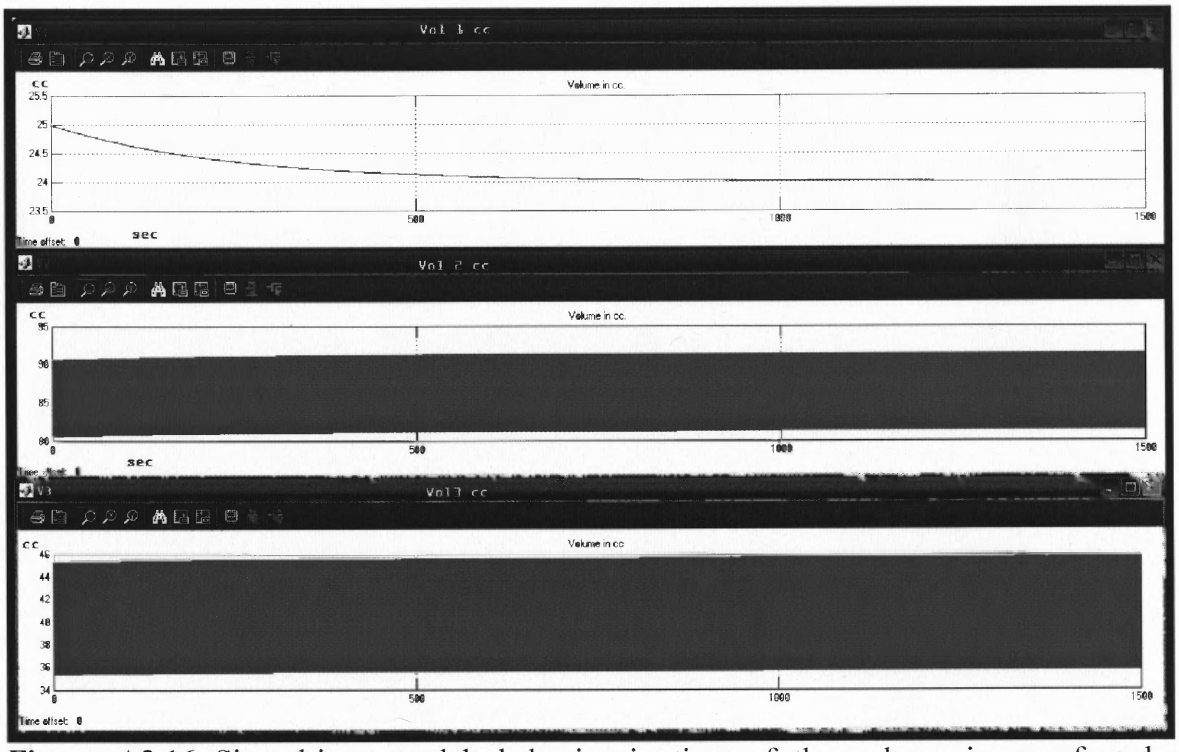

Figure A3.16 Sine driven model; behavior in time of the volume in cc of each compartment. R1=100 mmHg-sec/cc R2= 0.01 mmHg-sec/cc.

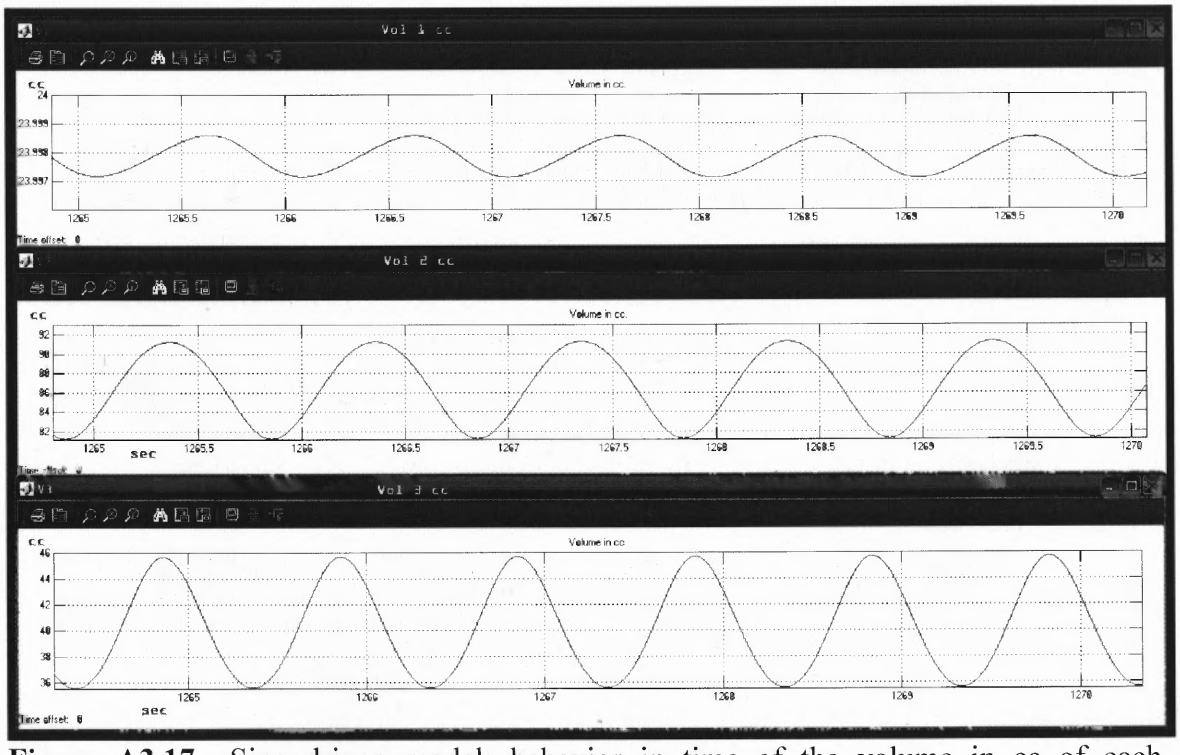

Figure A3.17 Sine driven model; behavior in time of the volume in cc of each compartment. R1= 100 mmHg-sec/cc R2= 0.01 mmHg-sec/cc.

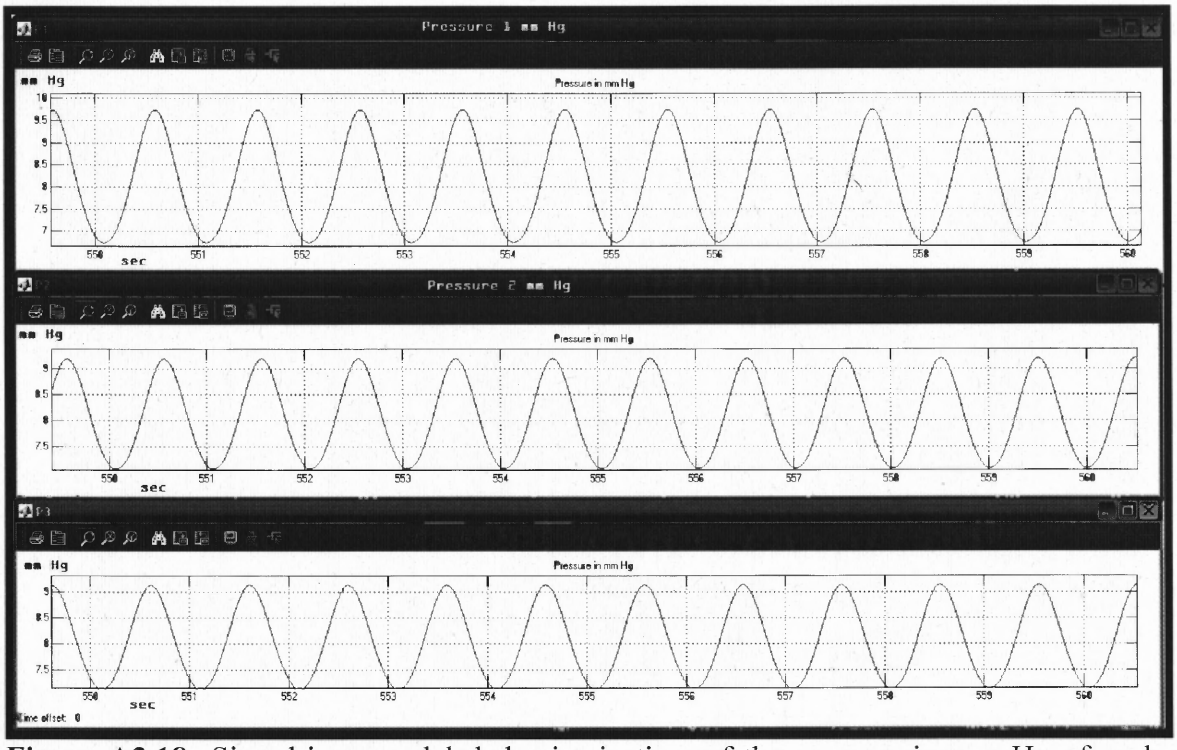

Figure A3.18 Sine driven model; behavior in time of the pressure in mm Hg of each compartment. R1= 100 mmHg-sec/cc R2= 0.01 mmHg-sec/cc.

Case #8:R1= 100 mmHg-sec/cc R2= 0.1 mmHg-sec/cc.

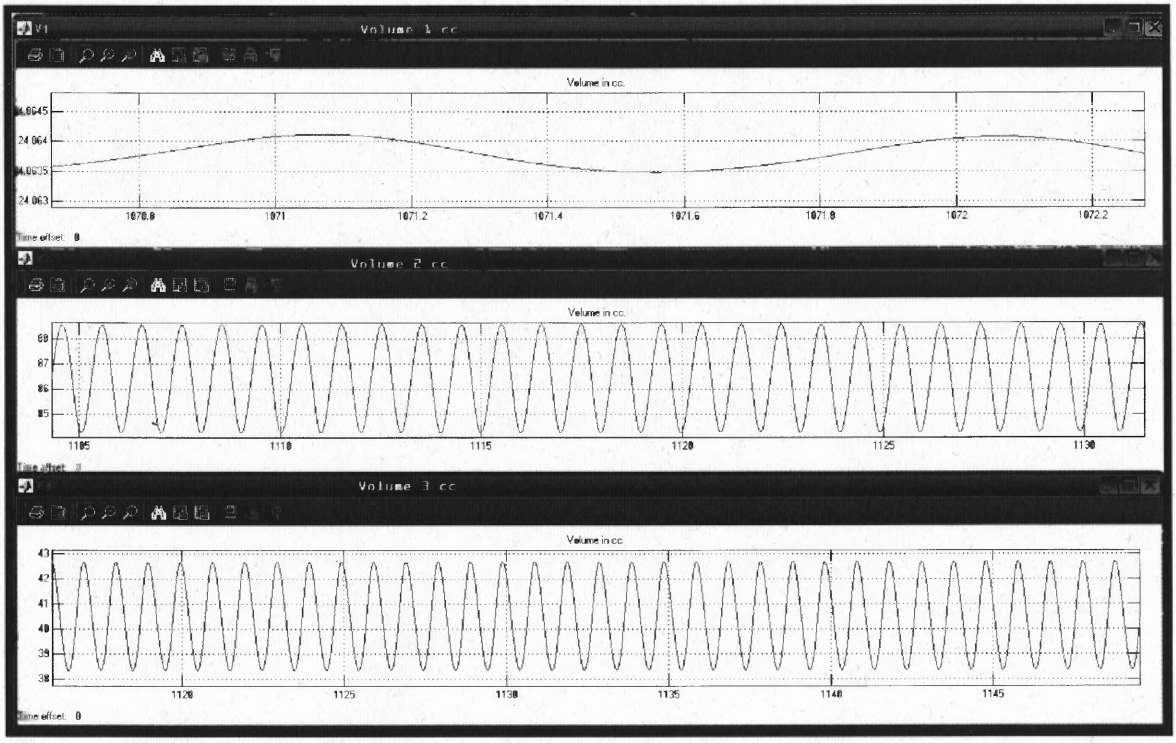

Figure A3.19 Sine driven model; behavior in time of the volume in cc of each compartment. R1= 100 mmHg-sec/cc R2= 0.1 mmHg-sec/cc.

It is really interesting to watch how the amount of exchange between Cp2 and Cp3 has now been diminished by the increased resistance between them The model is not descriptive anymore of what should have happened in normal physiology, due to the amount of CSF flow between the cranial cavity and the spinal compartment,. Thus the model fails to continue describing a normal CSF dynamics. (see figure A3.19 and A3.20)

This specific case could represent an altered craneo-vertebral junction, in which a partial obstruction at the level of the foramen magnum is present, like in the case of Arnold-Chiari syndrome.

Also interesting is the fact that Cp1's volume is still very stable.

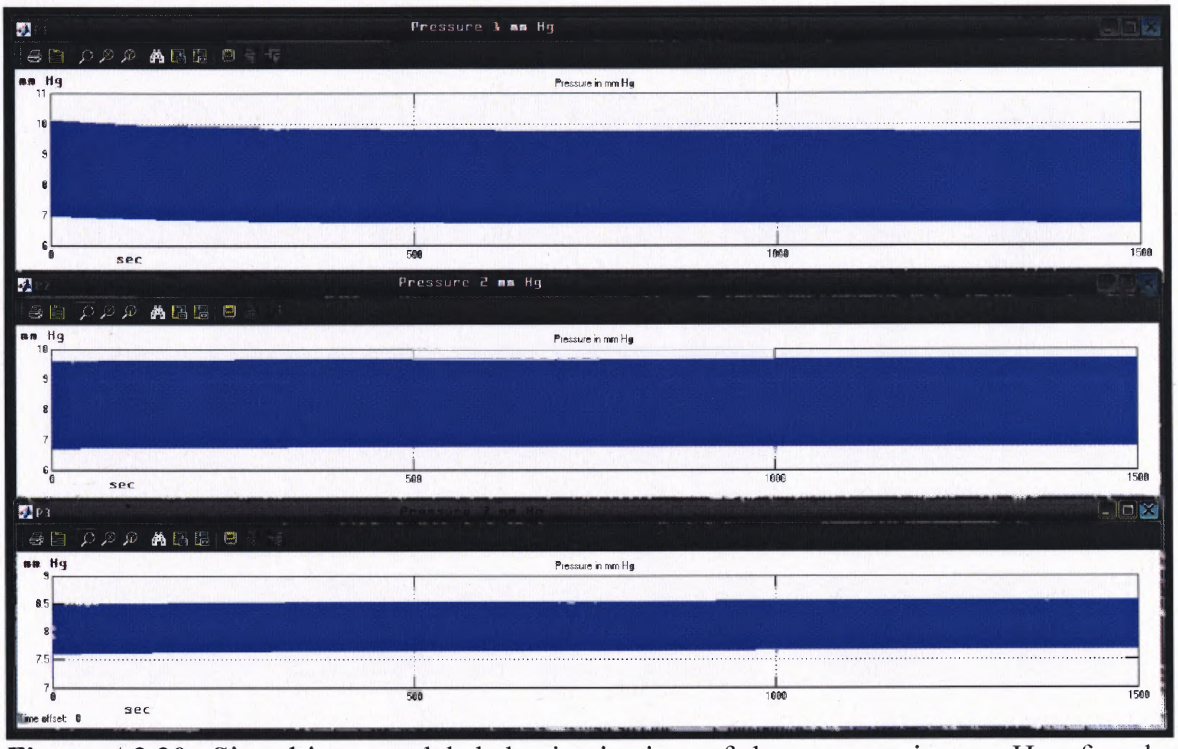

Figure A3.20 Sine driven model; behavior in time of the pressure in mm Hg of each compartment. R1= 100 mmHg-sec/cc. R2= 0.1 mmHg-sec/cc.

In respect to the pressure behavior, some interesting variations are present. The intracranial behavior is totally different from the spinal behavior. While the Cp1 and Cp2 have a similar range in their respective pressure, Cp3 has an independent behavior. The spinal pressure is not only much lower but also holds a diminished range between the lower and upper values.

The model is not representative any more of the normal CSF dynamics. It appears to be a threshold of R1 at 0.1 mmHg-sec/ml value for the system to enter into failure.

Case #9: R1= 10^8 mmHg-sec/cc R2= 0.001 mmHg-sec/cc. Increasing the R1 resistance up to values of 10^8 does not alter the volume distribution in a significant way, or the pressure behavior of the system. It only alters the amount of time required to reach equilibrium, extending the time up to 1900 sec.

Case #10:R1=0.1mmHg-sec/ to R1=10^{-6} mmHg-sec/R2= 0.001 mmHg-sec/cc. In the same manner as the CSF exchange per cycle between Cp2 and Cp3 is mainly controlled by the R2 resistance, it can be observed in next series of simulations that the fluid exchange per cycle between Cp1 and Cp2 are mainly controlled by the resistance R1.

If the R1 resistance is decreased to 0.1 mm Hg-sec/cc, the CSF exchange between Cp1 and Cp2 starts to increase as shown in figure A3.21, where the CSF volume interchange reach values of 1cc per cycle.

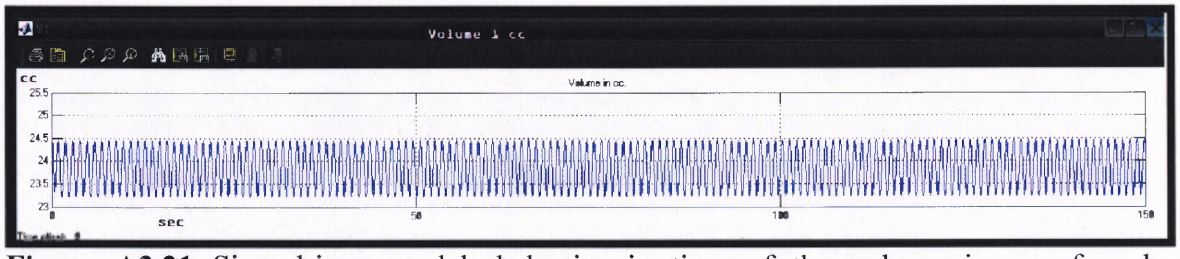

Figure A3.21 Sine driven model; behavior in time of the volume in cc of each compartment. R1= 0.1 mmHg-sec/cc R2= 0.001 mmHg-sec/cc.

If the R1 resistance is diminished to 0.01 mmHg-sec/cc, the CSF exchange between Cp1 and Cp2 continues to increase as shown in figure 5.37, where the CSF volume interchange reaches a final value of 2cc per cycle. The situation is very stable even at R1 values up to the order of 10^{-6} mmHg-sec/cc ; where the values for volume variation remain at the same level as when R1 value was 0.01 mmHg-sec/cc. Meanwhile the volume exchange between Cp2 and Cp3 dos not differ much from previous simulations.

Interestingly, no interaction between R1 and R2 is noticed, each one seems to be acting independently from each other.

Another fact of interest, is that the pressure behaves different when the model does not reflect the normal CSF dynamics. Two different and independent pressure dynamics are observed when R2 reaches 0.1 mmHg-sec/cc; one pressure dynamics inside the cranium, compartments Cp1 and Cp2; and, another pressure dynamics outside the cranium for compartment Cp3. In this case the increased resistance R2 alters not only the flow, but also the pressure communication between the intracranial and extracranial content.

In respect to pressure dynamics a very fast equilibrium is achieved at any of these relatively low R1 parameters, but still within normal values.

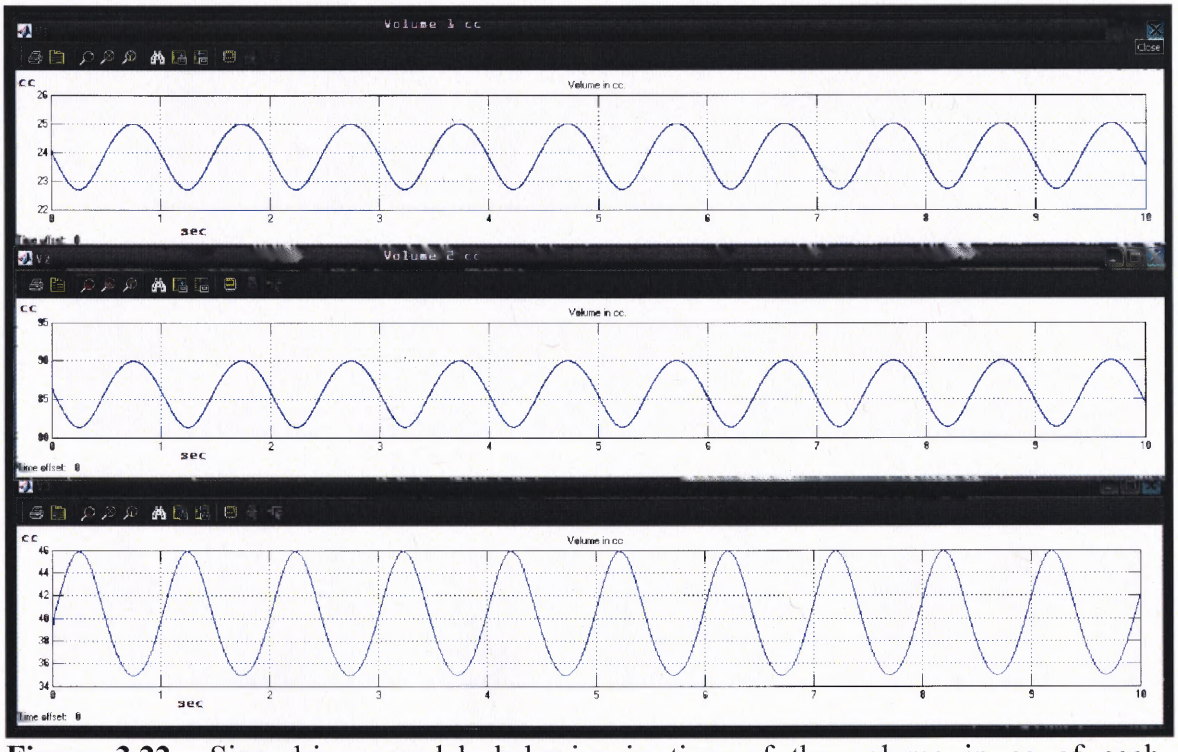

Figure 3.22 Sine driven model; behavior in time of the volume in cc of each compartment. R1= 10-6 mmHg-sec/cc R2= 0.001 mmHg-sec/cc.

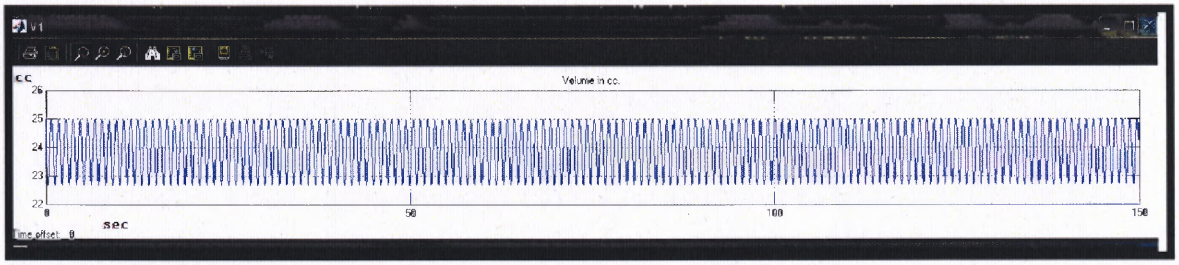

Figure A3.23 Sine driven model; behavior in time of the volume in cc of each compartment. R1= 10^{-6} mmHg-sec/cc R2= 0.001 mmHg-sec/cc.

REFERENCES

Andeweg, J. (1996). Consequences of the anatomy of deep venous outflow from the brain. Neuroradiology, 41, 233-241.

Andeweg, J. (1996). The anatomy of collateral venous flow from the brain and its value in aetiological interpretation of intracranial pathology. Neuroradiology, 38, 621–628.

Bateman, G. A. (2000). Vascular Compliance in Normal Pressure Hydrocephalus. AJNR, 21, 1574–1585.

Bateman, G, (2002), Vascular Hydraulics Associated with Idiopathic and Secondary Intracranial Hypertension. AJNR 23:1180–1186

Bateman,G, Christopher R. Levi, C, Schofield, P, Wang, Y, Lovett, E, (2005), The pathophysiology of the aqueduct stroke volume in normal pressure hydrocephalus: can co-morbidity with other forms of dementia be excluded? Neuroradiology 47: 741–748

Berry, J, Manoach, E, Mekkaoui, C, et al.(2002), Hemodynamics and Wall Mechanics of a Compliance Matching Stent: In Vitro and In Vivo Analysis. J Vasc Interv Radiol13:97–105

Bhadelia, R. A., Bogdan, A. R., Wolpert, S. M. (1998). Cerebrospinal fluid flow waveforms: effect of altered cranial venous outflow. A phase-contrast MR flow imaging study. Neuroradiology, 40, 283-292.

Bhadelia, R.A., .Bogdan, A.R., et al. (1997). Cerebrospinal fluid pulsation amplitude and its quantitative relationship to cerebral blood flow pulsations: a phase-contrast MR flow imaging study. Neuroradiology, 39, 258–264.

Bhadelia, R, Bogdan, A, Wolpert, S, (1995), Analysis of Cerebrospinal Fluid Flow Waveforms with Gated Phase-Contrast MR Velocity Measurements. AJNR 16:389–400.

Bradley, W, Safar, F, Hurtado, C, et al, (2004), Increased Intracranial Volume: A Clue to the Etiology of Idiopathic Normal-Pressure Hydrocephalus? AJNR 25:1479–1484.

Chestnut, R., Marshall, L. (1994). Intracranial Pressure: Monitoring and Management. Neurosurg Cli N Am, 5(4), 573- 606.

Chestnut, R., Marshall, L. (1991). Treatment of Abnormal Intracranial Pressure. Neurosurg Cli N Am, 2(2), 267- 284.

Chong, J., Mayer, S. A. (2002). Critical Care Management of Increased Intracranial Pressure. Journal of Intensive Care Medicine, 17(2), 55-67.

Czosnyka, M., et al. (1999). Vascular Components of Cerebrospinal Fluid Compensation. J Neurosurg, 90, 752-759.

Czosnyka, Z., Czosnyka, M., Whitfield, P., et al. (2002). Cerebral Autoregulation among Patients with Symptoms of Hydrocephalus. Neurosurgery, 50, 526–533.

Czosnyka, M, Czosnyka, Z, Momjian, S, Pickard, J, (2004), Cerebrospinal fluid dynamics. Physiol. Meas. 25: R51–R76

Dandy, W. (1919). Experimental Hydrocephalus. Ann Surg, 70129-142.

Edwards, R. J., Dombrowski, S. M., Luciano, M. G., Pople, I. K. (2004). Chronic Hydrocephalus in Adults. Brain Pathol, 14, 325-336.

Edsbagge, M, Tisell, M, Jacobsson, L, Wikkelso, C, (2004), Spinal CSF absorption in healthy individuals, Am J Physiol Regul Integr Comp Physiol 287: R1450–R1455

Egnor, M., Zheng, L., Rosiello, A., Gutman, F., Davis, R. (2002). A model of pulsations in communicating hydrocephalus. Pediatr Neurosurg, 36, 281–303.

Fin, L., Grebe, R, (2003), Three dimensional modeling of the cerebrospinal fluid dynamics and brain interactions in the aqueduct of Sylvius, Computer Methods in Biomechanics and Biomedical Engineering 6 : 163–170

Gray, H. (1977). The blood-vessels of the brain. In H Gray's Anatomy, Descriptive and Surgical, Grays Anatomy, 512 -514. New York, NY, Random House.

Gray, H. (1977). Sinuses of the Dura Mater. In H Gray's Anatomy, Descriptive and Surgical, Grays Anatomy, 602-606. New York, NY, Random House.

Gray, H. (1977). The nervous System in H Gray's Anatomy, Descriptive and Surgical, Grays Anatomy, 639-758. New York, NY, Random House.

Grant A. Bateman,G, (2004), Idiopathic intracranial hypertension: priapism of the brain? Medical Hypotheses 63, 549–552

Greitz, D., Wirestam, R., et al. (1992). Pulsatile movement and associate hydrodynamics studied by magnetic resonance phase imaging. The Monroe- kellie Doctrine revisited. Neuroradiology, 34, 370-380.

Greitz, D., Hannerz, J. (1996). A Proposed Model of Cerebrospinal Fluid Circulation: Observations with Radionuclide Cisternography. AJNR, 17, 431–438.

Hakim, C.A., et al. (2001). Normal Pressure Hydrocephalus. Neurosurg Cli N Am, 12, 761-773.

Hakim, S., et al. (1976). The Physics of the Cranial Cavity, Hydrocephalus and Normal Pressure Hydrocephalus: Mechanical Interpretation and Mathematical Model. Surg Neurology, 5, 187-210.

Hoppensteadt, F., Peskin, C., (2001)The Heart and Circulation, in Modeling and Simulation in Medicine and the Life Sciences, 5-69, New York Springer.

Holzapfel G.A., Gasser T.C., Ogden R.W. (2000). A New Constitutive Framework for Arterial Wall Mechanics and a Comparative Study of Material Models. Journal of Elasticity, 61, (1), 1-48

Johanson, C., Jones, H. (2001). Promising vistas in hydrocephalus and cerebrospinal fluid. Research Trends in Neurosciences, 24(11), 631-632.

Johnston, I., Teo, C. (2000). Disorders of CSF hydrodynamics. Child's Nerv Syst, 16, 776–799.

Kacsmarek, M., et al. (1997). Hydromechanics of Hydrocephalus Steady State Solutions for Cylindrical Geometry. Bull Math Biol, 59(2), 295-323.

Karahalios, D.G., Rekate, H.L., Khayata, M.H. (1996). Apostolides PJ Elevated intracranial venous pressure as a universal mechanism in pseudotumor cerebri of varying etiologies. Neurology, 46, 198–202.

Kondziella, D, Wolf Lu¨demann, W,Brinker, T, (2002) Alterations in brain metabolism, CNS morphology and CSF dynamics in adult rats with kaolin-induced hydrocephalus Brain Research 927 35–41

Kurtcuoglu, V., Poulikakos, D., et al. (2005). Computational Modeling of the Mechanical Behavior of the Cerebrospinal Fluid System. Journal of Biomechanical Engineering, 127, 265-269.

Kotani, J., Nitta, K., Sakuma, Y., Sugioka, S., Fujita, N., Ueda, Y. (1992). Effects of bilateral jugular vein ligation on intracranial pressure and cerebrospinal fluid outflow resistance in cats. Br J Oral Maxillofac Surg, 30(3), 171-173.

Lacolleya, P., Challandeb, P., Boumazaa, S. (2001) Mechanical properties and structure of carotid arteries in mice lacking Desmin. Cardiovascular Research , 51, 178–187

Lakes, R. (1993). Materials with Structural Hierarchy. Nature, 361(11), 511-515.

Levine, D. (1999). The Pathogenesis of Normal Pressure Hydrocephalus: A theoretical Analysis. Bull Math Biol, 61, 875-916.

Linninger, A.A., Tsakiris, C., Zhu, D.C., Xenos, M., Roycewicz, P., Danziger, Z., Penn, R. (2005). Pulsatile Cerebrospinal Fluid Dynamics in the Human Brain. Biomedical Engineering, IEEE Transactions on, 52 (4), 557 – 565.

Linninger, A, Xenos, M, Zhu, D, et al. (2007), Cerebrospinal Fluid Flow in the Normal and Hydrocephalic Human Brain. IEEE Transactions On Biomedical Engineering, 54, (2): 291- 302

Lorberboym, M., Lampl, Y., et al. (2001). Benign intracranial hypertension: correlation of cerebral blood flow with disease severity. Clinical Neurology and Neurosurgery, 103, 33–36.

Meier, U., Kiefer, M., Bartels, P. (2002). The ICP-dependency of resistance to cerebrospinal fluid outflow: a new mathematical method for CSF-parameter calculation in a model with H-TX rats. Journal of Clinical Neuroscience, 9(1), 58–63.

Nagashima, T., Tamaki, N., et al. (1987). Biomechanics of Hydrocephalus: a New Theoretical Model. Neurosurgery, 21(6), 898-904.

Naidich, T., et al. (1993). Phase Contrast Cine Magnetic Resonance Imaging: Normal Cerebrospinal Fluid Oscillation and Applications to Hydrocephalus. Neurosurg Cli N Am, 4(4), 677-706.

Nilsson, C., Stahlberg, F., et al. (1992). Circadian variation in human cerebrospinal fluid production measured by magnetic resonance imaging. AJP - Regulatory, Integrative and Comparative Physiology, 262(1,) 20-24.

Nonaka, H., Akima, M., Hatori, T., et al. (2002). The microvasculature of the human cerebellar meninges. Acta Neuropathol, 104, 608–614.

Penn, R., et al. (2005). Pressure Gradients in the Brain in an Experimental Model of Hydrocephalus. J Neurosurg, 102, 1069-1075.

Pena, A., et al. (1999). Effects of Brain Ventricular Shape on Periventricular Biomechanics. Neurosurgery, 45, 107-116.

Pena, A., et al. (2002). Communicating Hydrocephalus: the Biomechanics of progressive Ventricular Enlargement Revisited. Acta Neurochir, (S)81, 59-64.

Peterson, L, Jensen, R, Parnell, J, (1960), Mechanical Properties of Arteries in Vivo. Circulation Research, 8, 622-639

Piper, I., Chan, K., et al. (1993). An Experimental Study of Cerebrovascular Resistance, Pressure Transmission, and Craniospinal Compliance, Congress of Neurological Surgeons, 32(5), 805–816.

Rekate, H.(1994). The Usefulness of Mathematical Modelling in Hydrocephalus Research. Childs Nerv Syst, 10, 13-18.

Rekate, H., et al. (1998). Ventricular Volume Regulation: A mathematical Model and Computer Simulation. Pediatr Neurosci, 14, 77-84.

Sbarbati, A., Pietra, C., et al. (1996). The microvascular system in ischemic cortical lesions. Acta Neuropathol, 92, 56–63.

Schaller, B, (2004) Physiology of cerebral venous blood flow: from experimental data in animals to normal function in humans, Review. Brain Research Reviews 46 243–260

Scot, J.N., Farb, R.I. (2003). Imaging and anatomy of the normal intracranial venous system. Neuroimag Clin N Am, 13, 1–12

Sherwood, L. (2004). The Central Nervous System. In Human Physiology, 132 - 183. Belmont, CA: Thomson.

Shulman, K, and Marmarou, A, (1971 Pressure- Volume considerations in Infantile Hydrocephalus, Developmental Medicine and Child Neurology ,13,(s25): 90-95

Stemper, B,Yoganandan, N, Pintar, F, (2005), Methodology to study intimal failure mechanics in human internal carotid arteries.Journal of Biomechanics, 38: 2491–2496

Stevens, S., Lakin,W.,,(2003),A Differentiable, Periodic Function for Pulsatile Cardiac Output Based on Heart Rate and Stroke Volume , Mathematical Biosciences 182(2):201-211

Sunagawa, K, Kanai1, H, Tanaka, M, (2000), __Simultaneous Measurement of Blood Flow and Arterial Wall Vibrations in Radial and Axial Directions, IEEE Ultrasonics Symposium:1-4

Taveras, J., Word, E. (1978). Angiografia Carotidea. In Diagnostico Neuroradiologico, 588 – 778 .Buenos Aires, Arg :Panamericana.

Turner, R. (2002). How Much Cortex Can a Vein Drain? Downstream Dilution of Activation-Related Cerebral Blood Oxygenation Changes. NeuroImage, 16, 1062–1067.

Van Andel et al., (2003), Mechanical Properties of Porcine and Human Arteries: Implications for Coronary Anastomotic Connectors. Ann Thorac Surg 59 (76):58–65

Zofia H. Czosnyka, Z,Czosnyka, M,Whitfield, P, Donovan, T, Pickard, J(2002), Cerebral Autoregulation among Patients with Symptoms of Hydrocephalus. Neurosurgery, 50, (30): 526-533.